AMERICAN UNIVERSITY OF BEIRUT

LOW RESOLUTION PALEOCLIMATE RECONSTRUCTION, FROM STABLE ISOTOPE ANALYSIS OF TWO SPELEOTHEMS FROM THE EL-KASSARAT AND RAHWE CAVES, IN LEBANON

by
RENA DARWICH KARANOUH

A thesis
submitted in partial fulfillment of the requirements
for the degree of Master of Science
to the Department of Geology
of the Faculty of Arts and Sciences
at the American University of Beirut

Beirut, Lebanon
May 2014

AMERICAN UNIVERSITY OF BEIRUT

LOW RESOLUTION PALEOCLIMATE RECONSTRUCTION,
FROM STABLE ISOTOPE ANALYSIS OF TWO
SPELEOTHEMS FROM THE EL-KASSARAT AND RAHWE
CAVES, IN LEBANON.
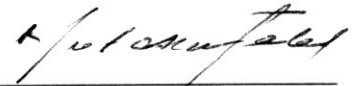

by

RENA DARWICH KARANOUH

Approved by:

_____   Advisor
Dr. Al Haidar
Assistant Professor, Geology
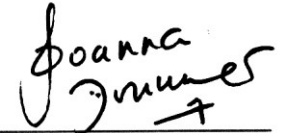

_____   Member of Committee
Dr. Mutasem Fadel,
Professor, Chairman, Environmental Engineering Program
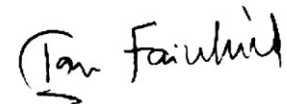

_____   Member of Committee
Dr. Joanna Doummar
Assistant Professor, Geology

_____   Member of Committee
Dr. Ian Fairchild
Professor and Head of School, GEES
(School of Geography, Earth and Environmental Sciences),
University of Birmingham, Edgbaston, Birmingham

Date of thesis defense: May 8th, 2014

AMERICAN UNIVERSITY OF BEIRUT
THESIS, DISSERTATION, PROJECT RELEASE FORM

Student Name:
____Karanouh_____Rena_____Darwich_____
   Last   First   Middle

● Master's Thesis   ◯ Master's Project   ◯ Doctoral Dissertation

[X] I authorize the American University of Beirut to: (a) reproduce hard or electronic copies of my thesis, dissertation, or project; (b) include such copies in the archives and digital repositories of the University; and (c) make freely available such copies to third parties for research or educational purposes.

[ ] I authorize the American University of Beirut, **three years after the date of submitting my thesis, dissertation, or project,** to: (a) reproduce hard or electronic copies of it; (b) include such copies in the archives and digital repositories of the University; and (c) make freely available such copies to third parties for research or educational purposes.

_____19.5.14_____

Signature   Date

This form is signed when submitting the thesis, dissertation, or project to the University Libraries

ACKNOWLEDGEMENTS

AN ABSTRACT OF THE THESIS OF

Rena Darwich Karanouh   for   Master of Science
                                           Major: Geology

Title: Low resolution paleoclimate reconstruction, from stable isotope analysis of two speleothems from the El-Kassarat and Rahwe caves, in Lebanon.

Two stalagmites were investigated from the coastal El-Kassarat cave, EKC-01 (located in central Lebanon), and a high elevation Rahwe cave, RC-01 (located in North Lebanon), respectively. The paleo-climatic records observed are based on oxygen and carbon stable isotope ratios, absolute dating of U/Th series, petrographic analysis, and growth patterns.

Groundwater, dripwater, rainwater, and snow samples were acquired for isotope analyses and physico-chemical parameter determination. Continuous temperature measurements were conducted for a whole year. Glass plates were placed inside each cave, and modern calcite precipitates were collected for calibration. All these measurements allowed for a detailed calibration of the stable isotopic and age data collected from the two stalagmites.

Four samples were drilled in the RC-01 stalagmite for U/Th dating. This stalagmite showed age reversals and alteration, thus requiring further assessment in the future.

The candlestick section of EKC-01 was drilled for U-series dating (3 samples). This stalagmite segment was also analyzed for carbonate $\delta^{18}O$ and $\delta^{13}C$ isotopes (64 samples), and for trace elements. Dating results show that this stalagmite started to grow at about 62 ka BP.

Isotopic results from the EKC-01 stalagmite indicates that major changes in local and global climatic records have been recorded in the stalagmites' laminae. These can be subdivided into five major climatic phases; Phase 1 (27.5 to 15.0 ka) was characterized by lower temperatures and lesser rainfall, with a mixture of C_3 (e.g. shrubs, wheat, trees) and C_4 (e.g. maize, sugar cane) vegetation types present in the region. As glaciers in much of the northern hemisphere melted, there was a sharp increase in temperature and rainfall, and a possible increase in C_3 vegetation between 15.0 and 13.0 ka. The climatic phase spanning from 13.0 to 9.0 showed comparatively more humid conditions, with an increase in rainfall during the early Holocene epoch. A short, relatively colder, period occurred approximately between 9.0 and 7.0 ka. This recorded cold event could coincide with that known at 8.2 ka event that occurred in the North Atlantic region. After about 7.0 ka, the conditions were close to those of present day environments, indicating a return to warmer temperatures and increased rainfall rates.

TABLE OF CONTENTS

LIST OF FIGURES

xi

xiii

xv

LIST OF TABLES

ABBREVIATIONS

BG   below ground level

BTD   Bureau Technique pour le Developpement

BP   before present

Hr   hour

km   kilometers

l/s   liters per second

m^3 cubic meters

masl   meters above sea level

μS   micro siemens

mg/l   milligrams per liters

ppm   parts per million

ppt   parts per thousand

TDS   total dissolved solids

MoEW   Ministry of Energy and Water

SST   Sea surface temperature

LNMS   Lebanese National Meteorological Station

$\delta^{13}C$ Ratio of Carbon-13 to Carbon-12 relative to a standard

$\delta^{18}O$ Ratio of Oxygen-18 to Oxygen-16 relative to a standard

ka   Kilo-annum (1000 years ago)

‰   Parts per thousand, or permil. Notation to express $\delta^{13}C$ and $\delta^{18}O$ values

ppm   Parts per Million

Dedicated to:

Issam Bou Jaoude,

my North, my South, my East and West,

my first and finest geology teacher,

thank you for always believing.

CHAPTER 1

INTRODUCTION AND OUTLINE

1.1 Forward

Today, climate change is a controversial issue as it impacts ecological and economical resources around the world. A number of processes have contributed to climate change, including the hole in the Ozone layer, the overuse of fossil fuels, and the natural climatic changes that the earth undergoes (Petit, 1999). The current debate stems around whether the cause for climate change is anthropogenic or it would have naturally occurred over geologic time, due to solar activity or volcanic eruptions (White, 2007).

Paleoclimatic studies provide a basis for possible causes of climatic change over a large span of geological time. Understanding past climates, and the reasons for their occurrence, provide the necessary material for which present day climate change can be understood.

How much has the anthropogenic input of CO_2 affected climate? Has this kind of warming occurred before or has human activity fueled the current climate change/global warming? White (2007) asked whether the present day warming is comparable to other warm periods of the past, or whether we are entering a new, and possibly dangerous, climatic regime. There has been a considerable warming over the last 140 years, and the increase within the 20th century seemed to be exceptional when compared with the last

1,200 years (*e.g.* Houghton, 2004). Understanding past climatic shifts and their causes can provide the necessary background baseline where present conditions can be modeled and studied. The ability to forecast climate changes might help countries in setting up preventive measures, ensuring the protection for their nationals.

Proxy data, influenced by climatic variations, can provide specific climatic signals. Many different environments can be used to access paleoclimatic conditions; marine deposits, lacustrine sediments, ice cores, paleosols, fluvial sediments, loess, lake levels, macrofossils, soils, calcretes, deep sea cores, pollen, corals, and tree rings are among the most utilised. The addition of speleothems to the former list is comparatively recent.

As rain and snowmelt waters percolate through the soil cover, its acidity increases as it absorbs soil CO_2, formed by root respiration, oxidation of dead plant material as well as microbial activities. On reaching the karstified limestone bedrock located below the soil layer, the slightly acidic water dissolves calcium carbonate in the rock as it flows through the varied sized conduits. This dissolution continues until thermodynamic equilibrium with the ambient partial pressure of CO_2 (pCO_2) is reached. Once this groundwater reaches the air filled cave chamber, speleothems are deposited slowly by degassing of dripwater as it passes from the rock fractures to the cave environment (McDermott *et al.,* 2004).

The earliest speleothem dating involved the use of radiocarbon methods to verify annual layering in a flowstone entombing a human thighbone (Broecker *et al.,* 1960). In order to reconstruct the paleoclimate over geologic time, scientists indirectly measure

components by analyzing various proxies/indicators that are sensitive to climatic or environmental parameters, and consequently are preserved in the speleothems (Campisano, 2012). The use of oxygen-isotope values in speleothems as a paleoclimate proxy started in the 1960s and 1970s (Hendy and Wilson, 1968 and Hendy, 1971). The way speleothems grow makes them ideal structures to measure such proxies. Dripwater in caves can capture surface climatic patterns and changes, which in turn are archived in the speleothems via the hydrological behaviour of the drips that form the speleothems' laminae (Baker *et al.,* 2000).

Speleothem growth rates are dependent on changes in surface conditions such as precipitation quality and quantity, changes in the type of vegetation cover, and changes in surface temperature (Fairchild *et al.,* 2006). Each cave has its unique geologic and environmental setting, which needs to be understood before stable isotopes, trace elements, annual bands or other proxies can be used with confidence for paleoclimatic reconstructions (Fleitmann *et al.*, 2009).

Speleothems have several advantages in comparison to other paleoclimate archives (Fleitman *et al.*, 2009, McDermott *et al.*, 2004). They:

- can be found in caves in almost all parts of the world;

- can be dated using the Uranium-series decay with exceptionally high precision, back to ~600 kyr BP. In contrast to radiocarbon dates, uranium-series dates are absolute ages and no calibration is needed;

3

- grow continuously over long time intervals, and thus have long and highly resolved time series covering several glacial-interglacial cycles;

- bear information about the environment above the cave, including rainfall, temperature, vegetation, soil productivity and glacier extent.

- precipitate close to isotope equilibrium;

- contain a number of physical and chemical proxy variables, such as annual growth layers, relatively rapid growth rates, stable isotope ratios and trace elements;

- can accurately reflect changes in the external environment if they grow in isotopic equilibrium.

The correlation and matching of different types of paleoclimatic records (*e.g.* ice cores, pollen) with the speleothem record can help show how geographically connected systems behave in a climatic time period as well as show the connection between land and sea systems with respect to heat transfer, rainfall generation, and timing of climatic events (Bar-Matthews *et al.,* 2003).

1.2 Stalagmites as natural archives

Speleothems is a term that encompasses the many different calcium carbonate precipitates that deposit in caves. The word is derived from the Greek words *spelaion* meaning cave, and *thema* meaning deposit. The term speleothem refers to the mode of occurrence - how a mineral looks rather than its composition (Hill and Forti, 1997). Stalagmites range in colour from white to ochre to brown, depending on the type of

4

contaminants present. Pure calcite is white or translucent in colour. The contaminants

are substances collected as the water percolates through the soil as well as the overlying

limestone rocks (Hill and Forti, 1997).
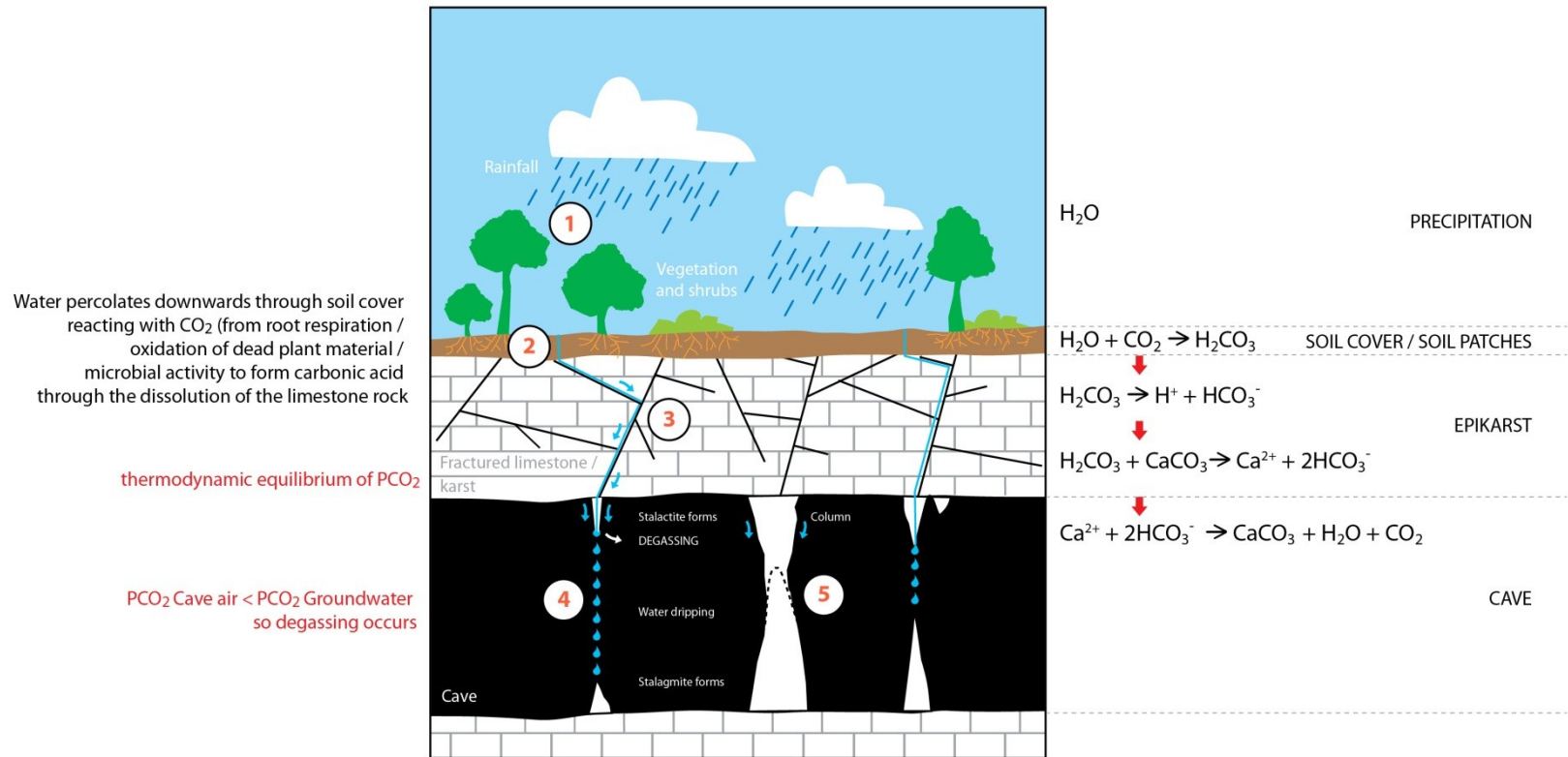
Figure 1. The system that rainwater follows from surface percolation until it reaches the cave environment (see text for explanation) (Formulas modified from Gillieson, 1996).

6

Figure 1 shows the possible flowpaths of rainwater and the subsequent formation of speleothems.

1- Rainfall / snowmelt are the main routes by which water reaches an aquifer.

2- The water percolates through the soil becoming more acidic as CO_2, from plant respiration / microbial activities / organic decay is dissolved.

3- Groundwater flows through the limestone rock through first, second and tertiary porosity, dissolving calcium carbonate.

4- When the groundwater reaches the cave air it undergoes degassing because of the change in pCO_2 depositing calcite with each drip. Calcite deposited in the ceiling is called a stalactite and calcite deposited on the ground is called a stalagmite. When a stalactite and a stalagmite meet, they are called a column.

Speleothem's growth period, isotopic and geochemical compositions reflect large scale surface processes such as precipitation, storm patterns, ocean-land heat transfer, vegetation cover type and soil-water-rock interactions (Bar-Matthews *et al*., 2003).

Speleothems are structures requiring different elements to grow. These are usually transported by dripping waters. It is essential to know the source and composition of the water from which stalagmites precipitate as it has a direct relation to the isotope ratio in the stalagmite. Water quality is dependent on the water mass the water originated from. Water quantity is reliant on air temperature, which affects rainfall and snow quantities.

Soil cover, vegetation type, evapotranspiration, precipitation rates, rock porosity, volcanic activities, and retention time are all factors that change the water composition

7

until it reaches the cave environment. Growth rate is considered a cumulative proxy since it is dependent on the many variables listed above. Stalagmite growth rates are characteristically measured by the yearly deposition of calcite bands which vary by at least two orders of magnitude (typically in the range of 0.01 -1.0 mm/year), depending on factors such as temperature, calcium ion concentration of the drip-waters (Baker *et al.*, 1998; Genty *et al.*, 2001a) as well as quantity of water available, which Fairchild and McMillan (2007) consider as the most important control on a speleothems' growth rate.

Effective precipitation, which is rainwater minus evapo-transpiration, controls drip rates (Genty and Deflandre, 1998) inside the cave. Drip rates are directly related to precipitation and water quantity in the epikarst and type of host rock above the cave. Usually, in arid and semi-arid regions, the water that drips inside a cave in summer comes from residual waters resident in the epikarst from winter precipitation.

Drip rates directly affect speleothem growth. Slow drip rates increase the amount of time that a drop spends on a stalactite, resulting in increased stalactite sizes and decreased stalagmite sizes (Baldini, 2001). Extremely high drip rates favour calcite deposition on the side of the stalagmite effectively increasing the stalagmite's diameter (Dreybrodt, 1980). Fast drip rates do not allow the time for degassing to occur on the stalactite, but rather on the stalagmite.

The morphology of the speleothem is controlled by the rate of the dripwater and the height of the point dripwater in stalagmites. The diameter of the stalagmite increases

with increased drip height due to splash effects. A falling drop may result in the formation of a depression where the drop impacts the stalagmite top. The stalagmite morphology is also dependent on the morphology of the stalactite above it and both can be viewed as an integrated system (Baldini, 2010).

It is important to understand that some stalagmite growth changes are due to global climatic shifts and some are due to local changes. The distinction between the two is difficult to interpret. Hiatuses could be due to changes in the environment (glacial/interglacial, flooding/removal of soil cover, lack of rainfall) or to tectonic activities which could affect the fracturing of the rock either closing or opening conduits. During glacial periods, the temperature in caves is below the freezing point, so the water is locked up as ice and does not flow effectively, stopping speleothem growth and thus forming a hiatus. Hiatuses often reflect uncomplimentary climate conditions for growth, and renewed growth often indicates a warming of the climate (*e.g.* Baker *et al.*, 1995; Frisia *et al.*, 2006). Speleothem growth is reduced with increasing latitude and altitude, and in cool and dry climates. In glacial periods, there are more detrital deposits in the cave due to an increase in erosion rate, and the lack of vegetation.

Each successive growth layer of a speleothem is assumed to have developed almost at the same time, for example during one season or one year (Frisia and Borsato, 2010). Speleothems are laminated and each lamina can be dated precisely. Each lamina can carry information about the environmental conditions under which it was precipitated. Laminations in speleothems typically show thousand-year, hundred-year, decadal,

annual or seasonal time scales. The laminations occur due to climatic changes or are the result of periodic events such as flooding.

Frisia *et al.* (2000) stated that variable crystal morphologies and sizes can account for visible laminations. Changes in mineralogy can also form laminations, such as when calcite and aragonite layers precipitate; this depends on the amount and variability of the temperature as well as the Mg/Ca ratio in the dripwater (Railsback *et al.,* 1994). Very often, lamination is the visual manifestation of changes in the quantity of organic, detrital or fluid inclusions (*e.g.* Shopov *et al*., 1994). Genty and Quinif (1996) stated that annual couplets, consisting of alternating white porous and dark compact laminae, can be explained by micro-porosity changes.

Comparison of annual bands in stalagmites with precipitation and temperature data reveal that thicker bands correlate with either higher temperatures (Frisia *et al.,* 2003) or higher effective moisture (Fleitmann *et al*., 2009). Effective moisture is defined as the amount of moisture retained in the soil after evapotranspiration and drainage processes (Fetter, 2007). Thick calcite laminae correlate well with high effective precipitation (Railsback *et al*., 1994). Effective precipitation is the total rainfall without the runoff, evaporation, and deep percolation amounts (Fetter, 2007).

Speleothems can undergo diagenetic changes, such as erosion, dissolution, micritization, and recrystallization. These processes can modify speleothem geochemistry and isotopic ratios and, thus, have critical implications for the

interpretation of environmental proxies and radiometric age-dating (Munoz-Garcia *et al*., 2012).

Diagenetic processes in stalagmites are often related to changes in the cave environment or in the hydrochemistry of the dripwater. These changes can induce the interruption of carbonate deposition, and a new interaction between drip waters and the carbonate minerals previously deposited can develop. This interaction geochemically alters the surface of the speleothem, and the resulting diagenetic features may be preserved as 'altered' stratigraphic intervals if carbonate deposition resumes after a period of no deposition (Muñoz-García *et al*., 2012). In some situations, the speleothem surface is permeable enough to allow water percolation, or the waters are corrosive enough to generate new percolation paths through the dissolution of existing carbonate. The water then enters the speleothem, promoting diagenetic transformations as it flows downwards via a network of connected pores (Frisia *et al.,* 2000). Stalagmites with large crystals can indicate re-crystallization or weak alteration of the speleothem (Kendall and Broughton, 1978).

1.3   Speleothem and related studies in the Eastern Mediterranean region

In the Eastern Mediterranean, speleothem isotope ratios have been studied in various places, including Turkey, Lebanon, Jordan and the West Bank.

During the last decade, intensive speleothem-based paleoclimate research has been written on the Eastern Mediterranean region, based on speleothem sampling and dating (a listing can be found in Finné *et al*. 2011 and in Robinson *et al*., 2006).

Only two speleothems have been sampled for paleoclimatic research from a Lebanese cave until now (Verheyden *et al*., 2008, Nader *et al*., 2013) These were collected from Jeita Cave (33° 56.617'N and 35° 38.632'E, ≈89 masl), a coastal cave located west of the Mount Lebanon range. The results showed high $\delta^{18}O$ and $\delta^{13}C$ values for the last interglacial period, low values in the early Holocene, and high values after 5.8 ka. The wettest period occurred between 9.2 and 6.5 ka. Between 6.5 and 5.8 ka a change to drier mid Holocene was observed. A two-step transition in the $\delta^{18}O$ and the $\delta^{13}C$ values, indicating a change from wet early Holocene to drier mid- Holocene conditions is observed between 6.5 and 5.8 ka. A first step of the transition occurs within ~500 years at around 6.5 ka, and is interrupted by a short (~100 year) return to wetter conditions. A second transition of equal intensity occurs more rapidly, seemingly in less than 200 years at 5.9 ka (Verheyden *et al*., 2008). The Jeita cave speleothem did not contain a glacial record.

Two stalagmites from the Junction Chamber in El-Kassarat cave, a coastal cave, have been dated by Nehme *et al*. (2013). Their dates of these speleothems, Kt12011 and Kt22011, were documented to be 37,590 ± 0.829 *a* and 33,921 ± 1.09 *a* respectively. No stable isotope dating was related with respect to these speleothems.

Lacustrine sediment sequence from the Yammouneh basin in Lebanon spans a 250 ka record (Develle *et al.*, 2010, 2011). They showed that isotopic changes in rocks can be due to air temperature changes rather than to increased rainfall. During the Holocene period, the effective moisture water isotope composition was probably the prime factor controlling the fluctuations of regional inland water composition. Develle (2010) stated that the isotopic enrichment in the Last Glacial Maximum (LGM) cannot be attributed to increased rainfall, but rather due to negative ground-temperature effect, possibly associated with changes in air mass trajectories over the Mediterranean Sea. She suggested that, at least in open lake systems, the source area effects during the Holocene and glacial–interglacial temperature changes had been important drivers on inland ^{18}O isotope signals in the Mediterranean region.

Other speleothem records from the Southern Levant region have been studied in Soreq, West Jerusalem , Pekiin, Mitzpe Shlagim, and Ma'ale Ephraim caves (*e.g.* Bar-Matthews *et al.*, 1996,1997, 1999, 2000, 2003; Ayalon *et al.*, 1998, 2013; Frumkin *et al.,* 1999a, 2000) providing a continuous record of the paleoclimate of the eastern Mediterranean region during the last 25 ka. The record from Soreq cave is made up of a composite of various stalagmites with overlapping ages. Speleothem deposition was continuous throughout the last 180 ka.

Bar-Matthews (2003) has shown a close correlation between speleothem δ^{18}O and marine record based upon planktonic foraminifera δ^{18}O values in the Eastern Mediterranean Sea. This suggests that climatic events in the Eastern Mediterranean Sea

were linked to terrestrial events for at least the last 250 ka. Bar-Matthews (2003) reported that a small peak of rainfall was recorded at about 4.7 ka, followed by increasing aridity. At about 5.1 ka, the annual rainfall was about 220 mm to 600 mm during the early Holocene (7.5-8 ka). Holocene temperature values varied from 14 to 17ºC between 8 and 10 ka BP to a maximum warmer temperature estimate of 20-22 ºC between 0.8 and 1.2 ka BP. Bar-Matthews (1999, 2000, 2003) reported a large positive carbon-isotope excursion from 8.5 to 7 ka in Soreq cave speleothems. They concluded that the positive $\delta^{13}C$ values are related to early Holocene rainfall events, associated with Sapropel S1, which stripped soil cover thereby reducing the influence of soil CO_2 and soil processes on the $\delta^{13}C$ of groundwaters. A general shift to more negative $\delta^{13}C$ values is recorded from 20 to 15 ka and a plateau from this point to 10 ka probably due to a shift from C_4-rich flora to a mixed C_3-C_4 vegetation cover (Robinson *et al*., 2006). Frumkin (2000) found no trace of this large $\delta^{13}C$ excursion in the Jerusalem West Cave record because maybe too few stalagmites had been sampled or it was a unique climatic event around Soreq cave.

Fundamental differences in the interpretation of the $\delta^{18}O$ data lead to different regional paleoclimate patterns. The $\delta^{18}O$ calcite data between Soreq cave and West Jerusalem cave are very similar. Bar-Matthews (1997, 1999) interpretation showed that the speleothems' $\delta^{18}O$ records are indicative of temperature change where glacial $\delta^{18}O$ values are 3.5 to 5‰ more enriched than interglacial periods. Frumkin (1999, 2000) stressed that the speleothems' $\delta^{18}O$ low values are due to a major increase in glacial

seawater $\delta^{18}O$ because of the evaporative enrichment of the Mediterranean Sea during glacial lowstands.

Long-term fluctuations in speleothem $\delta^{18}O$ records from Soreq and Peqiin Caves have been interpreted as primarily reflecting the 'amount effect' and 'temperature effect' (Dansgaard, 1964; Rozanski *et al.*, 1992). Thus, $\delta^{18}O$ values indicate dry-cold glacial and wet-warm interglacial periods respectively (Bar-Matthews *et al.,* 1997, 1999, 2003). This view suggests dry/wet Last Glacial/Holocene conditions, in contradiction with lake-level records. Kolodny *et al.* (2005), Enzel *et al.*, (2008) and Frumkin *et al.* (1999, 2000) all discussed that long-term changes in $\delta^{18}O$ the caves' carbonate records principally reflect changes of isotopic composition of the water vapor source, i.e. the source effect. High $\delta^{18}O$ values were credited to the isotopic enrichment of the Eastern Mediterranean sea waters, due to the changes in the global ice volume.

The analysis by Frumkin (1999) is in accord with the interpretation of the increased levels of Lake Lisan as representing significant increase in rainfall amounts whereas the Bar-Matthews (1997) interpretation does not agree with this interpretation, as it argues for drier conditions during these lake stands (Enzel *et al*., 2008).

Bar-Matthews (2000) showed how rainfall quantity above Soreq and Pekiin caves were different (as the Peqiin cave is found at a higher elevation) although the studied stalagmites showed the same $\delta^{18}O$ values for the same time. In this way two different controls of isotopic composition (temperature and elevation difference) apparently

cancel each other out causing speleothems in two different climatic regions to have similar $\delta^{18}O$ values.

None of these studies dealt with high elevation speleothems located in the karst region of the east 'Mediterranean Alpine zone' until Ayalon *et al*. (2013) was published. Speleothem deposition in this high altitude region was continuous during interglacials, but the Last Glacial growth was episodic. The main depositional period was from ≈56 ka to 51 ka. This coincides with the Dansgaarde Oeschger interstadials and warming in the northeastern basin of the Mediterranean Sea (Ayalon *et al.*, 2013*)*.

1.4   Aim of this study

The aim of this thesis is to construct highly resolved records of past climates using stalagmites collected from two Lebanese caves. This study constitutes the first scientific investigation conducted in the El-Kassarat cave and Rahwe caves. It seeks to contribute a better knowledge of the paleoclimate of the Eastern Mediterranean region during the last glacial / interglacial period, by using $\delta^{18}O$ and $\delta^{13}C$ isotopic signatures from two altitudinal different stalagmites. El-Kassarat cave has developed near the coast, while Rahwe cave is located at an elevation of over 2000m.

It is important to undertake such studies in Lebanon because, owing to its location, it is affected by major climatic systems from Africa, Asia and Europe. It is also a crossroads of major human societies throughout history. Understanding the paleoclimate can help explain the course of climate induced social migrations.

16

This study will attempt to correlate the records between two stalagmites; one taken from a coastal (El-Kassarat) and the other from a high elevation (Rahwe) cave. The comparison of the isotopic records of the speleothems from both caves allows for the testing of whether the cave records show similar paleoclimate signals or each cave records different local climatic variations.

CHAPTER 2

METHODS

2.1 Uranium-Thorium Dating

Radiogenic dating techniques are used to constrain the age of speleothems. The most widely applicable radiometric technique is ^{230}Th - ^{234}U - ^{238}U disequilibrium dating, which can be used between a few hundred years (limited by determination of ^{230}Th) to around 500 ka (Edwards *et al.,* 1986).

Rapid technological advancement during the last 20 years, from alpha-spectometry to Thermal Ionization Mass Spectrometry (TIMS) to Multi-Collector Inductively Coupled Plasma Mass Spectrometry (MC-ICPMS) dramatically increased the resolution and the precision of this dating system. The sample size decreased from 10 - 100 grams (α-spectrometry) to 10 - 500 mg (TIMS and MC-ICPMS), with the precision (2σ) in the ^{230}Th analyses improved from 2 - 10% to 0.1 - 0.4% (Fairchild *et al.*, 2006b).

The common uranium isotope, ^{238}U, undergoes a long and complicated decay chain before reaching the stable isotope ^{206}Pb. Along that chain of mostly short-lived intermediates are two long-lived isotopes, ^{234}U (half- life 5,248,000 years) and ^{230}Th (half-life 575,200 years). Measurement of the ratio of ^{234}U/^{238}U and ^{230}Th/^{234}U, assuming no thorium in the initial sample, allows the calculation of the age (White, 2007).

Both Uranium and Thorium have 4^+ valence states, which produce compounds that are highly insoluble. Uranium has also a 6^+ valence state, which usually appears as the Uranyl (UO_2^{2+}) ion, while Thorium does not have it. The Uranyl ion further complexes in carbonate waters, and becomes highly mobile (Langmuir, 1997). Uranium is relatively soluble, whereas thorium is insoluble. Since stalagmites form from groundwater degassing, very little thorium is present. As a result, speleothems often contain tens to hundreds of ppm Uranium but no Thorium. The radiogenic Thorium that accumulates in the calcite is a direct measure of the time elapsed since the calcite was deposited (White, 2007).

Speleothems are barely affected by erosion or other post-depositional processes. Moreover, because of the generally closed system conditions for the U/Th system, they can be precisely dated back (Plagnes *et al.*, 2002).

2.2   Stable isotopes

2.2.1   Concept of stable isotopes

The oxygen isotope time series has been used to interpret palaeoclimates (*e.g.* Hendy and Wilson,1968; Thompson *et al.*, 1974; Gascoyne *et al.*, 1980; Schwarcz,1986).

Stable isotopes are considered powerful tools in palaeoclimatology because strong links exist between some meteorological parameters, such as surface air temperature (Emiliani, 1955) or the amount of rainfall. Based on this link, there have been many

attempts to reconstruct past climatic conditions from records of the isotopic composition via proxies from various environmental archives (Darling, 2011).

Emiliani (1955) revealed that sea surface temperature decreased between 3°C and 8°C for glacial periods. He also established the fluctuating nature of paleoclimate variations in geological archives.

The Quaternary Period (from 2.6 million years to today), encompassing the Holocene and Pleistocene Epochs, was strongly influenced by bipolar glaciation (Gradstein *et al*., 2012). Paleoenvironmental changes throughout the Plistocene and Holocene Epochs, appear as isotopic changes in speleothems' laminae.

The changes in isotopic composition of precipitation in the speleothem may vary due to the extent of permafrost or glaciers, seasonal fluctuations, changes in local weather patterns, decrease in soil pCO_2, changes in water availability, and corresponding sources for precipitation (*e.g.* Spötl *et al.*, 2002).

Isotopes are atoms whose nuclei contain the same number of protons but a different number of neutrons. The term 'isotope' is derived from the Greek *iso* meaning equal, and *topos* meaning place. Isotopes have similar charges to the original atoms but different masses because of the difference in their number of neutrons.

The partitioning of isotopes into two substances, or the same substance with different isotopic ratios, is called isotopic fractionation (Hoefs, 1997). Mass differences are large enough to 'fractionate' or change the relative proportions of various isotopes.

Two different types of processes - equilibrium and kinetic isotope effects - cause isotopic fractionation. At equilibrium, the forward and backward reaction rates of fractionation, in any particular isotope, are identical. In kinetic equilibrium, the forward and backward reaction rates of fractionation are not identical, and the reactions may be unidirectional if the reaction products become physically isolated from the reactants. Processes like evaporation, diffusion or photosynthesis can cause kinetic fractionation.

As a consequence of the fractionation processes, waters and solutes often develop unique isotopic compositions that may indicate either their source or the processes that formed them (Kendall *et al.*, 1998).

Air cave temperature can remain constant during the year and this value is similar to the mean annual temperature above the cave. Humidity levels in caves tend to be very high, limiting the evaporation of dripwater, which would affect the fractionation of the isotopes that precipitate as the speleothem after degassing.

It is common practice to express isotopic composition in δ values, calculated by:

$\delta = (R_{sample}/R_{standard} - 1)1000$ ‰

Where: R_{sample} is the isotopic ratio of the samples

$R_{standard}$ is the corresponding ratio of the standard

The ratio of Oxygen-18 to Oxygen-16, relative to a standard, is known as $\delta^{18}O$. When the sample is more enriched in the heavy isotope than the standard it has a more positive δ value; and when it is more depleted and has a more negative δ value.

The relationship between oxygen and hydrogen isotope ratios in the hydrological cycle is governed by the fractionation processes associated with evaporation and precipitation. Using data from a global survey of precipitation, continental runoff and polar meltwater, Craig (1961) defined a Global Meteoric Water Line (GMWL) as:

$\delta D = 8\delta^{18}O + 10$

where δD and $\delta^{18}O$ are the ratios of $^2D/^1H$ and $^{18}O/^{16}O$, expressed as a per mil (‰) deviation from the international Vienna Standard Mean Ocean Water (VSMOW) reference standard, from the International Atomic Energy Agency in 1968.

2.2.2 *Oxygen isotopes*

2.2.2.1 <u>Oxygen and Hydrogen isotopes in water</u>

Oxygen has three naturally occurring stable isotopes ^{16}O, ^{17}O and ^{18}O. In water, the stable isotopes of oxygen are ^{16}O and ^{18}O, and those of hydrogen are ^1H and ^2H or Deuterium (D) and a radioactive isotope ^3H (Tritium, T).

99.765% of all oxygen atoms on earth are made up of ^{16}O. Changes in phases cause fractionation between both heavier ^{18}O and lighter isotope ^{16}O to occur. There is a relationship between rainfall ^{18}O signature, groundwater and surface water. The oxygen and hydrogen isotopes in water are measured using the Standard Mean Ocean Water, SMOW, where $\delta^{18}O$ and δ^2H (or δD) is 0‰ (Craig, 1961).

The use of D/H ratios as a proxy for the $\delta^{18}O$ of water is based on the correlation of the isotopic systems of meteoric waters. Worldwide, this is represented by the Global

Meteoric Water Line, MWL, relationship: $\delta D = 8\delta^{18}O + 10$ (Craig, 1961). The intercept

for the MWL is different for different regions. In the Eastern Mediterranean, the

intercept (deuterium excess parameter – d excess: defined as the difference $\delta^2 H - \delta^{18}O$) is

higher than 10 because evaporation processes at the sea-surface occur into low-humidity

air masses of continental origin (Saad, 2004). Gat and Carmi (1987) indicated that the

oxygen-hydrogen isotope relationship in the eastern Mediterranean is better expressed

by the Mediterranean Meteoric Water Line ($\delta D = 8\delta^{18}O + 22$). Years, with the highest

amount of precipitation, are usually the most depleted in $\delta^{18}O$ and δD.

$\delta^{18}O$ data in speleothems are determined by the isotopic composition of cave

dripwater, which in turn is dependent on the isotopic composition of rain (or snowmelt).

Climatic effects influence $\delta^{18}O$ in precipitation; these include temperature, seasonality,

and the origin and quantity of precipitation (Lachniet, 2009a). The empirical, inverse

relationship between rainfall amount and rainfall $\delta^{18}O$ is called the "amount effect"

(Rozanski *et al.*, 1993).

In Lebanon, the isotopic composition of rainwater is influenced by three main air

mass trajectories: one originates from Eastern Europe (humid and cold), another

originating from the Mediterranean Sea (warm and rainy), and the third made by warm

winds passing from the desert (Saad, 2005).

The topographic feature of the country induces a high altitude effect on the isotopic

fractionation in precipitation. In the Lebanon and Anti-Lebanon mountains ranges, the

average temperatures are lower than in the coastal areas, thus precipitation will be

isotopically depleted in the heavy isotope. The stable isotope composition of precipitation in Lebanon shows the Lebanese Meteoric Water Line (LMWL) defined by the following equation:

$$\delta D = 7.13\delta^{18}O + 15.98 \qquad \text{(Saad, 2005)}$$

The Regional Meteoric Water Line (RMWL), as estimated for data collected from Syria and Jordan is expressed using the following equation:

$$\delta D = 7.8\ \delta18O + 19.25 \qquad \text{(Saad, 2005)}$$

The calculated δD for LMWL (15.98) was found to be lower than the δD for RMWL (19.25) indicating a relatively less pronounced evaporation effect in Lebanon. In fact, the δD varies significantly depending on the temperature and the humidity at the vapor source region (Saad, 2005).

In Lebanon, the altitude effect varies from -0.1 to -0.23‰/100 m for $\delta^{18}O$, attributed to air masses of different origin and different degrees of rainout contributing to the formation of precipitation (Gourcy et al., 2004).

$\delta^{18}O$ variations are partly controlled by the change of season (rainy/dry) and partly by the annual amount of concurrent rainfall. The lowest $\delta^{18}O$ waters enter the cave during the rainy winter months, whereas evaporation in the epikarst zone during the dry summer causes these waters to become heavier (Bar-Matthews et al., 1996).

The higher salinity and water density in the Levantine Basin result in an increase in sea surface $\delta^{18}O$ values relative to the western Mediterranean (Pierre, 1999). This sharp

W–E gradient reflects strong evaporation of the incoming Atlantic Surface water flowing eastward (Almogi-Labin *et al.*, 2009).

During wet periods, ^{18}O values are depleted, and during dry periods enriched. The locality is an important factor as latitude affects the amount of precipitation.

Absolute changes in mean annual temperature cannot be entirely deduced because various effects can influence the isotope composition of dripwater and thus the precipitated cave carbonate (McDermott, 2004).

Significant evaporation in the vadose zone would increase both D/H and $^{18}O/^{16}O$ in groundwater, and would shift the dripwater compositions away from and below the MMWL. Some workers suggest that rapid outgassing of CO_2 from dripwater - a process that can cause non-equilibrium, kinetic fractionation (vapour-diffusion fractionation) of oxygen (and carbon) isotopes - is an important, and often overlooked, element of speleothem formation (Mickler *et al.,* 2006).

2.2.2.2   <u>Oxygen isotope in speleothem</u>

Calcite's oxygen and carbon isotopes are measured against the Pee-Dee Belemnite standard (Craig, 1957), a belemnite from the Pee-Dee Formation in South Carolina. This belemnite is now exhausted and the VPDB (Vienna Pee-Dee Belemnite) is used.

The oxygen isotopic composition of inorganic calcium carbonate deposited in isotopic equilibrium with the precipitating fluid depends on:

(1) The ^{18}O of the precipitating fluid;

(2) The oxygen fractionation between water and calcium carbonate, which is

controlled by the precipitation temperature (Verheyden, 2001).

The oxygen isotopic composition of calcium carbonate, $\delta^{18}O_c$, formed in isotopic

equilibrium with a water of fixed composition, $\delta^{18}O_{water}$, decreases with increasing

temperature. However, it is now recognized that changes in the water composition form

the main agent for change in $\delta^{18}O_{calcite}$ over time (*e.g.* McGarry *et al.*, 2004).

Evaporative processes in semi-arid/arid regions modify groundwaters in the vadose

zone, before reaching the point of speleothem formation. The interpretation of $\delta^{18}O$

records depends on the assumption that the carbonate has been precipitated in isotopic

equilibrium with cave drip-water throughout the interval of study (Hendy, 1971;

McDermott, 2004).

One way to test for disequilibrium processes is by comparing contemporaneous

$\delta^{18}O$ records of multiple speleothems from the same cave. Dorale (2002) called this the

'replication test' and concluded that a positive correlation between such records strongly

suggested that vadose zone and kinetic disequilibrium processes were not significant.

Dorale (2002) argued that by passing a replication test, a speleothem $\delta^{18}O$ record could

be considered a primary environmental record (Orland *et al.,* 2009). But the main test

used by most researchers to check for isotopic equilibrium is the Hendy test (Hendy,

1971) where the lack of correlation between $\delta^{18}O$ and $\delta^{13}C$ indicate that the speleothems

formed in isotopic equilibrium. In order for $\delta^{18}O$ calcite values of speleothems to be a

reliable record of paleoclimate conditions, the calcite needs to form under isotopic

26

equilibrium. There are two processes that might affect the process of isotopic equilibrium; the evaporation of groundwater in the vadose zone, and the rapid degassing of CO_2 from dripwaters.

2.2.3 Carbon isotopes in speleothem

Carbon has two stable isotopes, ^{12}C and ^{13}C and a radioactive isotope, ^{14}C. The half-life of ^{14}C is 5730 ±40 years (Leng, 2006).

Shifts in $\delta^{13}C$ in stalagmites are linked to changes in soil CO_2, and is mainly controlled by the degree of geographic extent of C3 and C4 vegetation (Robinson, 2006). During photosynthesis in plants, carbon isotopes will fractionate depending on the photosynthetic pathway used (O'Leary, 1981). The C3 pathway (Calvin cycle) fixates carbon using the enzyme rubisco, where it reacts with one CO_2 molecule to produce 2 molecules of 3-phosphogluceric acid. C3 plants include grasses, shrubs, trees and herbs, have $\delta^{13}C$ values that reach ≈ -25 to -32‰ PDB (Hoefs, 1997).

In the C4 pathway (Hatch-slack cycle) an acid of 4 carbon atoms is produced (Hoefs, 1997). Much smaller fractionation results from this pathway and C4 plants values range from ≈ -10‰ to -16‰ because they are adapted to water stressed conditions and high light (Cerling and Quade, 1993).

Carbon isotope ratios in speleothems usually reflect the balance between isotopically light biogenic carbon derived from the soil CO_2 and heavier carbon dissolved from the limestone bedrock (Leng, 2006). Changes in $\delta^{13}C$ values of

27

speleothem calcite have been inferred to reflect changes in vegetation (quantity and type) above the cave as well as in the catchment area. Differences between C3 and C4 vegetation, deduced from the quantity of rainfall, can be ascertained using $\delta^{13}C$ values (*e.g.* Bar–Matthews *et al.*, 1997; Frumkin *et al.*, 2000).

A high $\delta^{13}C$ value can indicate a period of rapid percolation of water, with little interaction between the water and the soil CO_2. If this is the primary factor responsible for elevated $\delta^{13}C$, then they should be associated with wetter periods. If seasonal evaporation of water in the unsaturated zone or within the cave itself is the dominant process, then high $\delta^{13}C$ should be associated with drier periods (Leng, 2006). To avoid this kind of ambiguity, results should be correlated with other proxies.

Strongly correlated carbon isotope and Mg/Ca ratios may point to a role for partial degassing of cave dripwaters and calcite precipitation in the hydrological flowpath above the cave that could produce elevated $\delta^{13}C$ values unrelated to changes in vegetation type or intensity (Leng, 2006).

2.2.4   *Trace element variations*

Trace element ratios of stalagmite calcite are used to reconstruct paleohydrology, paleorainfall, and potentially paleo-bioproductivity of soils (Baldini, 2010).

There are various sources for trace elements' incorporation in stalagmite laminae. These include aeolian particles; dry and wet atmospheric deposition; bedrock type; superficial sediment deposits; inorganic soil constituents; and elements recycled by soil

biota (Fairchild *et al.,* 2009). During colder and dryer periods, higher trace element concentrations reflect an increase in exogenic sources, such as sea spray and aeolian dusts, with a reduced contribution of weathering from the host (Verheyden *et al.,* 2004). Ayalon (1999) showed that changes in the influence of weathering, and changes in rainfall intensity explained changes in the Sr and Ba content of speleothems.

Drier and possibly warmer conditions are signified by elevated Mg, Sr, and Ba values. Variations in Mg, Sr, Ba ratios may be due to changes in the groundwaters' residence time (Fairchild *et al.,* 2006). When residence times are shorter due to higher rainfall rates, less limestone bedrock is being dissolved in the epikarst and so Sr/Ca ratios decreases. This manifests itself in dripwater rates. Fast drips can record heavy rainfall events by an increase in the drip rate and a negative peak in conductivity (Borsato, 1997).

Gascoyne (1992) and Fairchild (2009) showed that Mg concentrations in calcite is temperature dependent. Therefore, changes in the Mg content of a speleothem can be used to reconstruct air surface temperature changes, since in most shallow caves, the calcite precipitation temperature or cave temperature is an annual mean of the surface air temperature (Verheyden *et al.,* 2004). Bar-Matthews (1991) stated that the enrichment of Soreq cave waters in Mg^{2+} was due to prior low-Mg calcite precipitation from the cave waters, which are consequently enriched in Mg^{2+}. Fairchild (2009) cautioned, when dealing with Mg concentrations as a climate proxy for rainfall, because of the many parameters that can affect the values which include changes in dripwater,

29

marine input, dissolution, and re-routing of fluid causing mixing with other fluids or rock with a different Mg concentration.

High Sr/Ca and Ba/Ca ratios reflect longer residence times in the epikarst (Verheyden *et al.,* 2000) while high values in Mg/Ca are consistent with enriched $\delta^{18}O$ calcite. Both of these may be indicative of increased rainfall. Fe/Ca vary with high ratios possibly indicate increased soil redox potential. Positive correlations between Mg, Sr, Ba concentrations and changes in the $\delta^{13}C$ imply that similar processes influence their concentration changes (Verheyden, 2004).

Sr and Ba concentrations often have similar processes that control their concentrations. Temperature rise, warming soils and an increase in vegetation and soil biological activity affect Ba, and Sr concentrations (Hellstrom and McCulloch, 2000). Variations in Sr concentrations can also be controlled by calcite dissolution/precipitation processes in the epikarst, due to residence times, and these are reflected by rainfall rates (Fairchild *et al.,* 2000). In semi-arid regions, significant Sr changes can be due to the deposition of terrestrial dust above the cave surface (Goede *et al*., 1998). A sharp drop in the concentrations of Sr and Ba reflect enhanced weathering of the host-rock (Ayalon *et al.,* 1999).

The mixing of waters in the epikarst can overprint climatic signals due to the particular geology of the area (Verheyden, 2004) and this decreases the degree of correlation between the climatic changes and the isotopic values in the speleothem. The type of bedrock, the type of geological structures and fracturing (diffused or conduit

flow paths), type of soils, are all parameters that should be studied when isotopic values in the speleothem are measured.

2.2.5 *Petrography and microscopy*

Factors that control the morphology and fabric of calcite crystals of the speleothem include growth processes, discharge rates, fluid supersaturation, outgassing, the presence of growth inhibitors in the solution, and the mechanisms of transport of ions from the solution to the crystal surface and temperature (Frisia *et al.,* 2000).

There are four types of annual laminae found within speleothems: fluorescent laminae, formed by annual variations in organic matter flux; visible or petrographic laminae, formed by annual variations in calcite texture or fabric; calcite-aragonite couplets; and finally trace element laminae (Baker *et al.,* 2008).

Visible laminae are more abundant than fluorescent ones because of the many varied processes responsible for their formation. These processes include seasonal variations in drip rate, seasonal variations in drip water supersaturation, and/or cave climatology (*e.g.* relative humidity, pCO_2, cave surface temperature, and pH of the film of fluid wetting the speleothems (Frisia *et al.,* 2003).

Fluid inclusions can be formed when crystals coalesce and leave occasional fluid inclusions elongate parallel to the crystal boundaries (Fairchild and Baker, 2012).

Speleothem luminescent banding is different from the visible banding and is due to the inclusion of organic material in the crystal lattice during its growth, where organic

31

substances can be observed from their fluorescence under UV excitation (Baker *et al.,*
1997).

CHAPTER 3

SETTING OF THE STUDY SITES

3.1   Regional setting

Lebanon's morphology is shaped by the development of the Dead Sea Transform Fault in the Miocene epoch (Tortonian age, about five to ten million years ago) forming a restraining bend in Lebanon (Walley, 1998) (Figure 2). Compressional stresses formed two mountainous ranges; the anticlinoriums of Mount Lebanon and Anti-Lebanon, consisting mainly of carbonate rocks. Between these two ranges lies the syncline of the Bekaa Valley, consisting mainly of Quaternary and Eocene deposits (Walley, 1998).
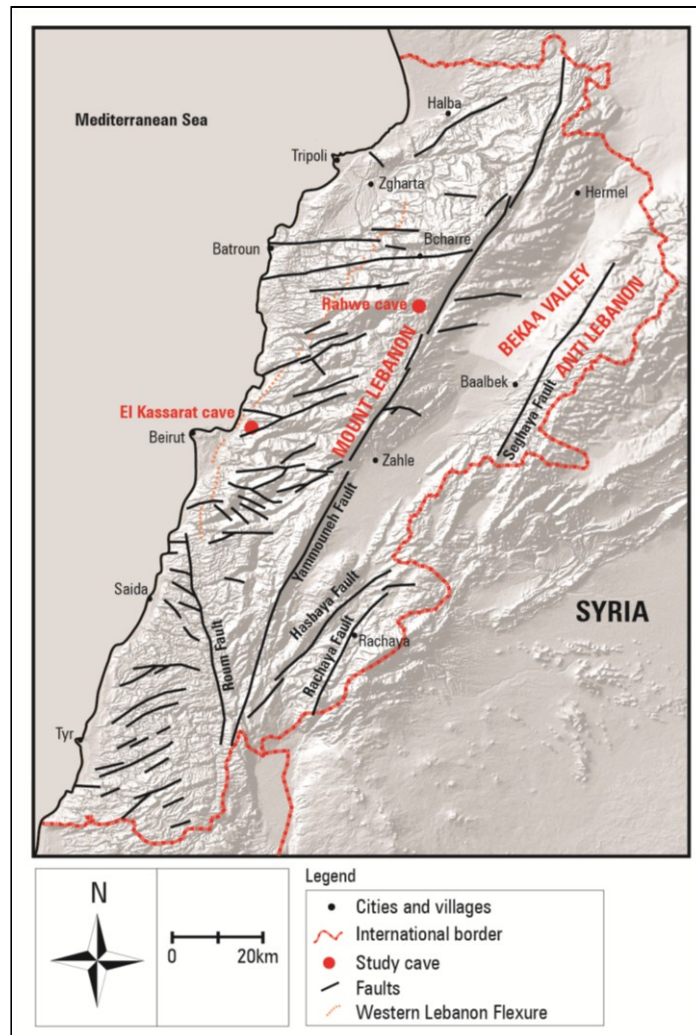
Figure 2. Simplified structural and topographic map of Lebanon, showing the location of the two investigated caves (modified from Walley, 1998)

Lebanon has a narrow coastal plain, and is about 250 km in length. It ranges 10 km to 60 km in width, with elevations up to about 250 m. The Lebanon Mountain Range rises to over 3,085 m at its highest point at Qornet el Saouda. The Bekaa plain, at an elevation of nearly 800 m, lies between the Lebanon and the Anti-Lebanon Mountain Ranges, and consists of agricultural land. The Anti-Lebanon Range rises to about 2,814

m at its highest point, Jabal el Sheikh. More than 65% of the surface area of Lebanon consists of fractured, highly karstic, carbonate rocks (Figure 3).
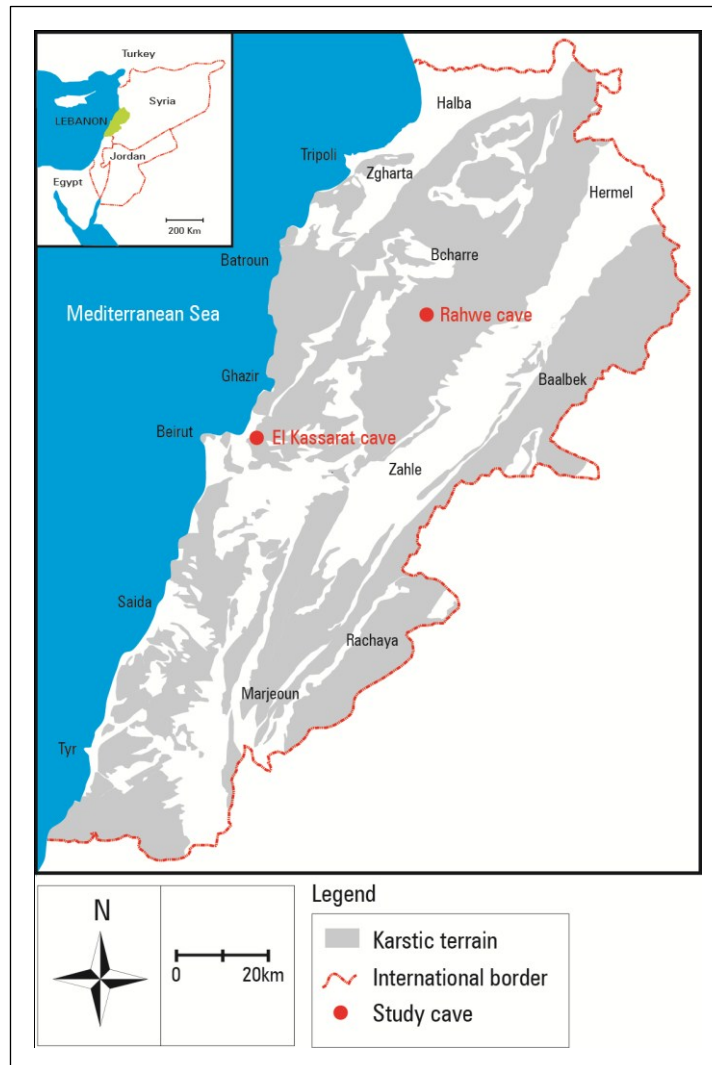
Figure 3. The extent of karstified terrain in Lebanon (Dubertret, 1955).

There are two major water aquifers in Lebanon. These are the Middle Jurassic Keserouane and the Cretaceous Sannine Formations, which are karstic indicating

emergence (subaerial exposure) over geological times. The El-Kassarat and the Rahwe caves have developed in the Keserouane and the Sannine Formations respectively.

The uplift of the carbonate platforms from beneath the sea due to tectonic activities has occurred several times in the geological history of Lebanon (Walley, 1998). Uplift began during the Turonian. The major uplift event occurred at the end of the Eocene resulting in widespread erosion during the Oligocene. Uplift also occurred during the Miocene (Walley, 1998).

The Levant region consists of contrasting climates which change from region to region depending on the topographic structures present. Lebanon's mountain ranges have a higher precipitation rate than the surrounding Levant countries, allowing for more vegetation and less desert areas. This makes it relatively unique as the mountain ranges are close to the coast.

3.1.1   *Climatic and Environmental Setting*

The Levant basin constitutes a climatic transitional region between the European and the African continents. The Levantine region spans the arid/semi-arid boundary and is therefore highly sensitive to climatic changes (Robinson *et al.*, 2006).

3.1.1.1   Regional climate

Modern rainfall in the Levant region is controlled by the Mediterranean Sea. Cold air masses from European or Atlantic sources, known as the Westerlies, sweep across

the Mediterranean and gain moisture while moving over the warmer sea waters. Changes in the NS precipitation gradient are linked to changes in air mass trajectories associated with sea-level pressure and sea surface temperature (SST) anomalies, which are in turn related to the upper-level (500 mbar) pressure pattern over the Mediterranean Sea (Develle *et al.*, 2011). The Mediterranean Sea's only connection to the Atlantic Ocean is via the Gibraltar Straits, causing the waters' conditions, from west to east, to be more saline and have a higher temperature. Climate in the Levant can also be influenced by the African Monsoon, moving in from Africa. The desert belt, which has shifted in a N-S direction throughout geological times, could be archived in the speleothem record.

3.1.1.2   Climate in Lebanon

The climate in Lebanon is semi-arid and consists of dry summers and relatively cold and humid winters. The average yearly temperature is approximately 15°C (LMS, 1977). The average annual precipitation on the coast of Lebanon is approximately

600 mm/yr, and about 1,200 mm/yr in mountainous regions, between November and March (LMS, 1977) (Figure 4). This precipitation provides the (acidic) waters circulating through the joints of the rocks which, over time, etch the caves.

Snow falls mainly above 1,500 m between December and February. The highest summit in Lebanon, Qornet el Saouda, at a height of 3,083 m, is below the present snowline which currently lies at about 3,700 m (Kurter, 1988). Mount Lebanon, which

comprises the mountain peaks just east of the Antelias Valley, creates an orographic effect resulting in most of the precipitation occurring on the western side of the mountain chain (Atlas Climatique du Liban, 1977). Rainfall and temperature gradients in Lebanon result in zones made up of specific vegetation from forests and woodlands to open plains (Abi-Saleh and Safi, 1988). The western slopes of Mount Lebanon mark climatic transitions as altitude increases, from Mediterranean belts with warm to more moderate climate, to subalpine belts consisting of conifer forests, Mediterranean oaks and junipers up to the treeline (Gasse *et al.,* 2011).
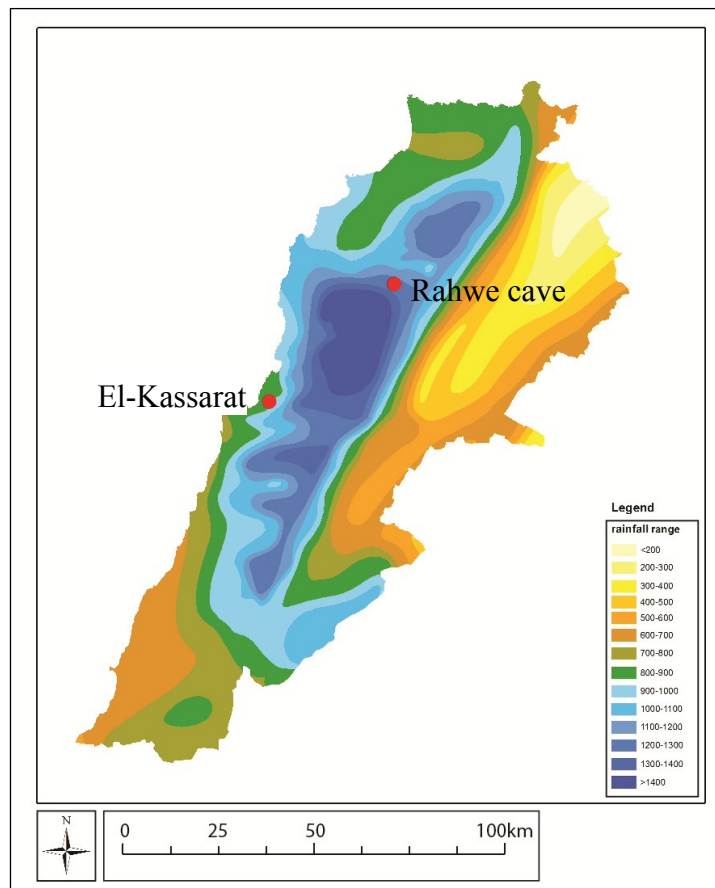
Figure 4. Precipitation rates in Lebanon (see text for explanation) (LMS, 1977).

38

The climate of the area of the El-Kassarat cave is typical of Eastern Mediterranean semi-arid conditions, with the majority of rainfall occurring during the winter months (November to March). Snow falls rarely at the El-Kassarat cave's elevation.

The climate around the area of Rahwe cave area is typical of Eastern Mediterranean mountainous conditions. Snow falls at the cave's elevation during winter months and persists until March (LMS, 1977). The snow is thick (nearly 2m) and usually completely covers the cave's entrance.

3.1.2 Isotopic variations

The high salinity and water density in the Levantine Basin result in an increase in sea surface $\delta^{18}O$ values by up to ≈1‰ relative to the western Mediterranean (Pierre, 1999).

Cold air masses from the Atlantic and northern Europe tend to propagate eastward (Develle *et al.,* 2011). Most storms occur in winter and follow the dominant direction of the westerlies (Develle *et al.,* 2011). The warmer Mediterranean Sea waters' cause these flows to become saturated with moisture. The dynamics of the Mediterranean cyclones imply the intersection of northwesterly–westerly flows with the Eastern Mediterranean coast and the mountain ridges result in rainfall events (Ziv *et al.,* 2006).

The Eastern Mediterranean basin constitutes a climate transition region between the European continent characterized by cold and dry weather and the African continent

39

characterized by hot weather. There are different air masses coming to this region. They are characterized by variable origins and several trajectories (Aouad Rizk, 2006).

The Mediterranean Sea is the major source of modern rainfall in the Eastern Mediterranean. Any changes in SST and salinity will affect rainfall. This in turn will affect the isotopic composition of the dripwaters in caves, and so consequently the isotopic composition of the speleothems. This implies that the low $\delta^{18}O$ events recorded in speleothems reflect changes in the hydrological activity due to an increase in the annual rainfall (Bar-Matthews *et al.,* 2000).

Seasonal variability of the isotopic rain signal, and particularly the deuterium excess is related to air mass trajectories and to evaporation over the Mediterranean Sea (Figure 5). Figure 5 shows that in: Trajectory 1 the air masses originating from East Europe reach Lebanon having crossed the "Anatolian Plateau", Turkey, Cyprus and a small distance over the Mediterranean Sea; Trajectory 2/3; Air masses coming from West Europe reach Lebanon by travelling across Italy, then the Mediterranean sea (Lebanon coast approach is from West), or by crossing the Mediterranean sea and then travelling along the North African coast (Lebanon coast approach is from South West). Trajectory 4; Air masses with an Atlantic origin enter from the West side of the Mediterranean Sea and travel along it before reaching the mount Lebanon. Usually these air masses are subjected to low pressure areas at the feet of Italy or over the triangle Turkey, Cyprus and Crete. (Aouad *et al.,* 2005). Also the isotopic content of the

snow cover does not strongly respond to sublimation, evaporation or melting-freezing

phenomena (Aouad *et al*, 2004).
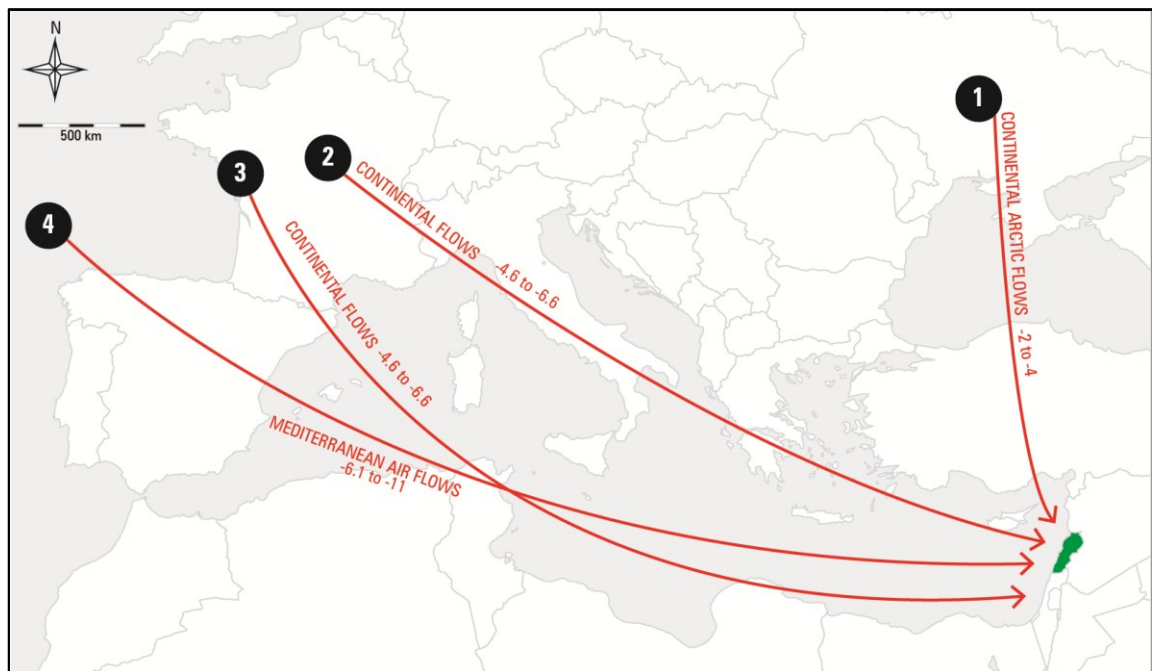
Figure 5. Trajectories of air masses that have produced rains over the western flank of Mount Lebanon during the winters 2001-2003, and corresponding δ^{18}O isotopic composition of precipitation close to Beirut (modified from Aouad, 2005).

The topography of Lebanon, with two SW-NE trending mountain ranges,

influences the isotopic composition of precipitation across the country. The Lebanon

Mountain range, closer to the Mediterranean Sea, is characterized by a humid

Mediterranean climate whereas the Anti-Lebanon Mountain range, located more inland,

is characterized by a humid to a semiarid climate. Due to this topographic effect in

Lebanon, the isotopic composition of rainwater changes and coastal precipitation is

41

isotopically enriched in the heavier isotope, while the colder inner continental regions

receive isotopically depleted precipitation with seasonal differences (Saad, 2005).

This is known as an orographic precipitation effect in Lebanon, where precipitation

occurs mainly on the western flank of Mount Lebanon. After the clouds reach the top,

they slide down into the Bekaa Valley on the eastern flanks of Mount Lebanon.

Consequently, the clouds have a lower amount of humidity on the eastern flank with

less rainfall on the eastern flank of the mountain (Figure 6). This effect causes isotopic

fractionation of the rainfall with different isotopic compositions for the same rainfall

cloud depending on the altitude from which the precipitation occurs.
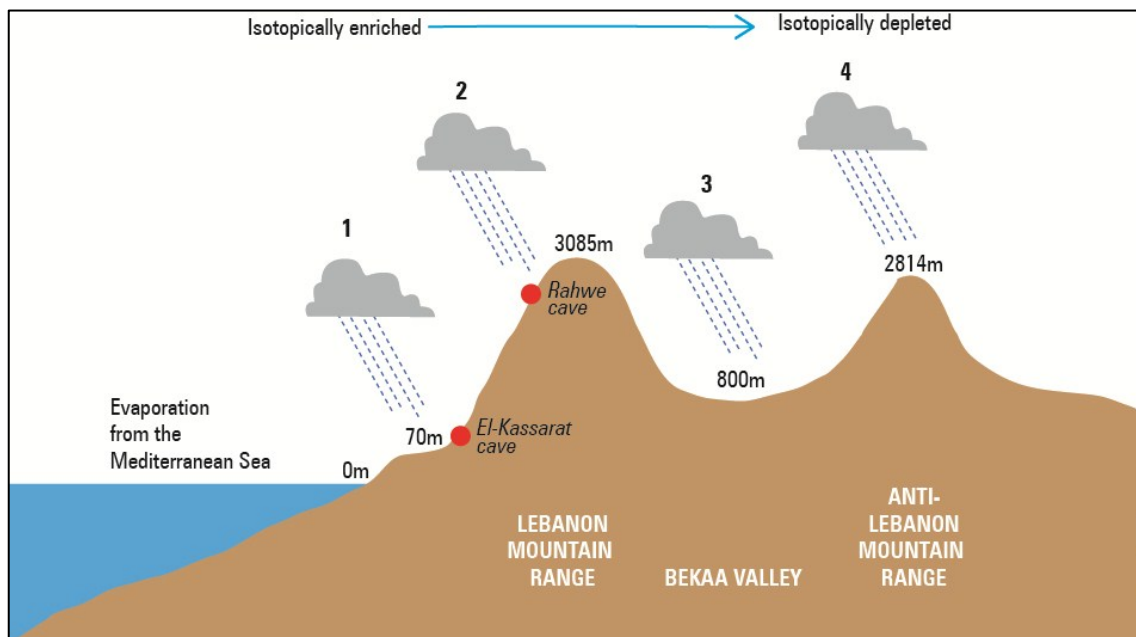
Figure 6.   Simplified model showing the isotopic depletion of rainfall over Lebanon, due to the orographic precipitation effect.

In the Levant, the oxygen and deuterium isotopic compositions of precipitation are primarily determined by the intensity of the sea-atmosphere interaction occurring, which in turn depends on the air-sea temperature differences and the duration of the interaction (Gat *et al.,* 2003).

90% of the isotopic composition of the rain waters are situated above the GMWL and show a d-excess between 10‰ and 30‰. High deuterium excess values are not only encountered along the European coast, but also when air masses originate from the Atlantic and cross North Africa (IAEA, 2005).

High d-excess values originate from cold and dry air from the continent, and from the air masses that originate from the Atlantic after crossing North Africa. It may be noted that air masses, coming from West Europe and crossing all the Mediterranean Sea, sometimes show high deuterium excess. The lack of relation between ^{18}O and d-excess and the space and time variability of the latter suggest that its interpretation is complex (IAEA, 2005).

On an annual time scale, rainfall amount, ground temperature, altitude and continentality apply controls on the mean rainfall isotopic composition (Rozanski *et al.,* 1993).

3.2 Study sites

The two studied caves are located in Lebanon, with the El-Kassarat cave being on the coast, and the Rahwe cave lying at a high elevation, in a mountainous region (Figure 7).
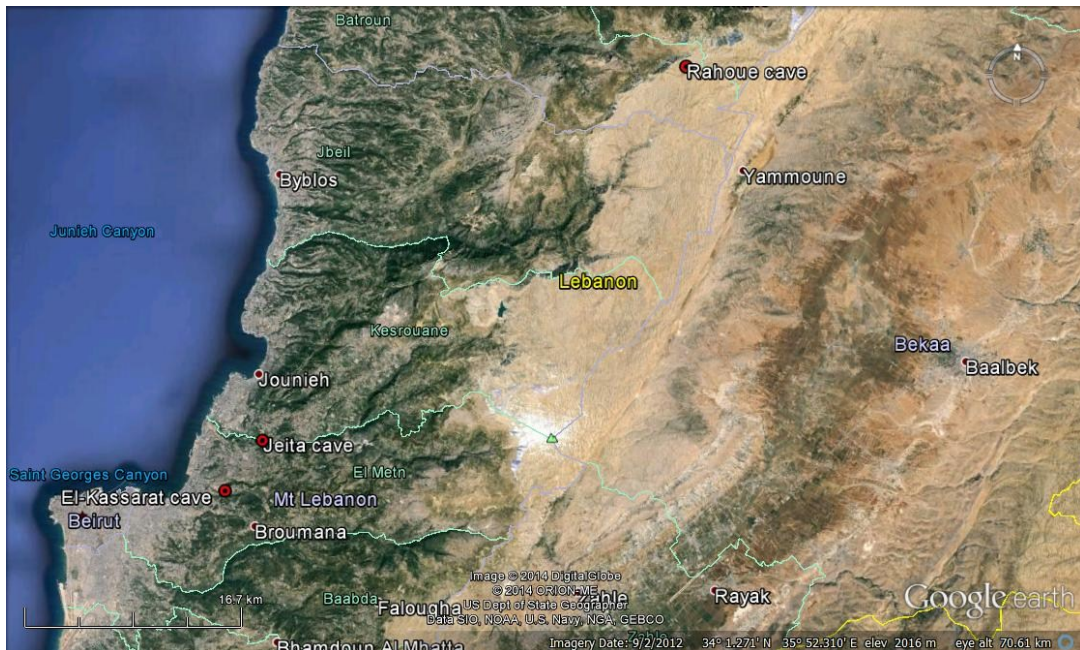
Figure 7. Map of Lebanon showing the location of the two study caves.

3.2.1 The El-Kassarat cave

The El-Kassarat cave is located in Nabay village in the coastal area of Mount Lebanon, Metn Caza, in the Antelias River Valley (Figure 8). The artificial entrance of the El-Kassarat cave is located at coordinates 33.910528° N and 35.608544°E at an elevation of approximately 85masl (Figure 9). The cave is situated between the villages

of Raboue and Bsalim from the North and South respectively, and villages of Antelias and Nabay from the East and West respectively.
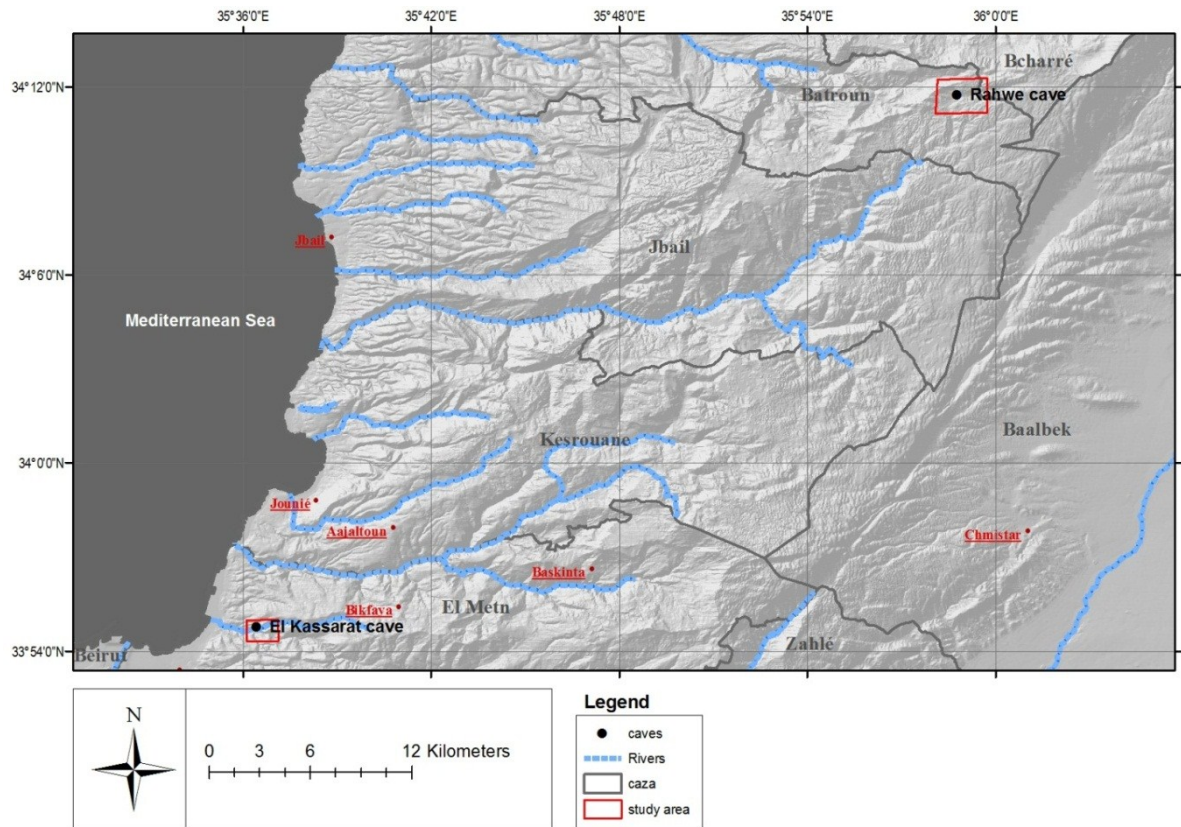
Figure 8. Topographic map of Lebanon showing the location of the two study areas (UNDP, 2013).
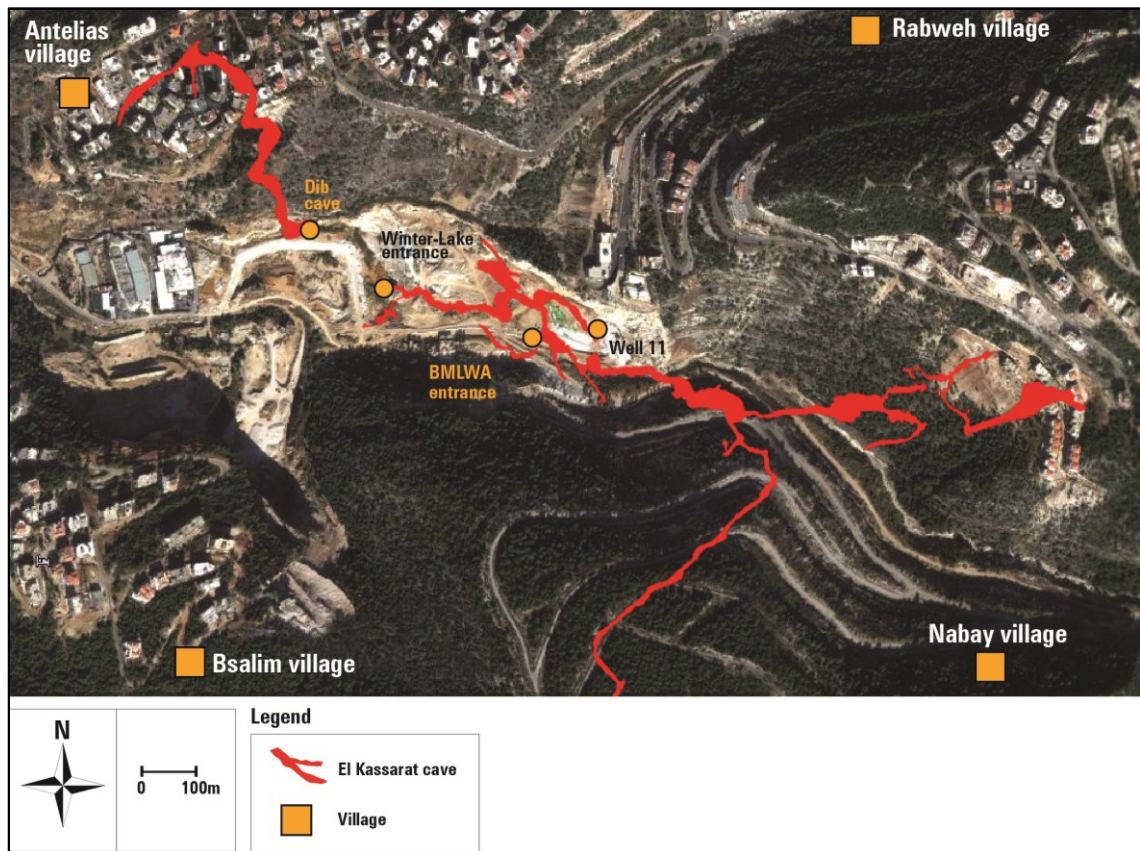
Figure 9. An image showing the location of the El-Kassarat cave and the surrounding villages. Note the cave entrances and its underground plan (from Google Earth).

It is one of a series of karstic caves situated within the Antelias valley. It is located approximately 2.7 km inland, in Jurassic-aged rocks of the Keserouane Formation.

The cave is 4,748 m long, with ceiling height reaching nearly 30 m in some locations. Thick soil pockets above the cave are distributed unevenly, and are mostly composed of terra rossa and rendsina soils.

The cave contains many speleothems containing several types of concretions ranging from flowstone, stalactites and stalagmites, helictites, 'popcorn' corals and cave

pearls (for more information on the different types of speleothems and how they are formed, refer to Hill and Forti,1997) . From Tinytags placed inside the cave, the cave air temperature averages around 17ºC, reflecting the mean annual temperature in the area. Humidity levels are around 95-100%.

3.2.1.1 <u>Cave history</u>

The El-Kassarat cave has no natural entrance. Although a cave was suspected to be located in Antelias valley (because of the large amount of water surfacing in this area in the form of springs) no cave was ever located until in 1969 when quarrying activities in Antelias valley broke a hole into the cave's ceiling, revealing the existence of the cave. Cavers from the Spéléo Club du Liban (SCL) subsequently explored the cave.

During the Lebanese civil war (1975-1990) continuous uncontrolled quarrying destroyed the cave's entrance and once again the cave became inaccessible. In 1996, work began to try to re-enter the cave. A company called the Bureau Technique pour le Development (BTD), with the aid of the SCL, conducted a study to exploit the underground river's water in order to increase the domestic water supply for Beirut and El Metn regions. Thirteen boreholes were drilled with the 11th borehole penetrating into the cave at the Forage Passage. This borehole was enlarged to allow members of the SCL to descend. Once again, after 28 years, El-Kassarat Cave was reopened with yet another artificial entrance. At the same time, another entrance was being excavated. This entrance turned out to be where the cave was destroyed by quarrying. Using

excavators, a huge amount of mud and debris was removed to open the 'winter-lake' entrance, so called because of a large lake located along its main axis. A sinkhole had also been located that could allow access of the cave in this area as well.

In 2006, the Beirut and Mount Lebanon Water Establishment (BMLWE) decided to build a dam inside the cave to exploit the underground river directly. A surge tunnel was excavated. A 5 m hole was drilled from the surface into the bedrock until the ceiling of the cave was reached. A staircase, approximately 30 m in length, was constructed from the surface through the ceiling of the cave to the underground river (Figure 10). The dam constructed at the bottom of the staircase holds back the waters of El-Kassarat cave's underground river flooding the cave passage up river in summer when the water level is low enough.

A concrete room was built over the 5 m artificial sinkhole and a nine-story staircase, 208 steps, has been built into the cave by the BMLWE. Currently, this is the only entrance to the cave since Well 11 has been blocked by river sediments and rocks from the surface, and the 'winter-lake' entrance has been completely clogged with mud and construction debris effectively also closing the sinkhole entrance.

Figure 10. The BMLWA staircase inside the cave.

3.2.1.2 <u>Cave description</u>

The main axis tunnel of El-Kassarat cave trends in an approximate E-W direction for nearly 650 m (App. 1). The cave is mostly horizontal, probably formed in phreatic conditions, with some areas filled with fluvial sediments. The underground river of El-Kassarat cave is perennial and effectively floods every spring with the onset of snowmelt between January and April removing some of the accumulated sediments. The water rises by about 15-25 m higher than in other months. The lowest level of water inside the cave occurs in the months of July and August when no precipitation occurs.

The galleries in the cave that are extensively filled with speleothems are the 'fossil galleries'. These occur mainly about 30 m above the current underground river water level. Extending for over 600 m collectively, these galleries are dry and filled with columns, stalactites, stalagmites and flowstone. In some parts, the concretions have reached several meters in height. The Forage and Salle du President Galleries are the two main 'fossil galleries' located close to the entrance (Figure 11, App. 1). They are each about 100 m in length and consist of a single passage trending in a SE-NW direction. The studied stalagmite was removed from the Salle du President Gallery (Figure 12).

Figure 11. The entrance of the Salle du President Gallery
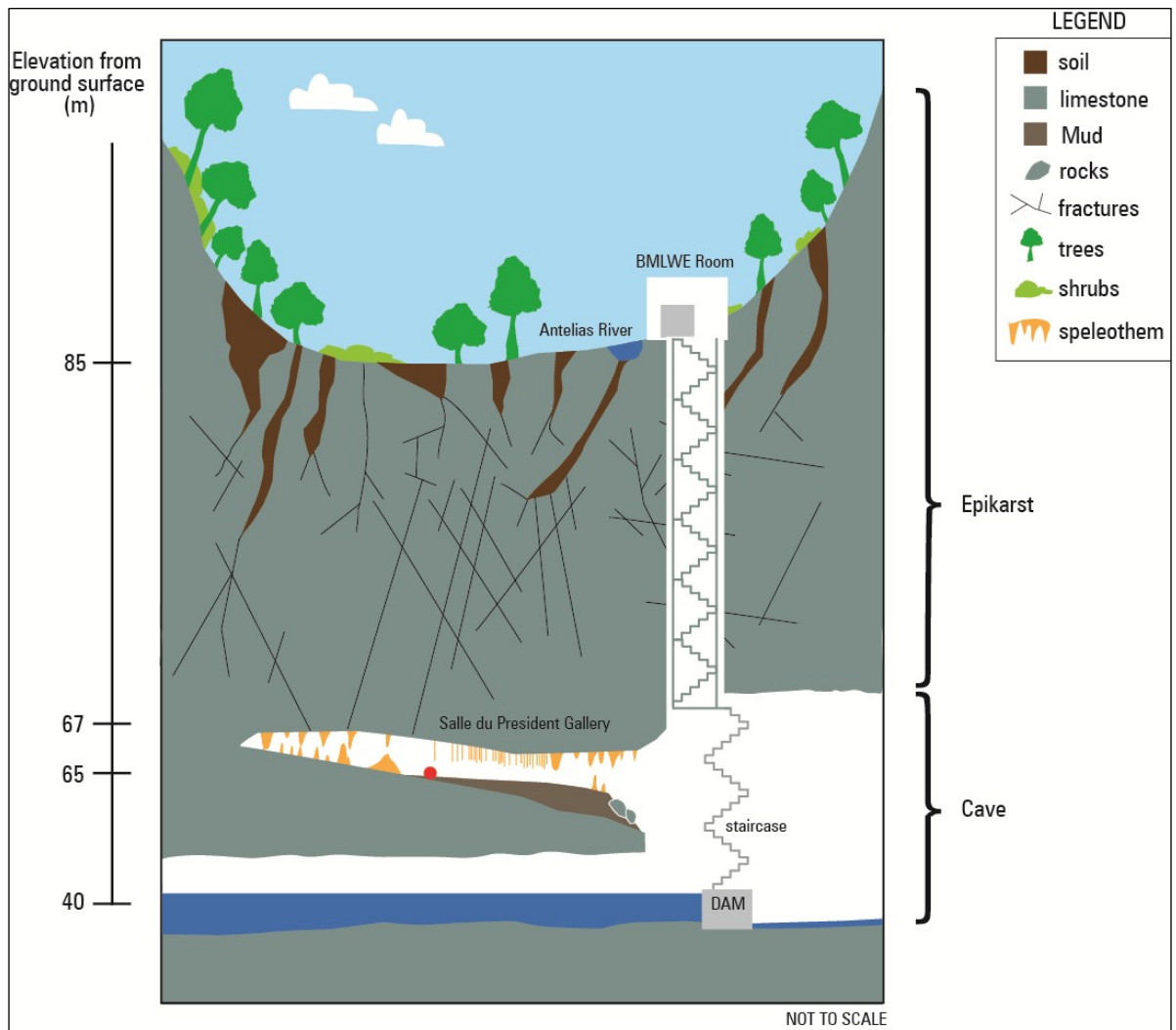
Figure 12. Diagram showing a cross-section of the El-Kassarat cave. El-Kassarat cave developed in a valley with patches of soil deposited in the karstic fracturing of the limestone rocks. The red dot is the approximate location of where the study stalagmite was removed.

3.2.1.3 Geology, geomorphology and hydrogeology

A geological map of the region around the El-Kassarat cave, at a scale of 1:15,000, was developed based on: 1) review of available maps (Dubertret 1956, geological maps of the area 1:50,000), 2) Google Earth satellite images and analysis of aerial

51

photographs, and 3) geological mapping and site visits. A cross-section was also constructed based on the El-Kassarat cave geological map.

The El-Kassarat cave lies in the quarries of Antelias, in the Antelias River Valley. It is surrounded by steep cliffs, some of which are natural and some are man-made (Figure 13).
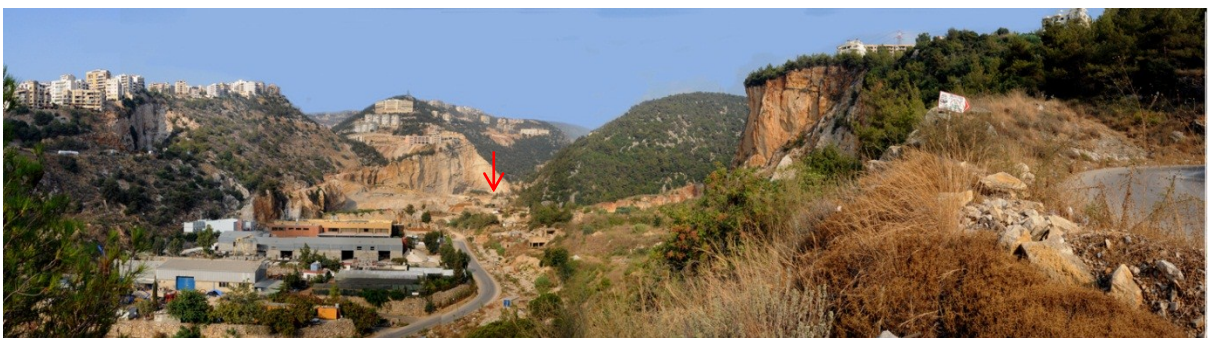
Figure 13. General view of the Antelias Quarry looking East. Arrow shows the location of the current cave entrance.

The catchment area of the surface river extends approximately 25 km^2 towards Broummana and Baabdat villages, to an elevation of approximately 700 masl (Figure 14). The El-Kassarat cave lies approximately 1 km up gradient from the Fouar spring. The underground river in the El-Kassarat cave is the main source of the Fouar Spring. The catchment area of the Fouar spring extends approximately for 280 km^2, to an elevation of approximately 1,600 masl to Tarshish and Aaintoura villages (Labaky,1998). Coloration tests in the bottom of the Qattine Azar sinkhole (-515m), in Majdel Tarchich, have shown that the groundwaters of the underground river of El-

Kassarat cave (and subsequently of Fouar Antelias spring) originate in the high

mountainous region of Majdel Tarchich (Labaky,1998).
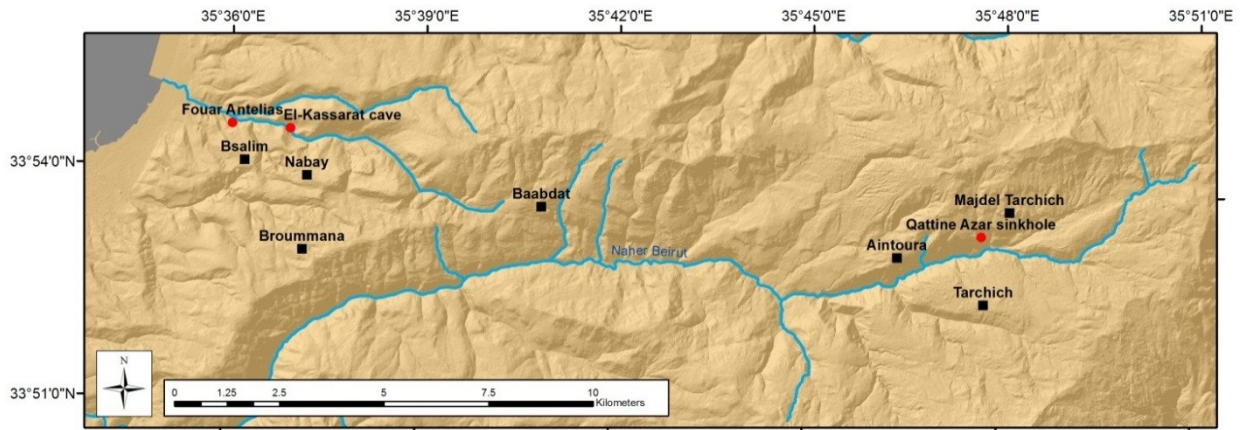
Figure 14. Map showing the approximate villages located in the catchment area of the El-Kassarat cave groundwater.

The geology of the area is characterized by the exposure of 6 different formations

dating from middle Jurassic to recent (Table 1, App. 2). The cave is formed in the lower

to middle Jurassic aged rocks, starting from 201 Ma (Hettangian age) to 164 Ma

(Callovian age) (Cohen *et al.*, 2012). The complete lithological succession and nature of

each formation is presented below. It consists mainly of massive to thickly bedded

limestone and dolomitic limestone, and is highly karstified.

53

Table 1. Lithostratigraphy of Lebanon. Highlighted in red is the formation in which the cave has been formed (modified from Walley, 1997)

PERIOD	FORMATION	LITHOLOGY	THICKNESS (m)
TERTIARY	QUATERNARY DEPOSITS	Alluvial deposits (gravel, sand, silt and clay)	20-30m
	PLIOCENE DEPOSITS	Thick conglomerates, marls and lignites. Some basalt deposits in the southwest area of the el Marj plain.	0-100m
	MIOCENE DEPOSITS	Marls, breccias, detrital clays, conglomerates, sandy silty marls, and lignites	150m
	EOCENE DEPOSITS	Nummulitic limestone, marly limestone, reefal limestone	900m
		Chalky marl, limestone with cherts	200-400m
CRETACEOUS	CHEKKA FORMATION	White chalks, and marly chalks, with cherts	100 – 500m
	MAAMELTEIN FORMATION	White grey marls, marly limestone	200 – 300m
	SANNINE FORMATION	Massive to thin bedded limestone and marly limestone – karstic	500 – 700m
	HAMMANA FORMATION	Variable sequence of thin bedded limestone, soft marls, and terrigenous sands. Creamish to greenish marly limestone. Highly fossiliferous with molded gastropods and fossilized oysters. Quartz geodes common.	170 – 200m
	MDAIREJ FORMATION	Grayish oolitic micro-crystalline and massive micritic karstic limestone	45 – 50m
	ABEIH FORMATION	Upper sections yellowish and brownish fossiliferous limestone, while lower sections intercalations of blue and green marls, and yellowish limestone	90 – 125m
	CHOUF SANDSTONE FORMATION	Often ferruginous brown to white sandstones interbedded with clays, shales, lignites, and tuffs, and locally basalts at the bottom. Cross bedded, hematitic sandstone and sands with impermeable lenses of bluish gray clay and marl with peat	200 – 230m
JURASSIC	SALIMA FORMATION	Brown yellow ferruginous oolitic limestone alternating with brown marl	0 – 45m
	BIKFAYA FORMATION	Blue gray massive oolitic hard and massive micritic limestone with chert bands and nodules	70 – 90m
	BHANNES FORMATION	Alternating ochre yellow oolitic limestone, friable brown shale and yellowish marl	70m
	KESEROUANE FORMATION	**Blue gray massive hard and massive micritic limestone**	**1000m**

El-Kassarat cave is located in the karstic limestone of the Middle-Jurassic aged Kesrouane Formation. The cave is structurally controlled and the fault observed in the Fault Gallery trends mainly in an E-W direction. This is the general direction of the cave's development.

A number of faults have been identified in the area from onsite mapping. A major strike-slip fault with a normal component, trends E-W, effectively emplacing Cretaceous rocks next to Jurassic ones in the Bsalim and Qalaat el Ousta region. This fault is part of the Nahr el-Mot fault which runs through Bsalim and Deir el Salib. The Nahr el Mot fault has a vertical displacement of approximately 500m, and a horizontal displacement of about 3 km. There are also some minor faults with a normal component and are smaller in scale.
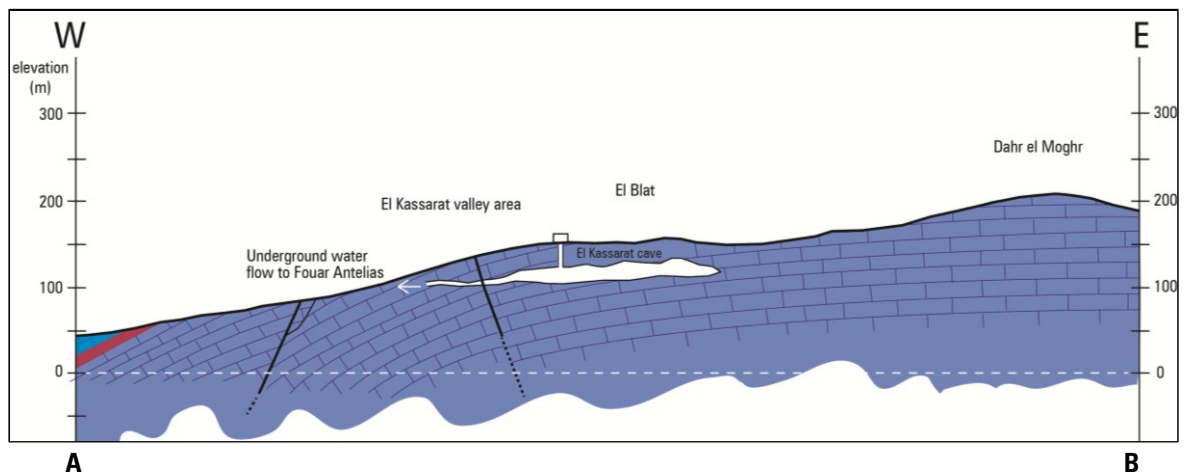
Figure 15. Cross-section of the El-Kassarat cave study area. The vertical scale has been expanded.

The bedding in the area dips towards the west. This is part of the coastal monocline of Lebanon (Figure 15). The water flowing in the cave runs towards the west until it

reaches the Bhannes Formation, which acts as the barrier of water that flows from east

to west because of the Bhannes Formation's lower permeability. Groundwater, after

reaching this barrier, banks against it and emerges as several springs in the area. The

underground river in the El-Kassarat Cave is the main source of water to the Fouar

Spring. The catchment area of the Foaur spring extends to an elevation of approximately

1,600 masl to Tarshish and Aaintoura villages (Labaky, 1998). The underground river

section runs for about 650m. When flooded, this river rises about 15 to 20m, depending

on precipitation amounts and the snow's thickness.

3.2.2   The Rahwe cave

The Rahwe cave is located in the high mountainous area of Harrisat Tannourine,

above Tannourine el-Fawka village in the Caza of Batroun. It lies on the northeastern

end of a big elongate doline, called the Sahlet Rahwe doline, (Figure 16, Figure 17).

The cave lies at the coordinates 34°11'46.66"N and 35°58'50.34"E, and at an elevation

of 2,208m. The distance of the cave to the Mediterranean Sea's shoreline is

approximately 32 km. The average groundwater temperature inside the cave is about

4.5°C, and air temperature is about 7°C. Humidity levels are around 95-100%.
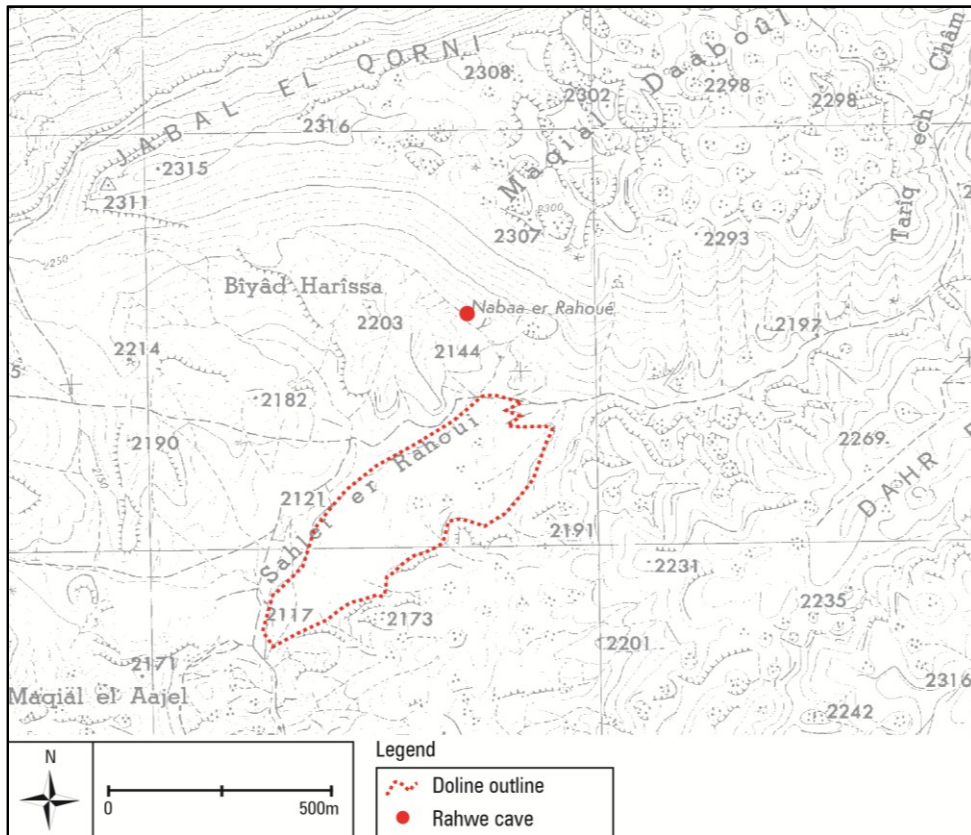
Figure 16. Topographic map showing the Sahlet Rahwe doline, and the location of the Rahwe cave (modified from the Lebanese Army topographic maps).

Figure 17. Photo of the Sahlet Rahwe doline. The location of the Rahwe cave is shown (red arrow). Photo looking Northeast.

3.2.2.1 <u>Cave history</u>

There was no natural entrance to the cave. The cave was only discovered when a project was proposed in the early sixties to provide Tannourine village with domestic water. A 45 m tunnel, perpendicular to the cave's main axis, was constructed to collect groundwater directly from the cave rather than from the Rahwe spring, whose flow was found to be too low. This tunnel led to the discovery of the Rahwe cave. Another larger tunnel was constructed in the late 1960's to increase the quantity of the water flow (Figure 18). Groundwater issuing from the Rahwe cave has been supplying Tannourine village with domestic water ever since.

Figure 18. The second artificial entrance (The Big tunnel) of the Rahwe cave (white arrow).

To date, the cave is still being mapped by members of the Speleo Club du Liban. It

currently measures 3,100 m in horizontal development. Rahwe cave is one of the

highest elevation caves in Lebanon that has been studied and explored.

3.2.2.2   <u>Cave description</u>

The cave consists of a meandering N-S trending 1 km main axis passage with an

underground river (Figure 19). The cave terminates at a terminal lake with a small tight

passage where groundwater emerges from the rocks. The stalagmite was collected from

this passage (Figure 19). Near the end of the main axis, there are some fossil galleries

trending in a general E-W direction. These passages contain speleothems with one

passage, the 'In My Lap' passage, is exceedingly filled with various types of

speleothems from rimstone dams, stalactites, stalagmites, columns, popcorn balls, and

flowstone. These passages have no running underground water flow but do have filled

water pools. The ceiling height in the cave varies from about 15 m along the main axis,

to 1.5 m in the E-W passages.
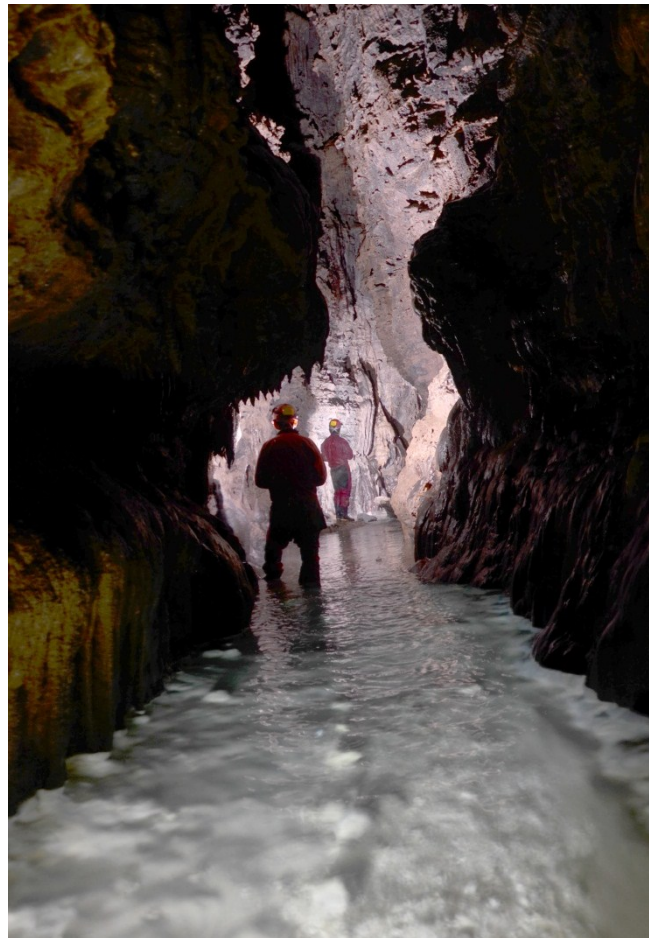
Figure 19. A general view of the main passage of the Rahwe cave with the perennial underground river.
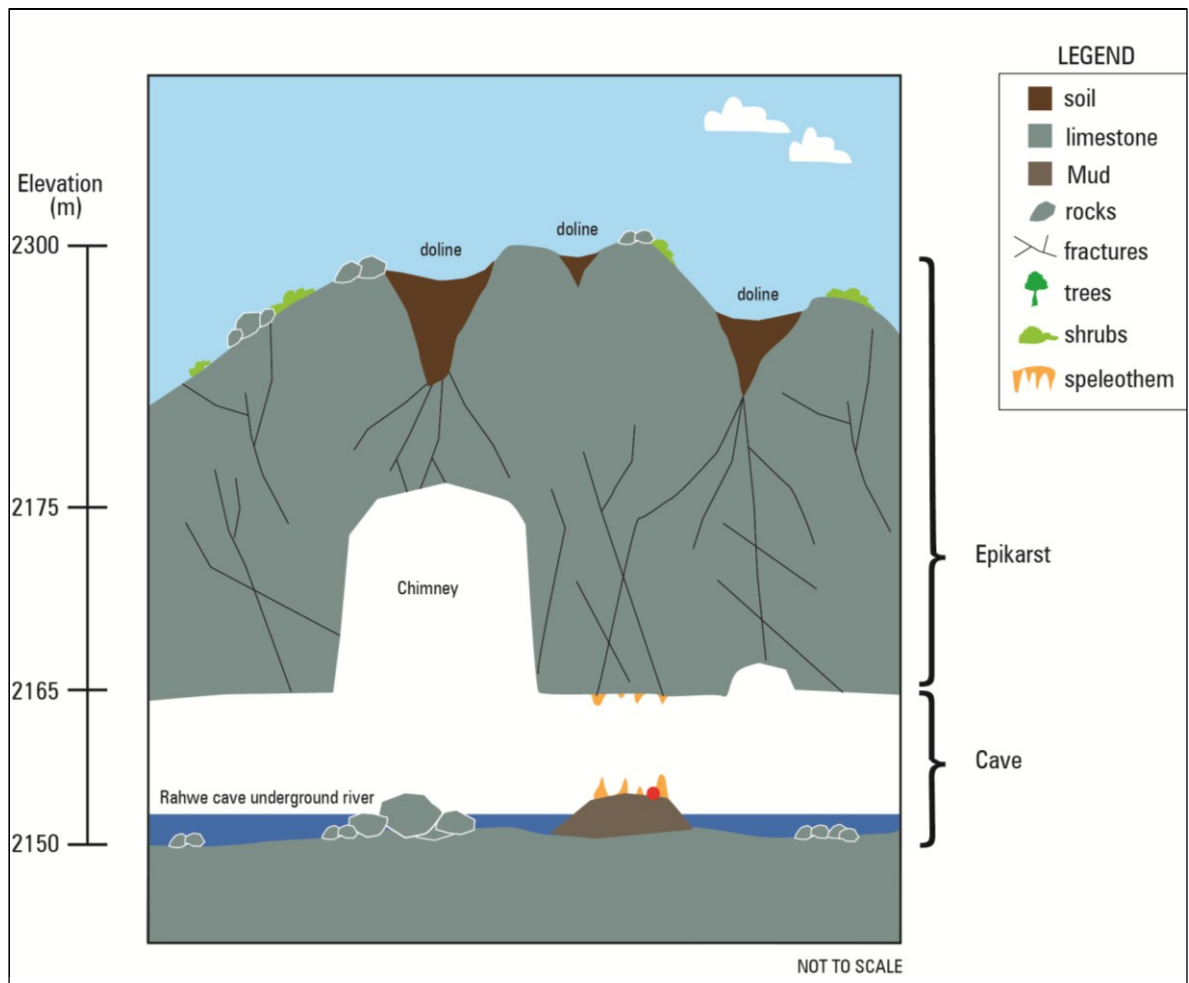
Figure 20. A cross section diagram of a section of the Rahwe cave. The red dot donates the location of where the studied stalagmite was removed.

3.2.2.3 Geology and geomorphplogy of the area

A geological map, at a scale of 1:15,000 was developed based on: 1) review of
available maps (Dubertret 1956, geological maps of the area 1:50,000), 2) analysis of
aerial photographs and Google Earth, and 3) geological mapping and site visits (App.

3). A cross-section was also constructed from the Rahwe cave geological map (Figure 21).

The Maqlal Daaboul Mountain, in which Rahwe cave has developed, consists of a 2,300 m top with many dolines, some of which are filled with terra rossa. The mountain consists of one formation, the Cenomanian aged limestone rocks of the Sannine Formation. It ranges from 100 Ma to 94 Ma (Cenomanian). This formation consists of marl, marly limestone, chert nodules, and massive to thinly bedded limestone. It is highly karstic in nature. The area surrounding the cave is made up of a series of highs, which surround a large doline called Sahlet el Rahwe. There are dolines dotted all around the area as well as on the top of the various highs. Some of the dolines are filled with terra rossa.

The Rahwe plateau is highly faulted, with a major E-W trending fault located in its northern section. This is a dextral strikeslip fault with a normal component. There are some minor faults in the area mainly trending in an E-W direction as well as N-S. The general bedding in the area is between 20º to 8º towards the SE.

The cave is formed along an impermeable marl layer that can be observed outside the cave in the drainage flow. This layer is probably the reason why the cave has formed, since it forms the barrier along which the underground water flows until it emerges as the Rahwe spring.
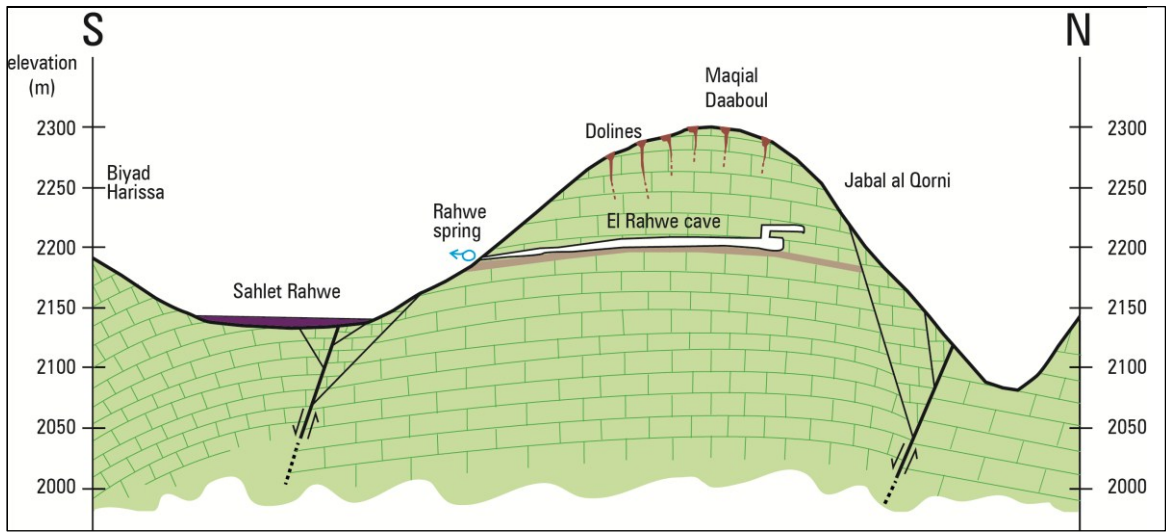
Figure 21. Cross-section of the Rahwe cave study area. The vertical scale has been expanded (x2).

Table 2 Summary of El-Kassarat and Rahwe caves parameters

NAME	EL-KASSARAT CAVE	RAHWE CAVE
X-coordinate	33.910528° N	34°11'46.66"N
Y-coordinate	35.608544°E	35°58'50.34"E
Elevation (m)	85	2208
Environment	Coastal valley	High Alpine mountain
Horizontal Development (m)	4748	<3000
Geology	Middle Jurassic, Keserouane Formation	Cenomanian, Sannine Formation
Approximate thickness of epikarst (m)	≈30	≈100
Approximate Ceiling height (highest) (m)	≈30	≈15
Distance from the sea (km)	2.7	32
Average cave air temperature (°C)	17	7
Average groundwater temperature (°C)	16	4.5
Average dripwater temperature (°C)	16	6
Cave Humidity	95-100%	95-100%
Cave entrance history	No natural entrance until 1960's	No natural entrance until 1960's
Name of stalagmite studied	EKC-01	RC-01
Date of stalagmite retrieval	24 September 2012	21 October 2012
Stalagmite location	Salle du President gallery	Main axis
Stalagmite location (distance from entrance, m)	100	80
Nearby dripwater rates	1 drip per 6 seconds	1 drip per 9 seconds

CHAPTER 4

SAMPLE COLLECTION, PREPARATION AND DESCRIPTION

This section will provide a description of the activities conducted from sample collection, sample preparation, monitoring, field and laboratory testing and the presentation of data.

One stalagmite was collected from the El-Kassarat and the Rahwe caves. Dripwater, groundwater and rainwater were also collected and tested for current physico-chemical conditions three times, while samples to be used for water isotope sampling were collected twice. The temperature inside each cave was also monitored.

4.1 El-Kassarat cave

One stalagmite was collected from the El-Kassarat cave on 24th of September 2012 and was labeled EKC-01 (Figure 22). This figure shows the location of the stalagmite inside the cave, the position of the collected samples as well as the location of other monitoring stations established. The EKC-01 was recovered from the Gallerie du President passage, about 100 m from the BMLWE entrance (App. 1). It was already broken when collected, although photos taken in the 2001 showed that the stalagmite was still attached to the ground but no longer growing (Figure 23). It is still unknown when exactly the stalagmite was broken or how.
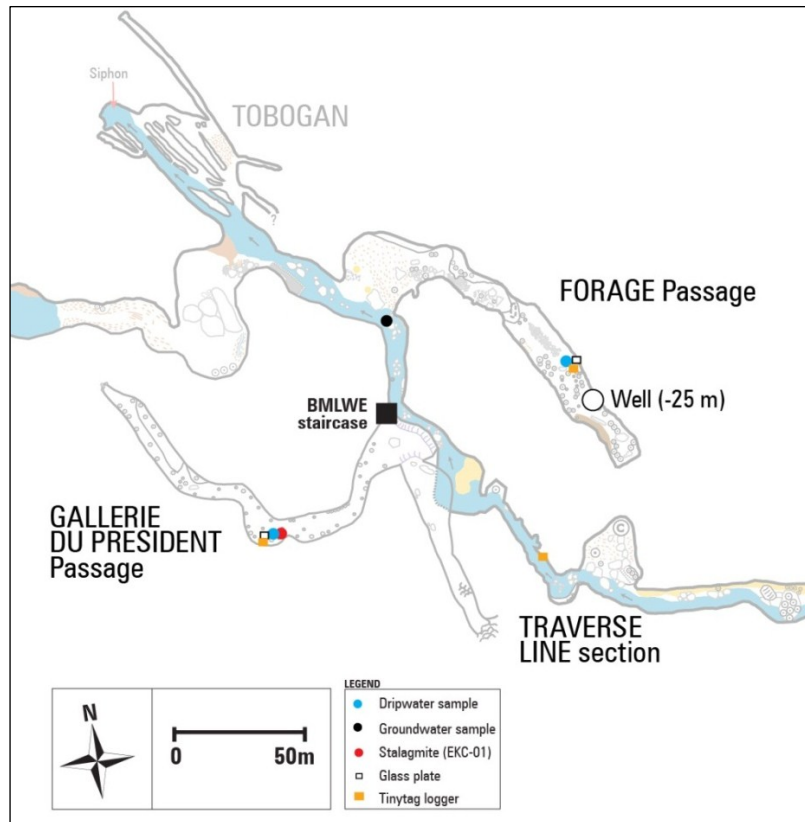
Figure 22. The El-Kassarat cave survey showing the locations of the stalagmite removal site, dripwater, groundwater and calcite collection glass plates. The BMLWE staircase is the present entrance into the cave.

Figure 23. Left: The EKC-01 stalagmite still standing (photogaph taken in 2001). Right: The EKC-01 stalagmite when collected (photograph taken in 2013).

The EKC-01 stalagmite was stabilized in epoxy, because of its fragility, and to avoid breakage during transportation and cutting. After the epoxy dried the stalagmite was cut into two halves along its growth axis at a rock cutting factory (Figure 24). One half was stored for future studies and the second half was polished with a handheld stone polisher. The polished part was then sliced, along the growth axis, using a stone saw, into ≈ 3 cm thick slabs (mainly to minimize shipping costs). The complete slab was photographed (Figure 24), packaged and shipped to the RSMAS center in Miami for isotopic analysis and dating.

Figure 24. Left: Removal of the EKC-01 from the cave in a protective pipe. Middle: Epoxy being poured around EKC-01. Right: Cutting EKC-01 into slabs.

The location where the EKC-01 was collected from is relatively dry most of the year. Mud deposits are present in the first section of the Gallerie du President passage, before the location of EKC-01, indicating that at some prior time groundwater did flow into the gallery (probably at high groundwater levels or during snowmelt events). Thus,

the dominant groundwater available for the growth of this stalagmite comes mainly from ceiling drips.

In addition to the stalagmite, other parameters were sampled and measured including dripwater, modern calcite deposits, cave air temperature, and humidity. Dripwater samples were collected from two locations: one in the Forage passage and one from the Gallerie du President's passage (Figure 22). Both were collected using a plastic funnel and bottle as shown in Figure 25, which were rinsed by the dripwater prior to collection, to minimize possible contamination effects. For the EKC-01 site the bottle was placed about 1 m away from the stalagmite removal site, and the drip-rate was approximately 1 drip every 6 seconds. This rate did not change considerably during the study year. Three sampling sessions on groundwater and dripwater were conducted in November 2012, June 2013 and August 2013 (App. 7).

Glass plates were also placed in the Gallerie du President's passage about 50 cm from the EKC-01 collection site (Figure 25). Two additional plates were placed in the Forage passage, close to the drilled well (Figure 22). These recent calcite deposits collected will be used for U/Th dating, mainly for the correction of the detrital ^{230}Th. In addition to recent calcite deposits collected, scraped calcite from the tips of an actively growing stalagmites close to the site of EKC-01 was also collected in order to obtain duplication in U/Th corrections, and in case no calcite growth occurred on the plates.

The pH, conductivity, temperature, and TDS of both groundwater and dripwater were tested on site using an OAKTON Handheld Water Meter, Eutec Instruments.

Figure 25. Left: the dripwater location and setup, Middle: modern calcite collection glass plate and Right: cave air temperature logger using a Tinytag monitor.

Temperature was collected using a Tinytag temperature logger (Gemini Data Loggers Co, Tinytag Plus 2 Internal Temperature, TGP – 4017). It was placed 1 m away from the EKC-01 removal site (Figure 25). The TGP – 4017 is a robust temperature logger contained in a waterproof case. The temperature readings range is -40°C to +85°C, with a reading resolution accuracy of 0.01°C (http://www.geminidataloggers.com/data-loggers/tinytag-plus-2), required for small variation in cave temperature. The logger was calibrated to measure a reading every 15 minutes. Two other Tinytag loggers were placed in the Forage Passage, and close to the Traverse line location (App. 1). The loggers were placed in different locations at different depths inside the cave to check for temperature variation (if present) between the different areas.

69

Humidity readings were collected using a Gemini TinyTag 2 Plus dual-channel temperature/relative humidity TGP-4500 data logger. The RH sensor collects data from 0-100%, and is accurate to ±3.0% at 25°C. But at high RH (between 95 and 100%) the sensor may give faulty reading (a flat line). When RH levels are very high (between 95 and 100%), the sensor becomes wet and will not function properly until it dries out again (personal communication with Nicola Hood, Gemini Data Loggers (UK) Ltd). Continuous measurements for humidity were not possible, and only spot measurements during site visits were undertaken. The humidity levels were measured in the Gallerie du President passage at the stalagmite site. The humidity level in this location measured an average of 90%.

4.1.1   The EKC-01 stalagmite visual description

Figure 26 outlines the general features of the stalagmite with close up images of certain areas described in subsequent sections. Stalagmite EKC-01 is 85 cm long. At its widest point the EKC-01 measures 18cm, and at its thinnest width it measures 5 cm. The stalagmite consists of two main growth periods. The first measures 54 cm in length, and the second is a candlestick and measures 31 cm in length. The candlestick section is noticeably thinner than the rest of the stalagmite. There appears to be some visual hiatuses (changes in growth directions, changes in colour, or changes in laminae thicknesses) in the stalagmite at 8.8cm, 50cm, 54.8 cm, and 70.4 cm from the bottom. Visually the laminae of the stalagmite curve at the apex, then thin and trail down the

70

sides of the stalagmite. In all cases, the curved growth morphology is interpreted to result from changes in the position of the drip location in the surface of the cave over time. This shift in dripwater location could be due to changes of flow paths due to blockages of discontinuities in the epikarst.
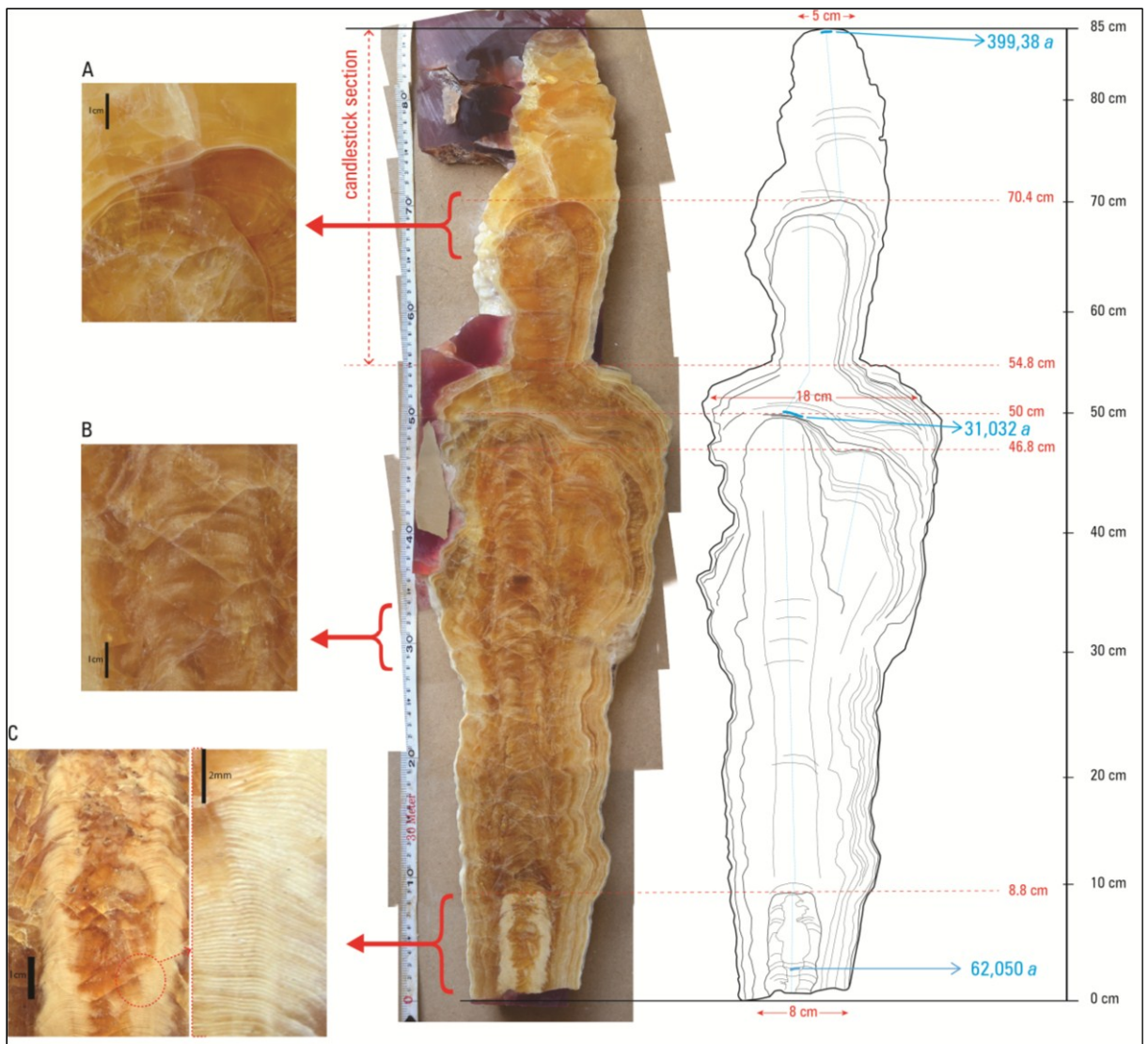
Figure 26. Details of the EKC-01 stalagmite. A, B, C are closeup images of different parts of EKC-01. Details of the measurments of the stalagmite as well as the age of different sections of the stalagmite.

From 0 to 8.8 cm (where zero is the bottom of the stalagmite), there is a cylindrical growth core with white opaque calcite material that appears to have laminations (Figure 26c). Opaque laminae are usually characterized by the input of detrital and colloidal material during periods of infiltration (Borsato *et al*., 2007) in seasonally high flows. Microcrystalline fabric forms milky, opaque layers, and is typical of Holocene stalagmites that show visible alternation of white and dark-brown laminae (Frisia *et al*, 2000). The laminae here are undulated and slope downwards towards the edges of the stalagmite (Figure 26c).

From the bottom of the stalagmite until 54.8 cm, the stalagmite's width increased from 8cm to 14cm. The stalagmite at around 30 cm began growing into two stalagmites with separate heads. These two amalgamate into one as the laminae covers both of them to form a flat top at around 50 cm. This part of the stalagmite consists of brownish transparent calcite (Figure 26b).

A candlestick top began to grow after 54 cm (Figure 26a). This part has a smaller diameter than the rest of the stalagmite, with the smallest width being 5 cm. This is the section that was isotopically sampled. The candlestick top begins as brown calcite and at around 70.4 cm becomes gradually less brown in colour and more transparent going through a series of lateral shifts as well as calcite colour.

4.1.2 Cave air temperature

Cave temperature was recorded for almost a year. The dates the loggers started to record cave air temperature in the El-Kassarat cave are shown in Table 3.

Table 3. The logging dates of the Tinytag loggers inside the El-Kassarat cave

	Salle du President's Passage El-Kassarat cave	Forage Passage El-Kassarat cave	Traverse line location El-Kassarat cave
Recording Started	11/04/2012 12:55:06	11/04/2012 12:53:10	03/17/2013 15:40:30
Recording Ended	08/22/2013 10:25:00	08/22/2013 08:38:00	08/22/2013 09:55:00

In El-Kassarat cave / President's passage, the logger's minimum reading was 16.3ºC, the maximum reading was 17.4ºC and the average air temperature was 16.9ºC. In the Forage passage the minimum reading was 16.6ºC, the maximum reading was 18.3ºC and the average air temperature was 17.4ºC. The Traverse line location is the farthest away from any entrances and is located above the El-Kassarat underground river. In the Traverse line location the minimum reading was 15.1ºC, the maximum reading was 16.9ºC and the average air temperature was 15.8ºC (Figure 27).
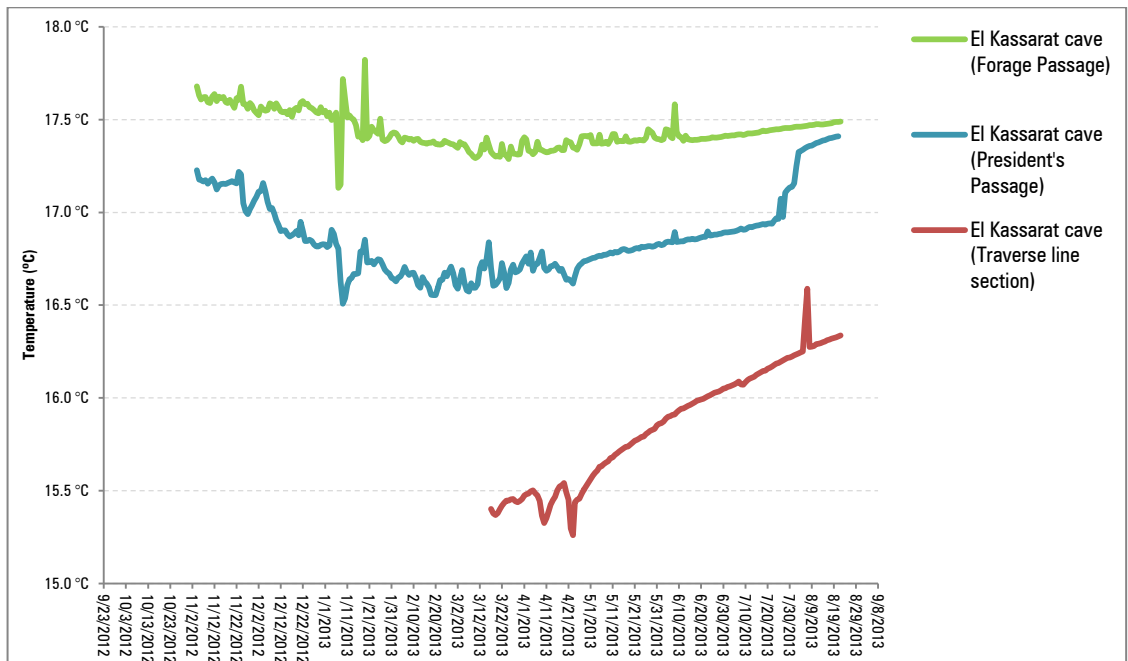
Figure 27. Temperature logging results from different locations in the El-Kassarat cave

Figure 27 shows that the temperature inside the cave did not stabilize in the winter months. From November 2012 to August 2013 the temperature was affected by outside conditions, decreasing steadily until May 2013 after which the cave temperature started to increase steadily. This effect is probably due to the presence of the cave openings, the Well and the BMLWE staircase, which are not properly sealed. The air current that is formed through these openings can affect the cave temperature.

The mid-January anomaly in the Forage Gallery and the Gallerie du President is due to a flooding period that occurred during this time, depositing mud on top of the Tinytag logger indicating that the water level must have reached higher than the

Tinytag. There is also clear evidence that water levels were high because nearby columns, which consisted of clean white calcite, were stained with mud up to about 2m.

It must be noted that the two entrances, the Well and the BMLWE staircase room, were only opened in 1996 and 2004 respectively. It can be inferred that current cave air temperature changes could not have affected the stalagmite's growth, since before the 1960's, the cave had no natural entrance and therefore no connection to the surface outside.
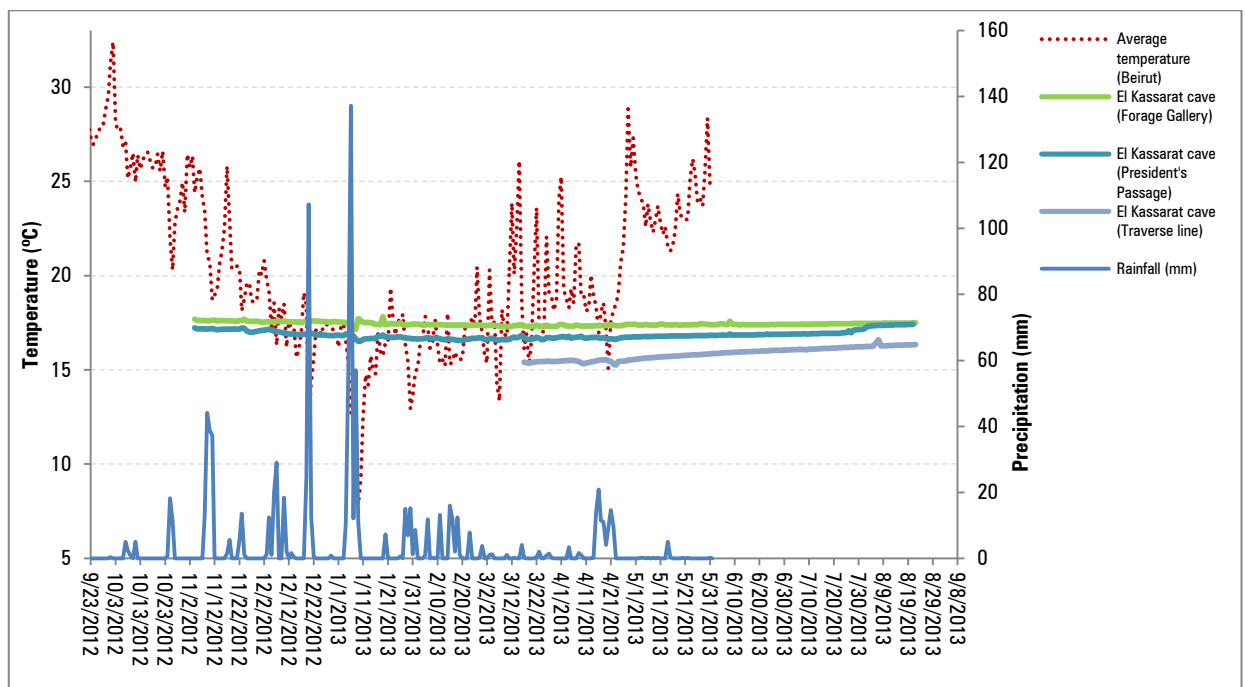
Figure 28. Temperature logging results correlated with surface temperature and rainfall in the El-Kassarat cave

In the El-Kassarat cave, temperature anomalies can be seen in different passages. The highest temperatures were measured in the Forage Passage, while the lowest were measured in the deepest sampled part of the cave, the Traverse line section. Their trends all correlate with each other although there is no major correlation with surface air temperatures as the latter tended to fluctuate a lot more (Figure 28). It can be deduced that maybe surface temperature is not affecting cave air temperature, but air currents could be formed inside the cave due to the rising and lowering of the underground river which could affect air pressure inside the cave.

Storm events have a short term effect on the cave environment, usually causing the underground river to flood for a short time and depositing sediments at higher levels. A drop in temperature and an increase in rainfall have shown dips in cave temperatures (Figure 29).
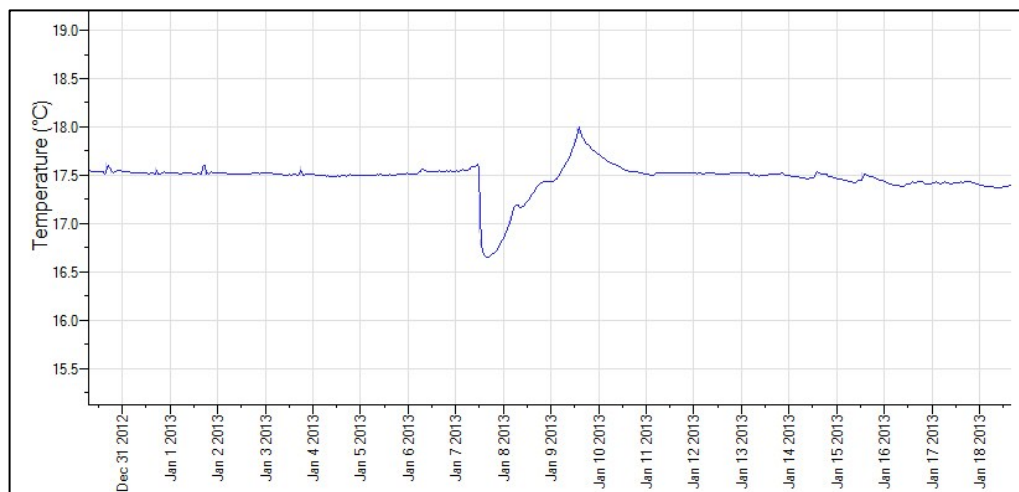
Figure 29. Flooding events seen as sudden temperature shifts in the El-Kassarat cave temperature log during January 2013.

76

As an example of this, after a large flood event on the 7th of January, 2013, the Tinytag in the Forage Gallery was submerged under the flood water, and mud was deposited on its top. The water flow reduced the temperature markedly, as seen in Figure 29, at a faster rate than the one in the Salle du President's Gallery. The water remained below the logger in this gallery, then the observed sudden increase then decrease in temperature from the 7th to the 9th of January may be due to this sudden flooding event.

4.1.3 *Precipitation collection*

Rainwater was collected in the Antelias quarry at coordinates 33°54'38.61"N and 35°36'27.83"E, at an elevation of 88 m. This location is approximately 360 m away from the BMLWE El-Kassarat cave entrance.

Data was obtained from the Meteorological office at the Beirut International Airport nearly 13 km away from the cave. Surface temperature and precipitation rates were obtained from the closest national gauging stations (Figure 30, Table 4).

Table 4. The closest gaging stations to the El-Kassarat cave

Cave name	Station name	Elevation (m)	x-coordinate	y-coordinate
El-Kassarat cave	**Beirut Golf Club**	14	33:51.123	35:29.513
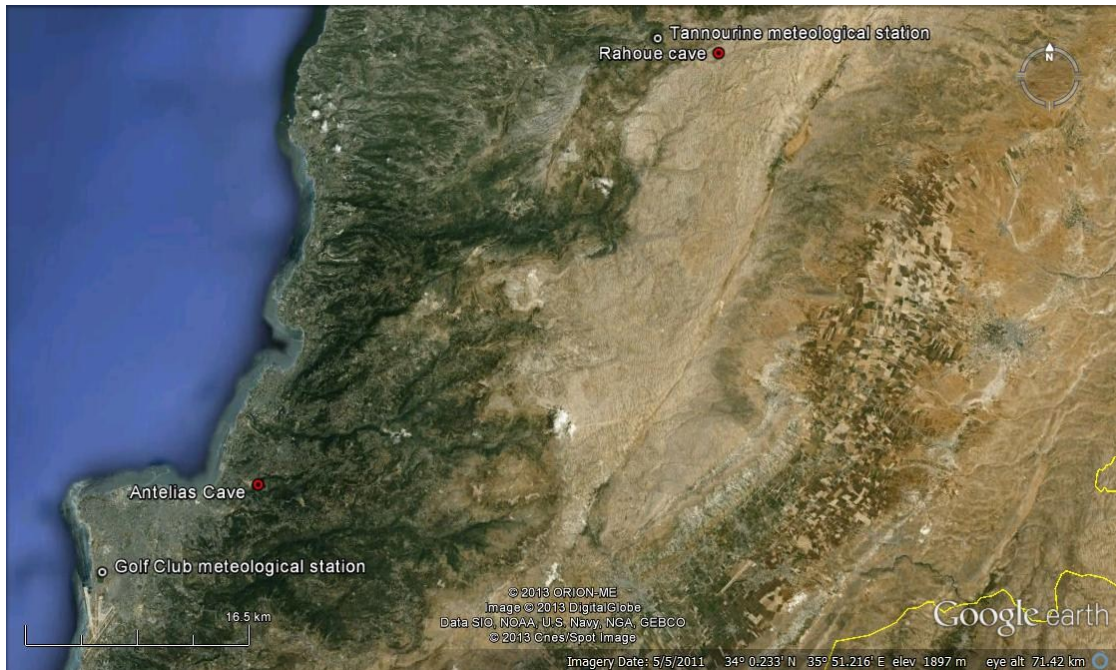
Figure 30. Locations of the closest meteological stations to the caves (Modified from Google Earth).

4.1.4 Uranium -Thorium dating

A ThermoFisher Scientific Neptune Plus MC-ICP-MS was used for the dating analysis. By default, an average crustal activity ratio of 0.6+/-0.2 for initial $[Th^{230}/Th^{232}]$ was used. Given that the true ratio for the samples is unknown, the corrected ages must be used with caution. A higher initial ratio will result in a larger corrected age.

An open-source algorithm in Mathematica application was used to process the U and Th data and calculate an accurate age (Pourmand *et al.,* 2014) (App. 15).

Results of the age dating and growth rate are presented in App.16. The EKC-01 stalagmite growth ranged from nearly 62 ka to 400 a. The growth was found to be 276 cm for approximately 30 ka. The growth rate for the candlestick section was found to be

relatively constant with no major shifts in growth rates throughout the nearly 26 ka

years of growth. It was found that it grew approximately 87 mm per year (Table 5,

Figure 31). The three dates do line up close to a straight line but the growth is not linear.

There are discrete growth phases, where the annual laminae near the base demonstrates

a faster growth rate (Figure 31).

Table 5. Table showing the growing rates of the ECK-01 stalagmite

YEAR	Growth length (mm)
0	0
399	5
31,032	356
62,050	820
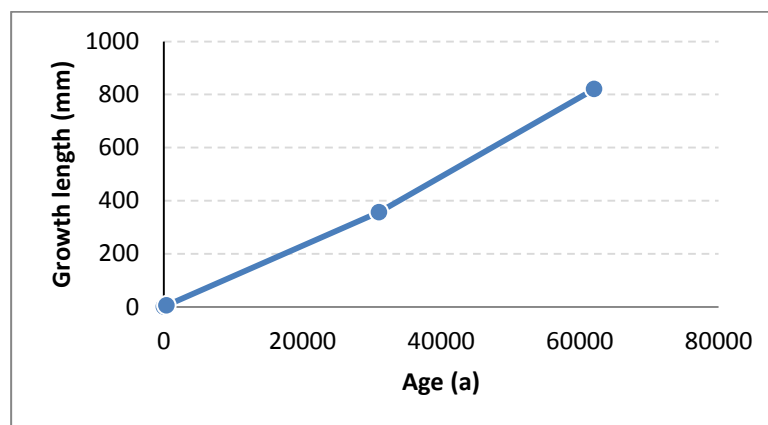
Figure 31. Graph showing the rate of growth in the candlestick section of EKC-01 stalagmite for the El-Kassarat cave.

4.1.5 $\delta^{18}O$ and $\delta^{13}C$ carbonate record from the EKC-01 stalagmite

This material was transferred to a glass reaction vessel, and analyzed for ^{18}O and ^{13}C stable isotopic composition using a Thermo-Finnigan DeltaPlus Mass Spectrometer. A Kiel III device was used to individually react powdered samples in glass vessels with 100% H_3PO_4 at 70°C. An in-house Optically Clear Calcite (OCC) standard was used for calibration, and corrected isotopic values are reported in per mil (‰) relative to Vienna Pee Dee Belemnite (VPDB). The reproducibility of the internal lab standard OCC over the course of the aragonite-calcite analyses was ± 0.02 ‰ for ^{13}C, and ± 0.06 ‰ for ^{18}O.

The EKC-01 candlestick results can be divided into three phases based on the $\delta^{18}O$ analysis (Figure 32, Figure 33). The $\delta^{18}O$ values from EKC-01 ranged from −6.23 to −2.7‰, with an average of -4.4‰. From 27.5 to 15 ka, the $\delta^{18}O$ values were above the average. At 15.2 ka the lowest value for $\delta^{18}O$ is measured at -2.7‰. The values increases rapidly to -6.23‰ at around 13.5ka. The high negative values remain relatively constant between 13.5 and 10.9 ka. Above this level there is an increase in values reaching -4.4‰ at 7.8 ka. This is close to the overall mean. Above the latter level, the values decrease and remain below the mean. Values begin to decrease towards the top of the stalagmite for intervals younger than 1.2 ka.

The $\delta^{13}C$ record follows a similar trend to that of the $\delta^{18}O$ record. The $\delta^{13}C$ values range between −12.4 and −6.9‰, with an overall mean of −11.1‰. High values are

observed between 27.5 ka and 17 ka, averaging about 11‰. Lower values occur between 17 and 14 ka with the higher value measured at 14 ka at -6.96‰. Values then increase to higher than average with some sharp decrease in values at -10.4 ka, -7.37 ka, -10.39 ka. Speleothem $\delta^{13}C$ records associated with C3 dominated vegetation typically have compositions of -14 to -6 ‰ (McDermott, 2004). Variations in the $\delta^{13}C$ record of EKC-01 suggest some variations in the C3/C4 vegetation ratio or in soil water residence time.

The $\delta^{18}O$ and $\delta^{13}C$ measurements have similar trends (Figure 33). Three changes have been recorded in the top section of the EKC-01 growth (the candlestick section). A first period, from 27.5 to 15 ka, shows relatively low $\delta^{18}O$ values with similarly low $\delta^{13}C$ values. The middle part, from 15.2 to 13.5 ka, has a sharp decrease at 14 ka in both $\delta^{18}O$ and $\delta^{13}C$ values following by a sharp increase at around 13 to 13.5 ka. The upper part of the stalagmite, from 13 to 0.0 ka, show a return to relatively high isotopic values for both $\delta^{18}O$ and $\delta^{13}C$. These isotopic values are higher than their corresponding values related to the first period. The $\delta^{18}O$ shows a higher increase between the first period and the final period than the $\delta^{13}C$ values.
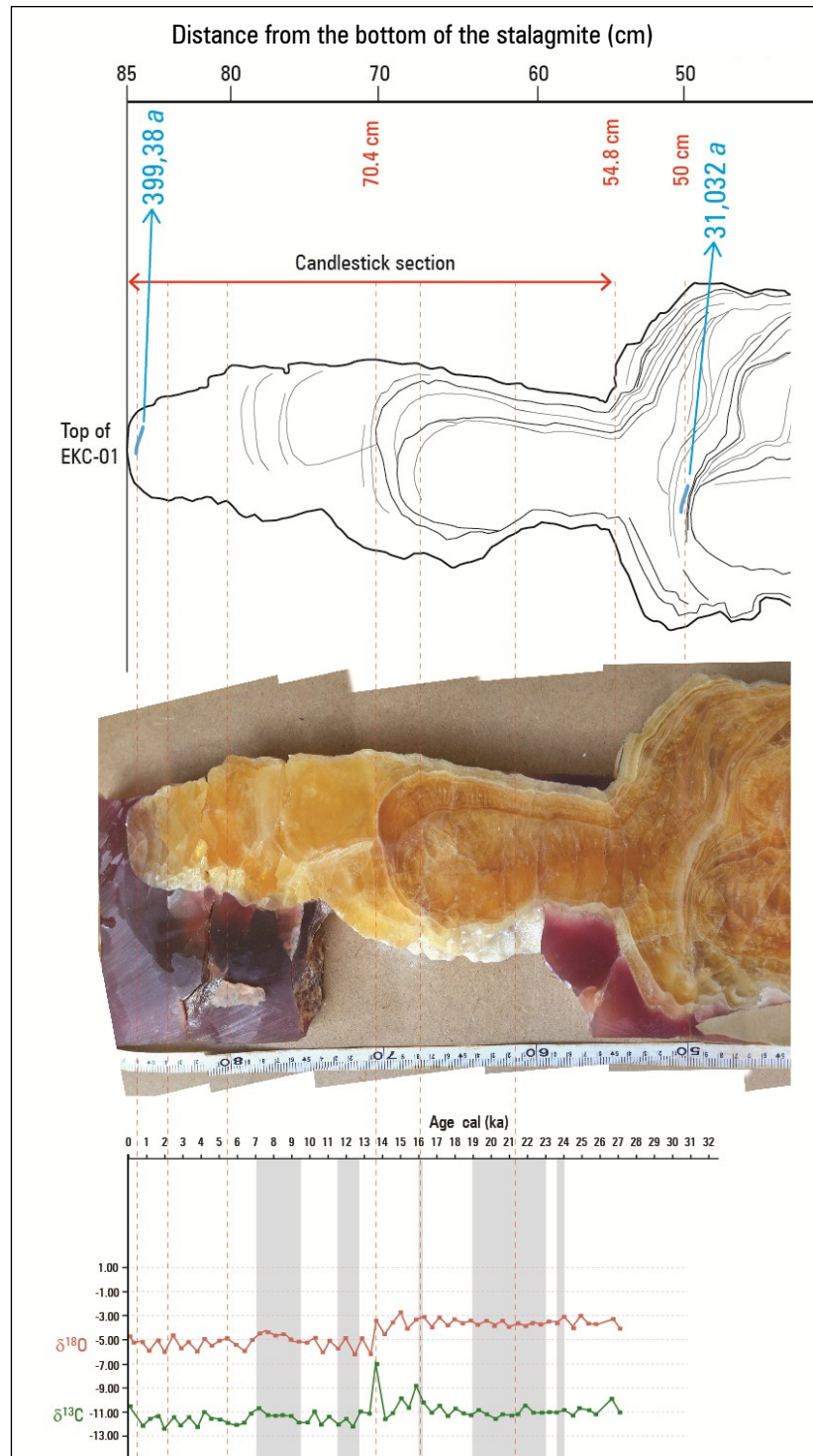
Figure 32. $\delta^{18}O$ and $\delta^{13}C$ variations showing the correlated section and ages of the EKC-01 stalagmite.
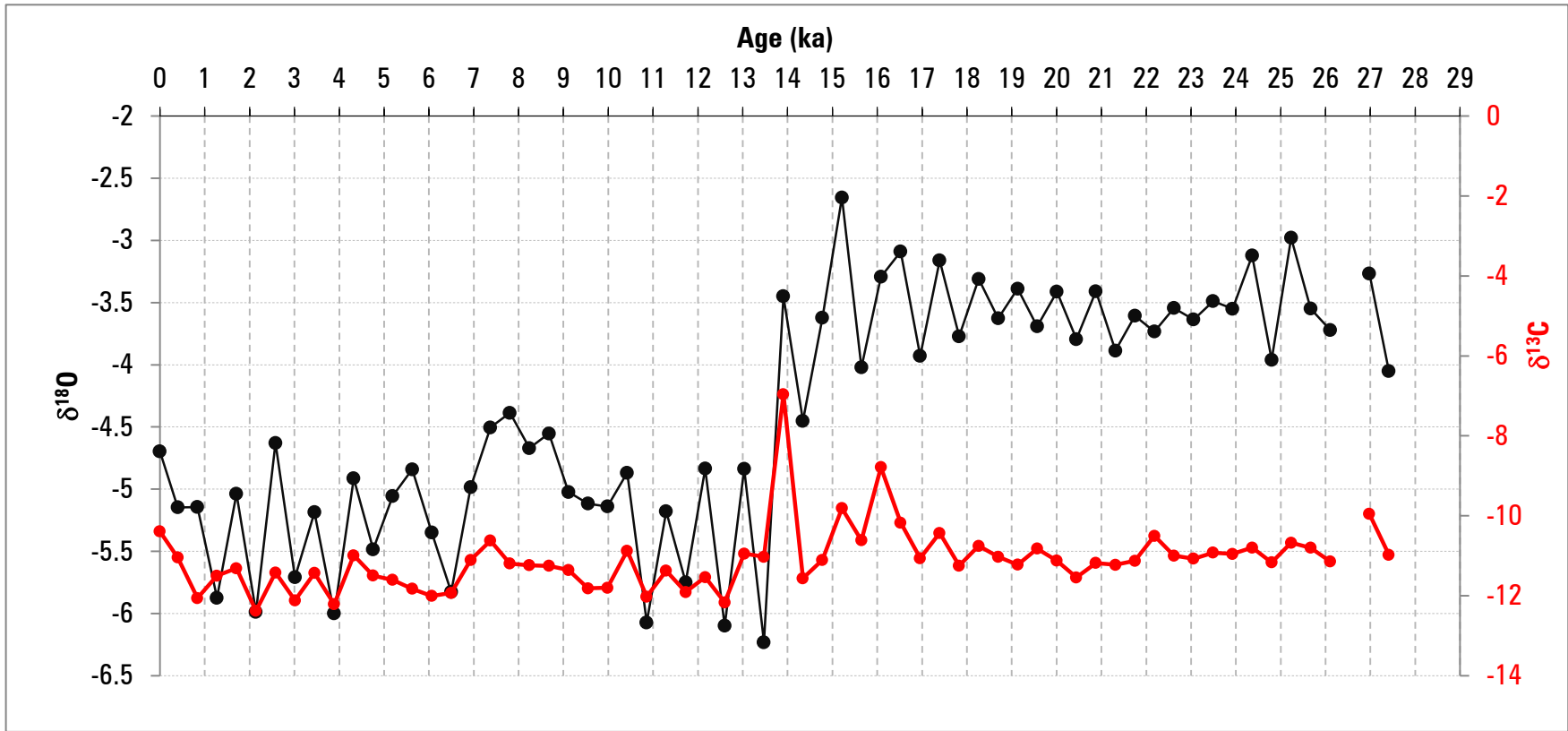
Figure 33. $\delta^{18}O$ and $\delta^{13}C$ variations in the candlestick section of EKC-01.

4.1.6 *Trace elements analysis*

The EKC-01 candlestick was analyzed for magnesium (Mg), strontium (Sr), barium (Ba), and iron (Fe) by Inductively Coupled Plasma Optical Emission Spectroscopy. For the replicate transects, splits of the milled sample were analyzed for elemental concentrations using a VarianTM Vista Pro Inductively Coupled Plasma Optical Emission Spectrometer (ICP-OES). Each sample was dissolved in 5 mL of a blank solution (4% OmniTrace HNO3 and 1 ppm yttrium) in an acid washed 15 mL poly test tube and introduced for analyses via an SPS-5 auto-sampler. Yttrium was used to normalize any instrument drift. Samples were initially analyzed for Ca^{2+}. Based on the results of this preliminary scan, the samples were diluted to a consistent Ca^{2+} concentration of between 3 and 5 ppm. This method reduced any matrix effects introduced by variations in sample size (De Villiers *et al.*, 2002). Once a uniform concentration was obtained, samples were reanalyzed using longer integration times.

4.1.7 *Institute and laboratory physico-chemical results of groundwater and dripwater*

4.1.7.1 In situ tests

4.1.7.1.1 *pH levels*

Rainwater near the El-Kassarat area measured a pH of 8.93. The dripwaters and groundwater in the El-Kassarat cave measured lower in values than that of rainwater, showing that the water was being effected by the aquifer and the epikarst. There is also

a pH difference between the two types of waters (groundwater and dripwater), as well as a difference between the two dripwater locations (Figure 34). This is probably due to the different paths and conduit channels the groundwater flows through to reach the cave cavity.

Throughout the sampling year, there was a decline in pH for the Gallerie du President Passage, where and initial high value in November 2012 declined in August 2013. This indicates that seasonality is influencing the waters' pH values. There is a steady decrease in groundwater pH through the same time period while that of the dripwater in the Forage Passage is steadier, with a slight decrease in June 2013. Since pH is characterized by the uptake of soil-originated CO_2, more CO_2 in the soil reduces the pH value of the water. Changes in soil pCO_2, alkalinity, pH values and the Ca^{2+} content of the groundwater usually follow seasonal variations (Kano *et al*., 1999).
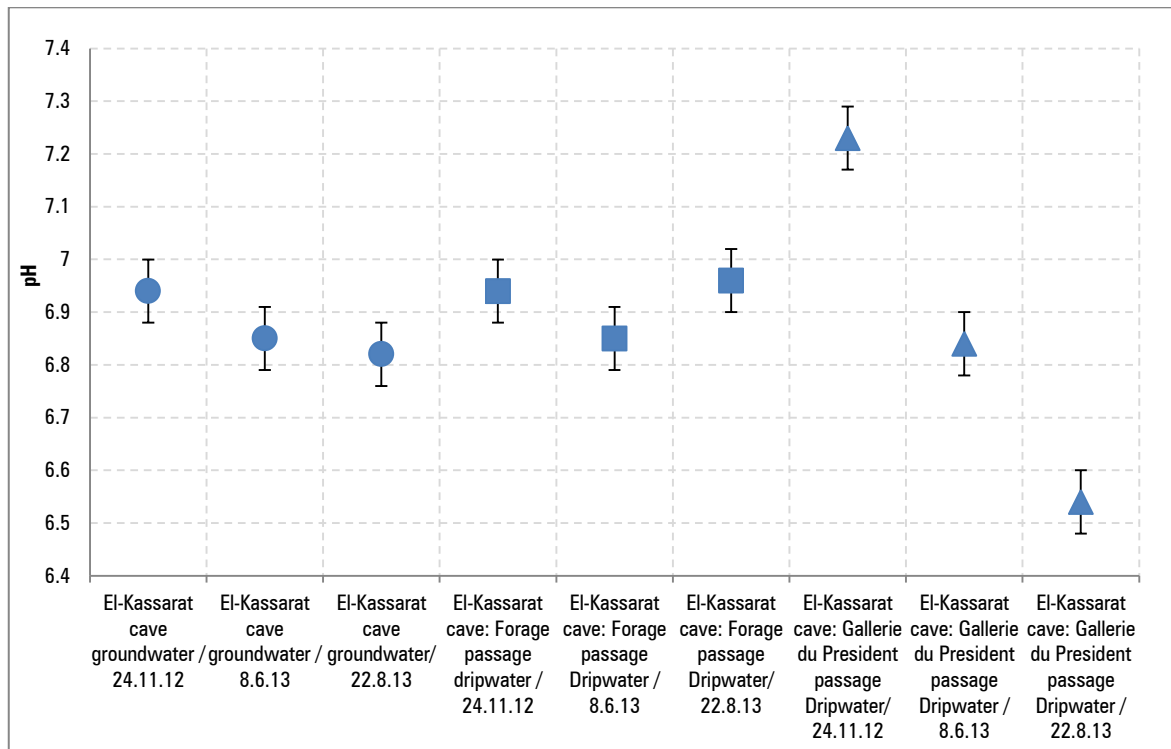
Figure 34. pH levels of various waters from the El-Kassarat cave.

4.1.7.1.2 *Water temperature levels*

In the El-Kassarat cave, the groundwater and dripwater temperature varied between 15.5° C and 17.8°C respectively (Figure 35). This difference could be due to the residence time of the water in the aquifer. Groundwater had lower temperaturethan dripwater, indicating that the two types of water could have different conduit paths through the aquifer. The dripwaters could be closer to the temperature of the rainwater of the El-Kassarat region since it seems to percolate through the epikarst (≈30m) and into the cave. The groundwater could have an initial input from higher elevations since

the catchment area is quite large, where the temperature of the water could be colder, where it travels underground eventually flowing as the El-Kassarat underground river.
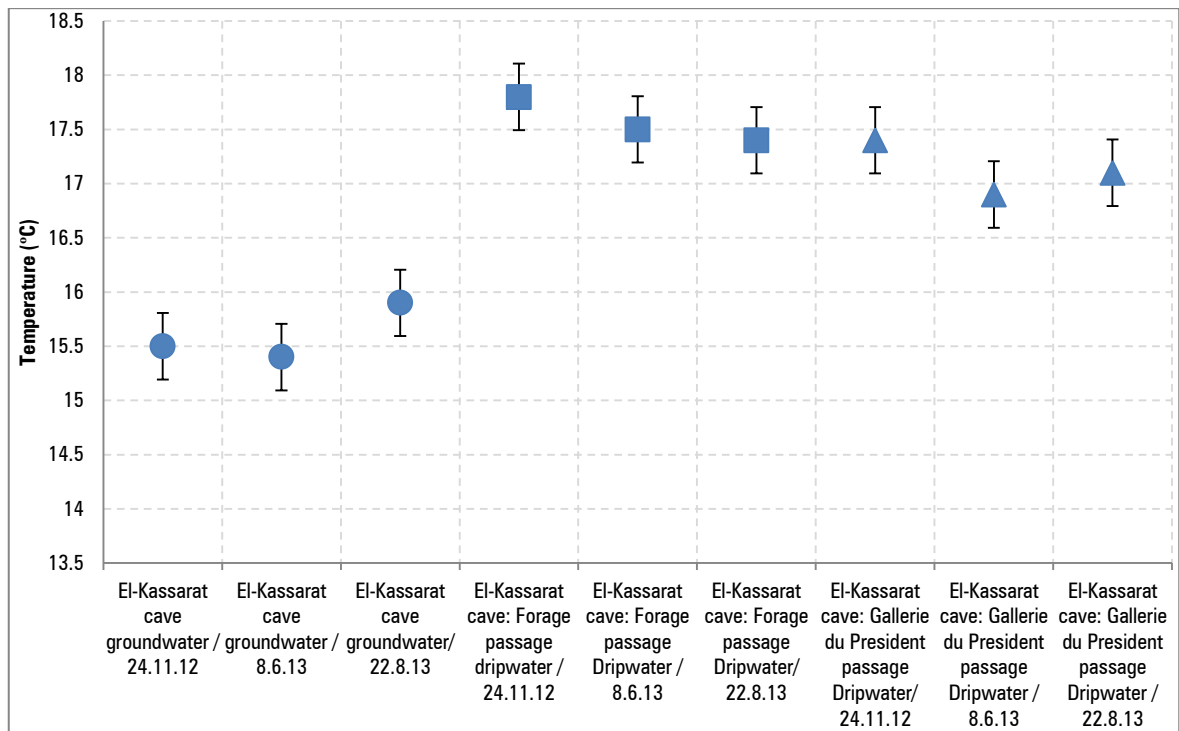
Figure 35. Groundwater and dripwater temperature in the El-Kassarat cave.

The catchment area of the El-Kassarat cave ($\approx$200 km^2) is large (Figure 36). The farthest that the El-Kassarat cave waters can travel in the aquifer is approximately 16 km. Groundwater flowing in the El-Kassarat cave has a very large catchment area. It commences its journey into the underground from a sinking stream called Fouar Dara sinkhole (Majdal Tarshish village) as well as from surface percolation. The catchment area is approximately 200 km^2 (Labaky, 1998) (Figure 36). The temperature of the

waters in Fouar Dara sinkhole is nearly 4ºC, since it consists mainly of snowmelt.

Tracer tests, conducted in these high elevation sinkholes (Labaky 1998), showed that

the groundwater reached El-Kassarat cave after about 12 days. Thus, temperature

increases approximately by 1ºC a day. The El-Kassarat cave dripwater temperature in

both sampled locations are very similar, but both are higher than those of the

groundwater. This relative difference is due to the origin and mixing of the waters.
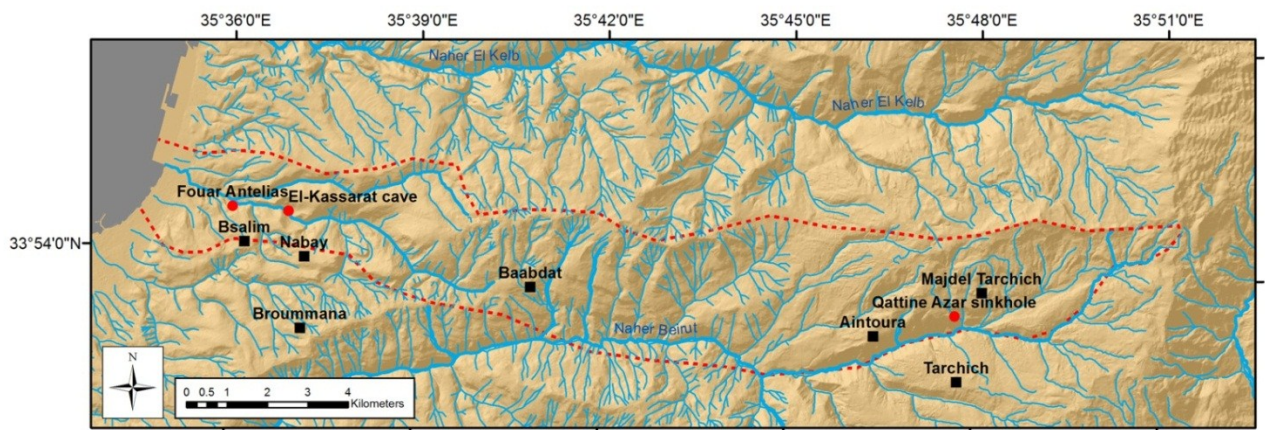
Figure 36 Possible catchment area of the Fouar Spring measuring nearly 200 km² in area (modified from Labaky, 1998).

4.1.7.1.3 *Conductivity levels*

With only three sample results it is difficult to identify a trend, but a general

variation does exist. There is a steady increase of conductivity values from winter to

summer months. Groundwater conductivity values ranged from 428 to 593 μs, 448 to

471 μs for the Forage gallery dripwater, and 450 to 470 μs for the Salle du President

gallery (Figure 37). The dripwater conductivity of the Salle du President passage and

Forage passages show this increase. From November to August, groundwater does

increase in values, although there is a dip in the middle value. This is indicative of the

higher residence time of the water in the aquifer. The higher the residence time and

higher the conductivity values.
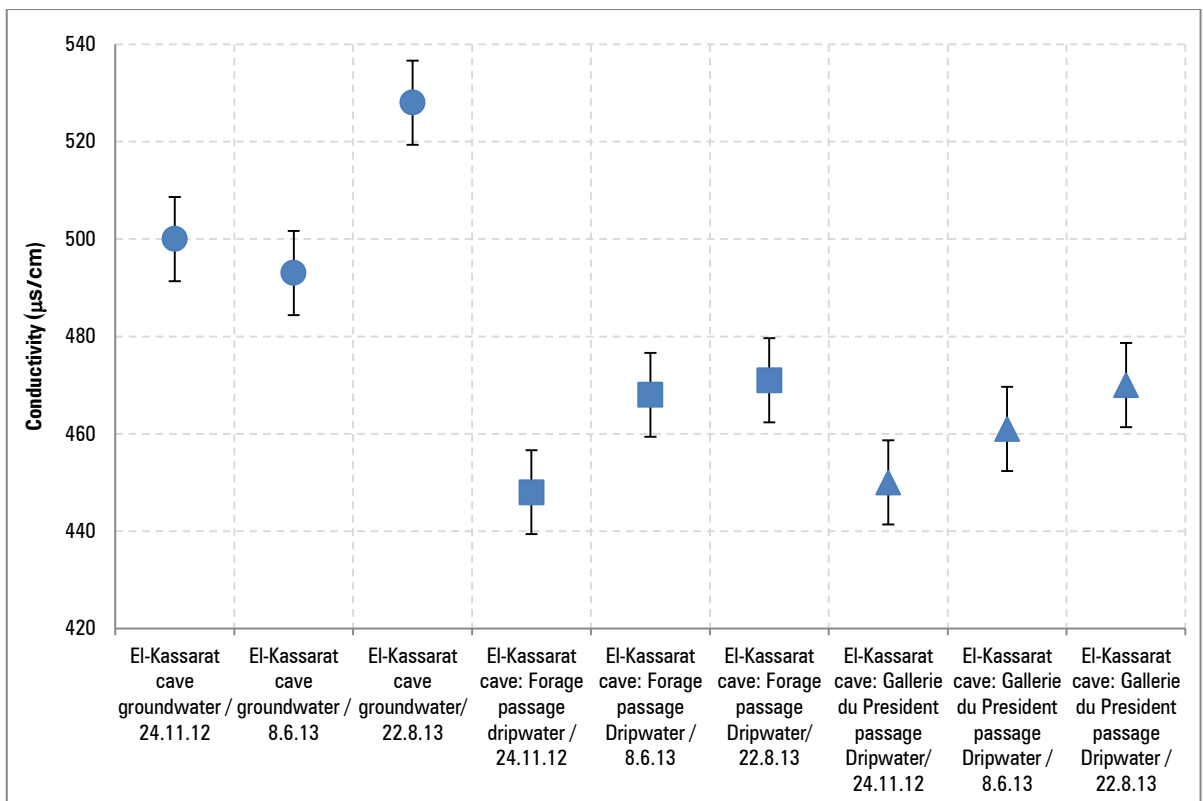
Figure 37. Groundwater and dripwater conductivity levels in El-Kassarat cave.

The El-Kassarat cave is close to a very large fault system making the aquifer

extremely fractured. The valley also has a surface soil sediments that can deposit inside

the conduits. The El-Kassarat Jurassic aged limestone also has a high dolomitic content. This dolomitic content could affect the rate at which the groundwater erodes the rock since dolomitic limestone is generally harder to erode than limestone. Temperature also plays an important role in this process as the CO_2 dissolving power (the more CO_2 dissolving into the groundwater, the more acidic the groundwater) is lesser at higher temperature.

4.1.7.2   Laboratory sampling results

Samples were tested at the AUB environmental Laboratory in the Engineering Faculty. App. 8 and App. 9 contain the results of the chemical and physical analyses of rainwater, snow, groundwater and dripwater.

Turbidity values in summer tend to be higher than in winter, with noticeable high values near the Well in the El-Kassarat cave, probably because the location of the well is close to a quarrying section of the valley where continued quarrying (beginning in the 1960's) and dynamiting of rock faces are still taking place. This could cause sediments to enter conduits and fractures causing an increase in turbidity values.

The results of the calcium parameter shows that the calcium range in summer and winter are affected by the quantity of water as well as the residence time, with conductivity values from winter to summer months 218 to 208 µs for groundwater, 88.6 to 208 µs for the Forage gallery dripwater, and 79.4 to 208 µs for the Salle du President gallery (Figure 38). The errors bars in the figures were calculated as a standard error.

90
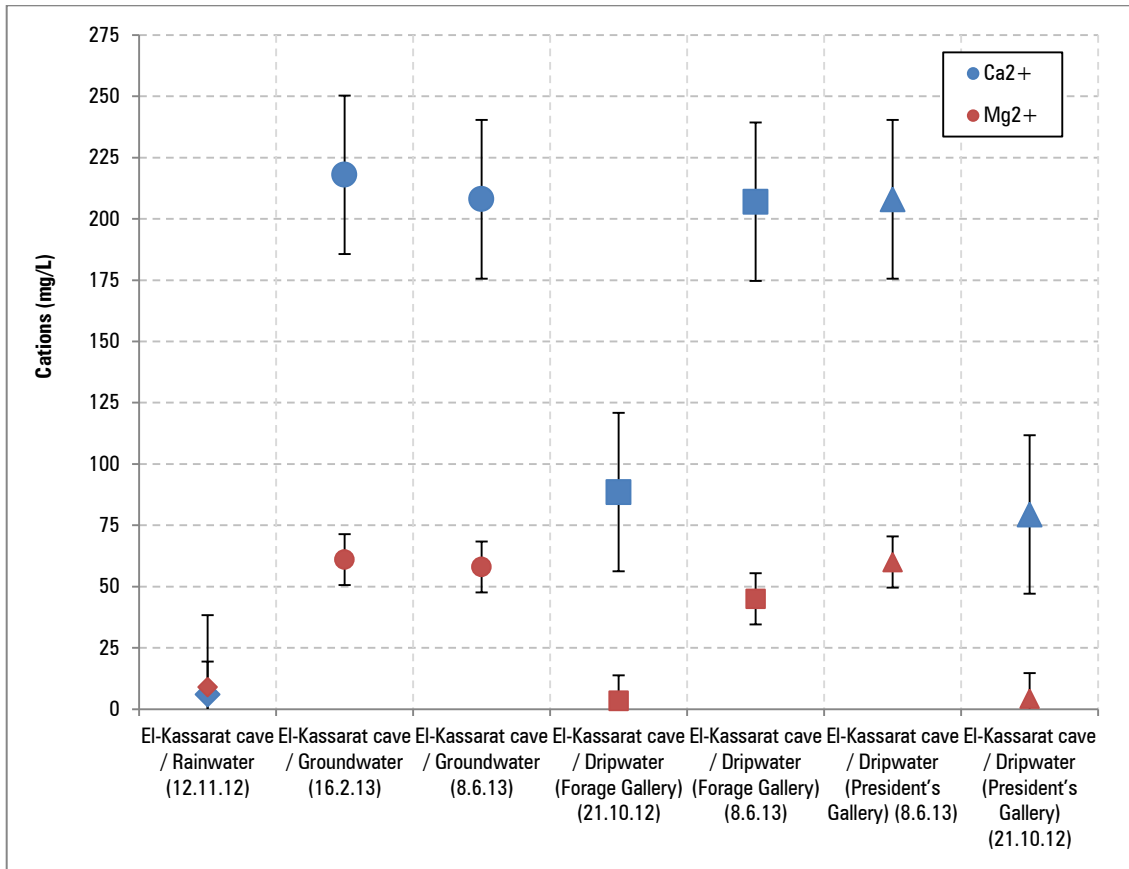
Figure 38. Mg^{2+} and Ca^{2+} concentrations of rainwater, snow, groundwater and dripwater for the El-Kassarat cave.

Conductivity levels between the El-Kassarat and Rahwe cave show higher values in the coastal region, which could be due to the seawater intrusion and agricultural activities (Figure 38). The concentrations of Ca2+ and Mg2+ are greater than those of Na+ and K+ (Figure 38). This reflects the chemical and mineralogical compositions of the rocks of the aquifer, which consist mainly of calcium carbonate and dolomite. The Na+ values are mainly due to the seawater intrusion that is present along the coast of Lebanon (e.g. Korfali et al., 2007). This occurs mainly near towns, due to the large

91

number of pumping wells extracting groundwater at a higher rate than that of recharge.

The K+ can come from fertilizers and pesticides used in agriculture. Seawater also has a

small percentage of Potassium.
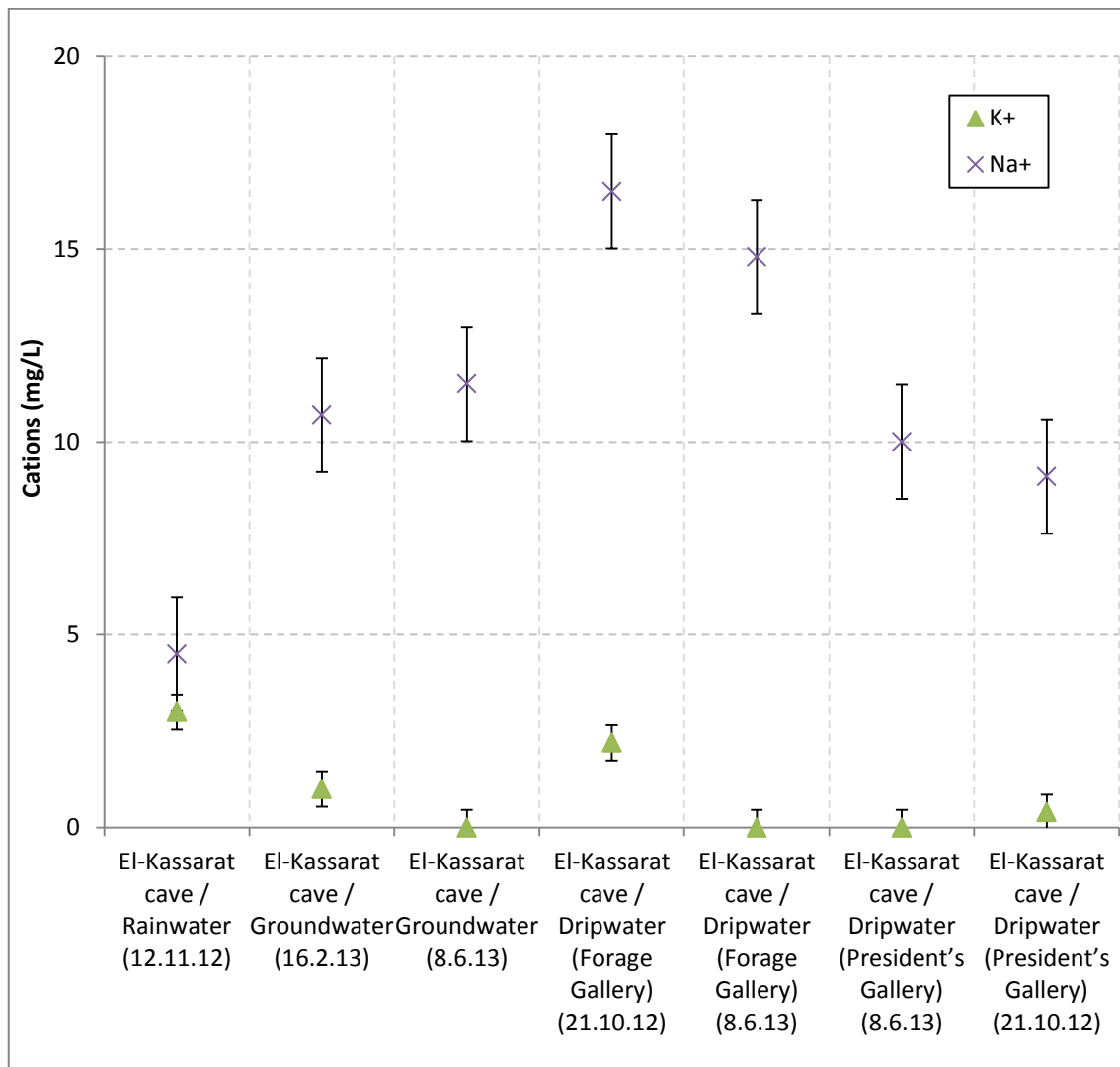
Figure 39. K$^+$ and Na$^+$ concentrations of rainwater, snow, groundwater and dripwater for the El-Kassarat cave.

4.1.7.3 Piper Diagrams

Piper diagrams are trilinear diagrams used to show percentages of three components. The major ionic species in groundwater are Na^+, K^+, Ca^{2+}, Mg^{2+}, Cl^-, CO_3^{2-}, HCO_3^-, and SO_4^2. The results of the chemical analysis are plotted on trilinear diagrams on the basis of percent of each cation or anion. A diamond shaped field between the two diagrams is used to represent the composition of water with respect to both cations and anions. Hydrogeochemical facies classification is used to describe groundwaters that differ in chemical composition (Figure 40) (*e.g.* Fetter, 1994).

The piper diagram shows that the El-Kassarat cave aquifer is a Calcium-Magnesium / Bicarbonate type hydro-chemical facies, which is indicative of a dolomitic limestone aquifer (Figure 41).

The winter and summer chemical composition of the groundwater and dripwater match indicating that the waters are coming from the same aquifers during winter high and summer low discharges.
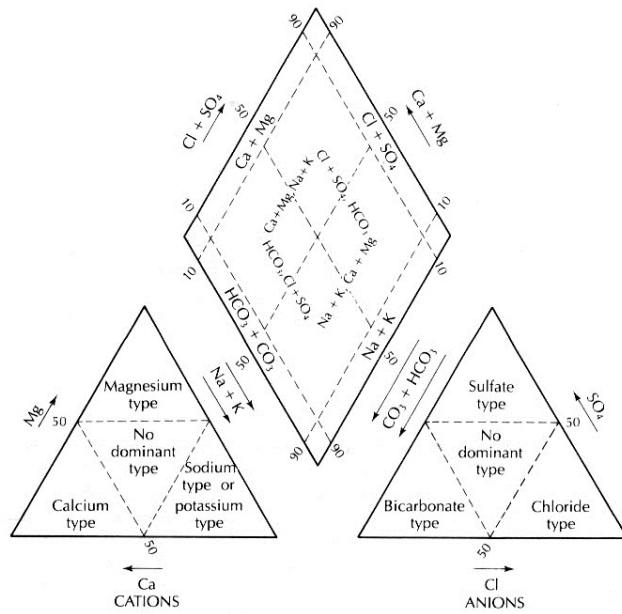
Figure 40. Hydrochemical facies based on percent of total equivalents of each ion (Fetter, 1994).
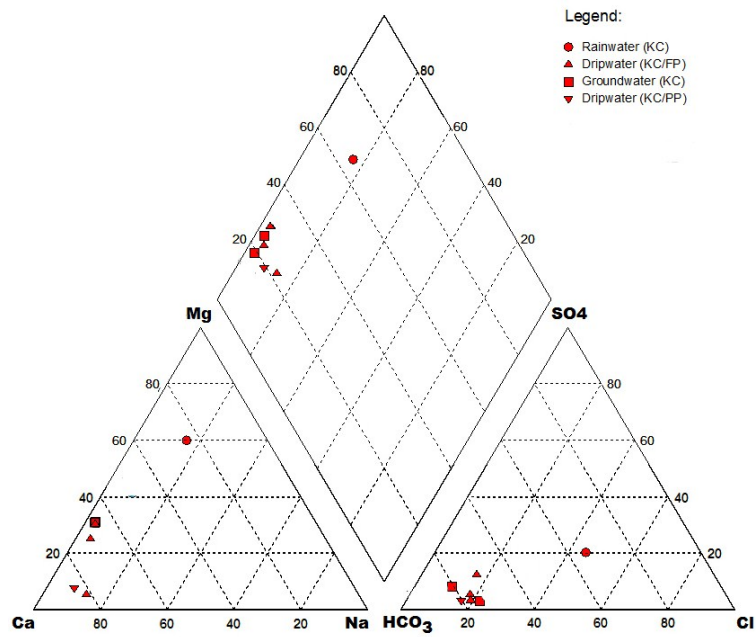
Figure 41. Piper diagram for October/November sampling results
(KC/FP: El Kassarat:cave/Forage Passage, KC/PP: El Kassarat cave/Salle du President's Passage).

94

4.1.8 Petrography and microscopy

Five thin sections for petrography and microscope analysis were collected from offcuts of the EKC-1 (Figure 42). The samples were collected close to the bottom of the candlestick section to visualize the change that might have taken place between those two sections of the stalagmite. Since EKC-01 was sent to the US at an earlier point in time, it was not possible to get thin sections directly from dated sections. They were polished to 180 μm, and the crystalline stratigraphy of the stalagmite was analyzed using an T-P meiji ml 9000 cannon 600D polarising microscope.

Small samples from the stalagmites were placed under a Tescan, Vega 3 LMU with Oxford EDX Detector (INCA XMAW20). The SEM was operated at an accelerating voltage of 30kV and a ~2nA beam. The sample was platinum coated and viewed under the scanning electron microscope.

Bands from the thin sections were microphotographed under plane and ultraviolet light using an Axiovert 200, Zeiss Flourescence and optical microscope with Zeiss Axiocam HRC and KS 300 V3 image analysis software. Microfabrics and banding were microphotographed under plane and ultraviolet light.

Figure 42. The locations of the thin sections collected and tested from the EKC-01 stalagmite.

All slides show compact columnar fabrics with large, composite crystals with

uniform extinction. These are typically forming in quasi-equilibrium conditions (low

supersaturation). The formation of columnar fabrics is mainly controlled by the constant

flow of waters that lacks impurities, which seems to be the case in the EKC-01. Those

columnar fabrics are composed of rhombohedral crystals faces.

96

In Figure 43, Slide 1 shows that crystals are elongated along the c-axis with alternating translucent and dark layers of calcite. Tips on the laminae are also visible with distinct growth bands created by layers of carbonate crystals. The photomicrograph show relatively thin, dark laminae of micritic impurities probably consisting of terra-rossa, clay or organic matter. In shallow caves, drip water is expected to carry some small amounts of organic material forming those dark bands, typical of the the El-Kassarat cave.

Figure 43. Straight composite crystal boundaries with uniform extinction (Slide 1 - 4x magnification, under crossed polars).

In addition, Figure 44 shows faint calcite laminae with blurry horizons of dark calcite laminae. These separate growth layers could be the result of seasonal changes of the growth.
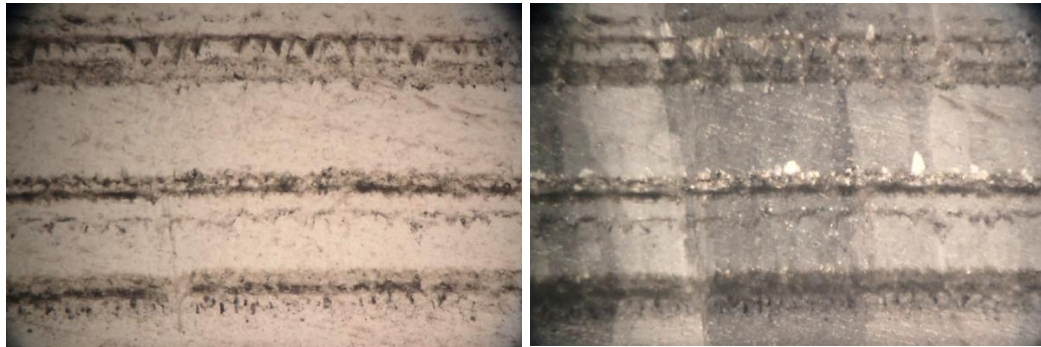
Figure 44. Photomicrograph of a thin section from the middle section of EKC-01 showing laminae of fluid inclusion horizons (Slide 1-4x magnification, Left: transmitted light, Right: crossed-polars).

Figure 44 and Figure 45 show the concentration of fluid inclusions aligned parallel to the growth layers of the stalagmite. They are thorn-shaped because of the constrictions that affect the inclusions (Figure 46). There is a clear horizon between inclusion rich and non-inclusion layers.
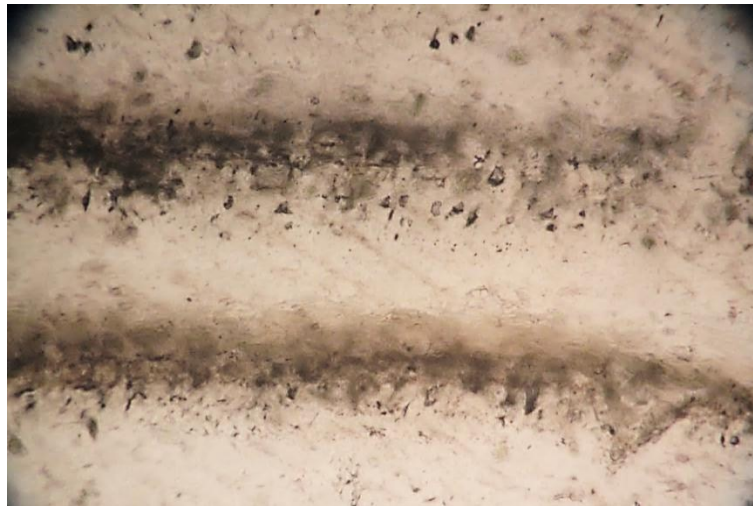
Figure 45. Fluid inclusions horizons (Slide 1-10x magnification).
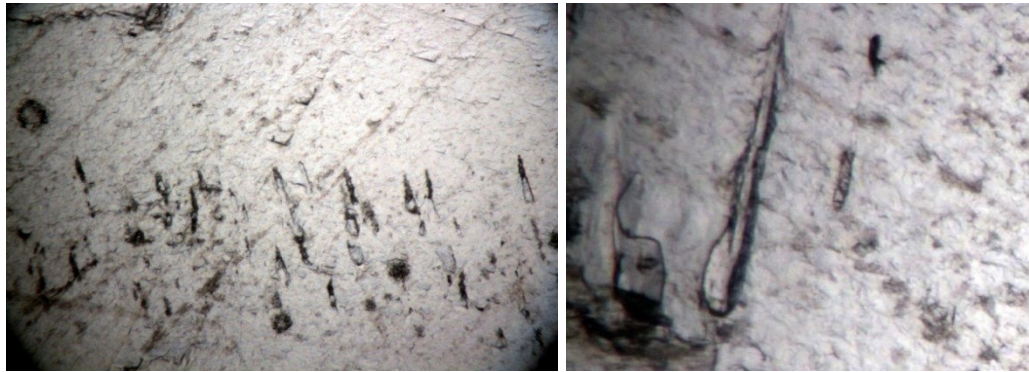
Figure 46. Left: Photomicrograph showing the thorn-shaped fluid inclusions (slide 2 - 4x magnification), Right: Photomicrograph shows a closeup view of a thorn-shaped fluid inclusion (slide 2 - 10x magnification).

Looking at those dark lamella in fluorescent light (Figure 47) reveals organic rich fluorescent laminae. Fluorescent laminae are caused mainly by changes of fluorescent constituents derived from the soil covers' humic material overlying the stalagmite location.
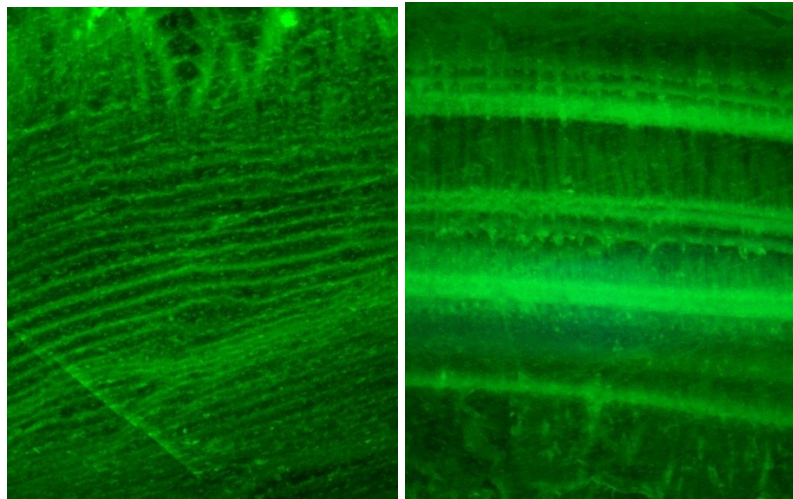
Figure 47. Left: Examples of luminescent excitation by UV light clearly showing laminations (slide 2 - 5x magnification, 0v, ph2, fs10). Right: luminescent excitation by UV light showing laminae (slide 1 - 5x magnification, ph2, fs10).

Figure 48 shows condensed dark laminae. It also shows the tips of the termination of crystals where dark impurities have deposited between the crystal tops.

Figure 49 shows dark calcite layers characterized by a high density of impurities. The tops of calcite crystals have euhedral terminations and micritic filling dissolution voids in the columnar crystal tips, as well as filling the depressions between crystal terminations. This fringe of crystals highlight the boundary between two calcite layers, and could be due to a thick film of water on the surface of the growing stalagmite.
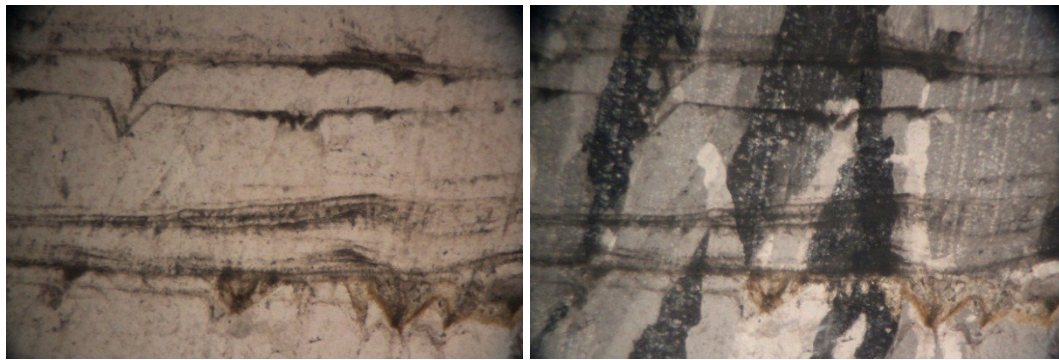
Figure 48. Crystal splitting can be observed in the transmitted light photomicrograph on the right (Slide 3, 4x magnification).
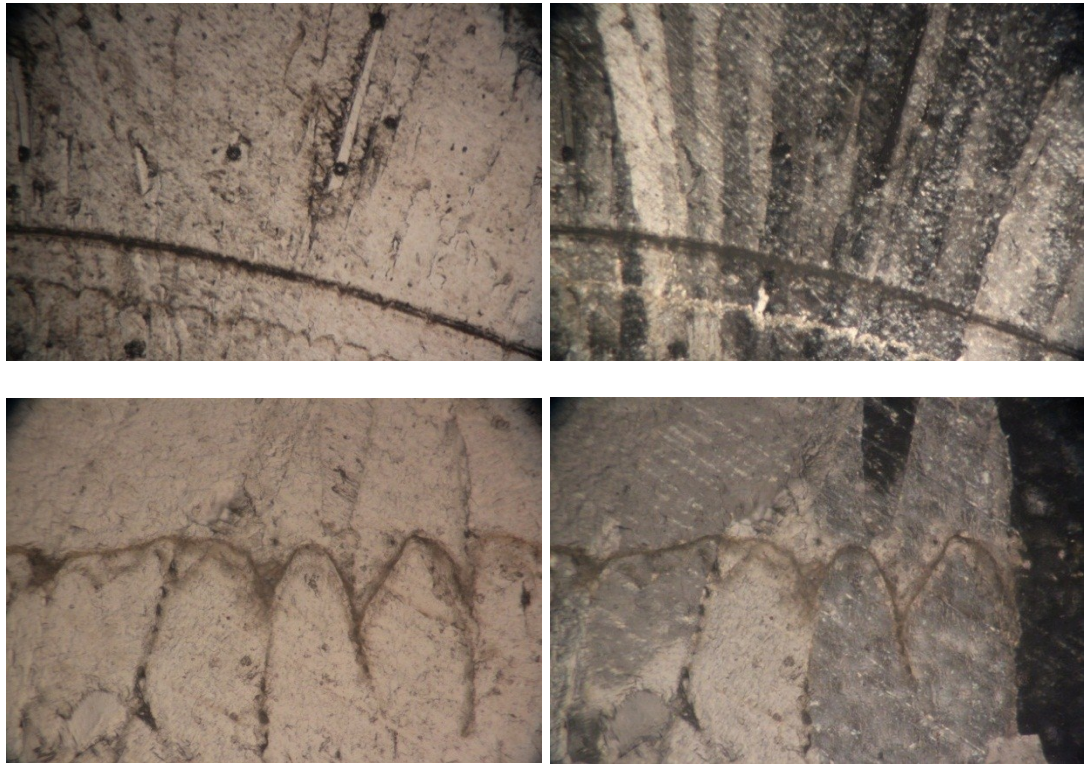
Figure 49. Slide 4 Truncated calcite crystal terminations. Detrital material and corrosion features (irregular crystal surfaces immediately below detrital layer) disrupt columnar calcite growth (4x magnification upper row and 10x magnification lower row).

Figure 50. Columnar fabric with irregular crystal boundaries, interfingered boundaries, growth laminae, dark, thin laminae organized in dark bands. Detrital material and corrosion features (irregular crystal surfaces immediately below detrital layer) disrupting columnar calcite growth. The photomicrographs on the left are taken in plane-polarized light while the right ones are using crossed-polars. (Slide 5,4x magnification upper row, 10x magnification lower row).

Figure 50 shows preserved bands with fine reddish-brown layers in columnar calcite. These dark layers could be iron oxide deposits or clay mineral. There is asymmetry in these layers, where clear calcite grades upward to cloudier calcite, then further upward to a dark layer. The whole pattern is vertically repeated but with different thicknesses.

4.2 Rahwe cave

One stalagmite was collected from Rahwe cave on the 21st October, 2012 and labeled RC-01. The Rahwe cave stalagmite was recovered about 80 m from the entrance of the cave, along the main axis of the cave. It was removed from a mud high about three meters above the groundwater level. Stalagmite RC-01 was not actively growing when it was collected. As mud deposits in this location were dry it was thought that water levels no longer reach the stalagmite level.

In addition to the stalagmite, other p-arameters were collected and measured including dripwater, recent calcite deposits, temperature and humidity readings were also collected. Dripwater samples were collected from two locations: one at the end of the constructed tunnel and the other close to the RC-01 removal site. Both were collected using a plastic funnel and bottle as shown in Figure 53, which were rinsed by the drip water prior to collection to minimize contamination effects. The drip-rate was approximately 1 drip every 9 seconds. Three sampling sessions on groundwater and dripwater were conducted in October 2012, June 2013 and August 2013. The pH, Conductivity, Temperature, and TDS of both groundwater and dripwater in the cave were tested on site using an OAKTON Handheld Water Meter, Eutec Instruments.

Glass plates, to collect modern calcite deposits, were collected from two locations close to the RC-01 removal site (Figure 51). Those recent calcite deposits collected were used for U/Th, mainly correction for detrital ^{230}Th. In additional to recent calcite deposits collected, scraped calcite from the tips of an actively growing stalagmites close

to the site of the harvested stalagmite was collected to obtain duplication in U/Th

corrections and in case no calcite growth occurred on the plates.

Figure 51. Calcite collection glass plate near RC-01.

A Tinytag temperature logger, Tinytag Plus 2 Internal Temperature, TGP – 4017

was placed 2 m away from the RC-01 removal site. The TGP – 4017 is a self-contained

temperature logger. The logger was calibrated to measure a reading every 15 minutes.

A Gemini TinyTag 2 Plus dual-channel temperature/relative humidity TGP-4500

data logger was used to measure the humidity level in the cave. The humidity in the

Rahwe cave averaged about 90%.

The RC-01 stalagmite was stabilized in epoxy. After the epoxy dried it was cut into

two halves along its growth axis at a rock cutting factory. The polished stalagmite half

was then sliced using a stone saw into $\approx$3 cm thick slabs (mainly to minimize shipping

costs). The complete slab was photographed (Figure 52) and then packaged and shipped

to the RSMAS center in Miami for isotopic analysis and dating.

Figure 52. Left: Rahwe cave locations of stalagmite removal site, Middle: Pouring epoxy resin to stabalize the stalagmite. Right: cutting the RC-01 into halves at a rock cutting factory.

The sampling locations inside the cave are shown in Figure 52. The location lies about 80 m from the tunnel entrance. All the devices were located approximately 3 m above the underground river level.
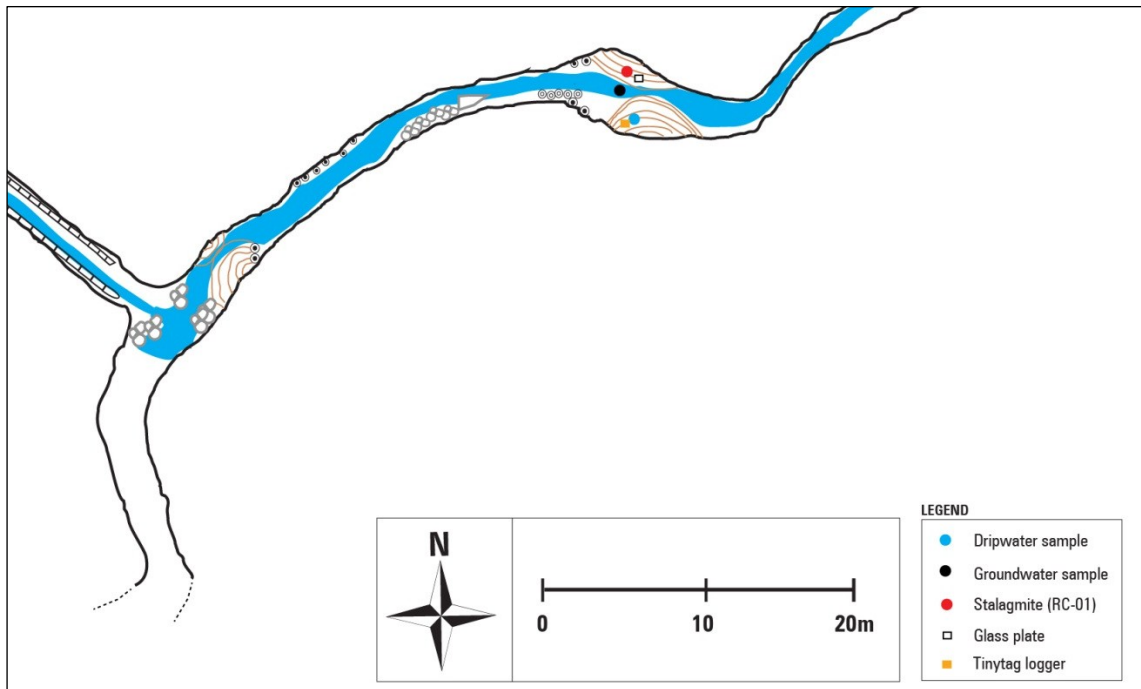
Figure 53. Rahwe cave locations of stalagmite removal site, dripwater, groundwater and calcite collection glass plate.

4.2.1   The RC-01 stalagmite visual description

Stalagmite RC-01 is 129.2 cm long. At its widest stalagmite RC-01 is 14 cm, and at its thinnest part it is 4cm. The laminae of the stalagmite curve at the apex, then thin and trail down the sides of the stalagmite (Figure 54). RC-01 has an inverted mushroom shaped base which still has some of the deposited clasts/pebbles from the cave deposits.

There appears to be some hiatuses in the stalagmite at 48.6 cm, 59.8 cm, 96.2 cm, 119 cm and 124.6 cm. These are seen as visual changes in the stalagmite's growth.

From the bottom of the stalagmite to around 18cm, the stalagmite consists of white laminated calcite. Then, at about 44cm, alterations of white and brown calcite laminae

are visible, with some dark brown layers that may be interpreted as flood zones (Gázquez *et al*., 2014). On these horizons, the calcite laminae tended to come apart from each other, and the mud deposits could be clearly identified. At around 60cm, there appears to be a major visual hiatus, where white calcite laminae changes to alterations between dark brown and white calcite. These dark and white alterations continue, until, closer to the top, at around 95cm, the stalagmite's white laminae become more numerous than the brown ones (Figure 54).

The stalagmite seems to have grown without any major lateral shifts. There are also some voids where mud was washed out during the cutting and polishing processes. The dark calcite tends to be with impurities such as mud.

There are small depressions at the top of some laminae indicating where the drips had penetrated the top of the stalagmite as it grew. There are also some corrosion areas throughout the stalagmite center.
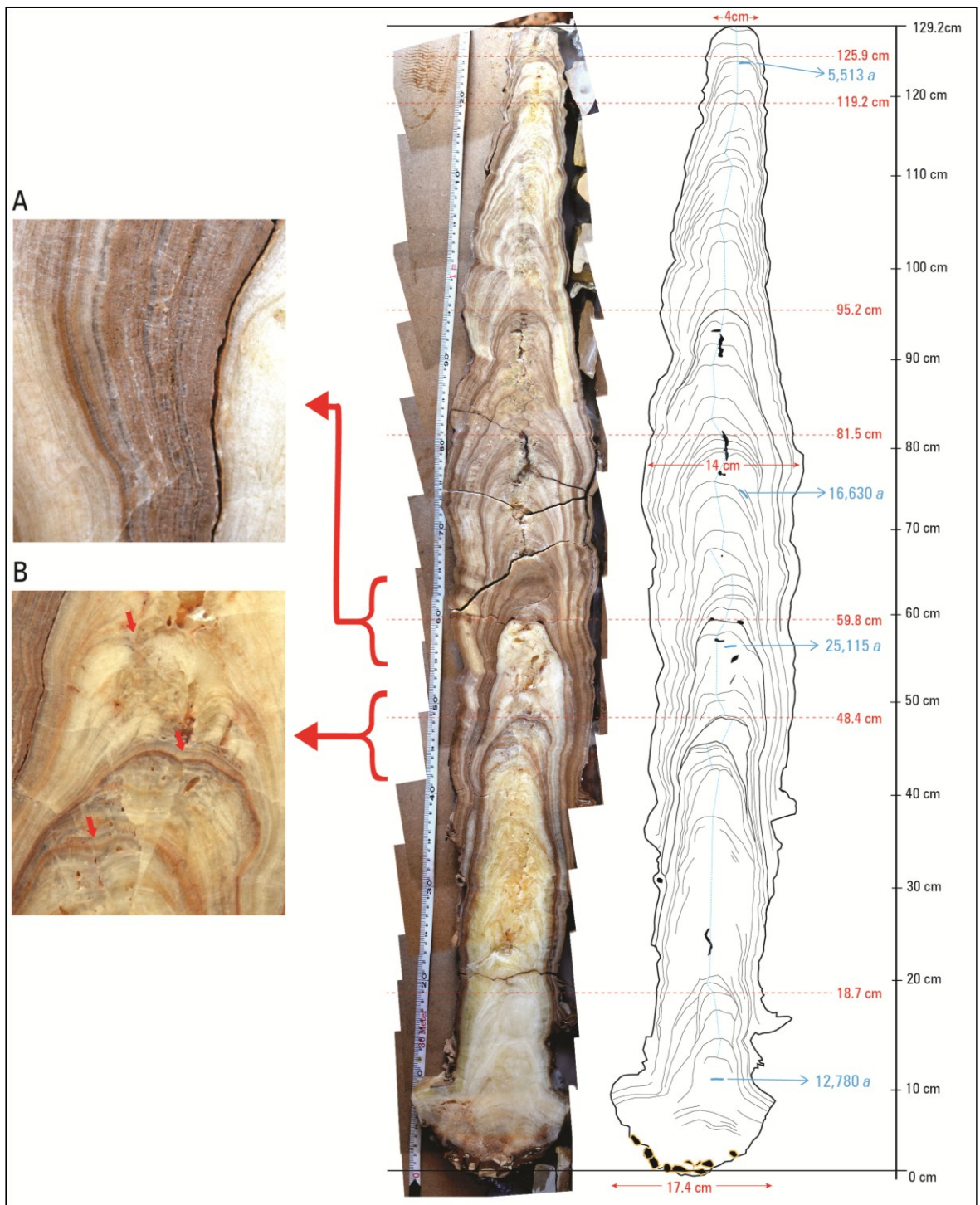
Figure 54. The RC-01 stalagmite measurement details with age sample locations. The breakages in the stalagmite occurred as a consequence of the slab cutting.

108

4.2.2 Cave air temperature

The minimum cave air temperature was measured from November 2012 to August 2013. The minimum reading recorded was -0.7ºC, and the maximum reading was 5.6ºC (Figure 55).
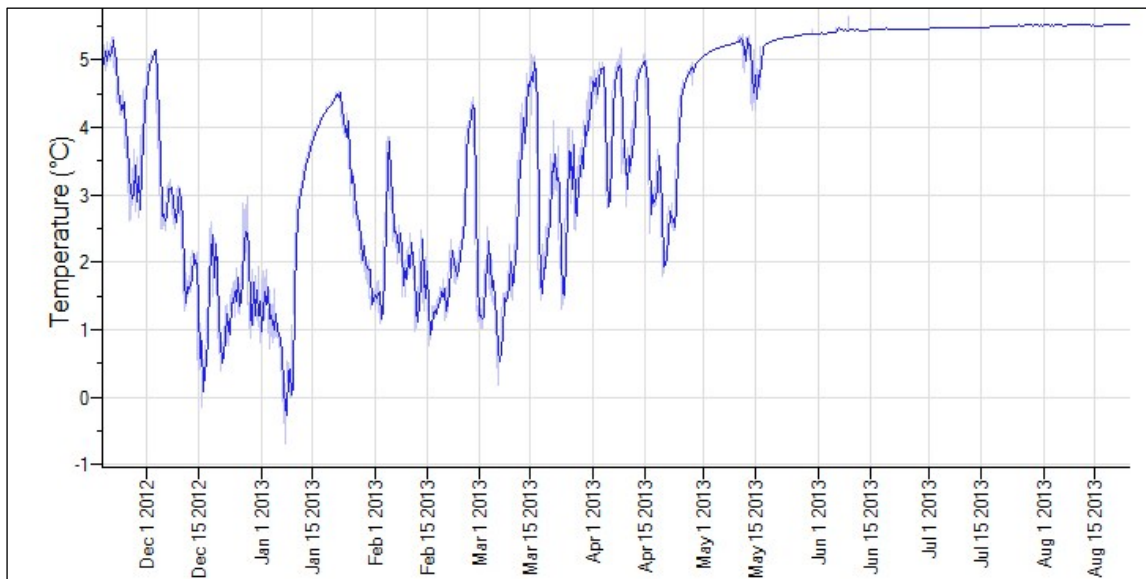
Figure 55. The Rahwe cave cave air temperature variations through time using the Tinytag logger.

Air temperature inside the cave was not stable from November 2012 to about May 2013, displaying sharp rises and falls. The air cave temperature only stabilized at the end of May 2013 where the temperature rose steadily with no spikes. This might be due to a direct interaction with surface temperatures or due to an increase/decrease in the groundwater flow, which in turn affected wind currents inside the cave. There is also a

possibility that snow blocked the entrances of the cave and groundwater flow banked

inside the cave, maybe submerging the Tinytag logger on separate occasions.

4.2.3   Precipitation collection

Rainwater near Rahwe cave was collected on the road leading to the cave, at

coordinates 34°11'56.33"N and 35°56'54.31"E, at an elevation of 1,696m. This location

is approximately 12.5 km away from the Rahwe cave entrance.

Precipitation and surface temperature data were obtained from the Meteorological

office at the Beirut International Airport for their Tannourine station. The Tannourine

gauging station is nearly 5 km from the cave's location. The location can be seen in

Table 6. The closest gaging station to the Rahwe cave. It shows the closest

meteorological station to the cave location.

Table 6. The closest gaging station to the Rahwe cave

Cave name	Station name	Elevation (m)	x-coordinate	y-coordinate
Rahwe cave	Tannourine	1838	34:12,467	35:55.896

From Figure 56 it is possible to correlate the surface air temperatures with the cave

temperature. An increase in precipitation with a decrease in surface temperature also

caused dips in the cave temperatures. This implies that current air temperatures are

directly affected by the surface temperatures, and the cave's temperature is not stable in

this location. It must be noted that the entrance of Rahwe cave was only opened in the

1960's. Before this date cave temperatures were probably more stable.

110
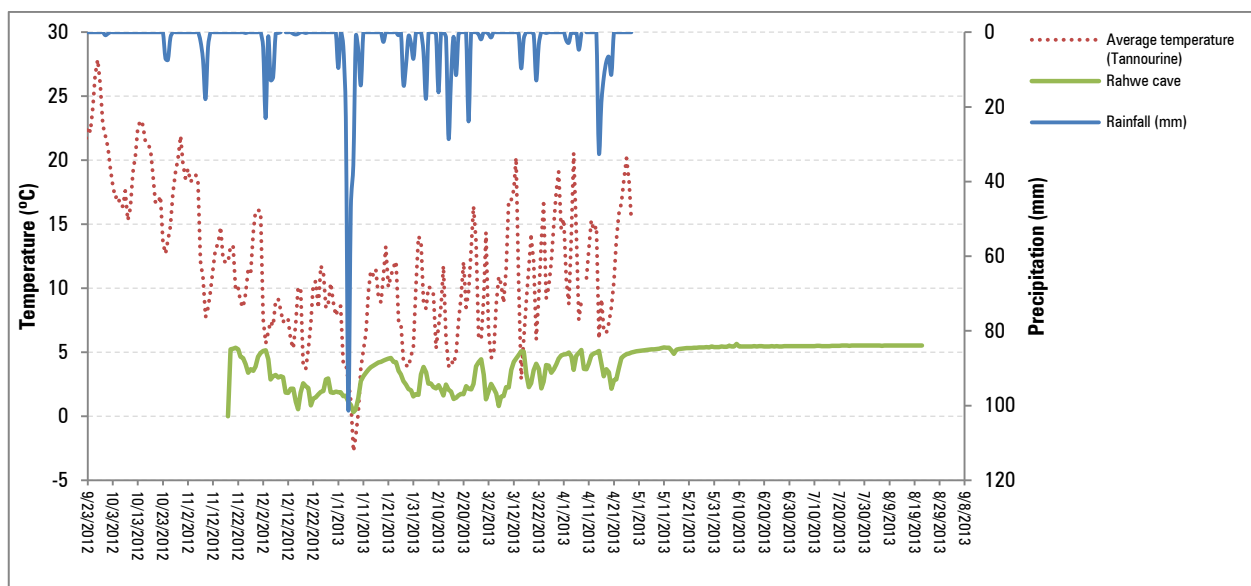
Figure 56. The Rahwe cave cave temperature chart with precipitation rates and surface temperature, for nearly a year.

4.2.4   Uranium-Thorium dating

The integration of detrital thorium in a stalagmite's laminae may occur due to the cementation of clay or sand on the growth surface of the speleothem. Clastic sediments can also be assimilated by flooding events where mud depositions are deposited on the growth surface of the stalagmite. These deposits are consequently sealed when they are later covered with calcite precipitation. Pure precipitated cave calcite's ^{230}Th value, with no added clastic sediments (*i.e.* time of deposition), is zero. Thorium present in the clastic sediments in stalagmite laminae is indistinguishable from that of the stalagmite and the sampling dating values become skewed.

111

An age reversal (isotopic ages are in opposite order to the stratigraphic ages) is present in the RC-01 stalagmite. At this time, a construction of the time series was not possible due to this. Carbon and Oxygen isotopic sampling were not undertaken on this stalagmite for this reason as well. No additional U/Th sampling on the RC-01 stalagmite was possible due to time and budgetary restraints. However, better investigation and sampling techniques of the RC-01 stalagmite might reveal that the reversals are simply due to bad sampling locations. Therefore, additional testing on this stalagmite is required, and it is beyond the scope of this investigation.

4.2.5 Institute and laboratory physico-chemical results of groundwater and dripwater

4.2.5.1 In situ tests

4.2.5.1.1 pH levels

The pH in the groundwater decreased from 8.38 to 8.06. While the dripwater at the entrance location increased from 8.02 to 8.08. And the entrance dripwater decreased from 8.18 to 8.13. The maximum decrease is around 3.5%, which is not that significant. However, the average Rahwe cave entrance site dripwater pH average value is 8.05, the stalagmite site dripwater pH average value is 8.16, and the groundwater average value is 8.13. These values are close to that of rainwater's pH value, 8.22 (Figure 57). This indicates that the groundwater has not had enough time to undergo considerable pH changes as it percolates through the soil and rock strata. The values indicate fast

112

recharge from rainfall, with a short residence time. The size of the catchment area is of importance with respect to residence time of the groundwaters, with the catchment area of the El-Kassarat cave being considerably larger than that of Rahwe cave.
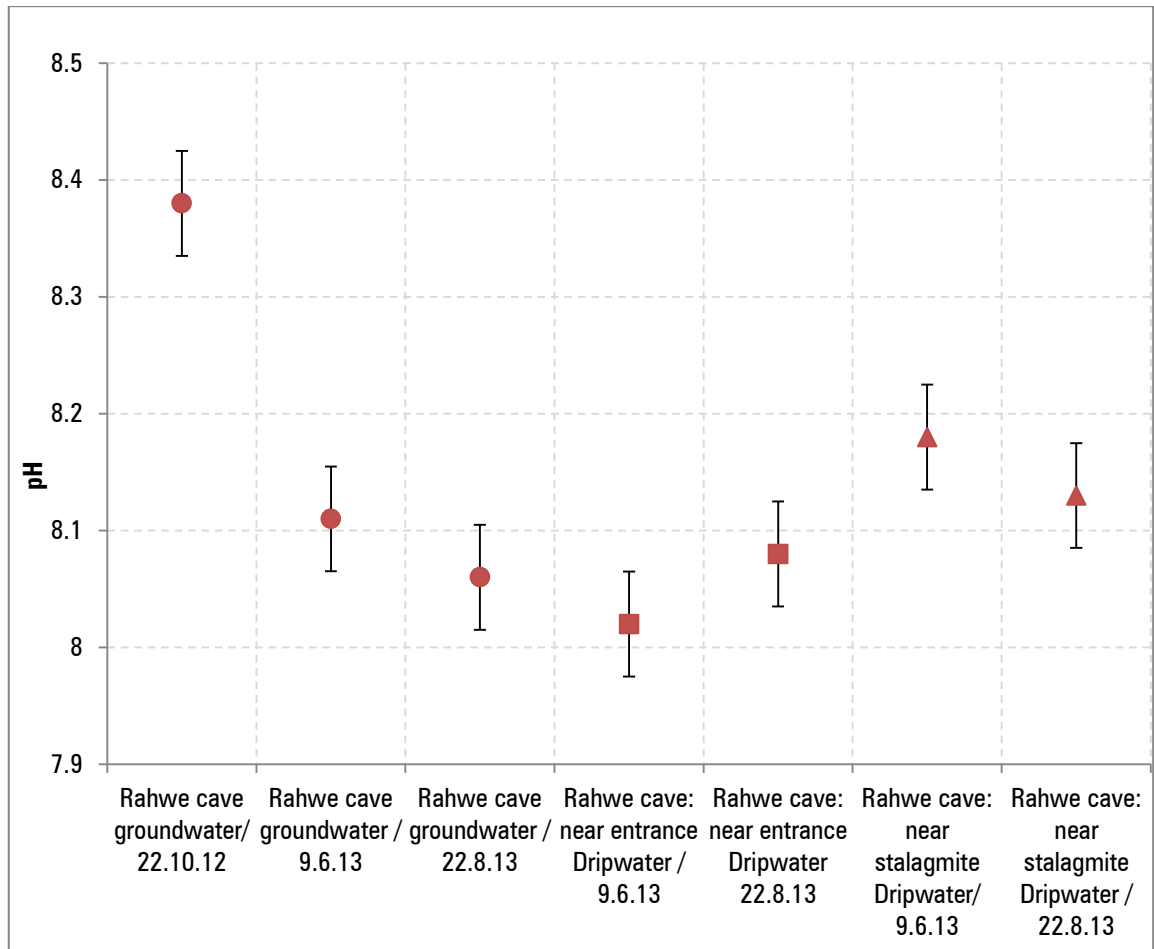
Figure 57. pH levels of various waters from the Rahwe cave.

4.2.5.1.2 Water temperature levels

The temperature in the groundwater decreased from 5 ºC to 4.9 ºC. While the
dripwater temperature at the entrance site was 7ºC while the dripwater temperature at
the stalagmite location was 5.9ºC (Figure 58). Although rainwater temperature was not
measured it is safe to assume that the groundwater is still a lot lower than that of El-
Kassarat cave indicating a faster percolation rate and less residence time.

The catchment area of the Rahwe cave is nearly 1.3 km^2. The farthest distance that
the water has to travel in the Rahwe cave catchment is approximately 1 km (Figure 59).
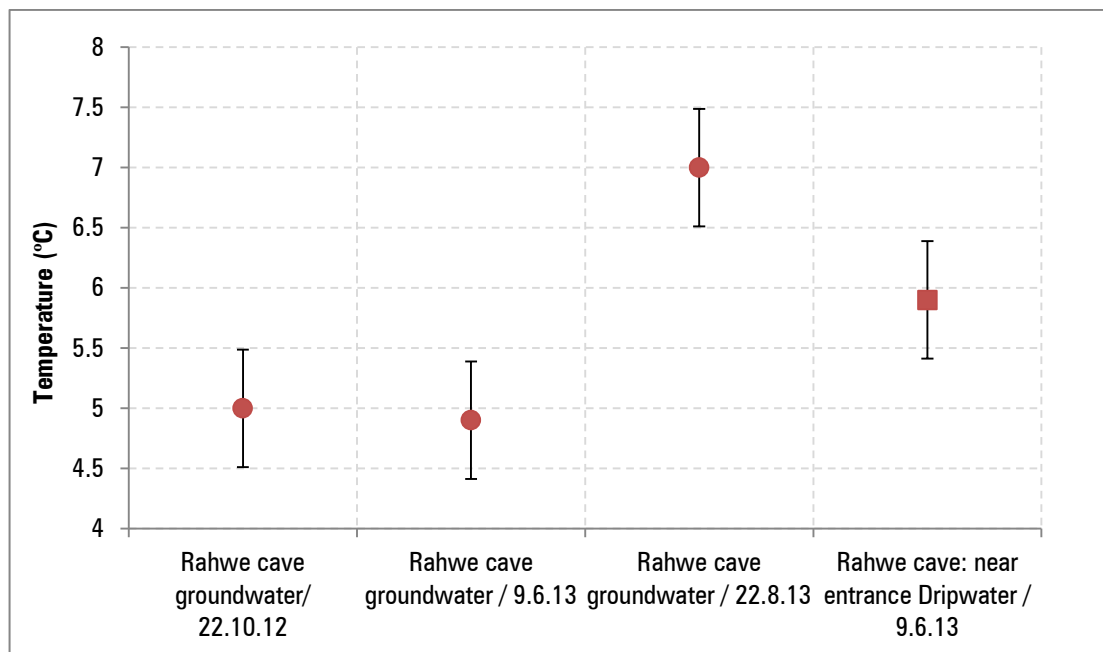
Figure 58. Groundwater and dripwater temperature in Rahwe cave.
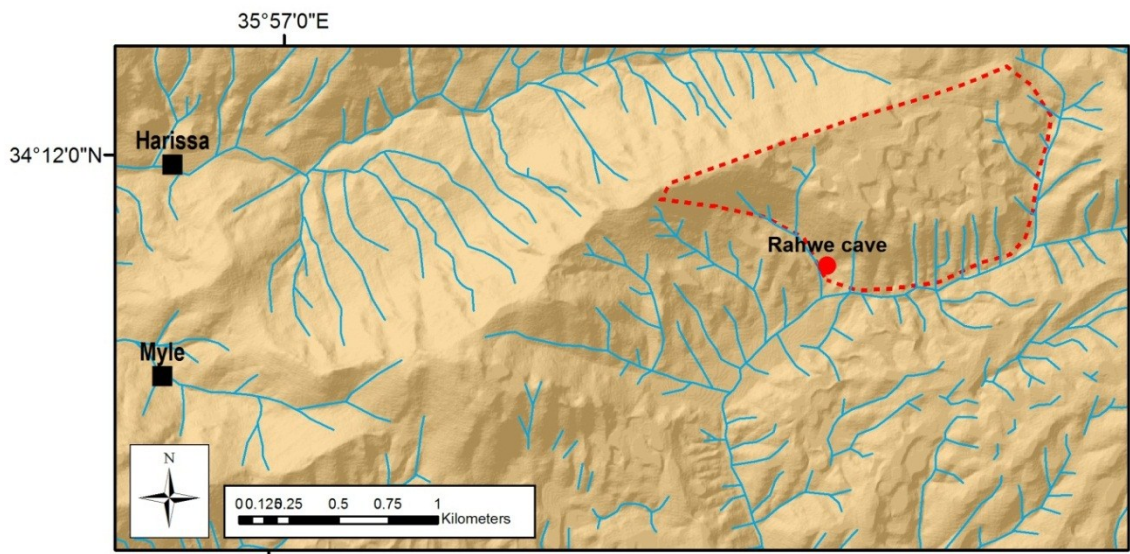
Figure 59. Possible catchement area of the Rahwe spring measuring nearly 1.3 km^2 in area.

Rahwe cave waters' temperature is lower than those of El-Kassarat cave because of the difference of altitude between the two caves. In Rahwe cave, the groundwater does not have to travel a very long distance to reach the cave so it does not have the time to decrease in temperature. The Rahwe cave dripwater temperature is slightly higher than the groundwater due to the residence time of the water due in turn to the size of the catchment area.

4.2.5.1.3 Conductivity levels

It is difficult to identify a trend for conductivity levels but a general variation can be assumed. There is steady values of conductivity from winter to summer months with only a few variations. The values of 243 to 226µs for groundwater, 213 to 198.3µs for

115

the entrance site dripwater location, and 264 to 198.7µs for the stalagmite site dripwater location are indicative of this (Figure 60). This is indicative of the residence time of the water in the aquifer. Lower residence time causes lower conductivity values.

The Rahwe cave aquifer consists mainly of karstified limestone with little or no surface soil cover. This allows for fast percolating of surface water into the aquifer with little surface evaporation or temperature changes. The average temperature of this high elevation cave also effects the rate at which CO_2 dissolves in the water since there is an increase in dissolution at lower temperature, making the water more carbonic and so there is an increase in water erosion.

The average air temperature at this high altitude cave ($\approx$13ºC for years 2001 to 2013 (Meteorological Office) influences the rate of solubility of CO_2 in the groundwater (Fetter, 1994). The increase in solubility of CO_2 will increase its acidity, thus lowering the pH values. When the groundwater comes into contact with the marly limestone of the Sannine-Maameltein Formation it dissolves it at a higher rate.
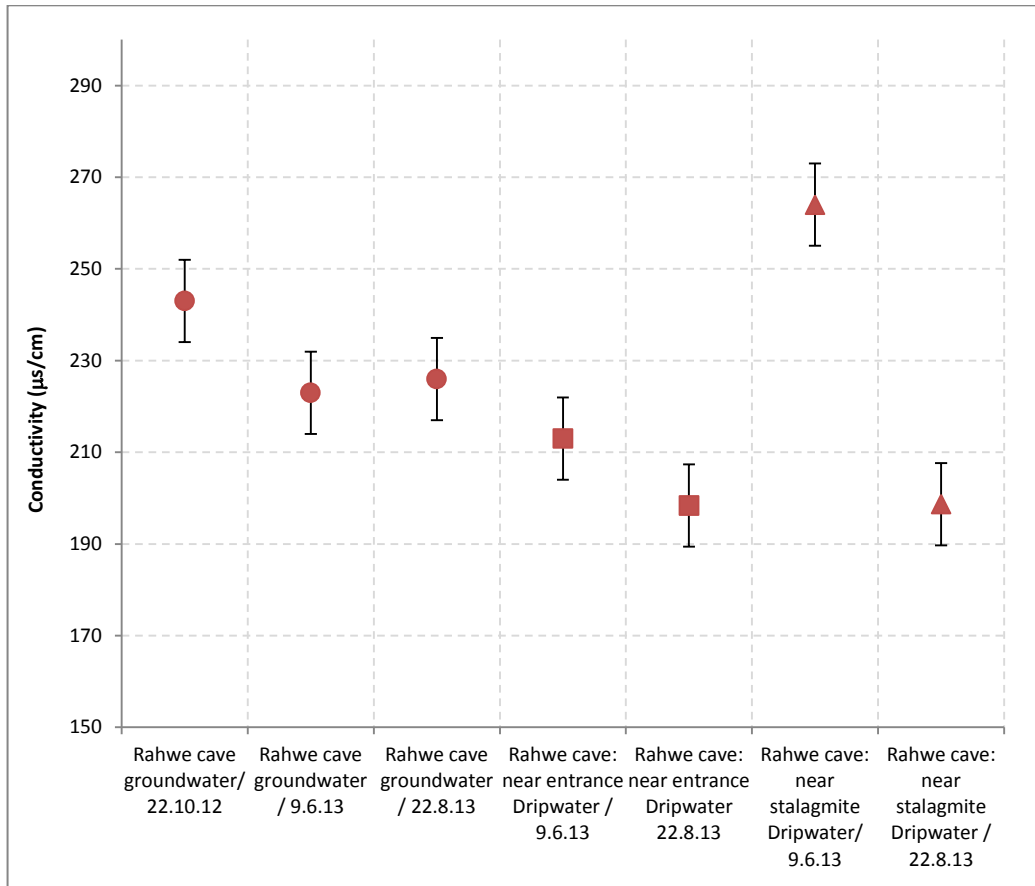
Figure 60. Groundwater and dripwater Conductivity levels in the Rahwe cave.

4.2.5.2 Laboratory sampling results

Samples were tested at the AUB environmental Laboratory in the Engineering Faculty. Appendces 8 and 9 shows the results of the chemical and physical analysis of rainwater, snow, groundwater and dripwater.

Turbidity values are low (the highest value measured is 2.2), due to the lack of extent of soil cover that could increase the sediment quantity with the percolating water.

The results of the calcium parameter show that the calcium range in summer and winter are affected by the quantity of water as well as the residence time, with conductivity values from winter to summer months varying, 153.8 to 136.1 μs for groundwater, 146.6 to 160.2 μs for the stalagmite site dripwater, and 142.2 μs for the entrance site dripwater. The calcium range in summer is higher than that in winter, indicating probably more flushing in winter months due to an increase in precipitation, and a shorter waters' residence time and less calcium from the host rock dissolving into the water. The magnesium levels are lower in winter, they increase during the summer, probably due to the same reasons as those of the calcium cations (Figure 61).

All measurements have lower Mg^{2+} values except for the snow. This could be because, when the snow is in contact with the rock, it dissolves calcium, allowing its concentration to increase.
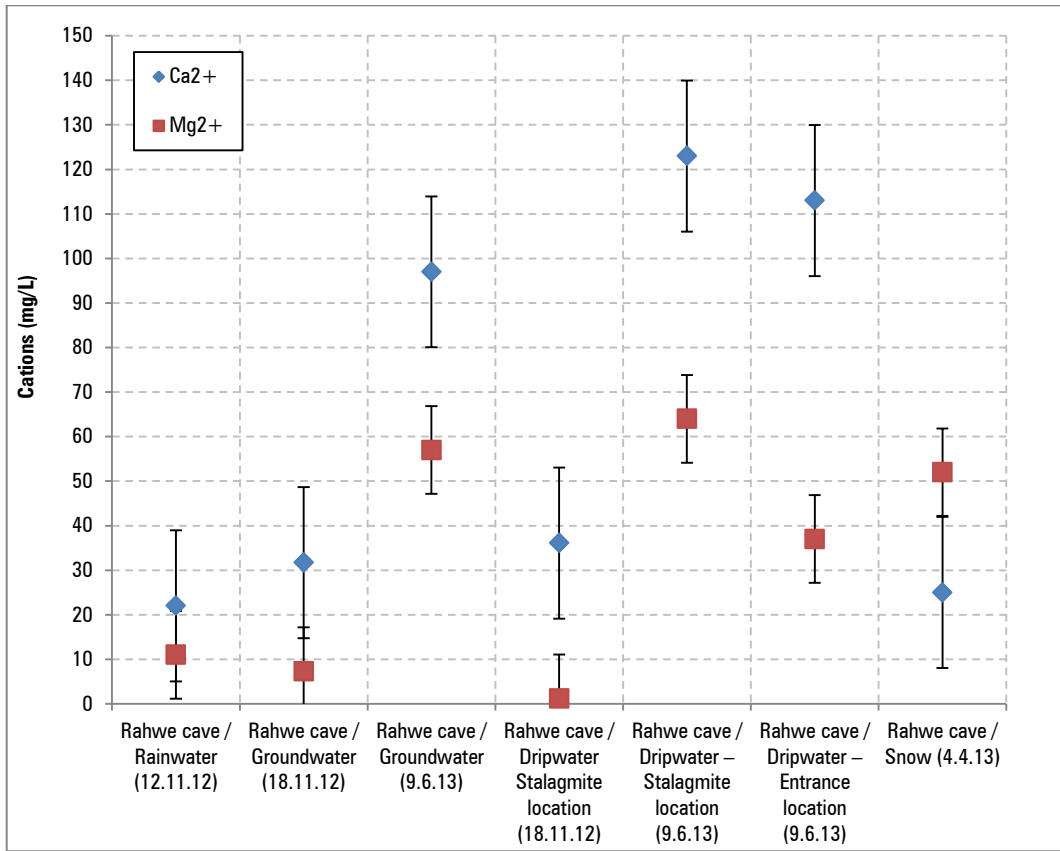
Figure 61. Ca^{2+} and Mg^{2+} concentrations of rainwater, snow, groundwater and dripwater for the Rahwe cave.

The potassium and sodium levels appear to remain similar for winter and summer probably implying that there is no added input from external sources (Figure 62).

119
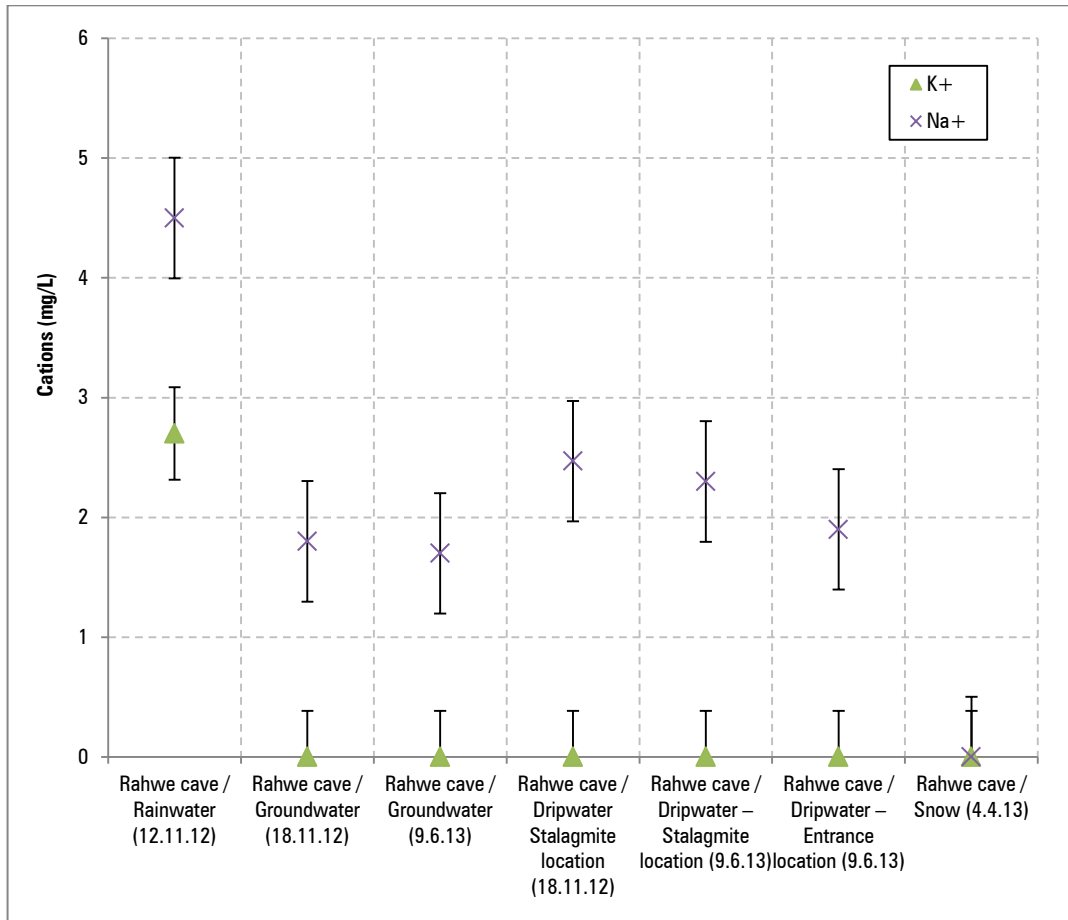
Figure 62. K$^+$ and Na$^+$ concentrations of rainwater, snow, groundwater and dripwater for the Rahwe cave.

Rainwater and snow K$^+$ and Na$^+$ values are different because they could be from different precipitation events. Snow was collected from a thick 1 m layer close to the rainfall collection site, while rainfall was collected from a onetime storm event. These two locations are approximately 3 km west of the cave entrance.

4.2.5.3   Piper Diagrams

The piper diagram shows that the Rahwe cave aquifer is a Calcium-Magnesium/ Bicarbonate type hydro-chemical facies, which is indicative of a limestone aquifer (Figure 63).

The winter and summer chemical composition of the groundwater and dripwater match, indicating that the waters are coming from the same aquifers during winter high and summer low discharges.
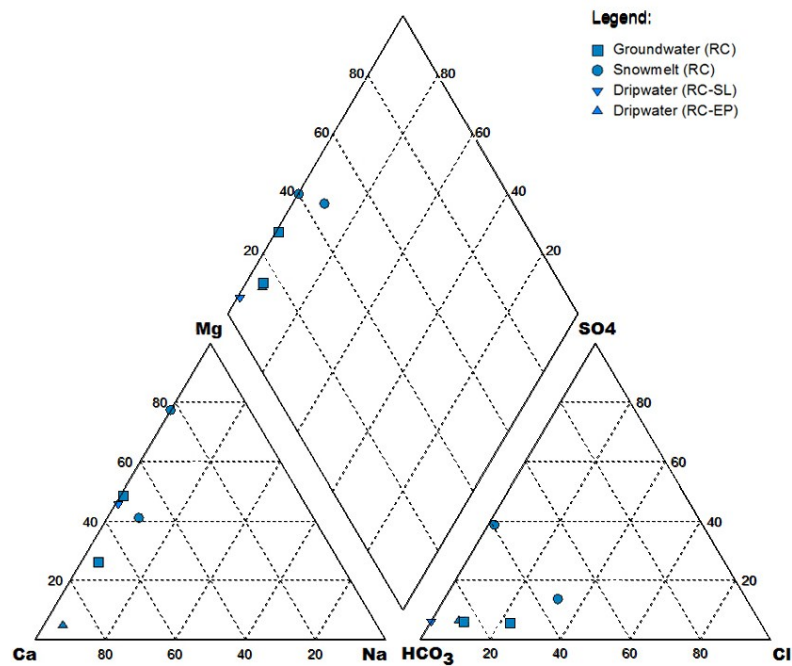
Figure 63. Piper diagram for June sampling results (RC: Rahwe cave, RC-SL: Stalagmite location, RC-EP: Entrance location).

4.2.6   Petrography and microscopy

Five thin sections for petrography and microscope analysis were collected from the offcuts of the RC-1 (Figure 64). The samples were collected close to the bottom of the stalagmite, with one close to the center section. The thin sections were polished to 180μm and the crystalline stratigraphy of the stalagmite was analyzed using an T-P meiji ml 9000 cannon 600D polarising microscope.

Small samples from the stalagmites were placed under a Tescan, Vega 3 LMU with Oxford EDX Detector (INCA XMAW20). The SEM was operated at an accelerating voltage of 30kV and a ~2nA beam. The sample was platinum coated and viewed under the scanning electron microscope.

Bands from the thin sections were microphotographed under plane and ultraviolet light using an Axiovert 200, Zeiss Flourescence and optical microscope with Zeiss Axiocam HRC and KS 300 V3 image analysis software. Microfabrics and banding were microphotographed under plane and ultraviolet light.

Figure 64. The locations of the thin sections collected and tested from the RC-01 stalagmite.
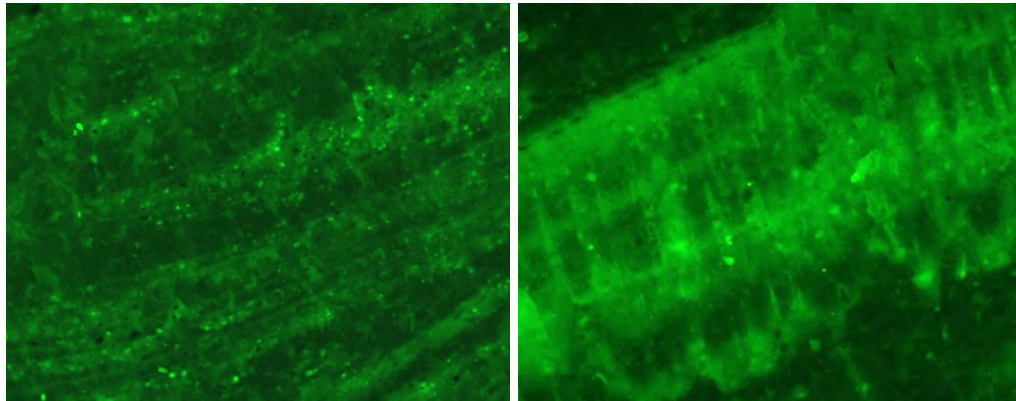
Figure 65. Left: Luminescent excitation by UV light from RC-01 thin sections showing fluorescent laminae not visible under transmitted light (Left: Slide 1 - 10x magnification, 4v, ph2, fs10) , Right: (Slide 5 - 10x magnification, 0v   ph2   fs10 – fl).

Figure 65 shows laminations under fluorescent light, with some laminae befainter than others. These laminations can represent annual layers where parameters (*e.g.* dripwater rates, pCO_2) afore mentioned make the laminae either thicker or thinner.
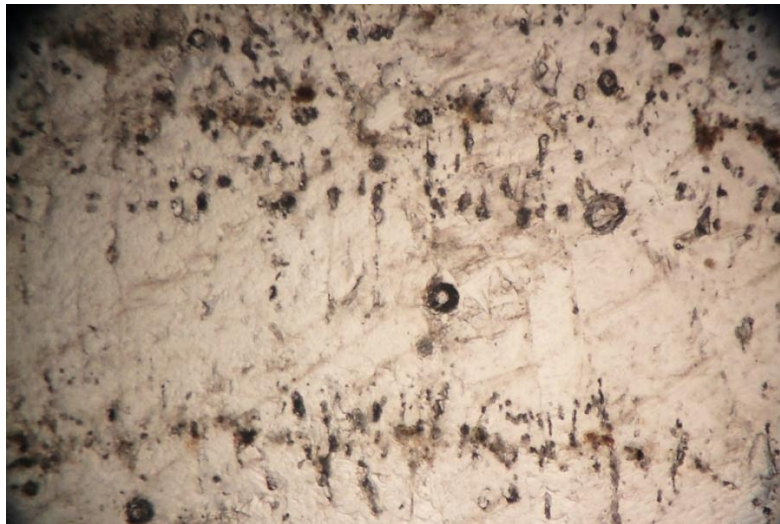
Figure 66. Fluid inclusion horizons under transmitted light (Slide 6 - 4x magnification).

Figure 66 shows a concentration of fluid inclusions aligned parallel to the growth layers of the stalagmite. They are ellipse-shaped inclusions and there is a distinctive horizon between inclusion rich and calcite layers. Thicker layers contain no major inclusions, and thinner layer have small and abundant inclusions.
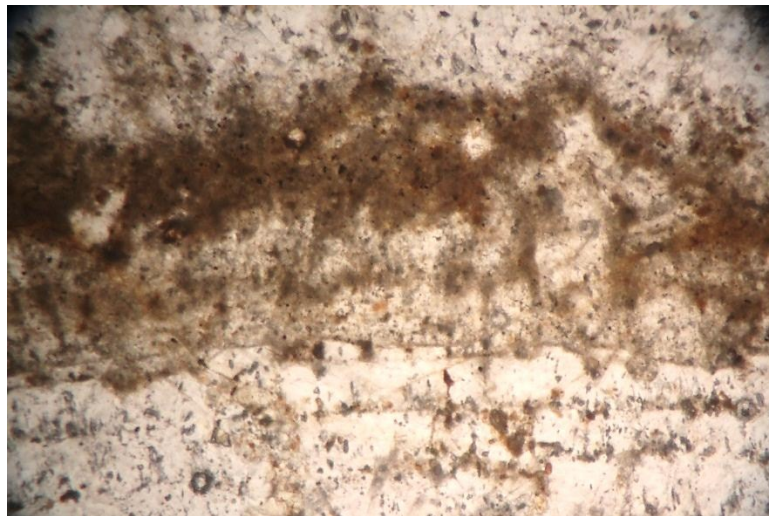
Figure 67. No clear laminae can be identified. There are some fluid inclusion horizons on the lower section of the photomicrograph (Slide 7, 4x magnification).

Figure 67 shows no clear lamina, but the bottom has some inclusion horizons. There appears to be some brown coloured material, which could be a detrital zone, where mud or terra-rossa was deposited over the calcite crystals. The brown material seem to have deposited in between the crystals.

125
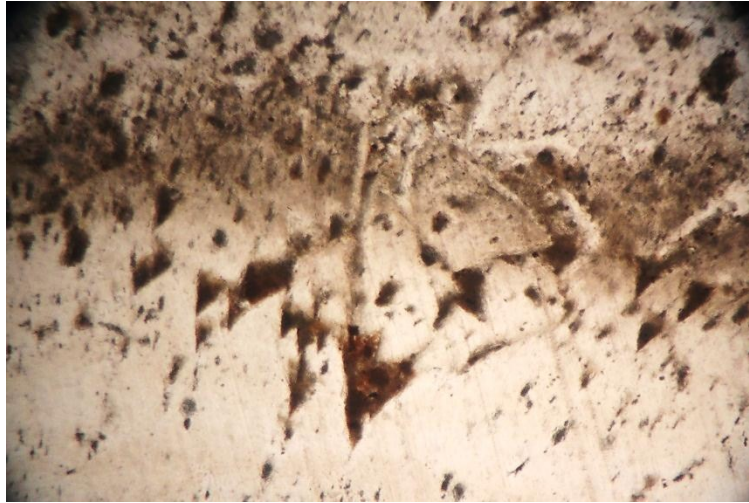
Figure 68. Trigonal calcite crystals – note the dark patches (Slide 7, 4x magnification).
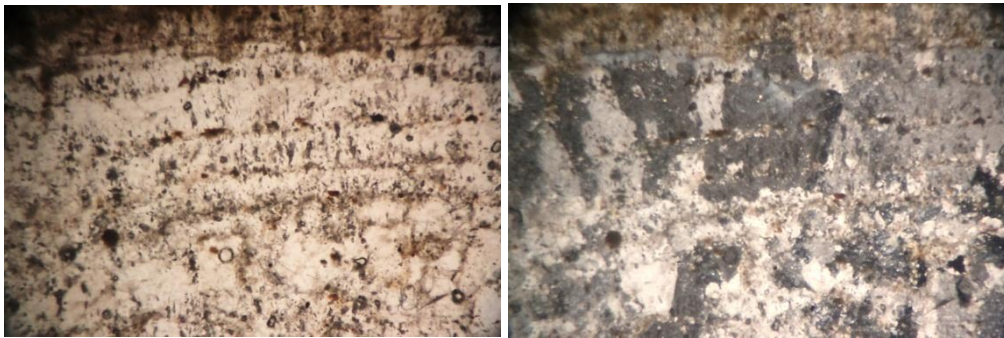
Figure 69. Faint laminations present, Left: transmitted light, Right: crossed polars (Slide 6, 4x magnification).

Figure 68 shows trigonal calcite crystals where dark patches could be impurities within intercrystalline porosity. Figure 69 shows how the crystals appear to become larger with the successive growth layers.
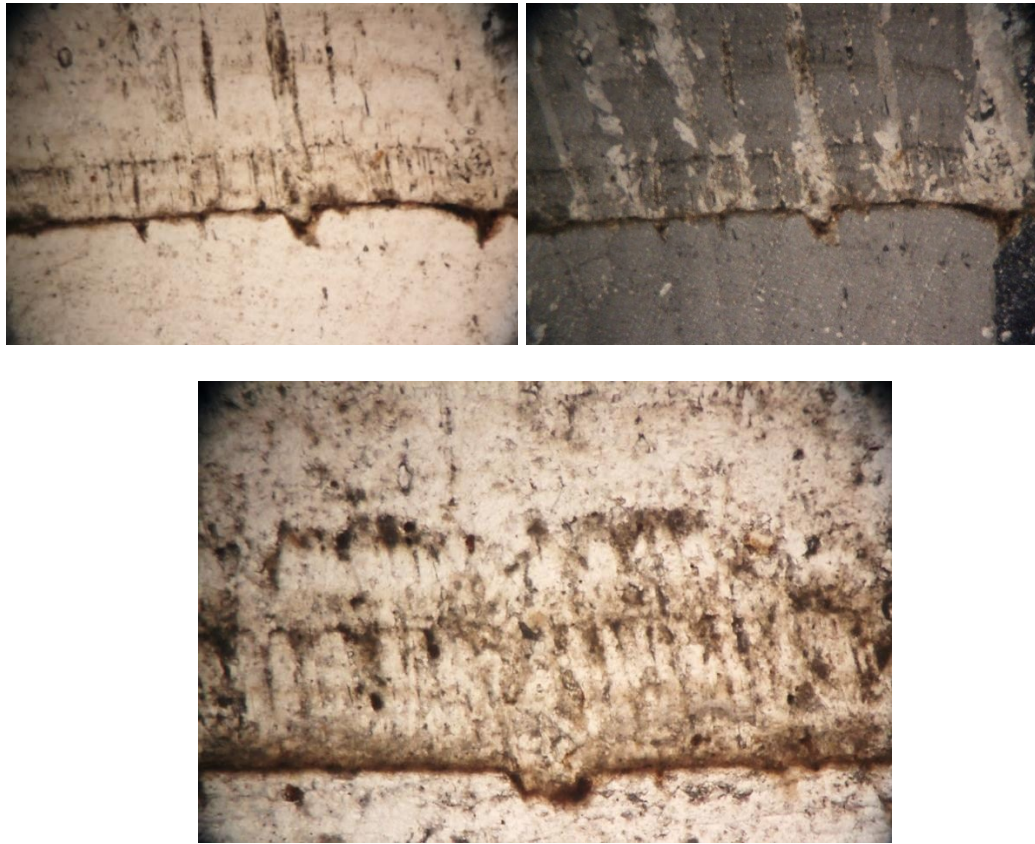
Figure 70. Top: transmitted light photomicrograph showing the "purification" of the mud-envelope by calcite spars (Left: transmitted light, Right: crossed polars - Slide 10, 4x magnification). Bottom: Dissolussion vug located at the bottom section of the photomicrograph (Slide 10, 10x magnification).

Figure 70 shows laminae with horizons made-up of calcite crystals, with tips infilled with brownish impurities. A dissolution vug can be observed in the bottom middle of the image, which has become infilled with detrital material. These dark impurities horizons could be interpreted as flood deposits.

127

4.3   Isotopic compositions of present day waters from the Rahwe and the El-Kassarat caves

In total, fourteen groundwater, dripwater and rainwater samples from El-Kassarat and Rahwe cave were collected at the end of 2012 and in the middle of 2013. They were analyzed for isotopic concentrations in Hacettepe University International Research and Application Center for Karst Water Resources Stable Isotope Laboratory in Turkey.

The cave dripwater isotopic composition depends upon differing factors such as the composition of the marine source, the evolution of the rainfall, the continentality, the altitude, the precipitation quantity, the air temperature, and changes of the water in the vadose zone due to its interaction with soil and rock. Thus, a potential relationship exists between the oxygen isotope composition of seawater, the climate and climatic controls of rainfall, and the isotopic composition of speleothems (Bar-Matthews *et al.*, 2003).

Figure 71 plots the $\delta^{18}O$ and $\delta^{2}H$ of the 14 samples collected. Detailed data are presented in Appendices 11 and 12. The isotopic values in $\delta^{18}O$ for the sampled rainwater collected were -12.37‰ for Rahwe cave and -5.75‰ for El-Kassarat rainwater. $\delta^{2}H$ values typically ranged between -70.45 and -31.67, for Rahwe cave and El-Kassarat cave respectively.

The isotopic values in $\delta^{18}O$ for the sampled groundwater collected were -8.23‰ for Rahwe cave and -6.84‰ for the El-Kassarat underground river in November, 2012. In June, 2013, the $\delta^{18}O$ isotopic values for the sampled groundwater collected were -

128

8.65‰ for Rahwe cave, and -7.48‰ for the El-Kassarat underground river. δ^2H values were -43.10 and -33.18 for Rahwe cave and El-Kassarat cave respectively in November 2012. δ^2H values were -45.33 and -36.54 for Rahwe cave and El-Kassarat cave respectively in June, 2013.

The isotopic values in δ^{18}O for the sampled dripwater collected were -8.51‰ for Rahwe cave (near stalagmite site) and -5.22‰ for the Salle du President's Gallery in November, 2012. In June, 2013, the δ^{18}O isotopic values for the sampled groundwater collected were -8.53‰ for Rahwe cave, and -5.41‰ for the Salle du President's Gallery. δ^2H values were -46.41 and -24.10 for Rahwe cave and El-Kassarat cave respectively in November, 2012. δ^2H values were -45.97 and -22.56 for Rahwe cave and El-Kassarat cave respectively in June, 2013.
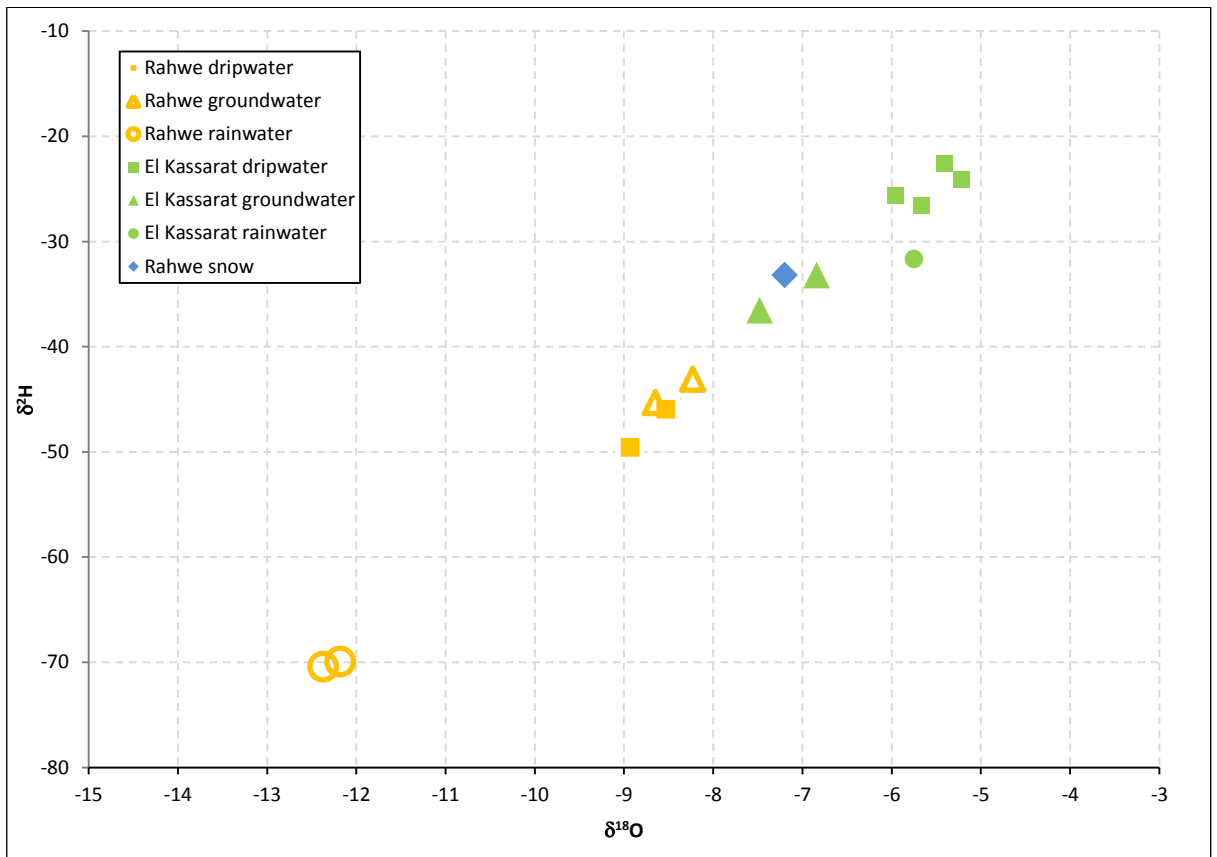
Figure 71. $\delta^{18}O$ and δ^2H values for the El-Kassarat and Rahwe caves groundwaters, rainwater and snow values.

CHAPTER 5

RESULTS AND DISCUSSION

This chapter will provide an in depth investigation of the results, mainly focusing on the El Kassarat cave and the EKC-01 stalagmite collected from it and the understanding of the paleo-environment from this calcite record.

5.1 Isotopic composition of rainwater and cave water

Lebanon is situated in the Eastern Mediterranean region. Its geomorphology, various climatic environments, and different air mass origins (Figure 5), make it complex to characterize the precipitation isotopically. This generates a diversity in the quantity, isotopic composition and chemical properties of the precipitation. This is an essential parameter that must be addressed for any isotopic study, as there have not been many such studies in Lebanon.
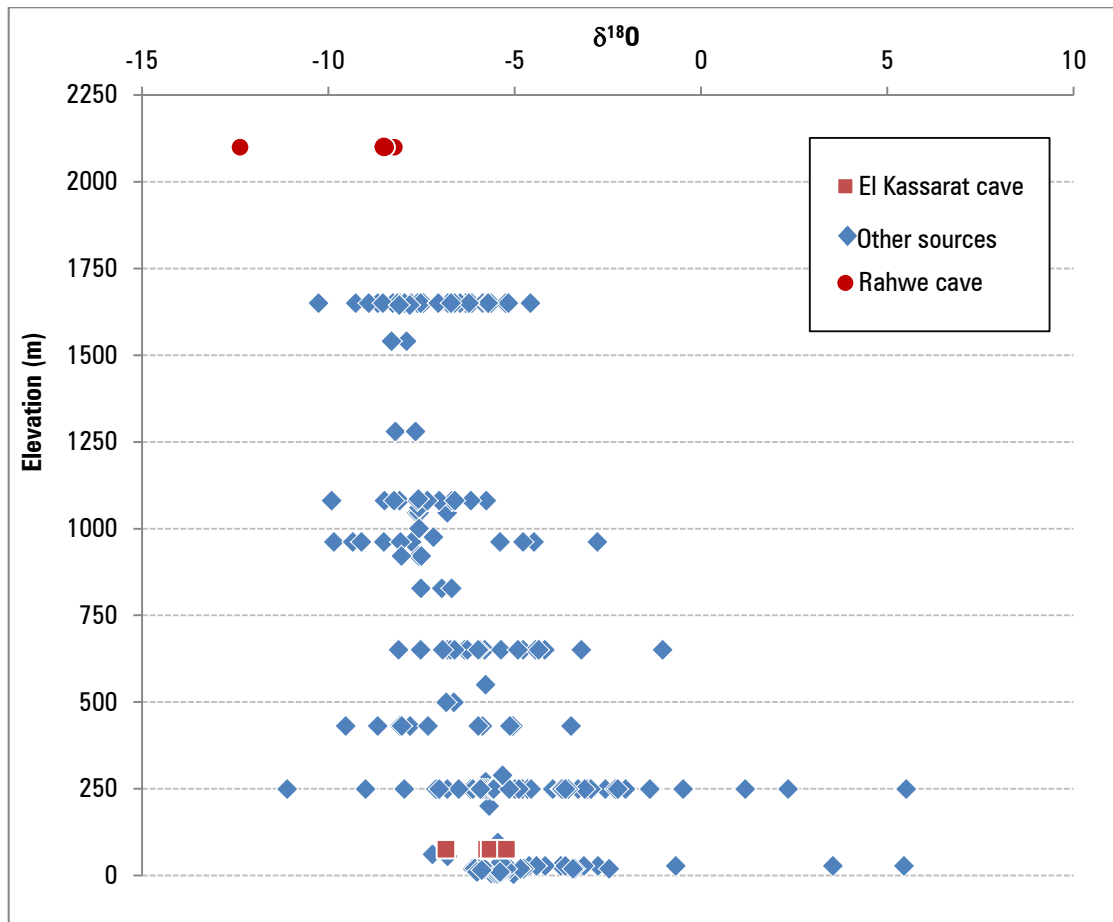
Figure 72. $\delta^{18}O$ **versus elevation from various locations in Lebanon. The blue dots represent data of water isotopes taken from various sources around Lebanon (App. 13).**

Figure 72 shows a plot of various $\delta^{18}O$ values versus elevation from a number of

different references (App. 13) as well as the results from the two study sites. Figure72

shows that in Lebanon, the isotopic values of water bodies that are more inland or at

higher altitudes have more depleted the $\delta^{18}O$ values. It also shows that there is a

considerable variation between coastal and high elevation $\delta^{18}O$ values. $\delta^{18}O$ water

values for Rahwe cave are clearly less enriched in heavy isotopes than those of the

coastal El-Kassarat cave. This indicates that the 'continental effect' is playing a role in the fractionation of the $\delta^{18}O$ isotopes.

Figure 73 schematically highlights the isotopic fractionation in precipitation as a result of topographic conditions and summarizes the values that can be obtained (Hoefs 1997 and Coplen *et al*., 2000). Altitude and topography causes the depletion of $\delta^{18}O$ and δ^2H at higher elevations, mainly due to rainout and topography (Figure 73).
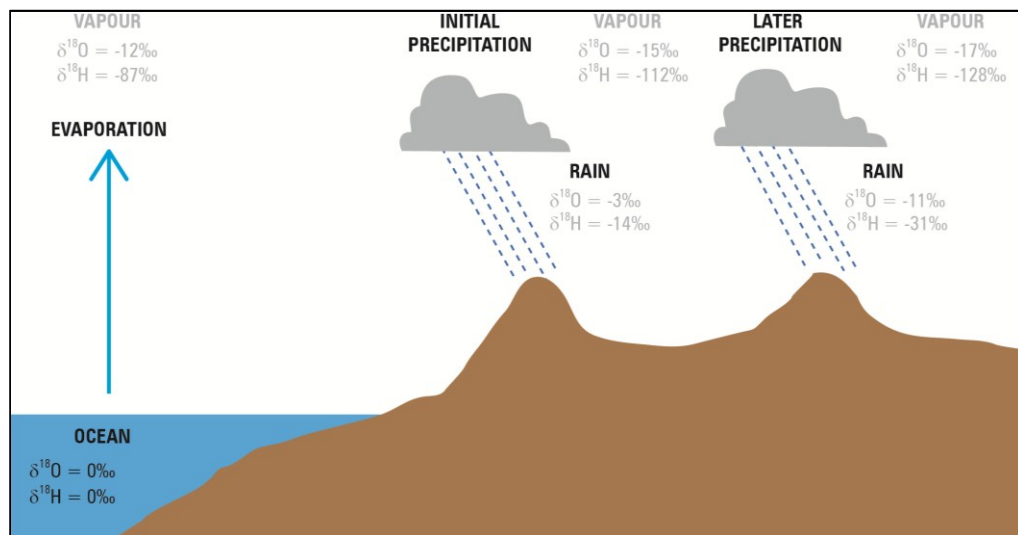
Figure 73. Rainout effect on δ^2H and $\delta^{18}O$ values (based on Hoefs 1997 and Coplen *et al*., 2000).

Present-day $\delta^{18}O$ of the eastern Mediterranean Sea surface water is $\approx$1.5‰ (Pierre, 1999), rainwater $\delta^{18}O$ near El-Kassarat cave is -5.75‰. So, there is an approximately 7.25‰ difference between the $\delta^{18}O$ values of the eastern Mediterranean Sea surface and the rainfall above the El-Kassarat cave. Present-day cave drip water is $\approx$0.3‰ less ^{18}O-

enriched relative to the rainfall, probably because of mixing processes that take place in the aquifer with pooled water that has had a longer residence time.

Figure 74 establishes the relationship between $\delta^2 H$ and $\delta^{18}O$ for the study area and outlines the Lebanese Meteoric Water Line (LMWL), the Eastern med Meteoric Water Line (MMWL), and the Global Meteoric Water Line (MWL). The deviation of the slope of the LMWL from that of the MMWL is influenced by secondary evaporation during rainfall (Saad *et al*., 2005). The isotope data distribution of the samples collected from the El-Kassarat and Rahwe caves scatter around the MMWL, suggesting that the water is of meteoric origin. The isotopic values generally follow the regional Mediterranean Meteoric Water Line, although the El-Kassarat rain value is closer to the Global Meteoric Water Line (MWL). These results suggest that the Eastern Mediterranean Sea could be the main source for meteoric vapours, which eventually becomes the caves' dripwater and groundwater.
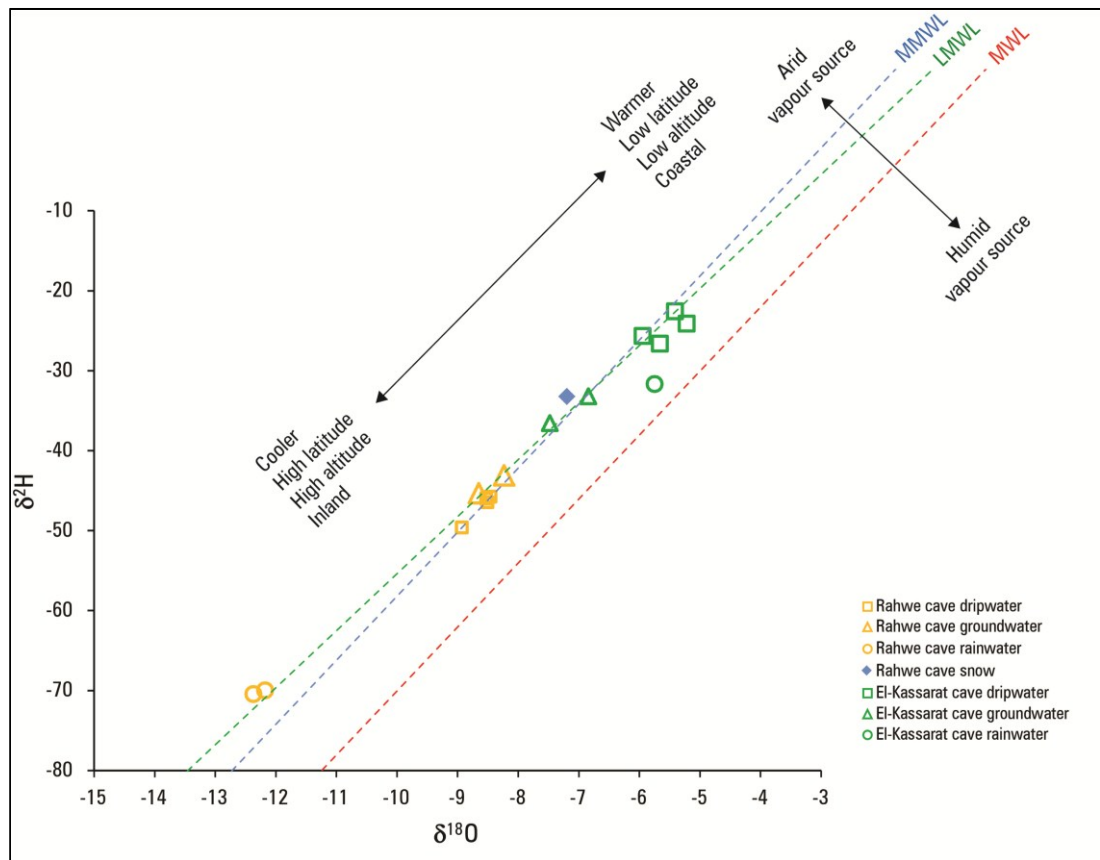
Figure 74. δ^2H-δ^{18}O relationships plot showing isotopic values of the rainwater/groundwater and dripwater of coastal and high elevation cave sites. (Lebanese Meteoric Water Line - LMWL, the Global Meteoric Water Line - MWL, the Eastern Mediterranean Meteoric Water Line - MMWL)(Gat and Carmi, 1987).

The El-Kassarat cave is located at an elevation of 75m. The precipitation in the location of the cave falls mainly as rain. The δ^{18}O values of rainwater were rich in the heavy isotopes, and measured -5.75‰, those of groundwater were at an average of -7.16‰, and of dripwater at an average of -5.22‰. The δ^{18}O for the coastal El-Kassarat cave scatter below the MMWL with higher δ^2H values. Groundwater δ^{18}O (-7.48‰ and

135

-6.84‰) is lighter than that of dripwater (-5.22‰ and -5.41‰), indicating that dripwater may represent short residence time of the water as it flows through the epikarst, while groundwater could represents water with a longer residence time because of the size of the catchment area. In the Gallerie du President's passage there was little dripwater $\delta^{18}O$ variation observed between the two samples taken in summer and winter seasons (-5.22‰ and -5.41‰). This indicates that the flowpath of the water is similar in terms of residence time and conduit structure. Additionally, temperature varied inside the cave by about 1°C. As a result, there are no observed seasonal variations in either cave temperatures or dripwater $\delta^{18}O$ that should affect the $\delta^{18}O$ of deposited calcite, leading to the conclusion that variations in speleothem $\delta^{18}O$ records are due to either significantly shifting rainfall rates or long-term temperature changes on the surface, or a mixture of both.

The Rahwe cave is located at an elevation of 2,208m. Most of its precipitation falls as snow rather than as rain. The $\delta^{18}O$ values of rainwater were depleted and measured -12.37‰, groundwater at -8.23‰, and dripwater at an average of -8.48‰. The water samples collected from Rahwe cave plotted on the lower section of the graph, indicating high altitude, inland or cooler climates. Many of the values plotted slightly below or on the MMWL line, suggesting some isotopic fractionation, perhaps due to evaporation. Note that the rain sample for Rahwe cave shows a deviation from the MMWL, and plots above the MMWL. This could be that some evaporation processes have occurred. In the RC-01 stalagmite site, there was little dripwater $\delta^{18}O$ variation observed between the

two samples taken (-8.51‰ and -8.53‰). However, temperature varied inside the cave by about 6°C. Since temperature variations have an effect on $\delta^{18}O$ fractionation, it could be an important parameter control on $\delta^{18}O$ variations in the stalagmite. This temperature change inside the cave could be due to snow blocking the entrance, forcing air currents inside the cave to change directions, or to the banking of groundwaters during flooding seasons inside the cave, causing a pressure difference inside it, thus a temperature change could occur. Since the entrance was only opened in the 1960's, the latter hypothesis could be more valid for the time of the stalagmite growth period. Aouad-Rizk (2006) sampled snow at Oyoun El-Simane (the highest site in Lebanon, at over 3,000m) from December 2011 to March 2012. This mountain is located about 17 km North-East of the Rahwe cave location. The results reveal that the $\delta^{18}O$ and δ^2H contents vary between -2.08 and -12.64 and between -0.9 and -86.00, respectively. The Rahwe cave snow $\delta^{18}O$ values fall within this range.

To conclude the isotope data distribution of the samples collected from the El-Kassarat and Rahwe caves scatter around the MMWL suggesting that the water is of meteoric origin. The isotopic values of the cave waters generally follow the regional Mediterranean Meteoric Water Line (Gat and Carmi, 1987), although the El-Kassarat rain value is closer to the Global Meteoric Water Line (MWL). These results also suggest that the Eastern Mediterranean Sea is the main source for meteoric vapours, which eventually becomes the caves' dripwater and groundwater.

137

The δ^{18}O in stalagmites is linked to the δ^{18}O content of the precipitation. But changes do occur as the water percolates through the epikarst, so it is important to understand the changes it undergoes since residence time and mixing can change the value of the δ^{18}O in the water and consequently in the precipitated calcite. Of course, more rigorous isotopic sampling is required that would yield more variation control as seasonality and source can be better considered, and the sampling resolution rate would be higher. However, from the results obtained, it is safe to say that the dripwater in both caves studied is not undergoing considerable changes as it flows through the epikarst (unlike the groundwater). It could therefore be safe to assume that the variations in the δ^{18}O values in the stalagmite are true proxies of the paleoclimatic changes and represent variations in the amount of rainfall and temperature at the surface.

5.2   Cave air and water temperatures

One year temperature measurements show that the modern temperature inside the studied caves is undergoing some variation (Figure 27, Figure 55). For the El-Kassarat cave temperature, the measurement points generally showed small variations (lowest 15.1ºC and maximum 18.3ºC). The cave temperature did not respond directly to surface temperature changes (the average outside air temperature was ≈21ºC) , and the average cave temperature was ≈16ºC), indicating that the epikarst has the capacity to store some of the surface heat. Rock and soil cover can act as heat insulators, preventing substantial

temperature variations. Such thermal insulation creates relatively stable temperature changes in the El-Kassarat cave. On the other hand, since the cave had no opening, it would be safe to assume that the temperature inside the cave at that time was stable. However, the temperature measurements obtained over the year of monitoring showed that the current cave openings do not impact greatly temperature variations inside the cave.

Rahwe cave temperature average for the year of monitoring ($\approx$4ºC) is lower than surface temperatures ($\approx$13ºC) outside the cave. The Rahwe cave temperature change trend loosely follows that of the surface temperature, indicating that the open entrance is affecting the cave temperature at the Tinytag location inside the cave ($\approx$80 m from the entrance). The cave temperature shows seasonal variations, and correlates well with the atmospheric temperatures outside, although they tended to have lower values. Rahwe cave was not connected to the outside environment until the tunnel entrances (which had no doors) were built. This has to be taken into account when interpreting the results of the isotopic composition of modern calcite from Rahwe cave, and when choosing the location from which the calcite has to be removed.

Temperature change can affect modern calcite deposits since Kim and O'Neil (1997) showed that the fractionation factor at the water/calcite interface was 1.02846 for a temperature range between 10-40°C, which increases by 0.00022 (0.22 ‰) per 1° temperature decrease between 10 and 25°C. Variations of less than 1°C can cause potential $\delta^{18}O$ shifts in speleothems, showing long-term changes of global climate

(Wigley and Brown, 1976). An increase of the cave air and water temperature of (+) 1°C will decrease the fractionation factor and speleothem $\delta^{18}O$ by approximately (-) 0.22‰, so less ^{18}O will be incorporated in the calcite (Nordhoff, 2005).

During the EKC-01 and RC-01 stalagmites' deposition, there was no natural opening to both caves, thus both stalagmites' $\delta^{18}O$ values are representative of surface temperature changes and precipitation rates. In addition, even after the openings were established some 60 years ago, the variation is still low suggesting that both stalagmites can be used for paleoclimatic considerations, and current calcite deposits can be utilized as climatic proxies.

As for water temperature, Rahwe cave waters' has lower temperature values than those of El-Kassarat cave because of the difference of altitude of the two caves, and so the difference in the average surface temperature (17ºC and 7ºC for El-Kassarat cave and Rahwe cave respectively). The differences are mainly due to the residence time of the waters in the aquifers which is mainly related to the size and extent of the catchment area. The catchment area of the El-Kassarat cave ($\approx$200 km^2) is much larger than that of Rahwe cave ($\approx$1.3 km^2). This affects the distance that water has to travel to enter the caves. The farthest distance that the water has to travel in the Rahwe cave catchment is approximately 1 km. The farthest that the El-Kassarat cave waters can travel in the catchment area is approximately 16 km^2.

On the other hand, the groundwater temperature values are a bit lower than dripwater temperature values in both cases (Figure 75). This is mainly also due to the

residence and travel times, which are longer for groundwater than for dripwater. Dripwater temperature is mainly related to the thickness and the structure of the epikarst above each stalagmite, ≈40 m for the El-Kassarat cave (Figure 12), and ≈150 m for the Rahwe cave (Figure 20). There is a slight difference in temperature between the different dripwaters sampled within each cave. This could be due to the different flowpaths that the groundwater undertakes as it percolates downwards.

Temperature values obtained from the dripwater further highlight the minimum interaction between the epikarst and the groundwater, which in turn allows for a better paleoclimatic assessment for these two caves.
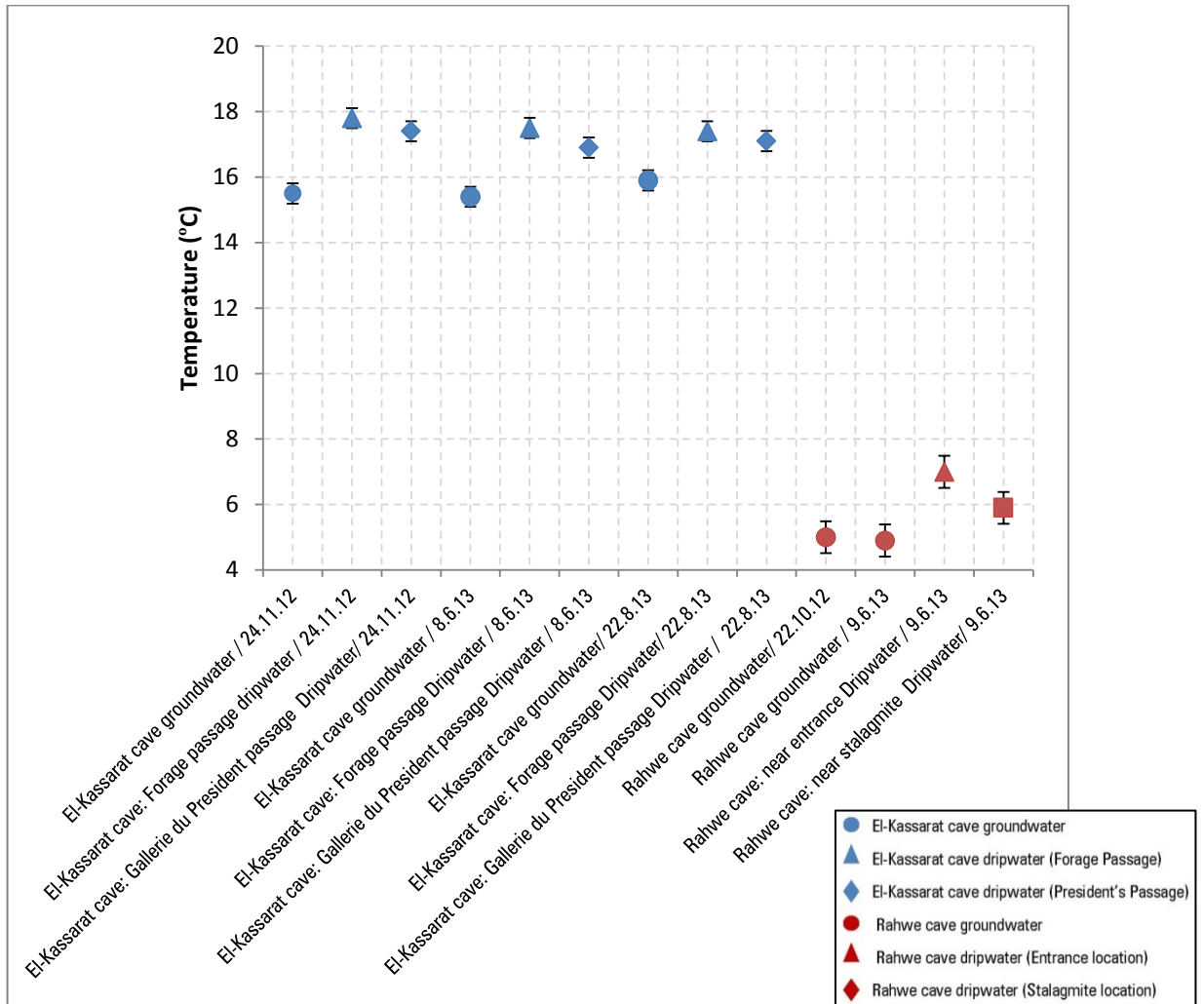
Figure 75. Groundwater and dripwater temperature in El-Kassarat and Rahwe caves.

5.3 Chemistry of groundwater

Regarding measured pH values in both caves, the Rahwe caves' waters are higher than those in the El-Kassarat cave (Figure 76). The Rahwe cave waters' pH level is close to that of rainwater (8.22), while the El-Kassarat cave rainwater pH value (8.93) have undergone considerable decrease in the order of 1 pH . The high Rahwe cave

values indicate fast recharge from rainfall, with a short residence time, since pH is characterized by the uptake of soil-originated CO_2 reducing it (Kano *et al*., 1999). This is what is occurring in the El-Kassarat cave site, where there is considerably more soil cover than in the Rahwe cave site. This also indicates that an increase in the acidity of the waters could be due to the higher residence time of the groundwater in the El-Kassarat cave aquifer.
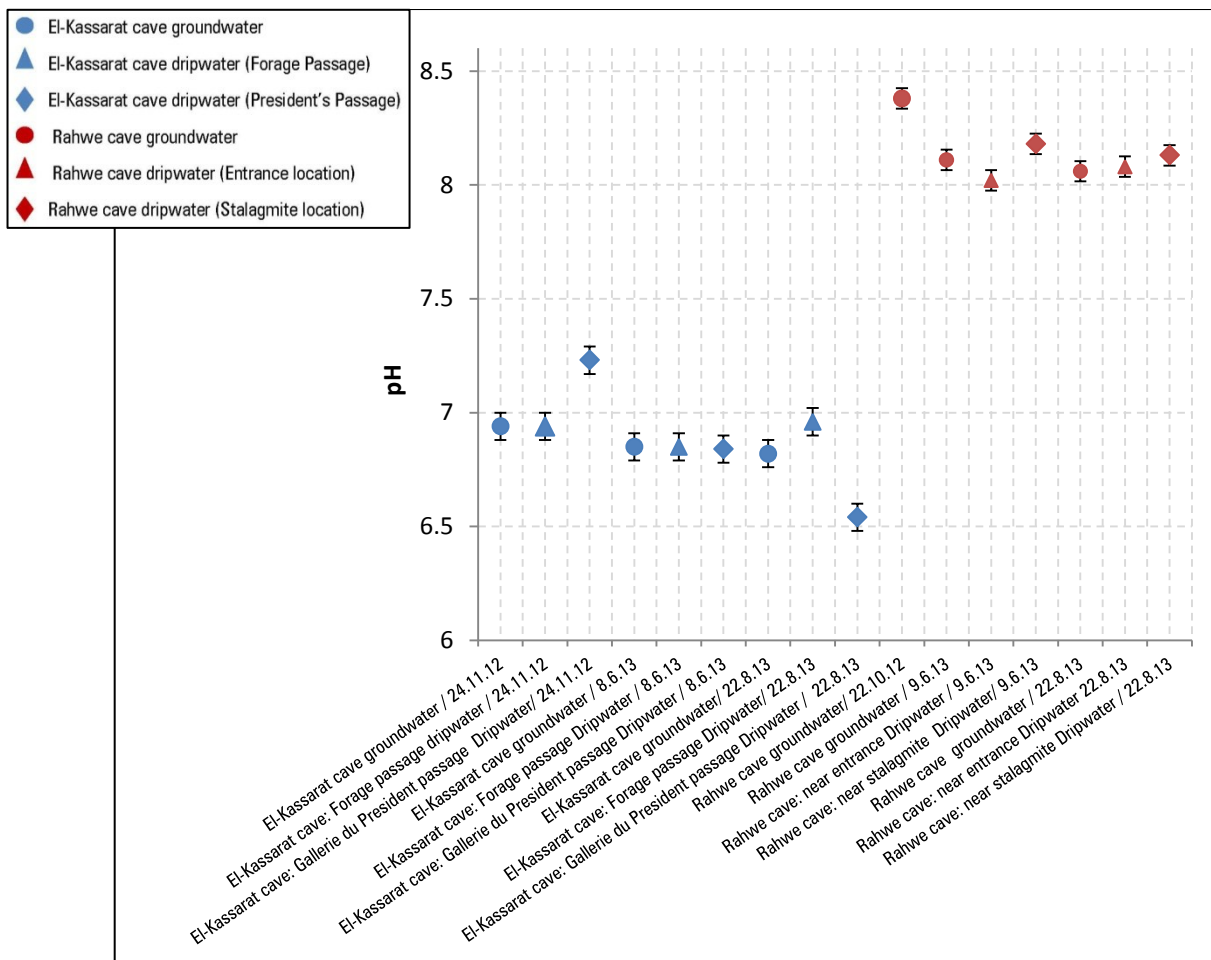
Figure 76. pH levels of various waters from the El-Kassarat and Rahwe caves.

143

In both caves, there is also a pH difference between the two types of waters, groundwater and dripwater, as well as a difference between the two dripwater locations. This is probably due to the different paths and conduit channels the groundwater flows through to reach the cave cavity.

Regarding conductivity values, the difference between the El-Kassarat and the Rahwe cave ($\approx 200\mu s$) dripwater and groundwater values are probably due to the extent of the residence time, the difference in the amount of mixing between groundwater from different parts of the aquifer, the rainfall percolation rate above the two caves and the nature of the aquifer in which each cave has developed.
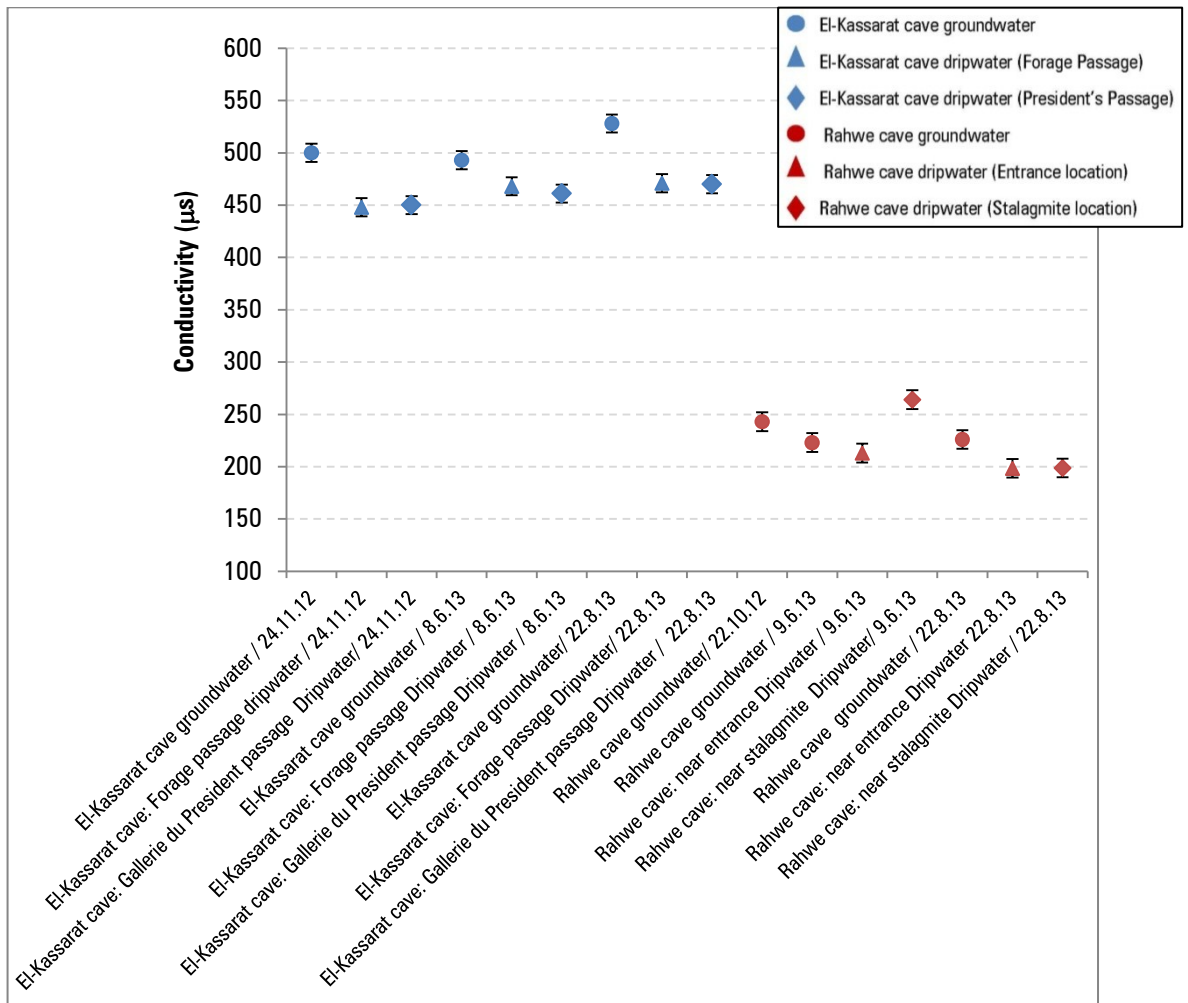
Figure 77. Groundwater and dripwater conductivity levels in El-Kassarat and Rahwe caves.

Both aquifers are limestone aquifers however, it seems that the Rahwe cave

groundwater and dripwater has a shorter residence time than those of the El-Kassarat

cave. Moreover the El-Kassarat cave is close to a large fault system, and so the

fracturing in the aquifer is extensive. The valley also has surface soil sediments that can

deposit inside the conduits as the water percolates downwards. The El-Kassarat cave's

145

Jurassic aged limestone also has a high dolomitic content. This dolomitic content could affect the rate at which the groundwater erodes the rock since dolomitic limestone is harder to erode than pure limestone. Temperature also plays an important role in this process as the CO_2 dissolving rate is lower at higher temperatures.

Turbidity levels in both caves tended to be slightly higher in the winter sampling sessions in comparison to the summer ones. This is probably due to the increased flushing that occurs through the conduits during increased rainfall in winter.

The chemical elements, such as Na^+, K^-, Ca^{+2}, Mg^{-2} , plotted on Figure 78 show that the increase of Na^+ values in El-Kassarat cave waters' could be mainly due to the proximity of the sea to that site. The K^+ values for both cave sampling is similar and low for both, indicating that there is no additional input of potassium cations from outside aquifer sources.
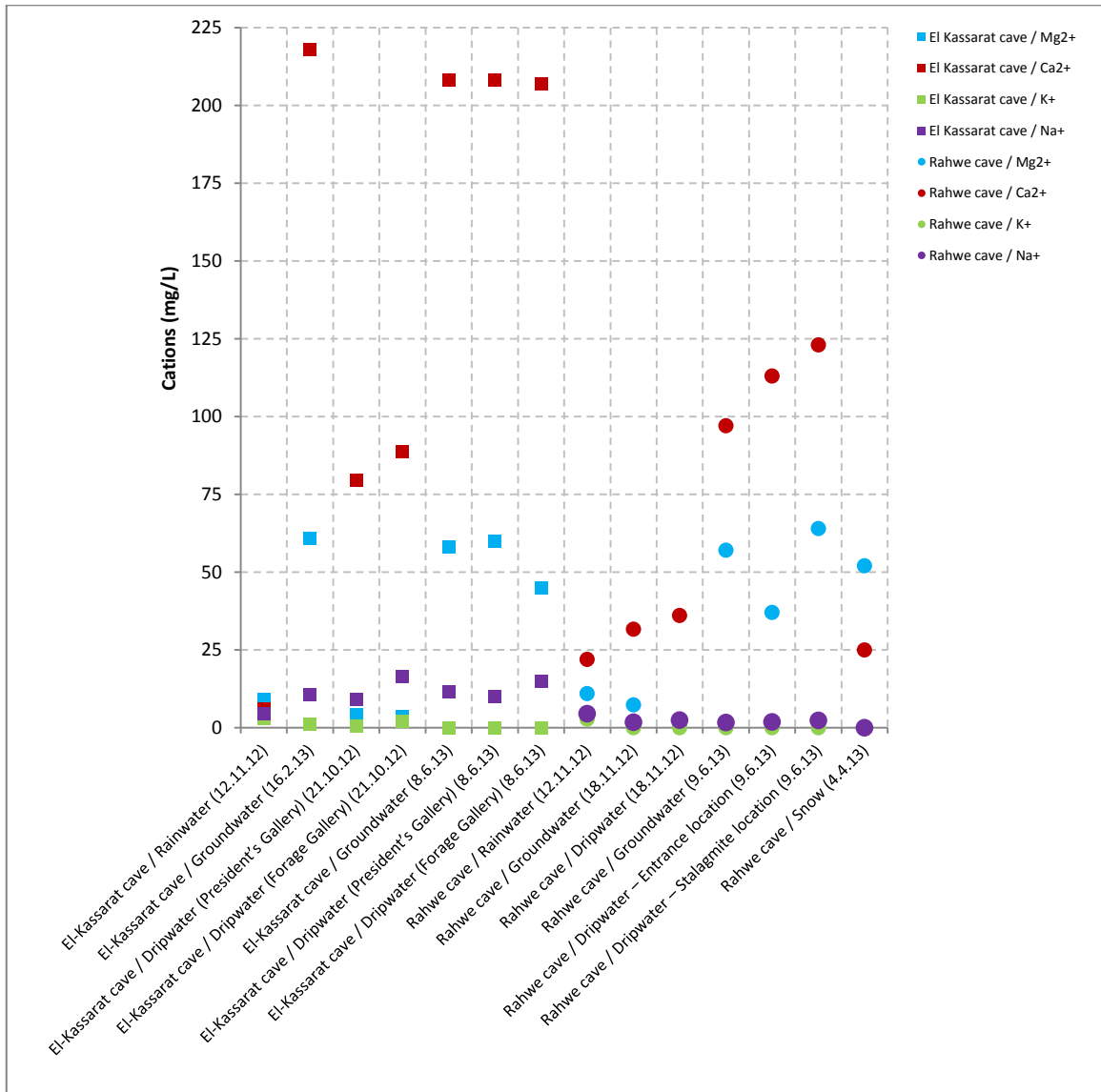
Figure 78. The results of the chemical analysis of rainwater, snow, groundwater and dripwater for the El-Kassarat and Rahwe caves.

In general, the El-Kassarat and Rahwe cave waters have higher concentrations of Ca^{2+} and Mg^{2+} than those of Na^+ and K^+ (Figure 78). This reflects the chemical and mineralogical compositions of the rocks forming the aquifer, which consist mainly of

147

calcium carbonate and dolomite. The values of Ca^{2+} of the El-Kassarat water tend to be higher than those in the Rahwe cave probably due to the increased residence time of the cave waters. The Mg^{2+} values are similar for both indicating a similar Mg^{2+} content from each aquifer.

The groundwater chemistry shows that the water is undergoing some changes in the epikarst during summer and winter seasons, mainly in Ca^{2+} and Mg^{2+} compositions, but not a major or alarming change that would alter the paleoclimatic data recorded in the stalagmites.

5.4   Petrographic assessment

The petrographic examination of both stalagmites has shown that laminae are seen in transmitted, fluorescent lights and under crossed-polars. The columnar crystals in the EKC-01 thin sections have shown that the laminae are well defined and have not been altered, and seasonal laminae growth were observed. The changes between the dark and light layers observed could be seasonal changes of wet and dry periods where white porous calcite and dark compact calcite are identified. Inclusions observed in some laminae can also signify a change in environmental parameters during deposition. The assessment of the EKC-01 thin section did not reveal any major recrystallization, diagenesis or alterations. The RC-01 thin sections are a little more disturbed and further work is needed on this stalagmite to assess the age reversal and the lack of well-defined laminae.

The EKC-01 stalagmite does not show any fractionation features since clear laminae and columnar crystals are observed and they do not show any visible alteration. This shows that the stalagmite EKC-01 can be used for paleoclimatic studies.

5.5 EKC-01 Stalagmite Isotopic Record Analyses

5.5.1 $\delta^{18}O$ and $\delta^{13}C$ modern calcite records

The $\delta^{18}0$ values of modern calcite inside El-Kassarat cave (collected from glass plates) and Rahwe caves (collected from scraped calcite powder from active stalagmites) where -5.1‰, and -5.14‰ respectively (Table 7).

The $\delta^{18}O$ values of the modern calcite from the El-Kassarat cave ($\approx$-5.1‰) are close to those of rainwater (5.75‰) and dripwater ($\approx$5.7‰) values, and so it can be assumed that the water is not undergoing any major changes due to mixing as it percolates through the epikarst. The $\delta^{18}O$ of rainfall is, therefore, translated to speleothem $\delta^{18}O$ with little fractionation in the epikarst, and climate processes can be correlated to variations in the stalagmite's $\delta^{18}O$ values.

On the other hand there is a marked decreasing shift between the $\delta^{18}O$ values of the rainfall (-12.275‰), dripwater (-8.52‰) and the modern calcite (-5.14‰) in the Rahwe cave (Table. 7). This decrease could be due to temperature shifts inside the cave, or the amount of prior calcite precipitation (PCP) that occurs. PCP can affect water isotopic values since as the water percolates through the epikarst it undergoes degassing and calcite deposition inside air-filled conduits (Fairchild and Baker, 2012). At this time it is difficult to evaluate which or if both these parameters are affecting modern calcite deposition in the Rahwe cave site of this study. Further monitoring will need to be attained in order to better assess what is happening.

Table 7. Modern calcite sampling results and their locations

Sample	Type	Modern calcite Average $\delta^{13}C$	Modern calcite Average $\delta^{18}O$	Dripwater Average $\delta^{18}O$	Rainwater Average $\delta^{18}O$
EKC - Plate 1	Plate	-9.21	-5.1	-5.805	-5.75
EKC - Plate 2	Plate	-8.93	-5.25	-5.805	-5.75
EKC Presidents Gallery	Scraped powder	-10.48	-4.49	-5.315	-5.75
EKC Forage Gallery	Scraped powder	-9.11	-4.22	-5.805	-5.75
Rahwe cave	Stalagmite tip	-2.53	-5.14	-8.52	-12.275

The $\delta^{13}C$ values of modern calcite inside El-Kassarat cave and Rahwe caves average -9.4‰ and -2.53‰ respectively. The El-Kassarat $\delta^{13}C$ values are high indicating a mixture of C4 and C3 vegetation cover (personal communication with Dr. Marc Beyrouthy, 2013). Speleothem calcite generally reflects $\delta^{13}C$ of the soil cover, which in turn is controlled by surface vegetation extent and type (Dorale *et al.*, 1992). El-Kassarat values lie within the expected range of C4 plants values range ≈ -10‰ to -16‰ (Cerling and Quade, 1993).

The $\delta^{13}C$ values from modern calcite in Rahwe cave is very low (-2.53‰) despite the fact that vegetation cover above Rahwe cave is dominated today by C3 type vegetation. This value could be the result of a thin soil horizon and low vegetation cover at this higher altitude. This contrasts with the El-Kassarat cave values where $\delta^{13}C$ values are higher.

Therefore the currently growing stalagmite sampled in the El-Kassarat cave can help in calibrating modern conditions (i.e. modern day $\delta^{18}O$ of calcite) with older records, since they represent current surface and cave conditions. Consequently, the

assumption can be made that this is the signal as proxy for interglacial conditions for this specific location.

5.5.2 $\delta^{18}O$ and $\delta^{13}C$ carbonate record from the EKC-01 stalagmite

The candlestick of the EKC-01 stalagmite showed variations in isotopic values that can be separated into five distinctive phases in the growth as observed in Figure 79. The phases as presented from older to younger are; Phase 1 from 27.5-15.0 ka; Phase 2 from 15.0-13.0 ka; and Phase 3 from 13.0 -9.0 ka; Phase 4 from 9.0-7.0 ka; Phase 5 from 7.0-0.0 ka (Figure 80). Due to the low time resolution (approximately one sampling point every 500 yr) of the EKC-01 stalagmite, short-term events and other climatic fluxes could not be detected, however major climatic events are still detectable and comparison is still possible.

152
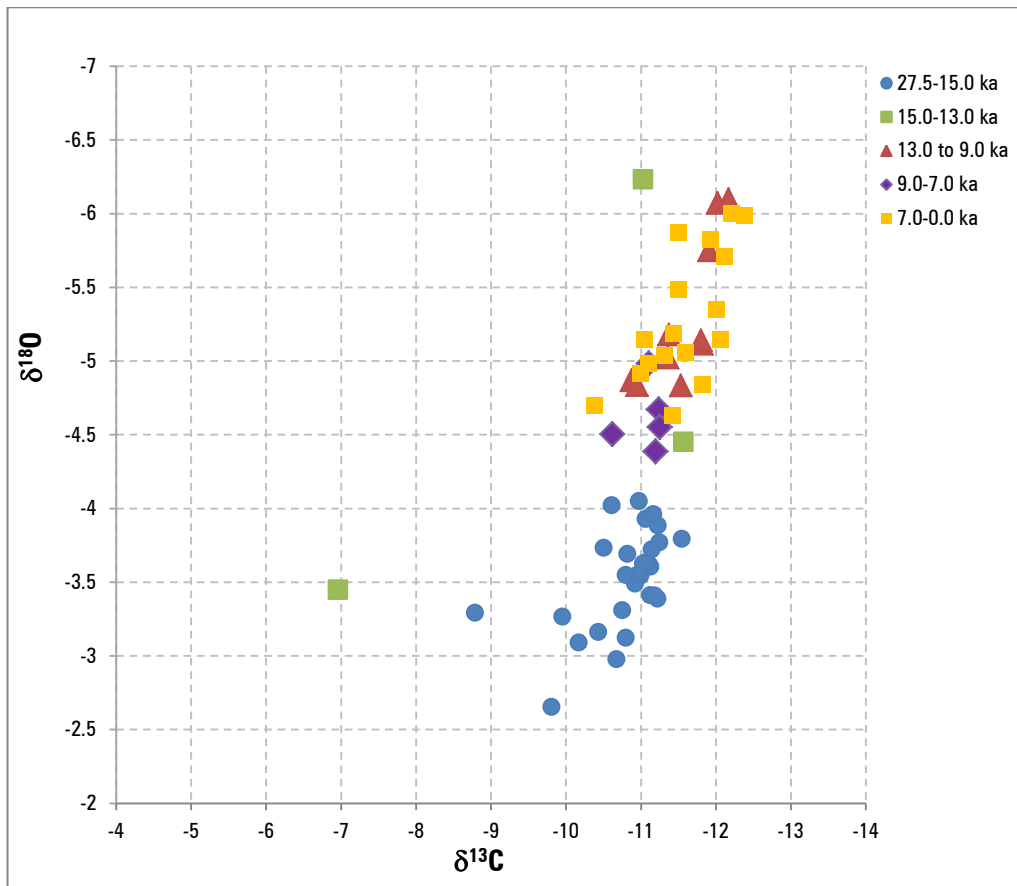
Figure 79. $\delta^{18}O‰$ vs $\delta^{13}C‰$ plot showing the isotopic compositions of 64 data points measured in stalagmite EKC-01 and the general grouping of the five major time periods.

Figure 79 shows a $\delta^{18}O‰$ vs $\delta^{13}C‰$ plot from the 64 data points measured in stalagmite EKC-01 and the general grouping of the five major phases. Phase 2 (15.0-13.0 ka) has a large scatter owing to the major climatic shift that occurred in this period. Phase 3 (13.0-9.0 ka) and Phase 5 (7.0-0.0 ka) scatter in the same field because they have similar climates. Another reason for the large scatter could be due to the sampling of more than one laminae during drilling and the mixing of various isotopic values from different layers.

153
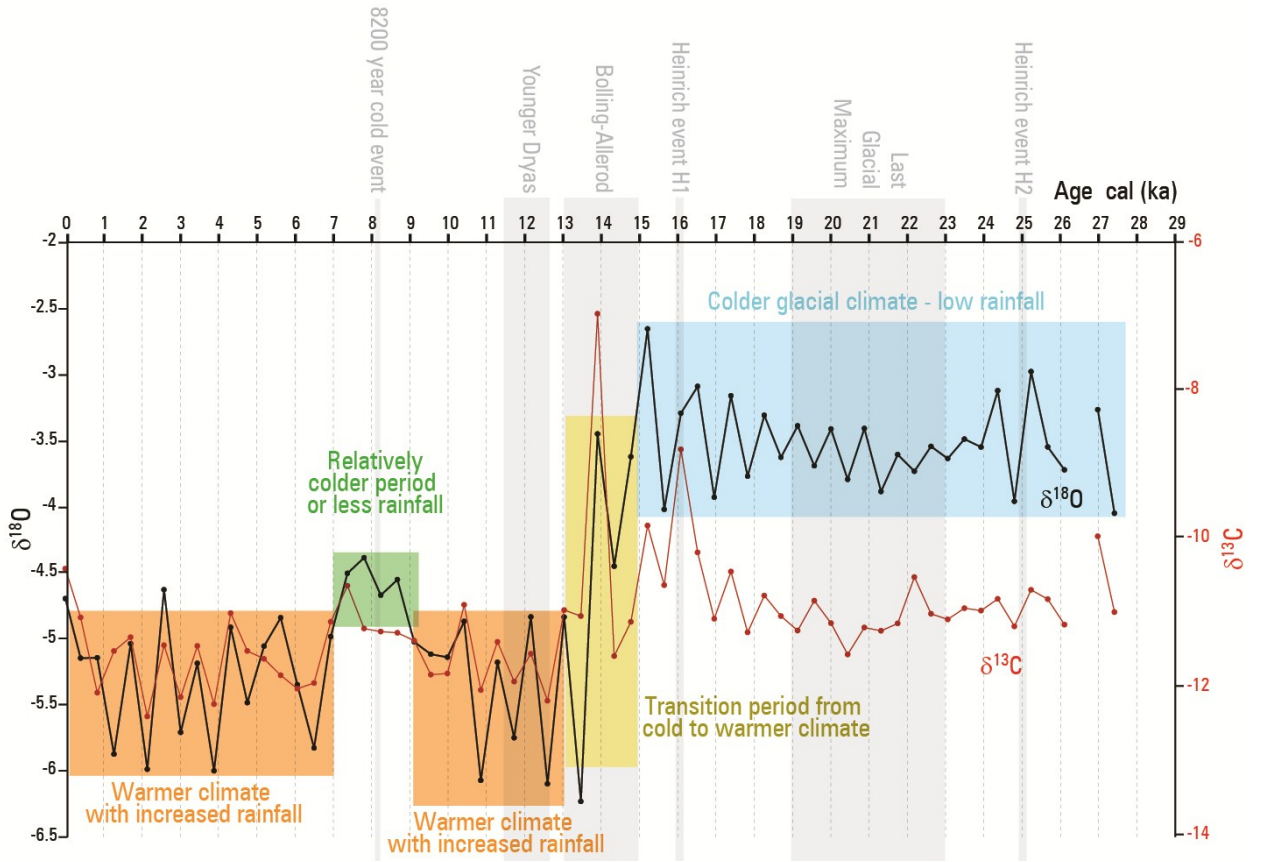
Figure 80. Summary of climate conditions inferred from the EKC-01 $\delta^{18}O$ and $\delta^{13}C$ values.

154

5.5.2.1   Phase 1 (27.5 to 15.0 ka)

In this phase the $\delta^{18}O$ and $\delta^{13}C$ values are well correlated with high heavy ^{18}O isotopic values from about 27.5 to 15.0 ka, with a decrease in values at around 14.5 ka (Figure 80). During this period the $\delta^{18}O$ and $\delta^{13}C$ values average about -3.53‰ and -10.8‰ respectively.

This period encompasses the Last Glacial Maximum ($\approx$23-19 ka). It is cooler and more arid than present conditions. In EKC-01 the $\delta^{18}O$ values are less negative indicating this event.

The Heinrich Event 2, H2, occurred at about 25 ka (Bar-Matthews *et al*., 1999). It was a time of intense cooling resulting from the addition of freshwater to the North Atlantic (Robinson *et al*., 2006). In EKC-01 this event correlates with a less negative $\delta^{18}O$ spike showing a cooler climate.

During Phase 1 the $\delta^{18}O$ values indicate a cold dry climate. The less negative $\delta^{18}O$ values correlate well with this period, which was characterized by the greatest extent of ice sheets in the northern Europe since (relative to the present day) the eastern Mediterranean region had colder temperatures (12º-16ºC) and less rainfall (300-450mm) (Bar-Matthews *et al*., 1997). Kolodny *et al*. (2005) interpreted $\delta^{18}O$ of Lisan Lake (Figure 83) sediments as primarily due to changes in evaporation to precipitation ratios rather than temperature or source $\delta^{18}O$ variations, making humidity and dry/wet environments the important parameter.

It is thus a possibility that due to the cold climate of this period there is a decrease of the ratio of evaporation to precipitation, permitting continuous dripping of water into the cave. This constant dripping at a slow rate can be observed in the continuous cylindrical shape (representing constant growth) of the candlestick section of the EKC-01 stalagmite.

During this period the $\delta^{13}C$ values average at about -10.8‰ for the EKC-01 stalagmite which are close to present day values albeit a little less negative. The rise in soil CO_2 (due to colder and/or less rainy conditions) could increase the ^{13}C enrichment and so the $\delta^{13}C$ values. Bar-Matthews (1997) demonstrated that this could be due to a mixture of C_3 and C_4 type vegetation on the surface

Close to the end of Phase 1 The Heinrich Event 1, H1, occurred at about 16.0ka. During this period the ice sheets began to melt and there was an increase in rainfall and temperature. This was the beginning of the transition from glacial to interglacial conditions. In EKC-01 this event correlates with a less negative $\delta^{18}O$ spike showing a cooler climate.

5.5.2.2   Phase 2 (15.0 to 13.0 ka)

There is a sharp increase in negative $\delta^{18}O$ values in this period. The highest and lowest $\delta^{18}O$ values in the sequence are recorded in this period, at -2.65‰ and -6.23‰. The highest $\delta^{13}C$ value recorded is -6.96‰ at around 14.0 ka (Figure 80).

These sharp increases for both $\delta^{18}O$ and $\delta^{13}C$ values are indicative of climatic changes. These spikes correlate with the Bolling-Allerod event which occurred due to the melting of the ice sheets and an increase in rainfall and temperature. This transition, from the last glaciation to the deglaciation, is characterized by $\delta^{18}O$ and $\delta^{13}C$ spikes which indicate that conditions were unstable (Bar-Matthews *et al.,* 1997).

Figure 80 also shows a cross section of the stalagmite (at the bottom) where a visible change in the colour of the calcite can be observed in this phase from darker ochre coloured to lighter yellow calcite (Figure 80, red arrow). This change could be due to the climatic transitions that were occurring in this period.

5.5.2.3   Phase 3 (13.0 to 9.0 ka)

This Phase occurred during the transition from the late glacial Pleistocene Epoch (10-26 ka) to the warmer Holocene Epoch (10 ka to present) (Figure 80).

Average $\delta^{18}O$ and $\delta^{13}C$ values recorded were -5.3‰ and $-$ 11.6‰ respectively. A relative increase in negativity in the $\delta^{18}O$ and $\delta^{13}C$ values can be indicative of relatively more humid and wet conditions. High $\delta^{13}C$ average values in this phase are indicative of C_3 vegetation type, indicating that the climate is wetter and warmer and similar to present day conditions.

Some spikes are observed in the data with a decrease in negative $\delta^{18}O$ values. This may be related to the Younger Dryas event which occurred between 12.7 and 11.5 ka.

157

5.5.2.4   Phase 4 (9.0 to 7.0 ka)

Average $\delta^{18}O$ and $\delta^{13}C$ values recorded in this phase were -4.6‰ and – 11‰

respectively.

The small decrease in negative $\delta^{18}O$ and $\delta^{13}C$ values observed might be

consequently inferred as an arid period. This may be related to the 8.2 ka event which

occurred due a large meltwater pulse from the final collapse of the ice sheets, causing

the climate to become colder and less humid.

5.5.2.5   Phase 5 (7.0 to 0.0 ka)

Average $\delta^{18}O$ and $\delta^{13}C$ values recorded in this phase were -5.3‰ and – 11.6‰

respectively. Phase 5 is very similar to Phase 3 in climatic conditions and isotopic

values (Figure 80).

High $\delta^{13}C$ average values in this phase are suggestive of C3 vegetation type,

indicating that the climate is wetter and warmer. Between 3.0 and 0.0 ka, soil activity

seemed to decrease, as indicated by increasing $\delta^{13}C$ values. It is not clear if the $\delta^{13}C$

increase is due to a dryer climate (with a parallel increase in $\delta^{18}O$ values) or credited to

a decrease in the extent of the soil cover due to growing agricultural and human

activities.

5.5.3 EKC-01 trace element record

The EKC-01 was analyzed for magnesium (Mg), strontium (Sr), barium (Ba), and iron (Fe) by Inductively Coupled Plasma Optical Emission Spectroscopy.

It was identified that in stalagmite EKC-01 trace elements were incorporated in the calcite and varied in values as the stalagmite grew. Distinct fluorescent bands, observed in the thin sections of EKC-01, can be related to trace element signatures.

App. 14 shows the full results of the trace element values in the candlestick section of EKC-01 (Figure 81). In the EKC-01 stalagmite a rise in Mg concentrations can reflect a reduction in rainfall during glacial periods. There are spikes in the Mg concentrations at around 21.3, 16.0, 13.7, 11.0, 2.0 ka with the highest values at 13.7 ka. This peak coincides with marked decreases in $\delta^{18}O$ and $\delta^{13}C$ values. Some rises do not correspond to glacial periods (red dots in Figure 82). This could be explained because during rapid climate events the relationships between Mg and rainfall may differ from those of the current interglacial period (Fairchild *et al*., 2009).
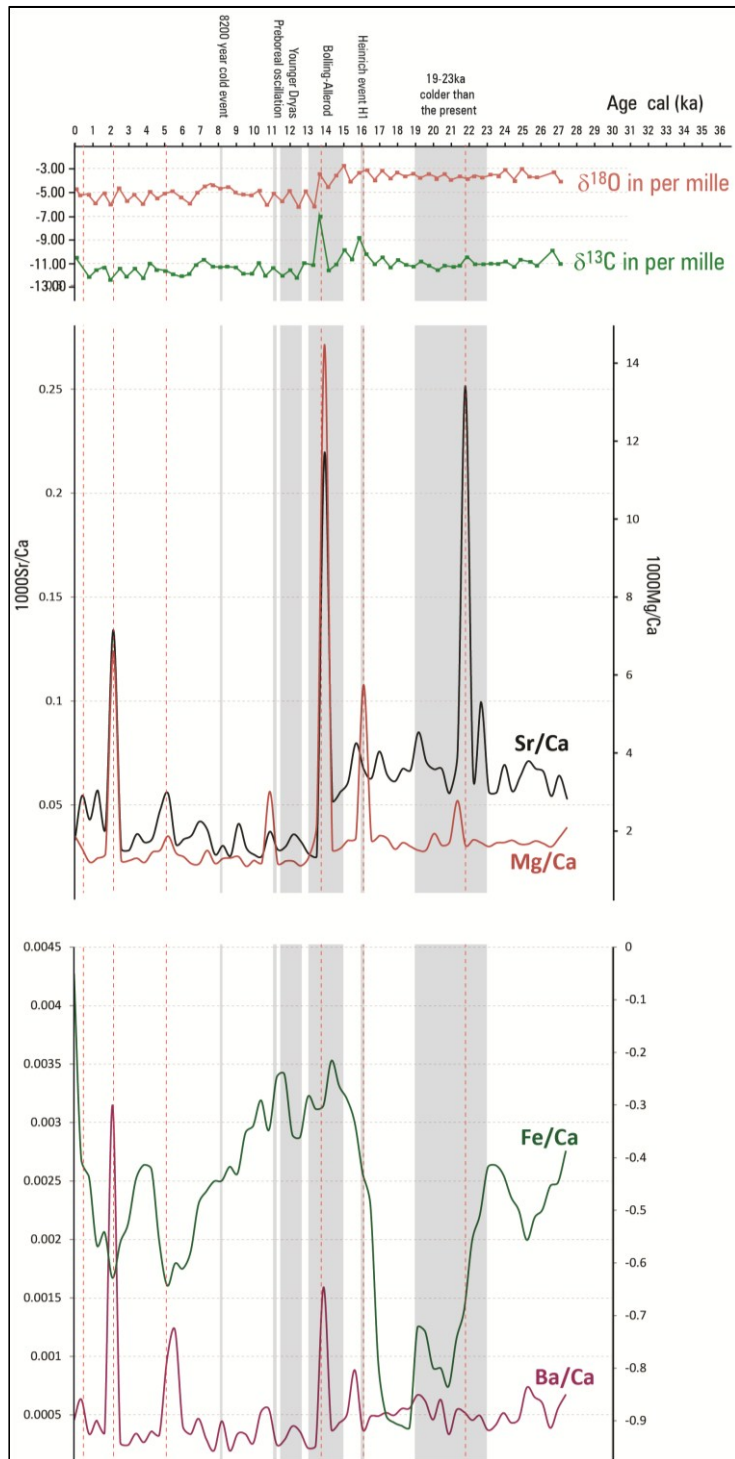
Figure 81. Data of Mg/, Sr/Ca, Ba/Ca and Fe/Ca correlated with $\delta^{18}O$ and $\delta^{13}C$ values in EKC-01.

160
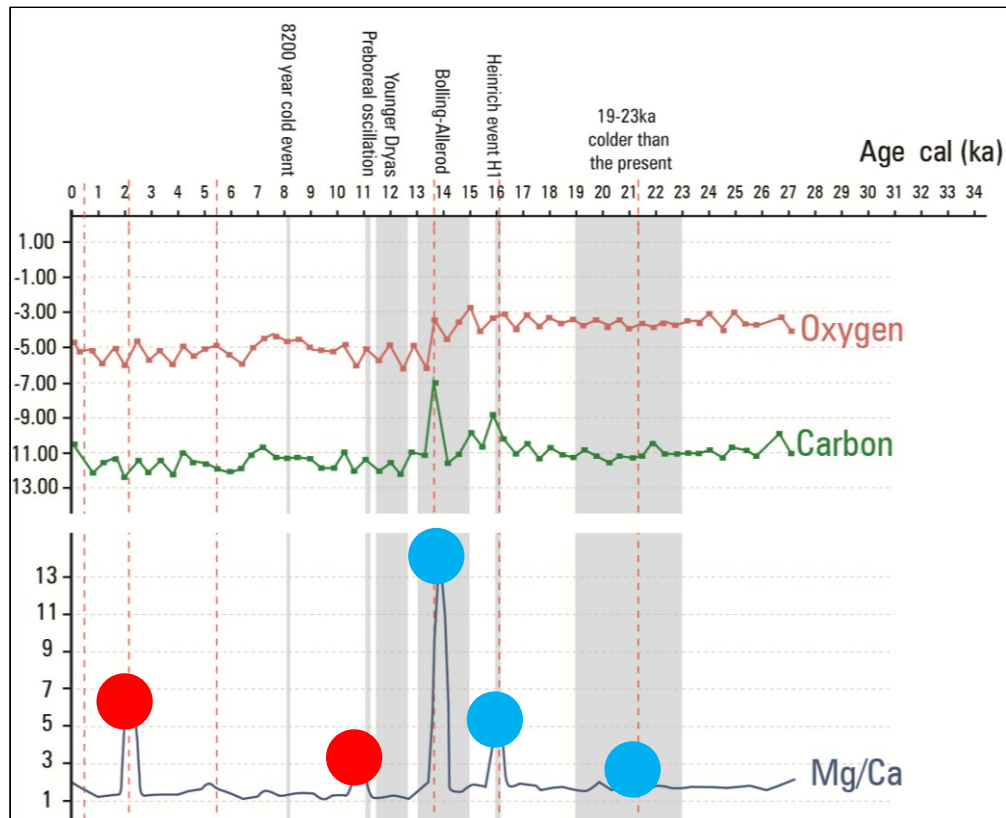
Figure 82. Mg concentrations in sampled EKC-01 stalagmite, compared with Oxygen and Carbon isotopic values. Blue dots on spikes signify peaks in cold/glacial periods and red dots signify peaks in warmer (Holocene) periods.

From approximately 27 ka to 14 ka there is a reasonable correlation between $\delta^{18}O$, Mg/Ca and Sr/Ca values. This could indicate that during this period the changes were not induced by rerouting since $\delta^{18}O$ are not affected by rerouting (Verheyden *et al*, 2000). The long term Mg/Ca and Sr/Mg decrease gradually in average values apart from the short term peaks. This decrease could be due to a decrease in residence time and so in the amount of Sr/Ca and Mg/Ca that dissolves into the water. After 14 ka the

correlation is less obvious and this could be due to human activity in the valley, as the area became more humid and warmer. Ksar Akil is an archeological site has shown that the Antelias valley was inhabited from a very early period (Douka *et al.*, 2013), dating between 50 to 10 ka. Agricultural activities and possible river diversions might have affected the conduits below the surface above the cave and caused rerouting of the water.

Several processes may affect dripwater composition as the groundwater flows through the epikarst as well as the amount of water to rock contact varies with water residence time or dissolution rates (*e.g.* calcite vs. dolomite). An increase in the dolomite to calcite ratio during weathering, caused by dry weather, leads to longer residence time, and thus a higher Mg/Ca concentrations. Degassing and prior calcite precipitation may affect the trace elements concentrations in the groundwater, resulting in an increase of Mg and Sr concentrations in times of low precipitation (Fairchild *et al.*, 2000). Trace element compositions often show a seasonal changeability since the processes are prone to seasonal variations (Treble *et al.*, 2003).

The Ba and Sr concentrations in the sampled ECK-01 correlate well except for a peak in Sr concentrations around 21 ka that does not appear in the Ba concentrations. Short-term and long-term fluctuations in Sr/Ca ratios can be interpreted as changes in water residence times. Low values represent periods of shorter residence times (i.e. humid conditions) (Verheyden *et al.*, 2000).

5.5.4 *Comparison of EKC-01 with other Eastern Mediterranean records*

5.5.4.1 Comparison of EKC-01isotopic results with other Eastern Mediterranean cave
records

Comparison of the isotopic profiles of the Jeita, Soreq, Pequiin, and West
Jerusalem caves to the El-Kassarat cave records reveal some similarities and
differences in the $\delta^{18}O$ trends (Figure 84). The oxygen isotope system is simpler to
analyze than that of carbon isotopes, so this section will only report on the $\delta^{18}O$
signatures for comparison.

El-Kassarat cave is approximately 5 km from Jeita cave. Both are less than 5 km
from the coast. The El-Kassarat cave is 154 km from the Peqiin cave, 240 km from the
West Jerusalem cave, and 278 km from the Soreq cave. All are located in an eastern
Mediterranean climate region but Lebanon, due to its mountain chains, has more annual
rainfall on its coast and more moderate temperatures (Figure 83) (Bar-Matthews *et al*.,
2003; Frumkin *et al*., 2000).

Jiita cave's stalagmite is the best one to compare to EKC-01, but with its limited
age range (only 12 ka) three other caves, although from slightly different climatic
zones, were compared.
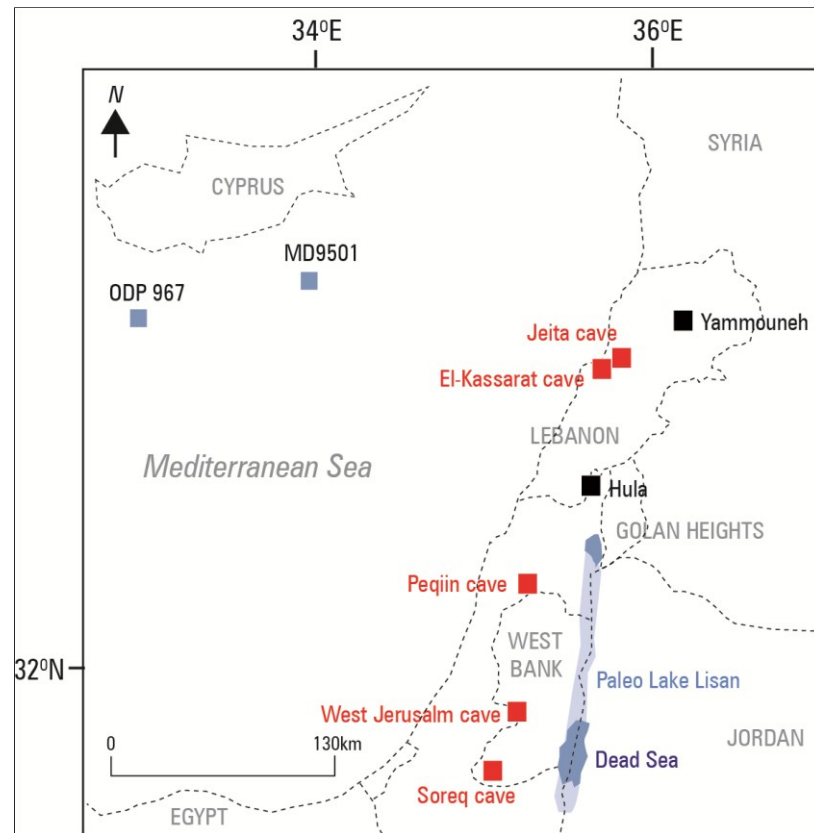
Figure 83. Map of the Levant region showing the location of caves, lakes and basins cited in the text (modified from Kolodny *et al*., 2005, Develle *et al*., 2010, Bar-Matthews *et al*, 2003).

The δ^{18}O signature of EKC-01 from 27.5 to 0.0 ka follows a similar general trend with the caves cited in Figure 83, but there are some differences.

5.5.4.1.1 Phase 1 (27.5-15.0 ka)

During Phase 1 the EKC-01 and West Jerusalem cave seem to follow the same trend and the δ^{18}O record is enriched. Soreq and Pequiin caves' records are more enriched in comparison to the El-Kassarat and West Jerusalem caves from 27 to 18 ka.

164

From 18 to 15 ka the El-Kassarat record follows a similar trend to that of Soreq cave record with differences occurring in the timing of the transition between the glacial and interglacial period. The drop in enrichment in Soreq and Pequiin caves occurs earlier than that of West Jerusalem and El-Kassarat caves (15.0 to 13.0 in El-Kassarat and 17.0 to 16.0 in Soreq and Pequiin caves). The peak enrichment $d^{18}O$ values in Soreq and Pequiin caves occurs earlier too (from 20.0 to 18.0 ka) than that in El-Kassarat and West Jerusalem caves (from 16.0 to 15.0 ka). Since the $\delta^{18}O$ values in this Phase are more enriched then the climate can be determined as dry and probably glacial since continental temperatures at this time are reported to have been 6ºC colder (12-16ºC) than present temperatures in the Eastern Mediterranean (Bar-Matthews *et al*., 1997). Lake Lisan was also at a high stand during this phase, probably due to low evaporation rates because of the low temperature although this analysis is contested (Horowitz and Gat, 1984, Goodfriend and Magaritz, 1988).

Bar-Matthews *et al*. (1997, 1999) interpreted the $\delta^{18}O$ as mostly linked to variations in amount of rainfall, but Frumkin *et al*. (1999b) interpreted $\delta^{18}O$ variations as mainly due to changes in the $\delta^{18}O$ values of the source waters.

Although Lebanon has a higher precipitation rate, the close regional proximity of the five caves shows comparable isotopic trends to climate in Phase 1.

5.5.4.1.2 Phase 2 (15.0-13.0 ka)

There is a lapse in the timing of the transition between the Pleistocene to early Holocene epochs (i.e. the drop into more negative $\delta^{18}O$ values) from the cave records.

Soreq and Pequiin caves $\delta^{18}O$ values drop first ($\approx$16 ka) and then El-Kassarat cave ($\approx$14ka) followed by West Jerusalem cave ($\approx$13 ka). This could be due to different local climatic changes, or different local rainfall rates.

5.5.4.1.3 Phase 3 (13.0 -9.0 ka)

During this time interval there is no record for the Pequiin cave any longer but the Jeita cave record begins. Jeita, Soreq and West Jerusalem caves all show more enriched $\delta^{18}O$ values than the El-Kassarat record. They all show a marked increase in negative $\delta^{18}O$ values indicating the shift to more humid conditions as well as increased rainfall.

5.5.4.1.4 Phase 4 (9.0-7.0 ka)

During this phase the Jeita, Soreq and west Jerusalem cave records all show an increase in negative values while the El-Kassarat record shows a decrease. This could be due to the low resolution sampling rate of EKC-01 or it could be due to the 8.2 ka event which was discussed earlier.

166

5.5.4.1.5 Phase 5 (7.0-0.0 ka)

During this time interval the cave records have similar $\delta^{18}O$ values except for jeita cave which is more enriched. The Soreq cave record (Bar-Matthews *et al*., 1997, 1999) and lake levels (Frumkin *et al*., 1994) suggest wet conditions for the period from 7.0 to 4.0 ka but the Jeita record shows a decrease in negative $\delta^{18}O$ values between 3.0 and 4.0 ka indicating a shorter wet period (Verheyden *et al*., 2008). The West Jerusalem records it most negative $\delta^{18}O$ value at nearly 4.5 ka. The El-Kassarat record is superimposed between the Jeita and Soreq caves records.
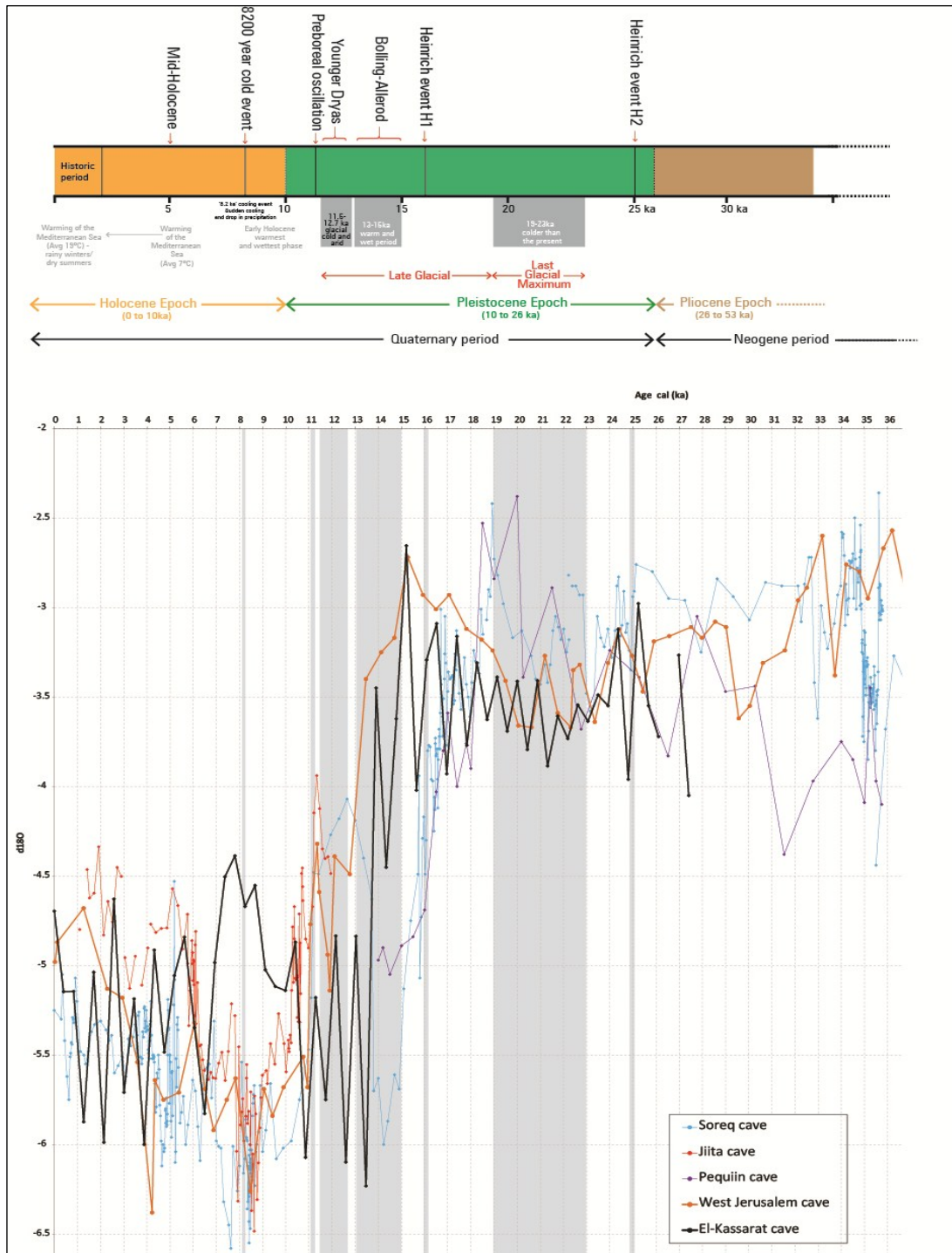
Figure 84. Correlation charts from various speleothem records, with the studied section of EKC-01, Jeita, Peqiin, West Jerusalm and Soreq caves records (modified from Bar-Matthew *et al*.1996, 1997, Verheyden *et al*., 2008, Frumkin *et al*., 2000; Robinson *et al*., 2006, Gradstein *et al*., 2012).

5.5.4.2 Sea-land climatic correlation of offshore core $\delta^{18}O$ record (*G.ruber*) and $\delta^{18}O$ values of the EKC-01 stalagmite

Since the source for the cave waters is mainly derived from the Mediterranean Sea than a comparison between land-based and marine isotope records has the potential to be comparable. A comparison is made between the marine record from the planktonic foraminifera species *G. ruber* , the SST values and the El-Kassarat cave record identified in this study. Figure 85 plots the isotopic results from the EKC-01, SST values from various studies, ODP 967 and core 9501 (modified from Almogi-Labin *et al*., 2009).

Two marine based cores were studied; The RV Marion Dufresnae – MDVAL core 9501, located in the northern Levantine basin, at the coordinates 34º32'N and 33º59'E, with a water depth of 980m, and a core length of 11m; and the ODP 967, also located in the northern Levantine basin, at coordinates 34°04.098'N and 32°43.523'E, with a water depth of 2553m, and a core length of 142m. Core 9501, SE off Cyprus. ODP site 967 is mostly under the influence of the North Atlantic/ Mediterranean climate system (Almogi-Labin *et al*., 2009).

The SST references are obtained from various references cited.

The El-Kassarat cave record does trend similarly to that of the marine records although the values of the $\delta^{18}O$ is generally more negative. This is to be expected due to the fractionation of the isotopic signature from the sea to the land. Land based $\delta^{18}O$ varies between 5 to 7‰ to the marine cores' record. The high $\delta^{18}O$ values are similar

from 27.5 to 15ka although there is a time lapse between the increase in negative $\delta^{18}O$ values from glacial to interglacial periods. The drop occurs from 19 to 13 ka in the marine cores, while it occurs from 15 to 13 ka in the El-Kassarat isotope values. The SST for this period shows low values which is expected for a glacial /cold period.

There is a warming trend in the eastern Mediterranean seawater from 13 ka to the present with average seawater temperature (SST) of approximately 18°C. Today the average seawater temperature is around 19°C (Verheyden *et al*., 2008).

The shift from the late Pleistocene to the Holocene was caused by a rise in temperature of about 10°C (Emeis *et al*., 2000). This large temperature change reflects the fact that the Mediterranean Sea is landlocked and isolated from the moderating effects of the Atlantic Ocean (Almogi-Labin *et al*., 2009). During interglacial period the SST varied between 17 and 21°C, and during the glacial the SST was lower, dropping to 11°C during the LGM. Bar-Matthews (2003) thought it fair to assume that any changes in SST in the past were also reflected in the land temperatures.

Kolodny *et al*. (2005) interpreted that the cave records $\delta^{18}O$ values mainly reflect sea surface $\delta^{18}O$ changes while Bar-Matthews *et al*. (2003), interpreted $\delta^{18}O$ changes during interglacial periods to largely reflect the decreasing $\delta^{18}O$ values in rainfall with the increase in precipitation rates.
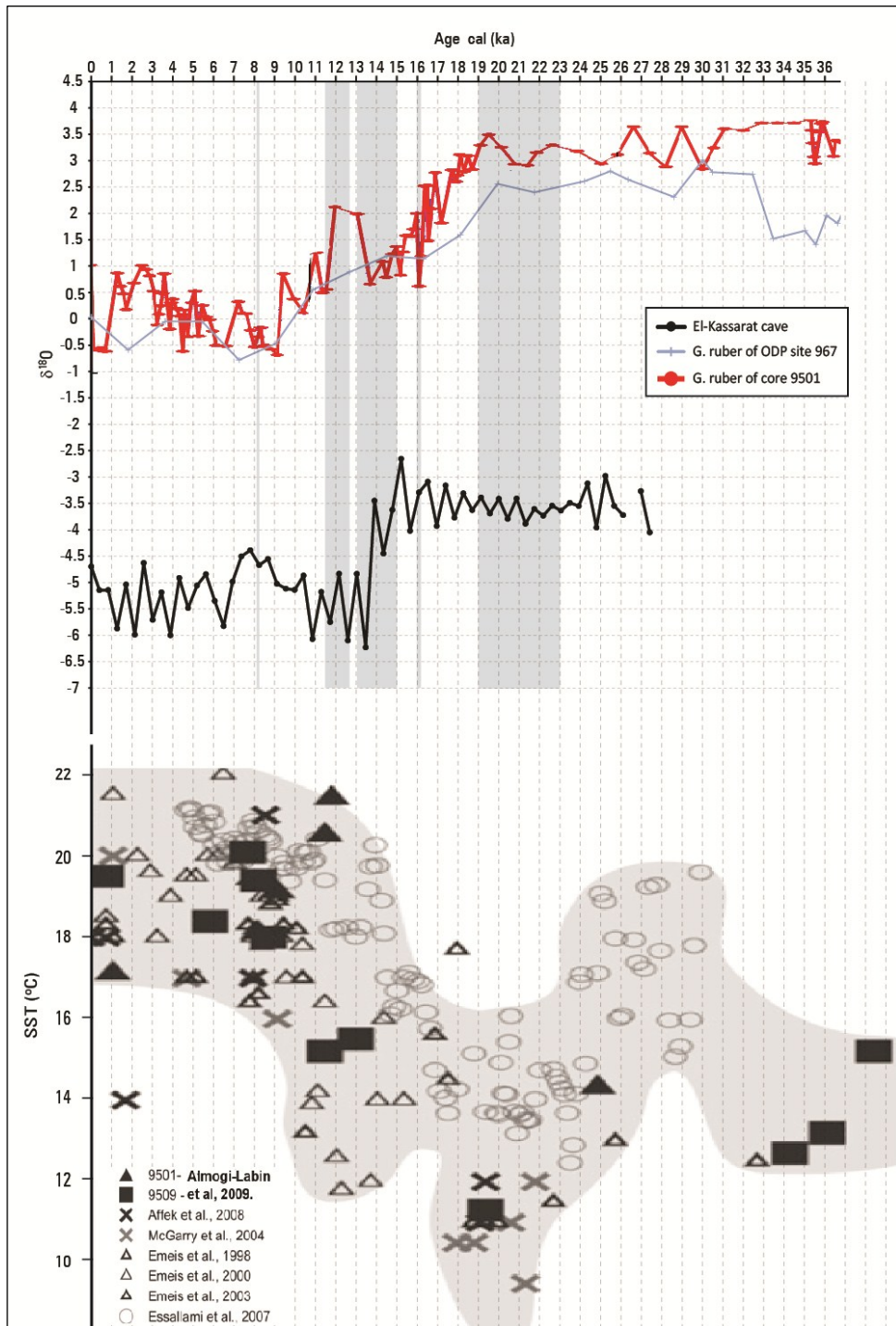
Figure 85. Plot of the isotopic results from the EKC-01, SST, ODP 967 and core 9501 (modified from Almogi-Labin *et al*., 2009 and Emeis *et al*., 2000).

171

CHAPTER 6

6.1   Conclusion

This study shows that a highly intricate collection of processes occur in cave settings and affect the final isotopic and trace element compositions in growing speleothems.

In order to understand paleoclimatic changes in the past, current conditions should be understood. Therefore the stratigraphic and structural setting, the extent of rainfall, the source of the rainfall and its chemical composition, the extent of soil cover and vegetation cover, thickness and nature of the epikarst, dripwater rates and chemical composition, the cave temperature and humidity, the shape of the stalagmite, the petrographic details, and isotopic compositions, and trace elements are required for a better all-around picture and understanding. Collecting all this data will not only allow us to understand the present conditions but will help in calibrating the past conditions, which will allow us to open a window into the past environment.

Two stalagmites, EKC-01 and RC-01, were removed from the coastal El-Kassarat cave and a high elevation Rahwe cave respectively. Groundwater, dripwater, rainwater and snow samples were acquired for isotope analyses and physico-chemical parameters. Continuous temperature measurements were conducted for a year. Glass plates were placed inside the two caves to collect modern calcite precipitates for calibration

purposes. All these allowed a better understanding and refinement of the isotopic and age data collected from the two stalagmites.

RC-01 sample of the Rahwe cave was drilled for U-series dating. Four samples were drilled for U/Th dating. The RC-01 stalagmite showed reversals and alteration and so requires further assessment which is beyond the scope of this study.

EKC-01 of the Kassarat cave was in good condition for isotopic and age studies. The top candlestick section was drilled for U-series dating (three samples), and analyzed for carbonate $\delta^{18}O$ and $\delta^{13}C$ isotopes and trace elements (64 samples). The EKC-01 stalagmite grew from approximately 62 to 400 ka period.

Isotopic sampling results have shown that the stalagmite recorded major changes in local and global climatic changes, at it has five major climatic phases.

Phase 1 (between 27.5 and 15.0 ka) revealed colder and low rainfall conditions, with a mixture of C_3 and C_4 vegetation types. As the glaciers melted there was a sharp increase in temperature and rainfall, and maybe an increase in C_3 vegetation occurred from 15.0 to 13.0 ka. The phase from 13.0 to 9.0 showed comparatively more humid conditions with an increase in rainfall representing the early Holocene epoch. A small relatively colder period occurred from around 9.0 to 7.0 ka that could be due to the 8.2 cold event. From around 7.0 ka the conditions were close to the present day environments with warm temperatures and more rainfall.

In this study it was also not possible to determine a correlation between high altitude and coastal paleoclimatic conditions because of the difficulties faced with the RC-01 stalagmite.

This study shows that global and local climatic changes are registered in Lebanese stalagmites and can be further investigate deeper into past climatic conditions. This is not only a window to the past but a possible door for the study of the future climatic changes.

Bar-Matthews (2000, 2003) showed that the amount effect was strong in controlling isotopes values and they have interpreted this for the Holocene record of Soreq cave. However, prior to the Holocene, boundary conditions were different so it is unsafe to conclude the same hypothesis. The El-Kassarat cave record appears to show the source effect control on isotope values during the glacial period and the Holocene.

The results of this study provide a valuable insight of the past climatic events that have happened in Lebanon and the Eastern Mediterranean. The study shows that climate changes have occurred for thousands, and probably for millions of years. These changes were due to many different reasons but essentially, all the changes have occurred due to some natural process that had taken place in geological times.

Today, the climate change issue is still being debated. Can we learn from the past to predict future climates? We can use past paleoclimatic shifts to predict what could happen with the local, and possibly, global climate. We know a lot concerning past

174

events with somewhat reliable confidence. However, future predictions will require more data collection and higher resolution analyses.

This study have provided some keystones in our knowledge of the paleo-environment, extended the Lebanese record, and set the stage for future works and future climatic studies.

6.2   Recommendations

In order to make a better assessment of stalagmite isotopic studies it is recommended that the following be undertaken:

Setting up *in situ* monitoring stations outside the two cave to measure temperature, rainfall rates, CO_2, and humidity levels continuously.

Setting up *in situ* monitoring stations inside the two cave to measure cave temperature, CO_2 concentration, air flow, and humidity levels continuously. Specific studies are required to determine the best location for these stations.

In addition long-term data collection of the following parameters is required:

- $\delta^{18}O/\delta^2H$ values of precipitation (rain and snow) - monthly

- $\delta^{18}O/\delta^2H$ of dripwater – monthly, and the drip rate

- $\delta^{18}O/ \delta^{13}C$ of present-day calcite precipitates (on glass tiles)

- Trace elements in the dripwater, as well as in modern calcite and speleothem calcite

Both these *in situ* monitoring stations and long term data collection will help determine the effect cave processes have on the modern calcite precipitation. In turn this could help in determining the processes that controlled the growth of the stalagmites under study.

As for the stalagmites themselves specifically (the EKC-01 and RC-01 stalagmites):

- More U/Th dating with very specific studied locations for the sampling far from any detrital deposits

- Continuation of the entire stalagmite's $\delta^{18}O/\delta^{13}C$ values

- Micromilling for a more high resolution isotope sampling

- Further petrographic studies based on locations of U/Th sampling as well as $\delta^{18}O/\delta^{13}C$ values

- Continued monitoring of the cave's waters (monthly) and temperature (yearly)

- Dripwater rates (drip plate for continuous logging)

- Modern calcite farming using glass plates

- The study of stable isotopic composition of the fluid inclusions.

REFERENCES

- Abi-Saleh, B., and Safi. S., 1988. Carte de la Végétation du Liban. Ecologia Mediterranean XIV (1/2); Carte de la Végétation du Liban. Ecologia Mediterranean XIV (1/2).

- Affek, H. P., Bar-Matthews, M., Ayalon, A., Matthews, A. & Eiler, J. M., 2008 Glacial/interglacial temperature variations in Soreq cave speleothems as recorded by 'clumped isotope' thermometry. Geochim. Cosmochim. Acta 72, 5351–5360.

- Almogi-Labin, A., Bar-Matthews, M., Shriki, D., Kolosovsky, E., Paterne, M., Schilman, B., Ayalon, A., Aizenshtat, Z., Matthews, A., 2009. Climatic variability during the last 90 ka of the southern and northern Levantine basin as evident from marine records and speleothems. Quatern. Sci. Rev. 28, 2882e2896.

- Aouad-Rizk A., Job J.O., Najem W., Travi Y., Blavoux B., Gourcy L., 2005-Oxygen-18 and deuterium contents over mount Lebanon related to air mass trajectories and local parameters. In: Isotopic composition of the precipitation in the Mediterranean Basin in relation to air circulation patterns and climate. AIEA-TECDOC-1453, Vienne, p: 75-82.

- Aouad-Rizk, A. 2006. Etude isotopique de la pluie et de la neige au Liban. PhD Thesis. L'Universite D'Avignon et de L'Universite Saint Joseph.

- Atlas climatique du Liban, Tome 1. 1977, Service Météorologique, Ministère des Affaires Publics, Beirut.

- Awad, S. 2011. Isotopic study (18O, 2H) of the ground water in the Bekaa's plain (Lebanon). Seventh International Conference on Material Sciences

(CSM7). Physics Procedia 21, 13 – 21.

- Ayalon A., Bar-Matthews M., and Kaufman A., 1999. Petrography, trace elements (Ba, Sr, Mg and U) and isotope geochemistry of strontium and uranium in speleothems as paleoclimate proxies, Soreq Cave, Israel. Holocene 9, 715–722.

- Ayalon A., Bar-Matthews, M., Sass, E., 1998 Rainfall-recharge relationships within a karstic terrain in the Eastern Mediterranean semi-arid region, Israel: d18O and dD characteristics. Journal of Hydrology 207 (1998) 18-21.

- Ayalon, A., Bar-Matthews, M., Frumkin, A., Matthews, A., 2013. Last Glacial warm events on Mount Hermon: the southern extension of the Alpine karst range of the east Mediterranean. Quaternary Science Reviews 59, pp43-56.

- Badini., J., 2010. The geochemistry of cave calcite deposits as a record of past climate. The sedimentary record, Vol 8, No 2.

- Baker, A. and Smart, P. L. ,1995, Recent flowstone growth rates: Field measurements in comparison to theoretical predictions, Chemical Geology, 122, 121-128.

- Baker, A., Genty, D., Dreybrodt, W., Grapes, J., Mockler, N.J., 1998. Testing theoretically predicted stalagmite growth rate with recent annually laminated stalagmites: implications for pastnstalagmite deposition. Geochimica et Cosmochimica Acta 62, 393–404.

- Baker, A., Genty, D., Fairchild, I.J., 2000. Hydrological characterisation of stalagmite drip waters at Grotte de Villars, Dordogne, by the analysis of inorganic species and luminescent organic matter. Hydrology and Earth System Sciences 4, 4392449.B.

- Baker, A., Smith, C.L., Jex, C., Fairchild, I.J., Genty, D., Fuller, L., 2008. Annually laminated speleothems: a review. International Journal of Speleology 37, 193–206.

- Baldini, J. U. L. 2001, Morphologic and dimensional linkage between recently deposited speleothems and drip water from Browns Folly Mine, Wiltshire, England. Journal of Cave and Karst Studies 63(3): 83-90.

- Bar-Matthews M, Ayalon A, Kaufmann, A., 2000. Timing and hydrological conditions of Sapropel events in the Eastern Mediterranean, as evident from speleothems, Soreq cave, Israel. Chemical Geology 169. 145–156.

- Bar-Matthews M, Gilmour M, Ayalon A, Vax A, Kaufmann A, Frumkin A & Hawkesworth C., 2000. Variation of Palaeoclimate in the Eastern Mediterranean Region – as Derived from Speleothems in Various Climate Regimes in Israel. Journal of Conference Abstracts Volume 5(2), 194, Cambridge Publications.

- Bar-Matthews M., Matthews A., Ayalon A., 1991 - Environmental controls of speleothem mineralogy in a karstic dolomitic terrain (Soreq cave). Journal of Geology 99: 189207.

- Bar-Matthews, M., Avalon, A. and Kaufman, A., 1997. Late Quaternary Paleoclimate in the Eastern Mediterranean Region from Stable Isotope Analysis of Speleothems at Soreq Cave, Israel. QUATERNARY RESEARCH 47, 155–168 (1997).

- Bar-Matthews, M., Avalon, A., Matthews, A., Sass, E., and Halicz, L., 1996, Carbon and oxygen isotope study of the active water-carbonate system in a karstic Mediterranean cave: Implications for paleoclimate research in semiarid regions: Geochimica et Cosmochimica Acta, v. 60, p. 337-347.

- Bar-Matthews, M., Ayalon, A., Kaufman, A., and Wasserburg, G. J., 1999. The Eastern Mediterranean paleoclimate as a reflection of regional events: Soreq Cave, Israel. Earth and Planetary Science Letters 166, pp. 85-95.

- Bar-Matthews, M.; Ayalon, A.; Gilmour, M.; Matthews, A.; Hawkesworth, C.J., 2003. Soreq and Peqiin Caves, Israel Speleothem Stable Isotope Data, IGBP PAGES/World Data Center for Paleoclimatology Data Contribution Series #2003-061. NOAA/NGDC Paleoclimatology Program, Boulder CO, USA.

- Borsato A., 1997. Dripwater monitoring at Grotta di Ernesto (NE Italy): a contribution to the understanding of karst hydrology and the kinetics of carbonate dissolution. Proc. of the 12th Int. Congr. of Speleology, La Chaux-de-Fonds, Switzerland 2: 57-60.

- Bradley R.S., 1999. Paleoclimatology - International Geophysics Series, Monograph, 64, Harcourt Academic Press, 610p.

- Broecker, W.S., Olsen, E.A., Orr, P.C., 1960. Radiocarbon measurements and annual rings in cave formations. Nature 185, 93–94.

- Campisano, C. J. 2012, Milankovitch Cycles, Paleoclimatic Change, and Hominin Evolution. Nature Education Knowledge 4(3):5.

- Cerling T.E. and Quade J., 1993. Stable carbon and oxygen isotopes in soil carbonates. Climate Change in Continental Isotopic Records, Geophysical Monograph 78 AGU: 217-231.

- Coplen, T.B., Herczeg, A. L., and Barnes, C., 2000. Isotope engineering: using stable isotopes of the water molecule to solve practical problems, in Environmental Tracers in Subsurface Hydrology, ed. by P.G. Cook and

A.L. Herczeg, Kluwer Academic Publishers, Boston.

- Craig, H., 1957, Isotopic standards for carbon and oxygen and correction factors for mass spectrometric analysis of carbon dioxide, Geochimica et Cosmochimica Acta, 12, 133-149.

- Craig, H., 1961. Isotopic variations in meteoric waters. Science 133, 1833-1834.

- Dansgaard, W. 1964, Stable isotopes in precipitation, Tellus, 16, 436.

- Darling, W.G., 2011, The isotope hydrology of quaternary climate changeq. Journal of Human Evolution 60, 417e427.

- Davies C. P., 2005. Quaternary paleoenvironments and potential for human exploitation of the Jordan plateau desert interior. Geoarchaeology 20:379–400.

- De Villiers, S., Greaves, M. and Elderfield, H. 2002, An intensity ratio calibration method for the accurate determination of Mg/Ca and Sr/Ca of marine carbonates by ICP-AES. Geochemistry Geophysics Geosystems, 3.

- Develle, A. L., Gasse, F., Vidal, L., Williamson, D., Demory, F., Van Campo, E., Ghaleb, B., Thouveny, N., 2011. A 250 ka sedimentary record from a small karstic lake in the Northern Levant (Yammoûneh, Lebanon) Paleoclimatic implications. Palaeogeography, Palaeoclimatology, Palaeoecology 305 - 10–27.

- Develle, A.-L., Herreros, J., Vidal, L., Sursok, A., Gasse, F., 2010. Controlling factors on a paleo-lake oxygen isotope record (Yammoûneh, Lebanon) since the Last Glacial Maximum. Quatern. Sci. Rev. 186, 416–425.

- Directorate General of Civil Aviation, Department of Meteorology, Beirut International Airport, Lebanese Republic, Ministry of Public Works and Transport.

- Dorale, J. A., Edwards, R. L., Onac, B. P. (2002), Stable Isotopes as Environmental Indicators in Speleothems, In Karst Processes and the Carbon Cycles, Final Report of IGCP379, Edited by Y. Daoxian and Z. Cheng, Geological Publishing House, Beijing, China, 107-120.

- Douka K, Bergman CA, Hedges REM, Wesselingh FP, Higham TFG., 2013. Chronology of Ksar Akil (Lebanon) and Implications for the Colonization of Europe by Anatomically Modern Humans.

- Dreybrodt, W., 1980, Deposition of calcite from thin film of calcareous solutions and the growth of speleothems, Chem. Geol., 29, 89-105.

- Dubertret L., 1945-1960. Geological map 1:50.000, Beirut Sheet, Beirut 1960.

- Dubertret L., 1945-1960. Geological map 1:50.000, Tannourine Sheet, Beirut 1960.

- Edwards, R. L., Chen, J. H., Wasserburg, G. J. 1986, 238U-234U-230Th-232Th systematics and the precise measurement of time over the past 500,000 years, Earth and Planetary Science Letters, 81, 175-192.

- Emeis, K.C., Struck, U., Schulz, H.-M., Rosenberg, R., Bernasconi, S.,Erlenkeuser, H., Sakamoto, T., Martinez-Ruiz, F., 2000. Temperature and salinity variations of the Mediterranean Sea surface waters over the last 16,000 years from records of planktonic stable oxygen isotopes and alkenone unsaturation ratios. Palaeogeography, Palaeoclimatology, Palaeoecology 158,

259–280.

- Emiliani, C., 1955. Pleistocene temperatures. Journal of Geology, 63, 538-78.

- Enzel, Y., Amit, R., Dayan, U., Crouvi, O., Kahana, R., Ziv, B. & Sharon, D., 2008 The climatic and physiographic controls of the eastern Mediterranean over the late Pleistocene climates in the southern Levant and its neighboring deserts. Global Planet. Change 60, 165–192.

- Fairchild I. J. and Tremble P. C., 2009. Trace elements in speleothems as recorders of environmental change. Quatern. Sci. Rev. 28, 449–468.

- Fairchild I., Borsato A., Tooth A. F., Frisia S., Hawkesworth C.J., Huang Y., Dermott F., Spiro B., 2000. Controls on trace element (Sr-Mg) compositions of carbonate cave waters: Implications for speleothem climatic records.- Chemical Geology, 166, 255-269.

- Fairchild I.J. and McMillan E.A. 2007. Speleothems as indicators of wet and dry periods. International Journal of Speleology, 36 (2), 69-74. Bologna (Italy).

- Fairchild I.J., Tooth A.F., Huang Y., Borsato A., Frisia S., Mcdermott F., Spiro B., 1999 - Bedrock and climatic controls on the cationic composition of karst waters. In: Geochemistry of the Earth's surface, Proc. of the fifth Int. Symp. on the geochemistry of the Earth's Surface, ed. Armannson H., Balkema, Rotterdam: 8790.

- Fairchild, I. J., Baker, A., 2012. Speleothem Science: From Process to Past Environments. Wiley-Blackwell, Pp450.

- Fairchild, I. J., Smith, C. L., Baker, A., Fuller, L., Spötl, C., Mattey, D., McDermott, F., E.I.M.F. 2006b, Modification and preservation of

environmental signals in speleothems, Earth-Science Reviews, 75, 105-153.

- Fairchild, Ian J; Bradby, Lawrence; Sharp, Martin; Tison, Jean-Louis., 1994. Earth Surface Processes and Landforms, Hydrochemistry of carbonate terrains in alpine glacial settings. Volume 19, Issue 1, pp. 33 – 54.

- Fairchild,I. J., Spotl, C. Frisia, S. Borsato, A. Susini, J. Wynn, P. M., Cauzid, J. 2010. Petrology and geochemistry of annually laminated stalagmites from an Alpine cave (Obir, Austria): seasonal cave physiology. Geological Society, London, Special Publications, 336:295-321.

- Fetter, C.W., 2007, Applied Hydrogeology. Macmillan College Publishing, Inc., New York, 616 p.

- Finne, M., Holmgren, K., Sundqvist,H. S., Weiberg,E., Lindblom, M., 2011. Climate in the eastern Mediterranean, and adjacent regions, during the past 6000 years e A review. Journal of Archaeological Science 38 (2011) 3153-3173.

- Finné, M., Holmgren, K., Sundqvist, H.S., Weiberg, H., Lindbolm, M., 2011. Climate in the Eastern Mediterranean, and adjacent regions, during the past 6,000 years review. Journal of Archaeological Science 38, 3153e 3173.

- Fleitmann, D., and Matter, A., 2009. The speleothem record of climate variability in Southern Arabia. C. R. Geoscience 341 (2009) 633–642.

- Fleitmann, D, Burns, S J., Neff, U; Mangini, A; Matter, A., 2003. Changing moisture sources over the last 330,000 years in Northern Oman from fluid-inclusion evidence in speleothems. Quaternary Research, Volume 60, issue 2, p. 223-232.

- Frisia S., Borsato A., Preto N., and McDermott F. (2003) Late Holocene

annual growth in three Alpine stalagmites records the influence of solar activity and the North Atlantic Oscillation on winter climate. Earth Plan. Sci. Lett. 216, 411–424.

- Frisia, S., Borsato A., 2010. Chapter 6, Karst Review Article, Developments in Sedimentology, Volume 61, Pages 269-318.

- Frisia, S., Borsato, A., Fairchild, I.J. & McDermott, F., 2000. Calcite fabrics, growth mechanisms, and environment of formation in speleothems from the Italian Alps and southwestern Ireland. Journal of Sedimentary Research 70, 1183-1196.

- Frisia, S., Borsato, A., Mangini, A., Spötl, C., Madonia, G., Sauro, U. 2006, Holocene climate variability in Sicily from a discontinuous stalagmite record and the Mesolithic to Neolithic transition, Quaternary Research, 66, 388-400.

- Frumkin A., Ford D.C., Schwarcz H.P., 1999. Continental Oxygen Isotopic Record of the Last 170,000 Years in Jerusalem. Quaternary Research, Volume 51, Number 3, pp. 317-327(11).

- Frumkin, A., D.C. Ford, and H.P. Schwarcz., 2000. Paleoclimate and Vegetation of the Last Glacial Cycles in Jerusalem From a Speleothem Record. Global Biogeochem. Cycles, 14(3), 863-870.

- Frumkin, A., BarYosef, O., Schwarcz, H. P., 2011. Possible paleohydrologic and paleoclimatic effects on hominin migration and occupation of the Levantine Middle Paleolithic.Journal of Human Evolution 60.

- Frumkin, A.; Barmatthews, M.; Vaks, A., 2008. Paleoenvironment of Jawa basalt plateau, Jordan, inferred from calcite speleothems from a lava tube. Quaternary Research, vol. 70, issue 3, pp. 358-367.

- Gascoyne M., 1992. Paleoclimate determination from cave calcite deposits - Quat. Sci. Rew., 11, 609-632.

- Gascoyne, M., Schwarcz, H.P., Ford, D., 1980. A palaeotemperature record for the mid-Wisconsin in Vancouver Island. Nature 285, 474–476.

- Gasse, F., Vidal, L. Develle, A.-L. and Van Campo, E. 2011, Hydrological variability in the Northern Levant: a 250 ka multi-proxy record from the Yammoûneh (Lebanon) sedimentary sequence. Clim. Past, 7, 1261–1284.

- Gat, J. R., and I. Carmi. 1987. Effect of climate changes on the precipitation patterns and isotopic composition of water in a climate transition zone: Case of the Eastern Mediterranean Sea area. ─ IAHS Publ. no. 168, pp. 513-523.

- Gat, J.R., Klein, B., Kushnir, Y., Roether, W., Wernli, H., Yam, R., Shemesh, A., 2003. Isotope compos   tion of air moisture over the Mediterranean Sea: an index of the air–sea interaction pattern. Tellus B Chem. Phys. Meteorol. 55, 953–965.

- Gázquez, F., Calaforra, J.M., Forti, P., Stoll, H., Ghaleb, B., Delgado-Huertas, A., 2014. Paleoflood events recorded by speleothems in cave, Earth Surface Processes and Landforms, Lane, S. N. (eds). Vol 39.

- Genty D. and Deflandre G., 1998, Drip flow variations under a stalactite of the Père Noël Cave (Belgium). Evidence of seasonal variations and air pressure constraints. Journal of Hydrology, Vol. 211, n° 1-4, pp. 208-232.

- Genty, D. and Quinif, Y. 1996, Annually laminated sequences in the internal structure of some Belgian stalagmites - importance for Paleoclimatology, Journal of Sedimentary Research, 66, 275-288.

- Genty, D., Baker, A., Massault, M., Procter, C., Gilmour, M., Pons- Banchu,

E., Hamelin, B., 2001a. Dead carbon in stalagmites: carbonate bedrock paleodissolution vs. ageing of soil organic matter. Implications for 13C variations in speleothems. Geochimica et Cosmochimica Acta 65, 3443–3457.

- Gradstein, F. M., Ogg, J. G., Schmitz, M. D., and Ogg, G. M., eds., 2012, The geologic time scale 2012: Elsevier, 1,144 p.

- Gillieson D., 1996. Caves: Processes, Development and Management. Blackwell, 324 pp.

- Goede, A., McCulloch, M., McDermott, F., Hawkesworth, C., 1998. Aeolian contribution to strontium and strontium isotope variations in a Tasmanian speleothem. Chem. Geol. 149, 37–50.

- Gourcy, L., Aouad-Rizk, A., Araguas, L., Argiriou, A., Bono, P., Diaz-Teijeiro, M.F., Dirican, A., El-Asrag, A.M., Gat, J., Gonfiantini, R., Horvatincic, N., Ouda, B., Carreira-Paquete, P., Rank, D., Saighi, O., Travi, Y., Vreca. P., 2004. Isotopic composition of precipitation in relation to air circulation patterns in the Mediterranean basin: Preliminary results. International Workshop on the Application of Isotope Techniques in Hydrological and Environmental Studies UNESCO, Paris, France, September 6-8.

- Gradstein, F. M., Ogg, J. G., Schmitz, M. D., and Ogg, G. M., eds., 2012, The geologic time scale 2012: Elsevier, 1,144 p.

- Hajar, L., Khater, C., Cheddadi, R., *et al*., 2008. Vegetation changes during the late Pleistocene and Holocene in Lebanon: a pollen record from the Bekaa Valley. Holocene 18 (7), 1089–1099.

- Hellstrom, J.C., McCulloch, M.T., 2000. Multi-proxy constraints on the climatic significance of trace element records from a New Zealand

speleothem. Earth and Planetary Science Letters 179, 287–297.

- Hendy, C., 1971. The isotopic geochemistry of speleothems. Geochimica et Cosmochimica Acta, 35: 801-824.

- Hendy, C.H., Wilson, A.T., 1968. Palaeoclimate data from speleothems. Nature 219, 48– 51.

- Hill, C.A. and Forti, P., 1986. Cave Minerals of the World. National Speleological Society, Hunstville.

- Hoefs, J., 1997. Stable Isotope Geochemistry, 4th ed., Springer-Verlag, Berlin.

- Houghton J., 2004. Global Warming - Cambridge University Press, 351p.

- http://www.gly.uga.edu/railsback/speleoatlas

- IAEA, 2005. Isotopic composition of precipitation in the Mediterranean Basin in relation to air circulation patterns and climate Final report of a coordinated research project 2000–2004.

- IPCC Fourth Assessment Report: Climate Change, 2007.

- Kano A, Kambayashi T, Fujii H, Matsuoka J, Sakuma K, Ihara T. 1999. Seasonal variation in water chemistry and hydrological conditions of tufa deposition of Shirokawa, Ehime Prefecture, southwestern Japan. Journal of the Geological Society of Japan 105 (4), 289–304.

- Kaufman, A, Wasserburg, GJ, Porcelli, D, Bar-Matthews, M, Ayalon, A and Halicz, L., 1998. U-Th isotope systematics from the Soreq cave, Israel and climatic correlations. *Earth and Planetary Science Letters*. Vol. 156, pp. 141-

- Kendall, A. C. and Broughton, P. L. 1978, Origin of fabrics in speleothems composed of columnar calcite crystals, Journal of Sedimentary Petrology, 48, 519-538.

- Kendall, C. 1998. Tracing nitrogen sources and cycling in catchments In: C. Kendall and J.J. McDonnell (Eds.), Isotope Tracers in Catchment Hydrology, Elsevier, Amsterdam, pp. 519-576.

- Kim S.T., O'Neil J.R., 1997. Equilibrium and non-equilibrium oxygen isotope effects in synthetic carbonates - Geochimica et Cosmochimica Acta, 61, 16, 3461-3475.

- Koeniger, P., Margane, A. & Himmelsbach, T., 2012. Stable isotope studies on altitude effect and karst groundwater catchment delineation of the Jeita spring in Lebanon. IAH congress, Niagara Falls,

- Kolodny, Y., Stein, M., Machlus, M., 2005. Sea-rain-lake relation in the Last Glacial East Mediterranean revealed by d18O–d13C in lake Lisan aragonites. Geochimica et Cosmochimica Acta 69, 4045–4060.

- Korfali, S., and Jurdi. M., 2007. Assessment of domestic water quality: case study, Beirut, Lebanon. Environ. Monit. Assess., 135:241–251.

- Kroon, D., Alexander, I. T., Little, M. G; Lourens, L., Matthewson, A; Robertson, A. H. F., Sakamoto, T., 1998. Oxygen isotope and sapropel stratigraphy in the eastern Mediterranean during the last 3.2 million years. In: Robertson, AHF; Emeis, K-C; Richter, C; Camerlenghi, A (eds.), Proceedings of the Ocean Drilling Program, Scientific Results, 160: College Station, TX (Ocean Drilling Program), 160, 181-189.

- Kuczumow A., Genty D., Chevallier P., Nowak J., Ro CU., 2003 - Annual resolution analysis of a SW France stalagmite by Xray synchrotron microprobe analysis. Spectrochimica Acta Part B 58:851865.

- Kurter, A. 1988, Glaciers of Turkey, glaciers of turkey,US Geological Survey professional paper 1386-g-1.

- Labaky, W., N. (1998), A hydrogeological and environmental assessment of the Faouar Antelias catchment - MS thesis, American University of Beirut, Lebanon.

- Lachniet, M.S., 2009a. Climatic and environmental controls on speleothem oxygen isotope values. Quaternary Science Reviews 28, 412-432.

- Langmuir, D. (1997), Aqueous Environmental Geochemistry, Prentice Hall, New Jersey, 600 pp.

- Lauritzen S.E., Lundberg J., 1999. Speleothems and climate.- The Holocene-sp. issue, 9,9, 643-647.

- Leng M. J. (ed.). 2006. Isotopes in Palaeoenvironmental Research. Springer, Dordrecht, The Netherlands. pp. 307.

- LMS, 1977. Atlas Climatique du Liban. Beirut: Lebanese Meteorological Service.

- Margane, A., 2013. Protection of Jeita cave. BGR, German/Lebanese Technical Cooporation paper.

- Matthews A., Ayalon A. and Bar-Matthews M. 2000, D/H ratios of fluid inclusions of Soreq Cave Israel speleothems as a guide to the Eastern

Mediterranean Meteoric Line relationships in the last 120 ky. Chem. Geol. 166, 183–191.

- McDermott, F., 2004. Palaeo-climate reconstruction from stable isotope variations in speleothems: a review. Quaternary Science Reviews 23, 901–918.

- McGarry S. F. and Baker A. (2000) Organic acid fluorescence. applications to speleothem palaeoenvironmental reconstruction. Quat. Sci. Rev. 19, 1087–1101.

- Mickler, P. J., Banner, J. L., Stern, L., Asmerom, Y., Edwards, R. L., Ito, E. (2004), Stable isotope variations in modern tropical speleothems: Evaluating equilibrium vs. kinetic isotope effects, Geochimica et Cosmochimica Acta, 68, 4381-4393.

- Miryam Bar-Matthews, M, Ayalon, A., Gilmour, M., Matthews, A, And Hawkesworth, C. 2003. Sea–land oxygen isotopic relationships from planktonic foraminifera and speleothems in the Eastern Mediterranean region and their implication for paleorainfall during interglacial intervals. Geochimica et Cosmochimica Acta, Vol. 67, No. 17, pp. 3181–3199.

- Muñoz-García, M.B., López-Arce, P., Fernández-Valle, M.E., Martín-Chivelet, J., Fort, R., 2012. Porosity and hydric behavior of typical calcite microfabrics in stalagmites. Sedimentary Geology 265-266: 72-86.

- Musgrove M., Banner J. L., Mack L. E., Combs D. M., James E. W., Cheng H., Edwards R. L., 2001. Geochronology of late Pleistocene to Holocene speleothems from central Texas: Implications for regional paleoclimate. GSA Bulletin, 113; 1532–1543.

- Nader, F., Cheng, H., Swennen, R., Verheyden, S. 2013, Holocene paleoclimate reconstruction based on stalagmite studies from Lebanon.

Presented at the 16th International Congress of Speleology, Brno, Czech Republic.

- Neev, D., and Emery, K. O., 1995. The Destruction of Sodom, Gomorrah, and Jericho. Oxford Univ. Press, London.

- Nehme, C. Delannoy, J.-J. Jaillet, S. Adjizian-Gerard, J. Hellstrom, J., Comaty, T., Arzouni, M., Matta, P. 2013 .sedimentary study and U-Th datations contribution to the morphodynamic reconstitution of the junction chamber (Kassarat cave, Nabay, Lebanon): A geomorphological approach for palaeohydrological records analysis. Presented at the 16th International Congress of Speleology, Brno, Czech Republic.

- Nordhoff, P., 2005. Stable isotope investigations on speleothems from different cave systems in Germany. PHD dissertation. Natural Sciences Faculties, Georg - August – University.

- O' Leary M.H., 1981 Carbon isotope fractionation in plants. Phytochemistry 20: 553-567.

- Orland, I J. Bar-Matthews, M. Ayalon, A., 2012. (in press) Seasonal resolution of Eastern Mediterranean climate change since 34 ka from a Soreq Cave speleothem, Geochimica et Cosmochimica Acta.

- Orland, I.J., Bar-Matthews, M., Kita, N.T., Ayalon, A., Matthews, A.,Valley, J. W., 2009. Climate deterioration in the Eastern Mediterranean as revealed by ion microprobe analysis of a speleothem that grew from 2.2 to 0.9 ka in Soreq Cave, Israel. Quaternary Research 71 (1), 27-35.

- Petit M. 1999. Le changement climatique d'origine humaine. Rappel de quelques résultats généraux. C.R.Acad.Sci.Paris Earth and Planetary Sciences, 328, 225-227.

- Pierre, C., 1999. The oxygen and carbon isotope distribution in the Mediterranean water masses. Marine Geology 153, 51–55.

- Plagnes V *et al*. 2002, A discontinuous climatic record from 187 to 74 ka from a speleothem of the Clamouse Cave (south of France), Earth and Planetary Science Letters 201: 87-103.

- Pourmand, A., Tissot, F. L. H., Arienzo, M. and Sharifi, A., 2014. Introducing a Comprehensive Data Reduction and Uncertainty Propagation Algorithm for U-Th Geochronometry with Extraction Chromatography and Isotope Dilution MC-ICP-MS. Geostandards and Geoanalytical Research. doi: 10.1111/j.1751-908X.2013.00266.x.

- Railsback, L. B., Brook, G. A., Chen, J., Kalin, R., Fleischer, C. J. 1994, Environmental controls on the petrology of a late Holocene speleothem from Botswana with annual layers of aragonite and calcite, Journal of Sedimentary Research, A64, 147-155.

- Rambeau, M.C., 2010. Palaeoenvironmental reconstruction in the Southern Levant: synthesis, challenges, recent developments and perspectives. Phil. Trans. R. Soc. A (2010) 368, 5225–5248.

- Riechelmann, D. F. C., Deininger, M., Scholz, D., Riechelmann, S., Schroeder-Ritzrau, A., Spoetl, C., Richter, D. K.; Mangini, A., Immenhauser, A., 2013. Disequilibrium carbon and oxygen isotope fractionation in recent cave calcite; comparison of cave precipitates and model data. Geochimica et Cosmochimica Acta 103: 232-244.

- Robinson, S. A., Black, S., Sellwood, B. and Valdes, P.J. 2006, A review of palaeoclimates in the Levant and Eastern Mediterranean from 25,000 to 5,000 years BP: setting the environmental background for the evolution of

human civilisation. Quaternary Science Reviews , 25 1517 – 1541.

- Rozanski, K., Araguâs-Araguâs, L. & Gonfiantini, R. 1993, Isotopic patterns in modem global precipitation. In: Climate Change in Continental Isotopic Records, ed. by P. K. Swart, K. C. Lohmann, J. McKenzie & S. Savin, 1-37. Geophysical Monograph 78, American Geophysical Union.

- Rozanski, K., Araguas-Araguas, L., Gonfiantini, R. 1992, Relation Between Long-Term Trends of Oxygen-18 Isotope Composition of Precipitation and Climate, Science, 258, 981-985.

- Saad, Z., Kazpard, V. A., Geyh, M. A., and Slim, K., 2005. Chemical and isotopic composition of water from springs and wells in the Damour river basin and the coastal plain in Lebanon. Journal of Environmental Hydrology. Vol 12, page 18.

- Schwarcz, H.P., 1986. Geochronology and isotopic geochemistry of carbonates in the weathering zone. In: Fritz, P., Fontes, J.Ch. (Eds.), Handbook of Environmental Isotope Geochemistry, The Terrestrial Environment, B, vol. 2. Elsevier, Amsterdam, pp. 271– 300.

- Shopov, Y. Y., Ford, D. C., Schwarcz, H. P. 1994, Luminescent microbanding in speleothems: high-resolution chronology and paleoclimate, Geology, 22, 407-410.

- Siddall, M., Rohling, E. J., Thompson, W. G., Waelbroeck, C. 2008. Marine isotope stage 3 sea level fluctuations: data synthesis and new outlook. Reviews of Geophysics. 46, 1-29.

- Spötl, C. and Mangini, A. 2002, Stalagmite from the Austrian Alps reveals Dansgaard-Oeschger events during isotope stage 3: Implications for the absolute chronology of Greenland ice cores, Earth and Planetary Science

Letters, 203, 507-518.

- Springer, G.S., Rowe, H.D., Hardt, B., Edwards, R.L., Cheng, H., 2008. Solar forcing of Holocene droughts in a stalagmite record from West Virginia in east-central North America. Geophysical Research Letters, 35.

- Stein, M., Torfstein, A., Gavrieli, I. & Yechieli, Y., 2010 Abrupt aridities and salt deposition in the post-glacial Dead Sea and their North Atlantic connection. Quatern. Sci. Rev. 29, 567–575.

- Thompson, P., Schwarcz, H.P., Ford, D.C., 1974. Continental Pleistocene climatic variations from speleothem age and isotopic data. Science 184, 893-895.

- Tohmé, G. and Tohmé, H., 2007. Illustrated Flora of Lebanon. CNRS.

- UNDP, 2013. (in press) Provision of Assessing the National Groundwater Resources through data collection and field assessment Campaign of Groundwater Resources across Lebanon.United Nations Development Programme (UNDP) & Ministry of Energy and Water (MoEW), Beirut Lebanon.

- Vaks , A., Bar-Matthews, M., Ayalon, A., Matthews, A., Frumkin, A., Dayan, U., Halicz, L., Almogi-Labin, A. and Schilman, B., 2006, Paleoclimate and location of the border between Mediterraneanclimate region and the Saharo-Arabian Desert as revealed by speleothems from the northern Negev Desert, Israel., Earth and Planetary Science Letters, 249, 3-4, 384-399.

- Vaks, A., Bar-Matthews, M., Ayalon, A., Schilman, B., Gilmour, M., Hawkesworth, C.J., Frumkin, A., Kaufman, A., Matthews, A., 2003, Ma'ale Efrayim Cave, Israel Speleothem Stable Isotope Data, IGBP PAGES/World Data Center for Paleoclimatology Data Contribution Series #2003-053.

NOAA/NGDC Paleoclimatology Program, Boulder CO, USA.

- Vaks, A., Bar-Matthews, M., Matthews, A., Ayalon, A., Frumkin, A., 2010, Middle-Late Quaternary paleoclimate of northern margins of the Saharan-Arabian Desert: reconstruction from speleothems of Negev Desert, Israel, *Quaternary Science Reviews*, 29, 19-20, 2647-2662.

- Vaks, A., Bar-Matthews, M.,Ayalon, A., Schilman, B., Gilmour, M., Hawkesworth, C., Frumkin, A., Kaufman, A., Matthews, A., 2003. Paleoclimate reconstruction based on the timing of speleothem growth and oxygen and carbon isotope composition in a cave located in the rain shadow in Israel. Quaternary Research 59, 182–193.

- Verheyden S., Genty D., Deflandre G., Quinif Y. and Keppens E. 2008, Monitoring climatological, hydrological and geochemical parameters in the Pe`re Noe¨l cave (Belgium): implication for the interpretation of speleothem isotopic and geochemical timeseries. Int. J. Speleol. 37, 221–234.

- Verheyden S., Keppens E., Fairchild I.J., Mc Dermott F., Weis D., 2000. Mg, Sr and Sr isotope geochemistry of a Belgian Holocene speleothem: implications for paleoclimate reconstructions. Chemical Geology 169: 131144.

- Verheyden S., Nader F. H., Cheng H. J., Edwards L. R. and Swennen R., 2008. Paleoclimate reconstruction in the Levant region from the geochemistry of a Holocene stalagmite from the Jeita cave, Lebanon. Quaternary Research 70: 368-381.

- Verheyden, S., 2001, Speleothems as palaeoclimatic archives. A study of the stable isotopic and geochemical behaviour of the cave environment and its Late Quaternary records. Ph.D. in science at the Vrije Universiteit Brussel, Belgium.

- Verheyden, S., 2004. Trace elements in speleothems. A short review of the state of the art. Int. J. Speleol., 33 (1/4), 2004: 95-101.

- Walley C., 1998. Some outstanding issues in the geology of Lebanon and their importance in the tectonic evolution of the Levantine region. Tectonophysics, Volume 298, Issues 1–3, 30 November 1998, Pages 37–62.

- Walley C.D., 1997. The Lithostratigraphy of Lebanon: A Review. Lebanese Scientific Research Reports, 10: 81-108.

- White, W. B. 2007, Cave sediments and paleoclimate. Journal of Cave and Karst Studies, v. 69, no. 1, p. 76–93.

- Ziv, B., Dayan, U., Kuschnir, Y., Roth, C., Enzel, Y., 2006. Regional and global atmospheric patterns governing rainfall in the southern Levant. Int. J. Climatol. 26, 55–73.

APPENDICES

8.2   Appendix 2: Geological map of the El-Kassarat cave study area
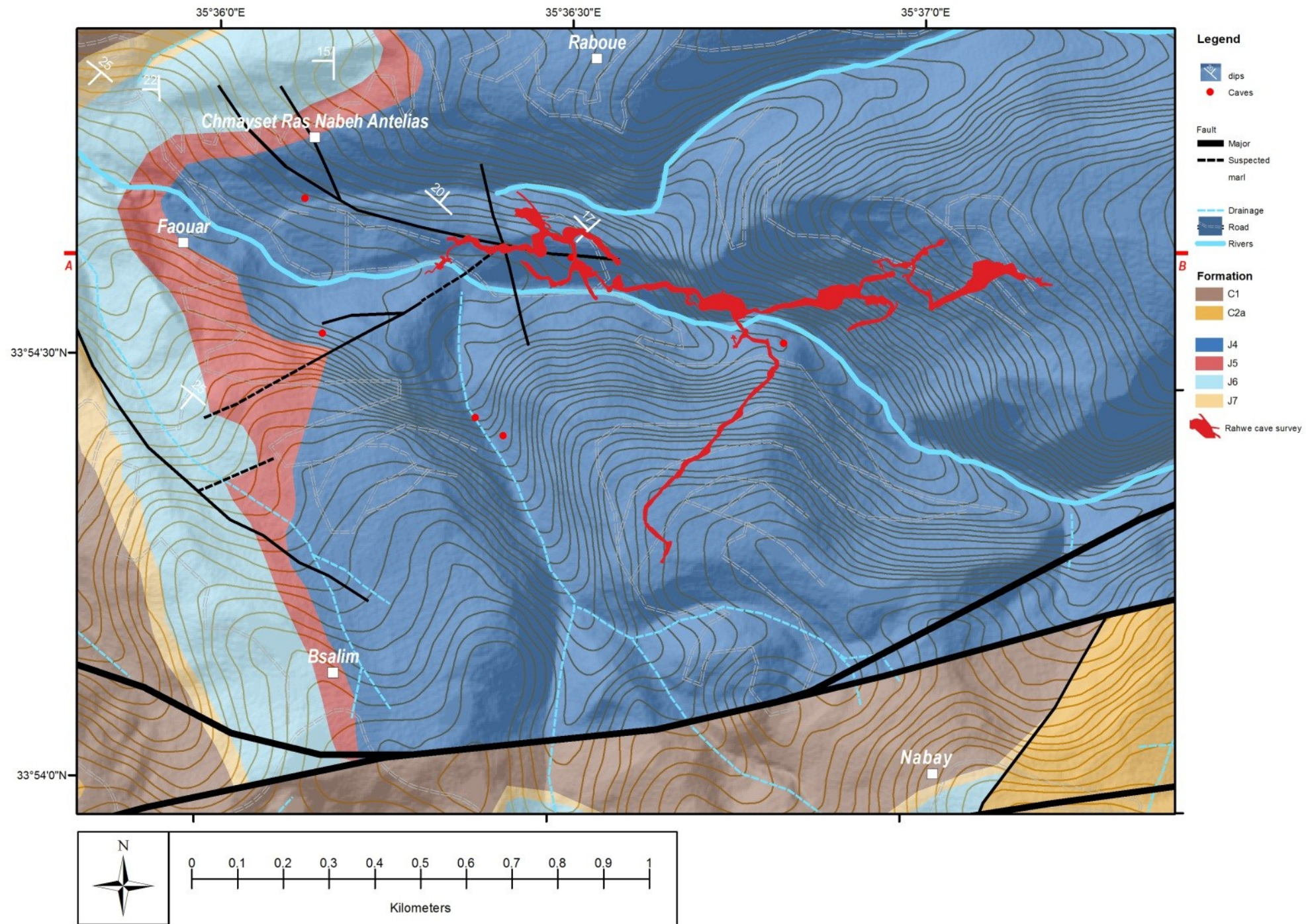
8.3   Appendix 3: Survey of Rahwe cave (2013, SCL Archives, drawn by Rena Karanouh, Issam bou Jaoude)
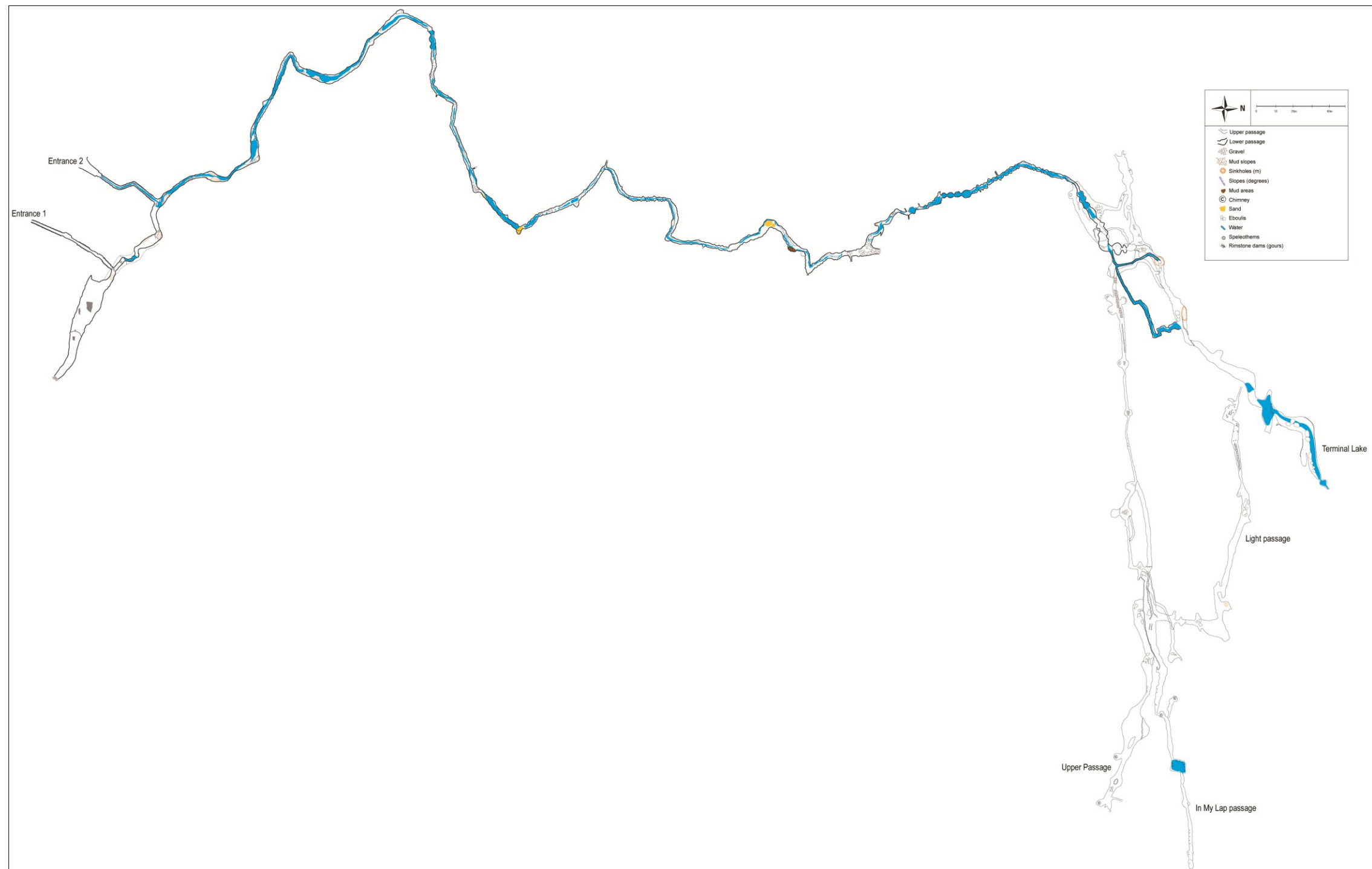
8.4   Appendix 4: Geological map of the Rahwe cave study area
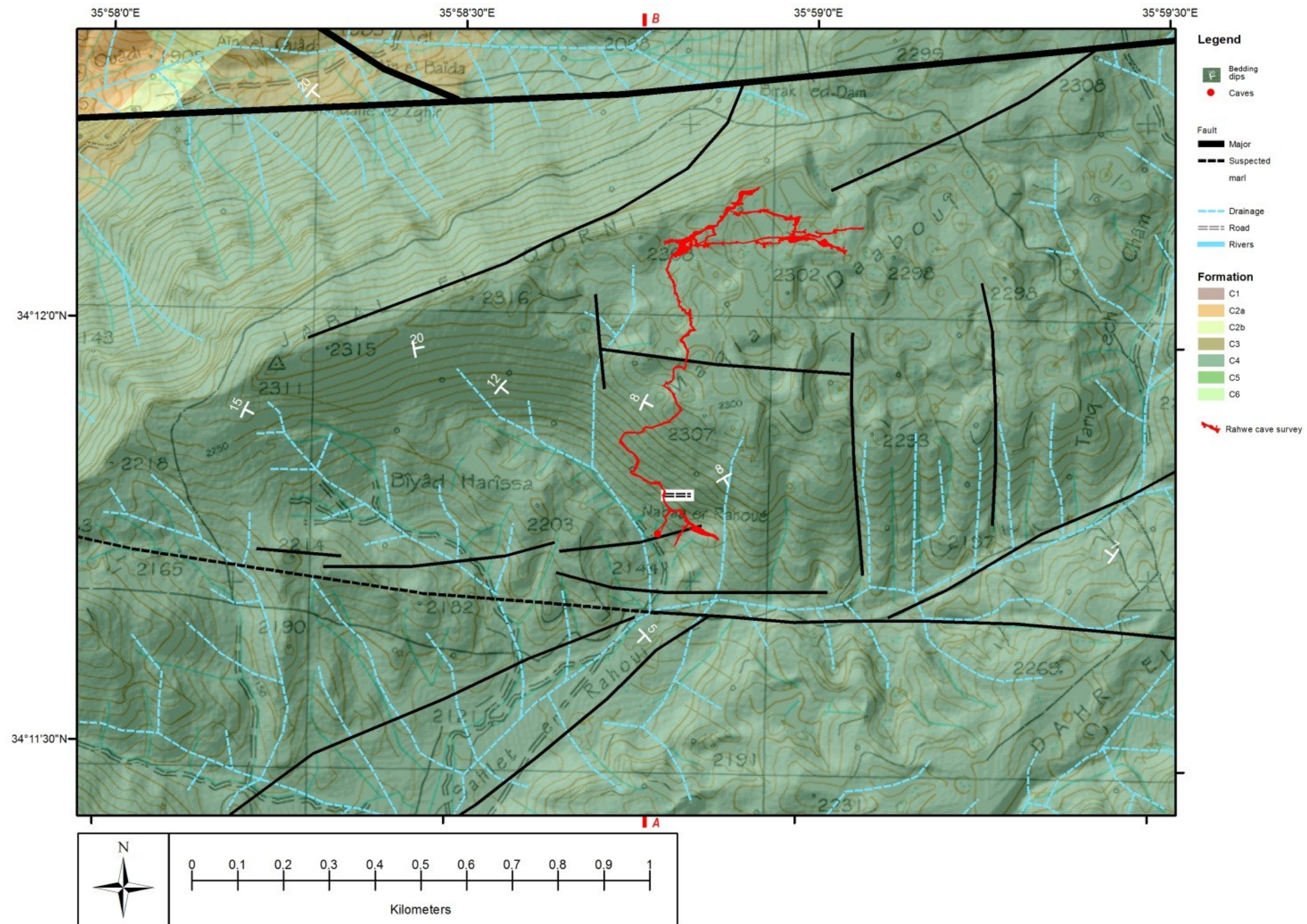
8.5 Appendix 5: Tinytag summary report table

S/N	661574	661584	661558	668266
LOGGER ID	TGP-4017	TGP-4017	TGP-4017	TGP-4017
Description	Rahwe cave	Salle du President's Passage El-Kassarat cave	Forage Passage El-Kassarat cave	Traverse line location El-Kassarat cave
Property	Temperature	Temperature	Temperature	Temperature
Logging Started	11/19/2012 05:47:10	11/04/2012 12:55:06	11/04/2012 12:53:10	03/17/2013 15:40:30
Logging Ended	08/24/2013 11:47:00	08/22/2013 10:25:00	08/22/2013 08:38:00	08/22/2013 09:55:00
Logging Duration	24040790.30 s	25133394.00 s	25127090.20 s	13630469.80 s
Offload Operator	user	user	user	user
Trigger Start	FALSE	FALSE	FALSE	FALSE
Start Delay	72000.00 s	7200.00 s	7200.00 s	22380.00 s
Interval	900.00 s	900.00 s	900.00 s	900.00 s
Stop Mode	When full	When full	When full	When full
Offload Time	08/24/2013 11:51:23	08/22/2013 10:40:50	08/22/2013 08:55:41	08/22/2013 10:09:28
Number of Readings	26713	27927	27920	15146
Stop Reason	Still Logging	Still Logging	Still Logging	Still Logging
Logging Mode	Minutes Mode	Minutes Mode	Minutes Mode	Minutes Mode
Statistics Start Time	11/19/2012 05:39:30	11/04/2012 12:47:30	11/04/2012 12:45:30	03/17/2013 15:32:30
Statistics End Time	08/24/2013 11:47:00	08/22/2013 10:25:00	08/22/2013 08:38:00	08/22/2013 09:55:00
Minimum Reading	-0.7 ℃	16.3 ℃	16.6 ℃	15.1 ℃
Maximum Reading	5.6 ℃	17.4 ℃	18.3 ℃	16.9 ℃
Average Reading	3.9 ℃	16.9 ℃	17.4 ℃	15.8 ℃
Mean Kinetic Temperature	4.0 ℃	16.9 ℃	17.4 ℃	15.9 ℃

8.6   Appendix 6: Results of Tinytag temperature logger in the El-Kassarat cave
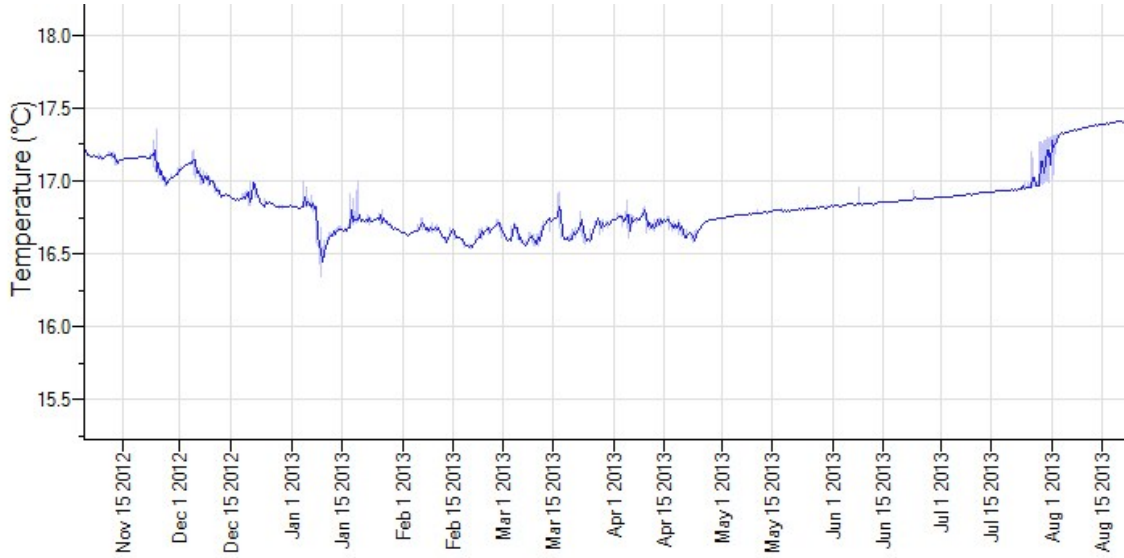
Salle du President Gallery's cave air temperature graph from the Tinytag logger
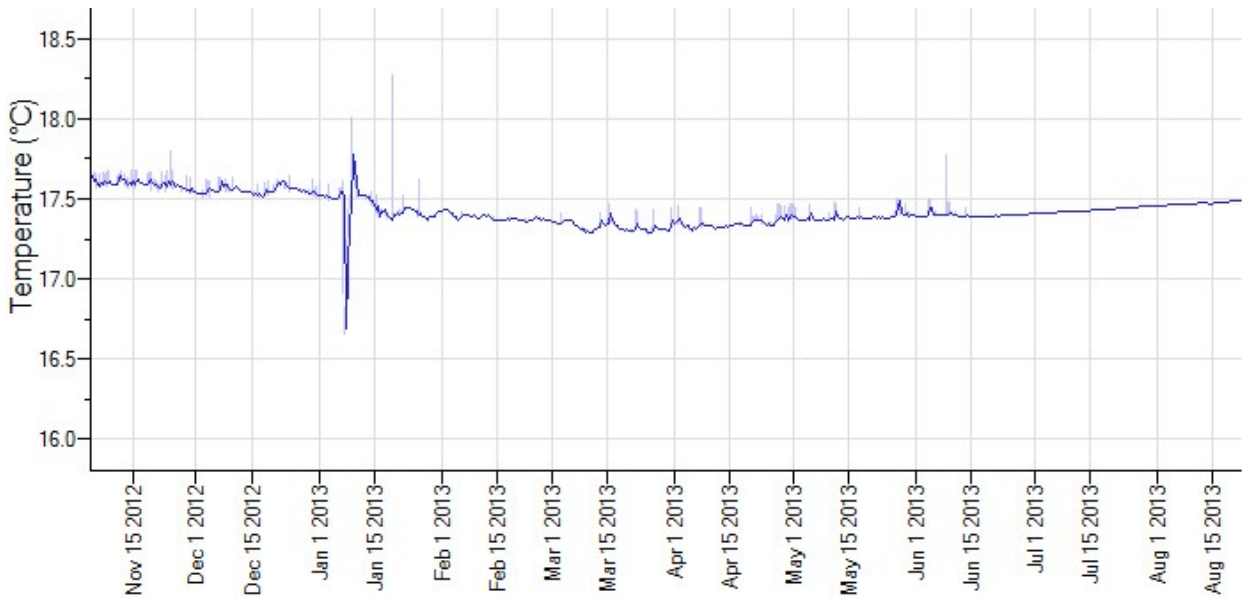
The Forage gallery's cave air temperature graph from the Tinytag logger. The mid-January anomaly is due to a flooding period that deposited mud ontop of the Tinytag logger indicating that the water level must have reached higher than the Tinytag.
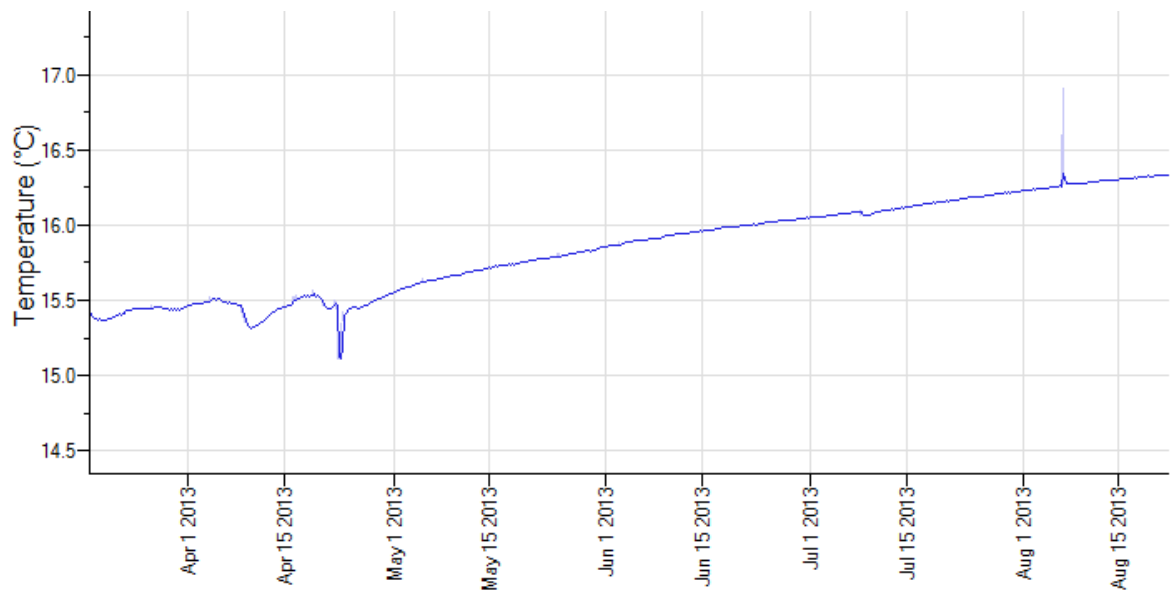
The Traverse line location cave air temperature graph from the Tinytag logger.

8.7   Appendix 7: pH, Temperature, Conductivity and TDS levels for the El-Kassarat and Rahwe caves' waters (measured from a handheld meter)

Parameter	Water type	pH	T (°C)	Conductivity (μs)	TDS (ppm)
El-Kassarat cave / 24.11.12	Groundwater	6.94	15.5	500	350
El-Kassarat cave: Forage passage / 24.11.12	Dripwater	6.94	17.8	448	313
El-Kassarat cave: Gallerie du President passage / 24.11.12	Dripwater	7.23	17.4	450	314
El-Kassarat cave / 8.6.13	Groundwater	6.85	15.4	493	345
El-Kassarat cave: Forage passage / 8.6.13	Dripwater	6.85	17.5	468	329
El-Kassarat cave: Gallerie du President passage / 8.6.13	Dripwater	6.84	16.9	461	322
El-Kassarat cave / 22.8.13	Groundwater	6.82	15.9	528	370
El-Kassarat cave: Forage passage / 22.8.13	Dripwater	6.96	17.4	471	329
El-Kassarat cave: Gallerie du President passage 22.8.13	Dripwater	6.54	17.1	470	328
Rahwe cave / 22.10.12	Groundwater	8.38	5	243	169
Rahwe cave / 9.6.13	Groundwater	8.11	4.9	223	155
Rahwe cave: near entrance / 9.6.13	Dripwater	8.02	7.0	213	148
Rahwe cave: near stalagmite / 9.6.13	Dripwater	8.18	5.9	264	185
Rahwe cave 22.8.13	Groundwater	8.06	-	226	156
Rahwe cave: near entrance 22.8.13	Dripwater	8.08	-	198.4	139
Rahwe cave: near stalagmite / 22.8.13	Dripwater	8.13	-	198.7	139.3

8.8   Appendix 8: Results of physico-chemical results for water sampling from groundwater, dripwater, snow and rainwater, for the El-Kassarat and Rahwe caves, conducted in November 2012 (Civil Engineering Service Laboratories, AUB)

Parameter	EL-KASSARAT CAVE				RAHWE CAVE		
	Rainwater (12.11.12)	Groundwater (16.2.13)	Dripwater (President's Gallery) (21.10.12)	Dripwater (Forage Gallery) (21.10.12)	Rainwater (12.11.12)	Groundwater (18.11.12)	Dripwater (18.11.12)
Turbidity	10.3	-	0.45	1.4	2.2	0.48	1.6
Conductivity (μS)	45.9	369	315	327	46.2	153.8	146.6
Total Dissolved Solids (mg/L 25ºC)	22.6	185	157	164	23.1	77	76
pH	8.93	6.67	7.01	6.71	8.22	8.16	8.19
Hydroxide alkalinity (mg/L as $CaCO_3$)	0	0	0	0	0	0	0
Carbonate alkalinity (mg/L as $CaCO_3$)	4	0	0	0	3.2	0	0
Bicarbonate alkalinity (mg/L as $CaCO_3$)	15.2	238	231	217	34.8	123	116.4
Total Hardness (mg/L as $CaCO_3$)	15	279	216	225	33	109	95
Calcium Hardness (mg/L as $CaCO_3$)	6	218	79.4	88.6	22	31.7	36.1
Magnesium Hardness (mg/L as $CaCO_3$)	9	61	4.3	3.4	11	7.3	1.2
Sulfate (mg/L SO_4^{2-})	7	19	<7	<7	<7	<7	<7
Chlorides (mg/L Cl^-)	11.6	19.1	27.6	31.3	12.1	7.7	6
Iron (mg/L)	0.22	<0.2	<0.1	0.15	<0.2	<0.1	<0.1
Manganese (mg/L)	< 0.2	<0.2	<0.1	<0.1	<0.2	<0.1	<0.1
Potassium (mg/L)	3	1	0.4	2.2	2.7	<1	<1
Sodium (mg/L)	4.5	10.7	9.1	16.5	4.5	1.8	2.47

8.9 Appendix 9: Results of physico-chemical results for water sampling from groundwater, dripwater, snow and rainwater, for the El-Kassarat and Rahwe caves, conducted in June 2013 (Civil Engineering Service Laboratories, AUB)

Parameter	EL-KASSARAT CAVE			RAHWE CAVE			
	Groundwater (8.6.13)	Dripwater (President's Gallery) (8.6.13)	Dripwater (Forage Gallery) (8.6.13)	Groundwater (9.6.13)	Dripwater – Entrance location (9.6.13)	Dripwater – Stalagmite location (9.6.13)	Snow (4.4.13)
Turbidity	<0.5	<0.5	<0.5	<0.5	<0.5	<0.5	<0.5
Conductivity (μS)	451	411	419	136.1	142.2	160.2	8.31
Total Dissolved Solids (mg/L 25ºC)	226	206	209	68.3	72.6	80	4.17
pH	6.76	6.77	6.77	7.57	7.58	7.62	7.24
Hydroxide alkalinity (mg/L as $CaCO_3$)	0	0	0	0	0	0	0
Carbonate alkalinity (mg/L as $CaCO_3$)	0	0	0	0	0	0	0
Bicarbonate alkalinity (mg/L as $CaCO_3$)	223	229	195	114	108	139	13.6
Total Hardness (mg/L as $CaCO_3$)	266	268	252	154	150	187	77
Calcium Hardness (mg/L as $CaCO_3$)	208	208	207	97	113	123	25
Magnesium Hardness (mg/L as $CaCO_3$)	58	60	45	57	37	64	52
Sulfate (mg/L SO_4^{2-})	31	<7	13	<7	<7	<7	<7
Chlorides (mg/L Cl^-)	30	33.3	31.2	21.2	19.5	15.6	13.8
Iron (mg/L)	<0.25	<0.25	<0.25	0.29	<0.25	<0.25	<0.25
Manganese (mg/L)	<0.2	<0.2	<0.2	<0.2	<0.2	<0.2	<0.2
Potassium (mg/L)	<0.2	<0.2	<0.2	<0.2	<0.2	<0.2	<0.2
Sodium (mg/L)	11.5	10	14.8	1.7	1.9	2.3	<0.1

8.10 Appendix 10: EKC-01, results δ^{18}O and δ^{13}C measurements

Age (yrs)	Distance (um)	Run	Sample	Number	std.dev. [o/oo]	std.dev. [o/oo]	δ^{13}C VPDB [o/oo]	δ18O VPDB [o/oo]	c	o
									5 pt running average	
0	0	D2001	EKC-01	1	0.02	0.02	-10.39	-4.70	-10.39	-4.70
399	5000	D2001	EKC-01	2	0.03	0.04	-11.05	-5.15	-10.72	-4.92
835	10000	D2001	EKC-01	3	0.02	0.05	-12.06	-5.14	-11.17	-5.00
1271	15000	D2001	EKC-01	4	0.02	0.10	-11.50	-5.87	-11.25	-5.22
1706	20000	D2001	EKC-01	5	0.03	0.04	-11.31	-5.04	-11.26	-5.18
2142	25000	D2001	EKC-01	6	0.03	0.03	-12.38	-5.99	-11.66	-5.44
2578	30000	D2001	EKC-01	7	0.04	0.10	-11.42	-4.63	-11.73	-5.33
3013	35000	D2001	EKC-01	8	0.02	0.04	-12.12	-5.71	-11.75	-5.45
3449	40000	D2001	EKC-01	9	0.02	0.04	-11.43	-5.19	-11.73	-5.31
3885	45000	D2001	EKC-01	10	0.02	0.04	-12.21	-6.00	-11.91	-5.50
4320	50000	D2001	EKC-01	11	0.02	0.06	-10.99	-4.91	-11.63	-5.29
4756	55000	D2001	EKC-01	12	0.02	0.03	-11.50	-5.48	-11.65	-5.46
5192	60000	D2001	EKC-01	13	0.02	0.03	-11.60	-5.06	-11.55	-5.33
5628	65000	D2001	EKC-01	14	0.03	0.12	-11.83	-4.84	-11.63	-5.26
6063	70000	D2001	EKC-01	15	0.02	0.01	-12.01	-5.35	-11.58	-5.13
6499	75000	D2001	EKC-01	16	0.02	0.03	-11.93	-5.83	-11.77	-5.31
6935	80000	D2001	EKC-01	17	0.02	0.03	-11.11	-4.98	-11.69	-5.21
7370	85000	D2001	EKC-01	18	0.03	0.09	-10.62	-4.50	-11.50	-5.10
7806	90000	D2001	EKC-01	19	0.04	0.05	-11.20	-4.39	-11.37	-5.01
8242	95000	D2001	EKC-01	20	0.02	0.03	-11.24	-4.67	-11.22	-4.87
8677	100000	D2001	EKC-01	21	0.05	0.13	-11.25	-4.55	-11.08	-4.62
9113	105000	D2001	EKC-01	22	0.04	0.07	-11.36	-5.02	-11.13	-4.63
9549	110000	D2001	EKC-01	23	0.06	0.08	-11.82	-5.12	-11.37	-4.75
9985	115000	D2001	EKC-01	24	0.03	0.08	-11.80	-5.14	-11.49	-4.90
10420	120000	D2001	EKC-01	25	0.07	0.07	-10.88	-4.87	-11.42	-4.94
10856	125000	D2001	EKC-01	26	0.02	0.02	-12.02	-6.07	-11.58	-5.24
11292	130000	D2001	EKC-01	27	0.03	0.06	-11.38	-5.18	-11.58	-5.28
11727	135000	D2001	EKC-01	28	0.10	0.15	-11.91	-5.75	-11.60	-5.40
12163	140000	D2001	EKC-01	29	0.03	0.05	-11.53	-4.83	-11.54	-5.34
12599	145000	D2001	EKC-01	30	0.02	0.04	-12.17	-6.10	-11.80	-5.59
13034	150000	D2001	EKC-01	31	0.03	0.08	-10.95	-4.84	-11.59	-5.34

Age (yrs)	Distance (um)	Run	Sample	Number	std.dev. [o/oo]	std.dev. [o/oo]	$\delta^{13}C$ VPDB [o/oo]	$\delta18O$ VPDB [o/oo]	c	o
									5 pt running average	
13470	155000	D2001	EKC-01	32	0.02	0.03	-11.03	-6.23	-11.52	-5.55
13906	160000	D2001	EKC-01	33	0.05	0.07	-6.96	-3.45	-10.53	-5.09
14341	165000	D2001	EKC-01	34	0.02	0.02	-11.57	-4.45	-10.53	-5.01
14777	170000	D2001	EKC-01	35	0.02	0.02	-11.11	-3.62	-10.32	-4.52
15213	175000	D2001	EKC-01	36	0.05	0.10	-9.81	-2.66	-10.09	-4.08
15649	180000	D2001	EKC-01	37	0.02	0.02	-10.61	-4.02	-10.01	-3.64
16084	185000	D2001	EKC-01	38	0.03	0.03	-8.79	-3.29	-10.38	-3.61
16520	190000	D2003	EKC-01	38	0.02	0.04	-10.17	-3.09	-10.10	-3.34
16956	195000	D2003	EKC-01	38	0.03	0.07	-11.06	-3.93	-10.09	-3.40
17391	200000	D2003	EKC-01	38	0.03	0.05	-10.43	-3.16	-10.21	-3.50
17827	205000	D2003	EKC-01	38	0.03	0.03	-11.25	-3.77	-10.34	-3.45
18263	210000	D2003	EKC-01	38	0.02	0.03	-10.75	-3.31	-10.73	-3.45
18698	215000	D2003	EKC-01	38	0.03	0.08	-11.03	-3.63	-10.90	-3.56
19134	220000	D2003	EKC-01	38	0.03	0.05	-11.22	-3.39	-10.94	-3.45
19570	225000	D2003	EKC-01	38	0.01	0.04	-10.82	-3.69	-11.01	-3.56
20005	230000	D2003	EKC-01	38	0.02	0.05	-11.12	-3.41	-10.99	-3.49
20441	235000	D2003	EKC-01	38	0.02	0.04	-11.54	-3.79	-11.15	-3.58
20877	240000	D2003	EKC-01	38	0.02	0.04	-11.18	-3.41	-11.18	-3.54
21313	245000	D2003	EKC-01	38	0.03	0.03	-11.23	-3.89	-11.18	-3.64
21748	250000	D2003	EKC-01	38	0.02	0.04	-11.13	-3.61	-11.24	-3.62
22184	255000	D2003	EKC-01	38	0.01	0.02	-10.50	-3.73	-11.12	-3.69
22620	260000	D2003	EKC-01	38	0.03	0.03	-11.00	-3.54	-11.01	-3.64
23055	265000	D2003	EKC-01	38	0.02	0.03	-11.07	-3.64	-10.99	-3.68
23491	270000	D2003	EKC-01	38	0.02	0.02	-10.92	-3.49	-10.93	-3.60
23927	275000	D2003	EKC-01	38	0.02	0.05	-10.95	-3.55	-10.89	-3.59
24362	280000	D2003	EKC-01	38	0.03	0.06	-10.80	-3.12	-10.95	-3.47
24798	285000	D2003	EKC-01	38	0.02	0.03	-11.17	-3.96	-10.98	-3.55
25234	290000	D2003	EKC-01	38	0.09	0.15	-10.68	-2.98	-10.90	-3.42
25670	295000	D2003	EKC-01	38	0.02	0.06	-10.80	-3.55	-10.88	-3.43
26105	300000	D2003	EKC-01	38	0.02	0.03	-11.14	-3.72	-10.92	-3.47
26541	305000	D2003	EKC-01	38					-10.95	-3.55
26977	310000	D2003	EKC-01	38	0.05	0.08	-9.95	-3.27	-10.64	-3.38
27412	315000	D2003	EKC-01	38	0.02	0.04	-10.98	-4.05	-10.72	-3.65

8.11 Appendix 11: Results of the $\delta^{18}O$ and δ^2H of rain/ground and dripwaters (samples collected November, 2012)

HACETTEPE UNIVERSITY
INTERNATIONAL RESEARCH AND APPLICATION CENTER
FOR KARST WATER RESOURCES
STABLE ISOTOPE LABORATORY
ANALYSIS RESULTS

Project : ELARD-LEBANON   Approval :   Dr. M. Ekmekci

Sample No.	Sample Name	d2H Reportable Value (permil)	d2H Standard Deviation (permil)	d18O Reportable Value (permil)	d18O Standard Deviation (permil)	Analysis Date	d2H Quality (stdev <2)	d18O Quality (stdev <0.3)
1	ASSAL	-40.28	0.66	-7.90	0.10	12/12/12	OK	OK
2	LABAN	-41.36	0.76	-7.81	0.17	12/12/12	OK	OK
3	AFQA	-38.96	0.90	-7.66	0.28	12/12/12	OK	OK
4	RAHWE GROUNWATER	-43.10	0.63	-8.23	0.09	12/12/12	OK	OK
5	RAHWE DRIP ENTRANCE	-45.76	0.87	-8.46	0.12	12/12/12	OK	OK
6	RAHWE DRIP STALAGMITE	-46.41	1.01	-8.51	0.17	12/12/12	OK	OK
7	ELKASSARAT DRIP FORAGE	-26.60	0.65	-5.66	0.16	12/12/12	OK	OK
8	ELKASSARAT GROUNDWATER	-33.18	0.63	-6.84	0.07	12/12/12	OK	OK
9	ELKASSARAT DRIP PRESIDENTS GALLERY	-24.10	1.17	-5.22	0.21	12/12/12	OK	OK
10	ELKASSARAT RAIN	-31.67	0.93	-5.75	0.14	12/12/12	OK	OK
	AVERAGE		0.82		0.15		OK	OK

211

8.12 Appendix 12: Results of the $\delta^{18}O$ and δ^2H of rain/ground and dripwaters (samples collected June, 2013)

HACETTEPE UNIVERSITY
INTERNATIONAL RESEARCH AND APPLICATION CENTER
FOR KARST WATER RESOURCES   STABLE UKAM
ISOTOPE LABORATORY
ANALYSIS RESULTS

Project : LEBANON-UNDP   Approval :   Dr. M. Ekmekci

Sample No.	Sample Name	d2H Reportable Value (permil)	d2H Standard Deviation (permil)	d18O Reportable Value (permil)	d18O Standard Deviation (permil)	Analysis Date	d2H Quality (stdev <2)	d18O Quality (stdev <0.3)
1	ELKASSARATT GROUNDWATER	-36.54	0.15	-7.48	0.09	22/06/13	OK	OK
2	ELKASSARATT DRIP WATER FORAGE GALLERY	-25.62	0.52	-5.95	0.09	22/06/13	OK	OK
3	ELKASSARATT DRIP WATER PRESIDENT'S GALLERY	-22.56	0.31	-5.41	0.05	22/06/13	OK	OK
4	RAHWE DRIP WATER ENTRANCE	-49.58	0.28	-8.93	0.03	22/06/13	OK	OK
5	RAHWE SNOW	-33.19	0.46	-7.20	0.17	22/06/13	OK	OK
6	RAHWE GROUNDWATER	-45.33	0.35	-8.65	0.25	22/06/13	OK	OK
7	RAHWE DRIP WATER STALAGMITE	-45.97	0.81	-8.53	0.10	22/06/13	OK	OK
8	RAHWE RAIN	-69.96	0.08	-12.18	0.03	22/06/13	OK	OK
Averages			0.37		0.10		OK	OK

8.13 Appendix 13: Various $\delta^{18}O$ and δ^2H values from numerous sources

Sample name	Water type	δ^2H reportable value (/mil)	$\delta^{18}O$ reportable value (/mil)	Analysis date	Reference	X-coordinates	Y- coordinates	Elevation (masl)
Afqa	Spring	-45	-8.2	mean 2011	Koeniger *et al*., 2012	34.068053	35.891986	1280
Afqa	Spring	-42.8	-8.33	5/7/2012	UNDP, 2013	34.068053	35.891986	
Afqa spring	Groundwater	-38.96	-7.66	12/12/2012	Turkey	34.06824º	35.8933º	1280
Ain el Karsab	Groundwater - spring	-27.3	-5.78	4/28/1972	UNDP, 2013	33.329167	35.390278	270
Ain ez Zarqa	Groundwater - spring	-25.9	-5.68	4/28/1972	UNDP, 2013	33.119444	35.199167	200
Ain Raha	spring	-43.12	-8.77	5/7/2012	UNDP, 2013	34.204638	35.909227	
Akaot	Damour river	-32.1	-6.65	5/4/2001	Saad et al, 2004			499
Akaot	Damour river	-31.4	-6.63	10/6/2001	Saad et al, 2004			499
Akaot	Damour river	-31.7	-6.83	1/8/2001	Saad et al, 2004			499

213

Sample name	Water type	δ^2H reportable value (/mil)	$\delta^{18}O$ reportable value (/mil)	Analysis date	Reference	X-coordinates	Y-coordinates	Elevation (masl)
Al Bas	Groundwater - borehole	-26.7	-5.62	4/25/1972	UNDP, 2013	33.25	35.211111	5
Al Chawakir	Groundwater - borehole	-26.4	-5.54	4/25/1972	UNDP, 2013	33.275	35.218056	6
Al Madik	spring	-37.41	-7.28	5/7/2012	UNDP, 2013	34.08328	35.70212	
Ali Arab	Groundwater - dug well	-24.2	-5.03	4/25/1972	UNDP, 2013	33.311667	35.233333	3
Alkaa	Damour river	-30.7	-6.81	5/4/2001	Saad et al, 2004			1045
Alkaa	Damour river	-37.7	-7.62	10/6/2001	Saad et al, 2004			1045
Alkaa	Damour river	-38.2	-7.56	1/8/2001	Saad et al, 2004			1045
Aramta	Precipitation - rain	-30.14	-5.86	3/15/2004	GNIP - Syrian Atomic Energy Commission	35.575	33.465	431
Aramta	Precipitation - rain	-12.46	-5.05	11/15/2004	GNIP - Syrian Atomic Energy Commission	35.575	33.465	431
Aramta	Precipitation - rain	-57.3	-9.53	12/15/2004	GNIP - Syrian Atomic Energy Commission	35.575	33.465	431
Aramta	Precipitation - rain	-40.72	-7.8	1/15/2005	GNIP - Syrian Atomic Energy Commission	35.575	33.465	431

214

Sample name	Water type	δ^2H reportable value (/mil)	$\delta^{18}O$ reportable value (/mil)	Analysis date	Reference	X- coordinates	Y- coordinates	Elevation (masl)
Aramta	Precipitation - rain	-20.94	-5.97	2/15/2005	GNIP - Syrian Atomic Energy Commission	35.575	33.465	431
Aramta	Precipitation - rain	-19.23	-5.12	1/15/2006	GNIP - Syrian Atomic Energy Commission	35.575	33.465	431
Aramta	Precipitation - rain	-44.38	-8.67	11/15/2003	GNIP - Syrian Atomic Energy Commission	35.575	33.465	431
Aramta	Precipitation - rain	-36.79	-8.08	12/15/2003	GNIP - Syrian Atomic Energy Commission	35.575	33.465	431
Aramta	Precipitation - rain	-39.03	-8.03	1/15/2004	GNIP - Syrian Atomic Energy Commission	35.575	33.465	431
Aramta	Precipitation - rain	-11.77	-3.48	2/15/2004	GNIP - Syrian Atomic Energy Commission	35.575	33.465	431
Aramta	Precipitation - rain	-32.33	-7.32	2/15/2006	GNIP - Syrian Atomic Energy Commission	35.575	33.465	431
Arbaeen	spring	-46.7	-8.57	5/7/2012	UNDP, 2013	34.126097	36.022199	
Assal spring	Groundwater	-40.28	-7.9	12/12/2012	Turkey	34.009747º	35.83852º	1540
Barouk	spring	-34.17	-7.35	5/7/2012	UNDP, 2013	33.712266	35.696963	
Barouk –	Damour river	-35.5	-7.54	5/4/2001	Saad et al, 2004			1060

Sample name	Water type	δ^2H reportable value (/mil)	$\delta^{18}O$ reportable value (/mil)	Analysis date	Reference	X-coordinates	Y-coordinates	Elevation (masl)
Barouk –	Damour river	-36.9	-7.55	10/6/2001	Saad et al, 2004			1060
Barouk –	Damour river	-38.2	-7.56	1/8/2001	Saad et al, 2004			1060
Beirut airport	Precipitation - unknown origin	1.3	-0.67	11/5/2002	International Atomic Energy Agency	35.494275	33.829311	27
Beirut airport	Precipitation - unknown origin	27.2	3.54	11/10/2002	International Atomic Energy Agency	35.494275	33.829311	27
Beirut airport	Precipitation - unknown origin	-14.7	-2.76	11/12/2002	International Atomic Energy Agency	35.494275	33.829311	27
Beirut airport	Precipitation - unknown origin	-23.4	-3.76	11/25/2002	International Atomic Energy Agency	35.494275	33.829311	27
Beirut airport	Precipitation - unknown origin	26.7	5.45	11/30/2002	International Atomic Energy Agency	35.494275	33.829311	27
Beirut airport	Precipitation - unknown origin	-25.5	-4.61	12/12/2002	International Atomic Energy Agency	35.494275	33.829311	27
Beirut airport	Precipitation - unknown origin	-24.9	-4.18	12/18/2002	International Atomic Energy Agency	35.494275	33.829311	27
Beirut airport	Precipitation - unknown origin	-26	-4.41	12/22/2002	International Atomic Energy Agency	35.494275	33.829311	27
Beirut airport	Precipitation - unknown origin	-9.5	-3.14	12/25/2002	International Atomic Energy Agency	35.494275	33.829311	27

Sample name	Water type	δ^2H reportable value (/mil)	$\delta^{18}O$ reportable value (/mil)	Analysis date	Reference	X- coordinates	Y- coordinates	Elevation (masl)
Beirut airport	Precipitation - unknown origin	-21.8	-3.64	12/27/2002	International Atomic Energy Agency	35.494275	33.829311	27
Bekaa	Precipitation - rain	-59.2	-9.85	12/15/2004	GNIP - Syrian Atomic Energy Commission	35.9	33.833333	961
Bekaa	Precipitation - rain	-55.31	-9.34	1/15/2005	GNIP - Syrian Atomic Energy Commission	35.9	33.833333	961
Bekaa	Precipitation - rain	-42.29	-8.51	12/15/2003	GNIP - Syrian Atomic Energy Commission	35.9	33.833333	961
Bekaa	Precipitation - rain	-12.76	-2.78	1/15/2006	GNIP - Syrian Atomic Energy Commission	35.9	33.833333	961
Bekaa	Precipitation - rain	-17.92	-4.46	2/15/2006	GNIP - Syrian Atomic Energy Commission	35.9	33.833333	961
Bekaa	Precipitation - rain	-17.42	-4.48	3/15/2006	GNIP - Syrian Atomic Energy Commission	35.9	33.833333	961
Bekaa	Precipitation - rain	-39.55	-7.76	1/15/2004	GNIP - Syrian Atomic Energy Commission	35.9	33.833333	961
Bekaa	Precipitation - rain	-33.44	-5.39	3/15/2004	GNIP - Syrian Atomic Energy Commission	35.9	33.833333	961
Bekaa	Precipitation - rain	-40.83	-8.06	2/15/2005	GNIP - Syrian Atomic Energy Commission	35.9	33.833333	961
Bekaa	Precipitation - rain	-47.14	-9.11	11/15/2004	GNIP - Syrian Atomic Energy Commission	35.9	33.833333	961

217

Sample name	Water type	δ²H reportable value (/mil)	δ¹⁸O reportable value (/mil)	Analysis date	Reference	X-coordinates	Y- coordinates	Elevation (masl)
Bekaa	Precipitation - rain	-21.94	-4.77	2/15/2004	GNIP - Syrian Atomic Energy Commission	35.9	33.833333	961
Berdawni	spring	-43.47	-8.13	5/7/2012	UNDP, 2013	33.88771	35.87149	
Beirut	Precipitation - rain	-11	-3.38	11/15/2003	GNIP - Syrian Atomic Energy Commission	35.509722	33.871944	19
Beirut	Precipitation - rain	-24.12	-5.79	12/15/2003	GNIP - Syrian Atomic Energy Commission	35.509722	33.871944	19
Beirut	Precipitation - rain	-23.23	-5.36	1/15/2004	GNIP - Syrian Atomic Energy Commission	35.509722	33.871944	19
Beirut	Precipitation - rain	-34.36	-6.13	12/15/2004	GNIP - Syrian Atomic Energy Commission	35.509722	33.871944	19
Beirut	Precipitation - rain	-21.99	-4.75	1/15/2005	GNIP - Syrian Atomic Energy Commission	35.509722	33.871944	19
Beirut	Precipitation - rain	-22.95	-5.12	1/15/2006	GNIP - Syrian Atomic Energy Commission	35.509722	33.871944	19
Beirut	Precipitation - rain	-22.62	-4.84	2/15/2006	GNIP - Syrian Atomic Energy Commission	35.509722	33.871944	19
Beirut	Precipitation - rain	-30.73	-2.46	3/15/2006	GNIP - Syrian Atomic Energy Commission	35.509722	33.871944	19
Beirut	Precipitation - rain	-16.41	-4.84	2/15/2005	GNIP - Syrian Atomic Energy Commission	35.509722	33.871944	19

218

Sample name	Water type	δ^2H reportable value (/mil)	$\delta^{18}O$ reportable value (/mil)	Analysis date	Reference	X- coordinates	Y- coordinates	Elevation (masl)
Beirut	Precipitation - rain	-18.15	-5.21	11/15/2004	GNIP - Syrian Atomic Energy Commission	35.509722	33.871944	19
Beirut	Precipitation - rain	-10.25	-3.43	2/15/2004	GNIP - Syrian Atomic Energy Commission	35.509722	33.871944	19
Bhamdoun	Precipitation - rain	-41.46	-8.09	1/15/2005	GNIP - Syrian Atomic Energy Commission	35.651111	33.808333	1080
Bhamdoun	Precipitation - rain	-41.92	-8.49	1/15/2006	GNIP - Syrian Atomic Energy Commission	35.651111	33.808333	1080
Bhamdoun	Precipitation - rain	-26.54	-5.76	2/15/2006	GNIP - Syrian Atomic Energy Commission	35.651111	33.808333	1080
Bhamdoun	Precipitation - rain	-31.86	-7.61	3/15/2006	GNIP - Syrian Atomic Energy Commission	35.651111	33.808333	1080
Bhamdoun	Precipitation - rain	-24.65	-6.17	11/15/2003	GNIP - Syrian Atomic Energy Commission	35.651111	33.808333	1080
Bhamdoun	Precipitation - rain	-35.51	-8.23	12/15/2003	GNIP - Syrian Atomic Energy Commission	35.651111	33.808333	1080
Bhamdoun	Precipitation - rain	-19.54	-6.68	1/15/2004	GNIP - Syrian Atomic Energy Commission	35.651111	33.808333	1080
Bhamdoun	Precipitation - rain	-57.48	-9.91	12/15/2004	GNIP - Syrian Atomic Energy Commission	35.651111	33.808333	1080
Bhamdoun	Precipitation - rain	-30.02	-7.02	2/15/2005	GNIP - Syrian Atomic Energy Commission	35.651111	33.808333	1080

Sample name	Water type	δ^2H reportable value (/mil)	$\delta^{18}O$ reportable value (/mil)	Analysis date	Reference	X- coordinates	Y- coordinates	Elevation (masl)
Bhamdoun	Precipitation - rain	-29.16	-6.6	2/15/2004	GNIP - Syrian Atomic Energy Commission	35.651111	33.808333	1080
Bhamdoun	Precipitation - rain	-29.25	-7.34	11/15/2004	GNIP - Syrian Atomic Energy Commission	35.651111	33.808333	1080
Creen	Precipitation - rain	-14	-2.56	4/15/2003	International Atomic Energy Agency	35.566667	33.866667	249
Creen	Precipitation - rain	-30.1	-5.72	3/26/2003	International Atomic Energy Agency	35.566667	33.866667	249
Creen	Precipitation - rain	-23.6	-4.77	3/13/2003	International Atomic Energy Agency	35.566667	33.866667	249
Creen	Precipitation - rain	-35.7	-5.79	3/8/2003	International Atomic Energy Agency	35.566667	33.866667	249
Creen	Precipitation - rain	-23.9	-5.94	2/27/2003	International Atomic Energy Agency	35.566667	33.866667	249
Creen	Precipitation - rain	-27.8	-5.86	2/22/2003	International Atomic Energy Agency	35.566667	33.866667	249
Creen	Precipitation - rain	-34.9	-6.18	2/16/2003	International Atomic Energy Agency	35.566667	33.866667	249
Creen	Precipitation - rain	-8.6	-4.01	2/12/2003	International Atomic Energy Agency	35.566667	33.866667	249
Creen	Precipitation - rain	-29.5	-5.58	2/5/2003	International Atomic Energy Agency	35.566667	33.866667	249

Sample name	Water type	δ^2H reportable value (/mil)	$\delta^{18}O$ reportable value (/mil)	Analysis date	Reference	X-coordinates	Y- coordinates	Elevation (masl)
Creen	Precipitation - rain	-1.1	-2.3	11/17/2001	International Atomic Energy Agency	35.566667	33.866667	249
Creen	Precipitation - rain	-33.2	-6.12	1/30/2003	International Atomic Energy Agency	35.566667	33.866667	249
Creen	Precipitation - rain	-47	-7.11	1/24/2003	International Atomic Energy Agency	35.566667	33.866667	249
Creen	Precipitation - rain	-14.6	-3.97	1/17/2003	International Atomic Energy Agency	35.566667	33.866667	249
Creen	Precipitation - rain	-6.5	-3.11	1/15/2003	International Atomic Energy Agency	35.566667	33.866667	249
Creen	Precipitation - rain	-13.9	-3.04	1/5/2003	International Atomic Energy Agency	35.566667	33.866667	249
Creen	Precipitation - rain	-27	-4.58	12/27/2002	International Atomic Energy Agency	35.566667	33.866667	249
Creen	Precipitation - rain	-17.8	-4.99	12/25/2002	International Atomic Energy Agency	35.566667	33.866667	249
Creen	Precipitation - rain	-21.5	-4.79	12/22/2002	International Atomic Energy Agency	35.566667	33.866667	249
Creen	Precipitation - rain	-30	-5.62	12/18/2002	International Atomic Energy Agency	35.566667	33.866667	249
Creen	Precipitation - rain	-33.8	-6.81	12/12/2002	International Atomic Energy Agency	35.566667	33.866667	249

Sample name	Water type	δ^2H reportable value (/mil)	$\delta^{18}O$ reportable value (/mil)	Analysis date	Reference	X- coordinates	Y- coordinates	Elevation (masl)
Creen	Precipitation - rain	-3.8	-2.95	11/11/2001	International Atomic Energy Agency	35.566667	33.866667	249
Creen	Precipitation - rain	16.9	2.34	11/30/2002	International Atomic Energy Agency	35.566667	33.866667	249
Creen	Precipitation - rain	-15.4	-3.76	11/25/2002	International Atomic Energy Agency	35.566667	33.866667	249
Creen	Precipitation - rain	-26.6	-5.59	12/13/2001	International Atomic Energy Agency	35.566667	33.866667	249
Creen	Precipitation - rain	-72.8	-11.1	12/7/2001	International Atomic Energy Agency	35.566667	33.866667	249
Creen	Precipitation - rain	-26.7	-4.65	12/3/2001	International Atomic Energy Agency	35.566667	33.866667	249
Creen	Precipitation - rain	0.6	-3.29	11/27/2001	International Atomic Energy Agency	35.566667	33.866667	249
Creen	Precipitation - rain	-16.5	-3.72	4/27/2003	International Atomic Energy Agency	35.566667	33.866667	249
Creen	Precipitation - rain	-8.9	-3.29	11/21/2001	International Atomic Energy Agency	35.566667	33.866667	249
Creen	Precipitation - rain	-14.7	-3.11	4/22/2003	International Atomic Energy Agency	35.566667	33.866667	249
Creen	Precipitation - rain	37.6	5.54	11/12/2002	International Atomic Energy Agency	35.566667	33.866667	249

Sample name	Water type	δ^2H reportable value (/mil)	$\delta^{18}O$ reportable value (/mil)	Analysis date	Reference	X-coordinates	Y- coordinates	Elevation (masl)
Creen	Precipitation - rain	38.8	5.51	11/10/2002	International Atomic Energy Agency	35.566667	33.866667	249
Creen	Precipitation - rain	11.5	-0.48	11/5/2002	International Atomic Energy Agency	35.566667	33.866667	249
Creen	Precipitation - rain	-1.1	-1.34	10/20/2002	International Atomic Energy Agency	35.566667	33.866667	249
Creen	Precipitation - rain	-5.4	-2.02	5/15/2002	International Atomic Energy Agency	35.566667	33.866667	249
Creen	Precipitation - rain	-29.4	-5.56	4/22/2002	International Atomic Energy Agency	35.566667	33.866667	249
Creen	Precipitation - rain	-20.7	-4.56	4/4/2002	International Atomic Energy Agency	35.566667	33.866667	249
Creen	Precipitation - rain	-25.5	-5.94	3/30/2002	International Atomic Energy Agency	35.566667	33.866667	249
Creen	Precipitation - rain	-25.7	-5.91	11/7/2001	International Atomic Energy Agency	35.566667	33.866667	249
Creen	Precipitation - rain	-24.5	-4.88	3/22/2002	International Atomic Energy Agency	35.566667	33.866667	249
Creen	Precipitation - rain	11.6	1.19	3/18/2002	International Atomic Energy Agency	35.566667	33.866667	249
Creen	Precipitation - rain	-6.6	-2.23	2/26/2002	International Atomic Energy Agency	35.566667	33.866667	249

Sample name	Water type	δ^2H reportable value (/mil)	$\delta^{18}O$ reportable value (/mil)	Analysis date	Reference	X-coordinates	Y- coordinates	Elevation (masl)
Creen	Precipitation - rain	-20.3	-5.14	1/29/2002	International Atomic Energy Agency	35.566667	33.866667	249
Creen	Precipitation - rain	-30.4	-6.5	1/22/2002	International Atomic Energy Agency	35.566667	33.866667	249
Creen	Precipitation - rain	-38.5	-7.96	1/9/2002	International Atomic Energy Agency	35.566667	33.866667	249
Creen	Precipitation - rain	-45.6	-9	1/7/2002	International Atomic Energy Agency	35.566667	33.866667	249
Creen	Precipitation - rain	-30.4	-7.02	1/4/2002	International Atomic Energy Agency	35.566667	33.866667	249
Creen	Precipitation - rain	-9.9	-3.56	12/29/2001	International Atomic Energy Agency	35.566667	33.866667	249
Creen	Precipitation - rain	6.1	-1.37	12/24/2001	International Atomic Energy Agency	35.566667	33.866667	249
Creen	Precipitation - rain	-8.8	-3.64	11/3/2001	International Atomic Energy Agency	35.566667	33.866667	249
Daelm	spring	-35.26	-7.67	5/7/2012	UNDP, 2013	34.23882	35.8055	
Dardara	spring	-27.7	-6.31	5/7/2012	UNDP, 2013	33.332228	35.59164	
Dier el Qamar	Damour river	-35.5	-7.51	5/4/2001	Saad et al, 2004			827

Sample name	Water type	δ^2H reportable value (/mil)	$\delta^{18}O$ reportable value (/mil)	Analysis date	Reference	X- coordinates	Y- coordinates	Elevation (masl)
Dier el Qamar	Damour river	-30.6	-6.95	10/6/2001	Saad et al, 2004			827
Dier el Qamar	Damour river	-30.7	-6.69	1/8/2001	Saad et al, 2004			827
Ein el Delb	spring	-34.7	-7.12	5/7/2012	UNDP, 2013	33.825932	35.685727	
El Arbiin spring, Yammouneh	Groundwater	-55.91	-9.61	22/04/2003	Awad, 2011			
El Kassarat cave	Groundwater	-33.18	-6.84	12/12/2012	Karanouh, 2014	33.909493º	35.611437º	75
El Kassarat cave	Rainwater	-31.67	-5.75	12/12/2012	Karanouh, 2014	33.909493º	35.611437º	75
El Kassarat cave - Forage passage	Dripwater	-26.6	-5.66	12/12/2012	Karanouh, 2014	33.909493º	35.611437º	75
El Kassarat cave - Presidents gallery	Dripwater	-24.1	-5.22	12/12/2012	Karanouh, 2014	33.909493º	35.611437º	75
El Laboueh Source	Spring	-55.11	-7.84	9/4/2003	Awad, 2011			

Sample name	Water type	δ^2H reportable value (/mil)	$\delta^{18}O$ reportable value (/mil)	Analysis date	Reference	X-coordinates	Y-coordinates	Elevation (masl)
El Mansouri	Groundwater - dug well	-26	-5.45	4/28/1972	UNDP, 2013	33.173056	35.191667	4
El Moghr spring, Yammouneh	Groundwater	-51.23	-8.52	22/04/2003	Awad, 2011			
El Rachidiye 1	Groundwater - spring	-28.7	-5.97	4/25/1972	UNDP, 2013	33.240833	35.220833	20
El Rachidiye 2	Groundwater - spring	-27.8	-6.07	4/25/1972	UNDP, 2013	33.240833	35.220833	20
En Naqoura-Ouadi El Ain	Groundwater - spring	-24.7	-5.37	4/28/1972	UNDP, 2013	33.116667	35.136667	37
Freidis	spring	-34.04	-7.26	5/7/2012	UNDP, 2013	33.779835	35.606747	
Hachich	spring	-29.57	-6.2	5/7/2012	UNDP, 2013	33.831685	35.752982	
Hermel S6 Aîn el zarqa Source	Spring	-50.85	-8.62	9/4/2003	Awad, 2011			
Hermel S8 Ras el mal Source	Spring	-62.01	-9.07	10/4/2003	Awad, 2011			
Hermel S7 Bdaîta Source	Spring	-58.88	-9.6	10/4/2003	Awad, 2011			
Hermel S9 El adim Source	Spring	-60.91	-9.91	10/4/2003	Awad, 2011			

Sample name	Water type	δ^2H reportable value (/mil)	$\delta^{18}O$ reportable value (/mil)	Analysis date	Reference	X-coordinates	Y- coordinates	Elevation (masl)
Iskanderoun	Groundwater - spring	-23.7	-5.39	4/28/1972	UNDP, 2013	33.1625	35.151667	5
Jabal el Sheikh	Rainwater	-29	-7.44	19/02/01	Ayalon et al, 2013	301520 N	222306 E	1650
Jabal el Sheikh	Rainwater	-25.5	-6.6	12/11/2001	Ayalon et al, 2013	301520 N	222306 E	1650
Jabal el Sheikh	Rainwater	-28.8	-7.63	13/01/02	Ayalon et al, 2013	301520 N	222306 E	1650
Jabal el Sheikh	Rainwater	-30.5	-7	22/04/02	Ayalon et al, 2013	301520 N	222306 E	1650
Jabal el Sheikh	Rainwater	-31.9	-8.27	17/03/03	Ayalon et al, 2013	301520 N	222306 E	1650
Jabal el Sheikh	Rainwater	-34	-6.66	10/4/2003	Ayalon et al, 2013	301520 N	222306 E	1650
Jabal el Sheikh	Rainwater	-38.2	-6.32	15/05/03	Ayalon et al, 2013	301520 N	222306 E	1650
Jabal el Sheikh	Rainwater	-13.6	-6.15	25/11/03	Ayalon et al, 2013	301520 N	222306 E	1650
Jabal el Sheikh	Rainwater	34.1	-8.08	24/12/03	Ayalon et al, 2013	301520 N	222306 E	1650
Jabal el Sheikh	Rainwater	39.2	-7.74	29/01/04	Ayalon et al, 2013	301520 N	222306 E	1650
Jabal el Sheikh	Rainwater	28.9	-6.69	25/02/04	Ayalon et al, 2013	301520 N	222306 E	1650
Jabal el Sheikh	Rainwater	27.8	-5.85	12/4/2004	Ayalon et al, 2013	301520 N	222306 E	1650
Jabal el Sheikh	Rainwater	-24.7	-6.58	12/12/2004	Ayalon et al, 2013	301520 N	222306 E	1650
Jabal el Sheikh	Rainwater	-35	-7.79	6/1/2005	Ayalon et al, 2013	301520 N	222306 E	1650
Jabal el Sheikh	Rainwater	-51.3	-10.28	24/1/05	Ayalon et al, 2013	301520 N	222306 E	1650

227

Sample name	Water type	δ^2H reportable value (/mil)	$\delta^{18}O$ reportable value (/mil)	Analysis date	Reference	X-coordinates	Y- coordinates	Elevation (masl)
Jabal el Sheikh	Rainwater	-16	-5.73	22/3/05	Ayalon et al, 2013	301520 N	222306 E	1650
Jabal el Sheikh	Rainwater	-7	-5.63	3/5/2005	Ayalon et al, 2013	301520 N	222306 E	1650
Jabal el Sheikh	Rainwater	-31.2	-6.65	10/11/2005	Ayalon et al, 2013	301520 N	222306 E	1650
Jabal el Sheikh	Rainwater	-27	-6.31	14/12/05	Ayalon et al, 2013	301520 N	222306 E	1650
Jabal el Sheikh	Rainwater	-42.2	-8.67	1/1/2006	Ayalon et al, 2013	301520 N	222306 E	1650
Jabal el Sheikh	Rainwater	-36.2	-9.26	18/1/06	Ayalon et al, 2013	301520 N	222306 E	1650
Jabal el Sheikh	Rainwater	-42.3	-7.95	12/2/2006	Ayalon et al, 2013	301520 N	222306 E	1650
Jabal el Sheikh	Rainwater	-25.6	-6.79	29/3/06	Ayalon et al, 2013	301520 N	222306 E	1650
Jabal el Sheikh	Rainwater	-43.1	-7.61	20/4/06	Ayalon et al, 2013	301520 N	222306 E	1650
Jabal el Sheikh	Rainwater	-24.8	-5.15	10/25/2006	Ayalon et al, 2013	301520 N	222306 E	1650
Jabal el Sheikh	Rainwater	-33.2	-6.46	11/28/2006	Ayalon et al, 2013	301520 N	222306 E	1650
Jabal el Sheikh	Rainwater	-43.3	-6.43	12/28/2007	Ayalon et al, 2013	301520 N	222306 E	1650
Jabal el Sheikh	Rainwater	.46.2	-7.52	1/16/2007	Ayalon et al, 2013	301520 N	222306 E	1650
Jabal el Sheikh	Rainwater	.43.6	-6.46	2/15/2007	Ayalon et al, 2013	301520 N	222306 E	1650
Jabal el Sheikh	Rainwater	-49	-6.61	3/28/2007	Ayalon et al, 2013	301520 N	222306 E	1650
Jabal el Sheikh	Rainwater	-58.3	-5.24	4/26/2007	Ayalon et al, 2013	301520 N	222306 E	1650
Jabal el Sheikh	Rainwater	-37.2	-7.06	11/28/2007	Ayalon et al, 2013	301520 N	222306 E	1650

Sample name	Water type	δ^2H reportable value (/mil)	$\delta^{18}O$ reportable value (/mil)	Analysis date	Reference	X- coordinates	Y- coordinates	Elevation (masl)
Jabal el Sheikh	Rainwater	-27.3	-7.03	12/31/2007	Ayalon et al, 2013	301520 N	222306 E	1650
Jabal el Sheikh	Rainwater	-43	-8.91	2/4/2008	Ayalon et al, 2013	301520 N	222306 E	1650
Jabal el Sheikh	Rainwater	-42.9	-8.14	3/4/2008	Ayalon et al, 2013	301520 N	222306 E	1650
Jabal el Sheikh	Rainwater	-31.4	-5.74	3/31/2008	Ayalon et al, 2013	301520 N	222306 E	1650
Jabal el Sheikh	Rainwater	-24.7	-5.17	10/29/2008	Ayalon et al, 2013	301520 N	222306 E	1650
Jabal el Sheikh	Rainwater	-18.3	-4.57	11/27/2008	Ayalon et al, 2013	301520 N	222306 E	1650
Jabal el Sheikh	Rainwater	-32.7	-7.05	12/31/2008	Ayalon et al, 2013	301520 N	222306 E	1650
Jabal el Sheikh	Rainwater	-31.9	-5.71	1/28/2009	Ayalon et al, 2013	301520 N	222306 E	1650
Jabal el Sheikh	Rainwater	-44.1	-8.53	2/25/2009	Ayalon et al, 2013	301520 N	222306 E	1650
Jabal el Sheikh	Rainwater	-71.1	-10.26	3/3/2009	Ayalon et al, 2013	301520 N	222306 E	1650
Jabal el Sheikh	Rainwater	-38.4	-6.22	3/31/2009	Ayalon et al, 2013	301520 N	222306 E	1650
Jabal el Sheikh	Rainwater	-43.1	-6.7	4/30/2009	Ayalon et al, 2013	301520 N	222306 E	1650
Jdita C1 Well	Well	-43.99	-7.74	5/4/2003	Awad, 2011			
Jeita	Spring	-36	-7.2	mean 2011	Koeniger et al., 2012	33.947214	35.689668	60
Jeita - Terminal Siphon	spring	-38.68	-7.34	5/7/2012	UNDP, 2013	33.947214	35.689668	

Sample name	Water type	δ^2H reportable value (/mil)	$\delta^{18}O$ reportable value (/mil)	Analysis date	Reference	X-coordinates	Y- coordinates	Elevation (masl)
Jezzine	Groundwater - spring	-35.5	-7.18	4/25/1972	UNDP, 2013	33.505	35.586111	975
Jezzine	spring	-33.38	-7.21	5/7/2012	UNDP, 2013	33.546868	35.601556	
Kefrayia Source	Spring	-40.93	-7.16	17/04/2004	Awad, 2011			
Kefrayia Well	Well	-36.84	-6.15	17/04/2004	Awad, 2011			
Laban	spring	-48.24	-8.54	5/7/2012	UNDP, 2013	33.994797	35.828675	
Laban spring	Groundwater	-41.36	-7.81	12/12/2012	Turkey	33.994805°	35.828403°	1644
Lehfed	spring	-37.34	-7.36	5/7/2012	UNDP, 2013	34.167157	35.777296	
Litani	Groundwater - spring	-30.4	-6.01	4/25/1972	UNDP, 2013	33.330556	35.261111	10
Litani right	Groundwater - spring	-25.1	-5.39	4/28/1972	UNDP, 2013	33.322222	35.252778	10
Nabaa al Assal	Spring	-45	-8.3	mean 2011	Koeniger et al., 2012			1540
Nabaa al Labbane	Spring	-44‰	-8.1	mean 2011	Koeniger et al., 2012	33.994797	35.828675	1644

230

Sample name	Water type	δ^2H reportable value (/mil)	$\delta^{18}O$ reportable value (/mil)	Analysis date	Reference	X-coordinates	Y- coordinates	Elevation (masl)
Nabaa el Barouk	Groundwater - spring	-38.5	-7.58	4/25/1972	UNDP, 2013	33.71	35.693333	1085
Nabaa el Izziye	Groundwater - spring	-24.2	-5.45	4/28/1972	UNDP, 2013	33.174167	35.238889	95
Nabaa el Qassaibe	Groundwater - spring	-24.7	-5.32	4/28/1972	UNDP, 2013	33.341389	35.390278	288
Nabi eila Source	Spring	-42.98	-7.05	7/4/2003	Awad, 2011			
Nabi eila Well	Well	-44.62	-7.64	7/4/2003	Awad, 2011			
Niha source	Spring	-46.1	-7.72	7/4/2003	Awad, 2011			
Rahwe cave	Rainwater	-70.45	-12.37	12/12/2012	Karanouh, 2014	34.196243º	35.980482º	2100
Rahwe cave	Groundwater	-43.1	-8.23	12/12/2012	Karanouh, 2014	34.196243º	35.980482º	2100
Rahwe cave - Entrance location	Dripwater	-45.76	-8.46	12/12/2012	Karanouh, 2014	34.196243º	35.980482º	2100
Rahwe cave - Stalagmite location	Dripwater	-46.41	-8.51	12/12/2012	Karanouh, 2014	34.196243º	35.980482º	2100
Ras el Ein	spring	-27.48	-6.17	5/7/2012	UNDP, 2013	33.99825	36.217583	

231

Sample name	Water type	δ^2H reportable value (/mil)	$\delta^{18}O$ reportable value (/mil)	Analysis date	Reference	X-coordinates	Y- coordinates	Elevation (masl)
Ras-el-Ain petite source	Groundwater - spring	-27.9	-5.88	4/25/1972	UNDP, 2013	33.229167	35.216667	15
Rihan	Damour river	-36.6	-7.57	5/4/2001	Saad et al, 2004			921
Rihan	Damour river	-37.3	-7.5	10/6/2001	Saad et al, 2004			921
Rihan	Damour river	-39	-8.04	1/8/2001	Saad et al, 2004			921
Safa	Groundwater - spring	-38.1	-7.56	4/28/1972	UNDP, 2013	33.751667	35.706944	1000
Safa	spring	-35.19	-6.94	5/7/2012	UNDP, 2013	33.749599	35.699827	
Sarbin	Groundwater - borehole	-27.9	-5.78	4/28/1972	UNDP, 2013	33.153056	35.356667	550
SHAILEH	Precipitation - rain	-39.8	-7.52	12/30/2002	International Atomic Energy Agency	35.666667	33.966667	650
SHAILEH	Precipitation - rain	-9.5	-1.03	12/27/2002	International Atomic Energy Agency	35.666667	33.966667	650
SHAILEH	Precipitation - rain	-32.9	-6.34	12/18/2002	International Atomic Energy Agency	35.666667	33.966667	650
SHAILEH	Precipitation - rain	-39.5	-6.69	12/15/2002	International Atomic Energy Agency	35.666667	33.966667	650

Sample name	Water type	δ^2H reportable value (/mil)	$\delta^{18}O$ reportable value (/mil)	Analysis date	Reference	X- coordinates	Y- coordinates	Elevation (masl)
SHAILEH	Precipitation - rain	-33.4	-6.8	12/12/2002	International Atomic Energy Agency	35.666667	33.966667	650
SHAILEH	Precipitation - rain	-25	-4.77	12/6/2002	International Atomic Energy Agency	35.666667	33.966667	650
SHAILEH	Precipitation - rain	-15.5	-4.34	11/30/2002	International Atomic Energy Agency	35.666667	33.966667	650
SHAILEH	Precipitation - rain	-19.3	-4.4	4/27/2003	International Atomic Energy Agency	35.666667	33.966667	650
SHAILEH	Precipitation - rain	-18.9	-4.44	4/22/2003	International Atomic Energy Agency	35.666667	33.966667	650
SHAILEH	Precipitation - rain	-16.9	-3.21	4/15/2003	International Atomic Energy Agency	35.666667	33.966667	650
SHAILEH	Precipitation - rain	-40.3	-8.11	3/26/2003	International Atomic Energy Agency	35.666667	33.966667	650
SHAILEH	Precipitation - rain	-24.8	-5.8	3/21/2003	International Atomic Energy Agency	35.666667	33.966667	650
SHAILEH	Precipitation - rain	-18.6	-5.36	3/13/2003	International Atomic Energy Agency	35.666667	33.966667	650
SHAILEH	Precipitation - rain	-28.9	-5.93	3/8/2003	International Atomic Energy Agency	35.666667	33.966667	650
SHAILEH	Precipitation - rain	-9.2	-4.19	3/4/2003	International Atomic Energy Agency	35.666667	33.966667	650

233

Sample name	Water type	δ^2H reportable value (/mil)	$\delta^{18}O$ reportable value (/mil)	Analysis date	Reference	X-coordinates	Y- coordinates	Elevation (masl)
SHAILEH	Precipitation - rain	-21.4	-4.35	11/25/2002	International Atomic Energy Agency	35.666667	33.966667	650
SHAILEH	Precipitation - rain	-24.5	-6.72	2/27/2003	International Atomic Energy Agency	35.666667	33.966667	650
SHAILEH	Precipitation - rain	-25.5	-6.27	2/22/2003	International Atomic Energy Agency	35.666667	33.966667	650
SHAILEH	Precipitation - rain	-33.3	-6.61	2/16/2003	International Atomic Energy Agency	35.666667	33.966667	650
SHAILEH	Precipitation - rain	-11	-4.91	2/12/2003	International Atomic Energy Agency	35.666667	33.966667	650
SHAILEH	Precipitation - rain	-27	-5.97	2/5/2003	International Atomic Energy Agency	35.666667	33.966667	650
SHAILEH	Precipitation - rain	-39.4	-6.93	1/30/2003	International Atomic Energy Agency	35.666667	33.966667	650
SHAILEH	Precipitation - rain	-49.1	-7.53	1/24/2003	International Atomic Energy Agency	35.666667	33.966667	650
SHAILEH	Precipitation - rain	-21.4	-5.15	1/17/2003	International Atomic Energy Agency	35.666667	33.966667	650
SHAILEH	Precipitation - rain	-14	-4.68	1/15/2003	International Atomic Energy Agency	35.666667	33.966667	650
SHAILEH	Precipitation - rain	-14.4	-3.47	1/5/2003	International Atomic Energy Agency	35.666667	33.966667	650

Sample name	Water type	δ^2H reportable value (/mil)	$\delta^{18}O$ reportable value (/mil)	Analysis date	Reference	X-coordinates	Y- coordinates	Elevation (masl)
SHAILEH	Precipitation - rain	-23.2	-4.98	11/12/2002	International Atomic Energy Agency	35.666667	33.966667	650
Tannourine	spring	-40.22	-7.95	5/7/2012	UNDP, 2013	34.19226	35.9241	
Tasseh	spring	-35.96	-7.46	5/7/2012	UNDP, 2013	33.452758	35.532312	
Tasseh	spring	-30.06	-6.64	5/7/2012	UNDP, 2013	33.452758	35.532312	
TRIPOLI	Precipitation - rain	-30.12	-6.67	11/15/2003	GNIP - Syrian Atomic Energy Commission	35.849722	34.436667	20
TRIPOLI	Precipitation - rain	-20.29	-6.32	12/15/2003	GNIP - Syrian Atomic Energy Commission	35.849722	34.436667	20
TRIPOLI	Precipitation - rain	-36.05	-6.62	1/15/2004	GNIP - Syrian Atomic Energy Commission	35.849722	34.436667	20
TRIPOLI	Precipitation - rain	-18.71	-5.95	2/15/2004	GNIP - Syrian Atomic Energy Commission	35.849722	34.436667	20
TRIPOLI	Precipitation - rain	-16.14	-4.89	11/15/2004	GNIP - Syrian Atomic Energy Commission	35.849722	34.436667	20
TRIPOLI	Precipitation - rain	-39.34	-7	12/15/2004	GNIP - Syrian Atomic Energy Commission	35.849722	34.436667	20
TRIPOLI	Precipitation - rain	-26.98	-5.05	1/15/2005	GNIP - Syrian Atomic Energy Commission	35.849722	34.436667	20

Sample name	Water type	δ^2H reportable value (/mil)	$\delta^{18}O$ reportable value (/mil)	Analysis date	Reference	X-coordinates	Y-coordinates	Elevation (masl)
TRIPOLI	Precipitation - rain	-17.48	-4.83	2/15/2005	GNIP - Syrian Atomic Energy Commission	35.849722	34.436667	20
TRIPOLI	Precipitation - rain	-42.79	-8.18	1/15/2006	GNIP - Syrian Atomic Energy Commission	35.849722	34.436667	20
TRIPOLI	Precipitation - rain	-22.47	-4.71	2/15/2006	GNIP - Syrian Atomic Energy Commission	35.849722	34.436667	20
TYR	Precipitation - rain	-36.1	-6.3	11/15/2003	GNIP - Syrian Atomic Energy Commission	35.193889	33.273333	5
TYR	Precipitation - rain	-37.35	-7.41	1/15/2006	GNIP - Syrian Atomic Energy Commission	35.193889	33.273333	5
TYR	Precipitation - rain	-30.38	-6.22	12/15/2003	GNIP - Syrian Atomic Energy Commission	35.193889	33.273333	5
TYR	Precipitation - rain	-15.13	-4.82	1/15/2004	GNIP - Syrian Atomic Energy Commission	35.193889	33.273333	5
TYR	Precipitation - rain	-17.76	-4.15	2/15/2004	GNIP - Syrian Atomic Energy Commission	35.193889	33.273333	5
TYR	Precipitation - rain	-8.85	-4.06	11/15/2004	GNIP - Syrian Atomic Energy Commission	35.193889	33.273333	5
TYR	Precipitation - rain	-39.27	-6.59	12/15/2004	GNIP - Syrian Atomic Energy Commission	35.193889	33.273333	5
TYR	Precipitation - rain	-32.85	-6.27	1/15/2005	GNIP - Syrian Atomic Energy Commission	35.193889	33.273333	5

236

Sample name	Water type	δ^2H reportable value (/mil)	$\delta^{18}O$ reportable value (/mil)	Analysis date	Reference	X-coordinates	Y- coordinates	Elevation (masl)
TYR	Precipitation - rain	-11.99	-4.44	2/15/2005	GNIP - Syrian Atomic Energy Commission	35.193889	33.273333	5
Wadi el karm Well	Well	-61.31	-9.33	10/4/2003	Awad, 2011			
Yammoune	spring	-47.84	-8.66	5/7/2012	UNDP, 2013	34.125542	36.023733	
Yammouneh El Arbiin source	Spring	-55.91	-9.61	22/04/2003	Awad, 2011			
Yammouneh El Moghr source	Spring	-51.23	-8.52	22/04/2003	Awad, 2011			
Yatar	Groundwater - borehole	-27.3	-5.93	4/28/1972	UNDP, 2013	33.153333	35.322778	642
Yohmor	Precipitation - rain	-24.96	-4.67	11/15/2003	GNIP - Syrian Atomic Energy Commission	35.516944	33.310278	514
Yohmor	Precipitation - rain	-38.41	-7.8	12/15/2003	GNIP - Syrian Atomic Energy Commission	35.516944	33.310278	514
Yohmor	Precipitation - rain	-25.07	-6.33	1/15/2004	GNIP - Syrian Atomic Energy Commission	35.516944	33.310278	514
Yohmor	Precipitation - rain	-20.85	-4.78	2/15/2004	GNIP - Syrian Atomic Energy Commission	35.516944	33.310278	514
Yohmor	Precipitation - rain	-8.93	-2.85	3/15/2004	GNIP - Syrian Atomic Energy Commission	35.516944	33.310278	514

Sample name	Water type	δ^2H reportable value (/mil)	$\delta^{18}O$ reportable value (/mil)	Analysis date	Reference	X- coordinates	Y- coordinates	Elevation (masl)
Zarka	spring	-51.41	-8.37	5/7/2012	UNDP, 2013	33.49457	35.659781	

8.14 Appendix 14: Trace elements sampling in ECK-01

Age (yrs)	Distance	Run	Sample	Number	Sr/Ca	Mg/Ca	Ba/Ca	Fe/Ca
0	0	i1405	EKC-01	1	0.033294	1.875065	0.000456	-0.05022
399	5000	i1405	EKC-01	2	0.054457	1.549286	0.000634	-0.75254
835	10000	i1405	EKC-01	3	0.043	1.198463	0.000338	-0.50776
1271	15000	i1405	EKC-01	4	0.056981	1.307035	0.000452	-0.95425
1706	20000	i1405	EKC-01	5	0.039335	1.426014	0.000353	-0.44602
2142	25000	i1405	EKC-01	6	0.134121	6.615833	0.003148	-0.48237
2578	30000	i1405	EKC-01	7	0.029101	1.253543	0.000266	-0.41632
3013	35000	i1405	EKC-01	8	0.028186	1.241171	0.000242	-0.32794
3449	40000	i1405	EKC-01	9	0.035999	1.29983	0.00034	-0.53409
3885	45000	i1405	EKC-01	10	0.03201	1.193472	0.000266	-0.30922
4320	50000	i1405	EKC-01	11	0.033963	1.45505	0.00036	-0.52637
4756	55000	i1405	EKC-01	12	0.047721	1.511716	0.000331	-1.10795
5192	60000	i1405	EKC-01	13	0.05548	1.867499	0.000985	-0.73642
5628	65000	i1405	EKC-01	14	0.031182	1.439592	0.001224	-0.32634
6063	70000	i1405	EKC-01	15	0.033548	1.335546	0.000405	-0.35711
6499	75000	i1405	EKC-01	16	0.035388	1.159931	0.000335	-0.3657
6935	80000	i1405	EKC-01	17	0.04205	1.165957	0.000468	-0.65701
7370	85000	i1405	EKC-01	18	0.03819	1.498378	0.000293	-0.61469
7806	90000	i1405	EKC-01	19	0.026207	1.167531	0.000196	-0.23115
8242	95000	i1405	EKC-01	20	0.030368	1.292404	0.000446	-0.34874
8677	100000	i1405	EKC-01	21	0.025647	1.30983	0.000194	-0.2345
9113	105000	i1405	EKC-01	22	0.040948	1.340665	0.000337	-0.72078
9549	110000	i1405	EKC-01	23	0.029368	1.093777	0.000336	-0.23159
9985	115000	i1405	EKC-01	24	0.026094	1.246461	0.000258	-0.16162
10420	120000	i1405	EKC-01	25	0.025486	1.195933	0.000526	-0.10688
10856	125000	i1405	EKC-01	26	0.037199	3.010779	0.000551	-0.51796
11292	130000	i1405	EKC-01	27	0.028615	1.174388	0.000248	-0.22049
11727	135000	i1405	EKC-01	28	0.02995	1.228662	0.000286	-0.20284
12163	140000	i1405	EKC-01	29	0.035847	1.22456	0.000403	-0.73056
12599	145000	i1405	EKC-01	30	0.032294	1.109951	0.000356	-0.13225
13034	150000	i1405	EKC-01	31	0.026347	1.344468	0.000216	-0.13434
13470	155000	i1405	EKC-01	32	0.02549	2.196075	0.00024	-0.33761
13906	160000	i1405	EKC-01	33	0.219524	14.4713	0.001592	-0.1666

Age (yrs)	Distance	Run	Sample	Number	Sr/Ca	Mg/Ca	Ba/Ca	Fe/Ca
14341	165000	i1405	EKC-01	34	0.052278	1.525222	0.000377	-0.3093
14777	170000	i1405	EKC-01	35	0.056189	1.550826	0.000431	-0.37049
15213	175000	i1405	EKC-01	36	0.06102	1.759428	0.000505	-0.26065
15649	180000	i1405	EKC-01	37	0.079668	1.821046	0.000883	-0.56534
16084	185000	i1405	EKC-01	38	0.067336	5.748246	0.000378	-0.64301
16520	190000	i1405	EKC-01	39	0.062907	1.764262	0.000486	-0.61409
16956	195000	i1405	EKC-01	40	0.075724	1.879754	0.00049	-1.86635
17391	200000	i1405	EKC-01	41	0.064536	1.807017	0.000519	-0.75918
17827	205000	i1405	EKC-01	42	0.061408	1.533995	0.000497	-0.63378
18263	210000	i1405	EKC-01	43	0.067469	1.697822	0.000553	-0.67427
18698	215000	i1405	EKC-01	44	0.066848	1.60095	0.000557	-0.62818
19134	220000	i1405	EKC-01	45	0.084953	1.502911	0.00067	-0.92185
19570	225000	i1405	EKC-01	46	0.070895	1.516438	0.000619	-0.79406
20005	230000	i1405	EKC-01	47	0.06719	1.933065	0.00046	-0.977
20441	235000	i1405	EKC-01	48	0.067292	1.631378	0.00063	-0.68022
20877	240000	i1405	EKC-01	49	0.055722	1.723387	0.000335	-0.79856
21313	245000	i1405	EKC-01	50	0.075084	2.776939	0.000541	-0.47169
21748	250000	i1405	EKC-01	51	0.251522	1.636668	0.000523	-0.51163
22184	255000	i1405	EKC-01	52	0.063795	1.772665	0.000455	-0.3299
22620	260000	i1405	EKC-01	53	0.099514	1.698967	0.000494	-0.43026
23055	265000	i1405	EKC-01	54	0.056528	1.601904	0.000371	-0.35214
23491	270000	i1405	EKC-01	55	0.05608	1.694348	0.000412	-0.44858
23927	275000	i1405	EKC-01	56	0.069304	1.705539	0.000517	-0.60271
24362	280000	i1405	EKC-01	57	0.056568	1.758127	0.000433	-0.54284
24798	285000	i1405	EKC-01	58	0.063576	1.662405	0.000467	-0.55988
25234	290000	i1405	EKC-01	59	0.071033	1.664629	0.000734	-0.62819
25670	295000	i1405	EKC-01	60	0.067455	1.742478	0.000652	-0.23599
26105	300000	i1405	EKC-01	61	0.065866	1.675172	0.000598	-0.52638
26541	305000	i1405	EKC-01	62	0.054257	1.59698	0.000389	-0.3187
26977	310000	i1405	EKC-01	63	0.064098	1.827372	0.000557	-0.52484
27412	315000	i1405	EKC-01	64	0.053057	2.092171	0.000675	-0.32923

8.15 Appendix 15: U/Th age model results

Sample Name	EKC01	RC-01-3	RC-01-4	RC-01-1	RC-01-2	EKC01top	EKC01bot
Age CORRECTED	399.3797277	25115.72295	12780.25991	5513.857531	16630.94415	31032.02177	62050.1814
± (95% CI = (Q97.5-Q2.5)/2 from MC var.)	49.65147273	1063.216918	69.52454987	129.3069741	745.0052709	192.7153606	396.1729459
Activity ratio 234U/238U initial	0.88146703	1.050612327	1.119063151	1.041458684	1.047088483	0.935276181	0.893862856
± (95% CI = (Q97.5-Q2.5)/2 from MC var.)	0.002227448	0.003824979	0.002690456	0.002469565	0.002560233	0.002367858	0.002528642
Age UNCORRECTED	463.0933748	28302.8966	12836.40996	5888.176711	18861.19459	31170.41468	62096.47508
± (95% CI = (Q97.5-Q2.5)/2 from MC var.)	45.56932315	179.4908464	66.68991774	37.75494696	109.3536198	186.4132294	395.3245639
Activity ratio 234U/238U initial	0.881445674	1.051070427	1.119082055	1.041502585	1.047386342	0.93525085	0.893848963
± (95% CI = (Q97.5-Q2.5)/2 from MC var.)	0.002228039	0.003868361	0.002692907	0.002471287	0.002568152	0.002367767	0.002527348
233/238U	0.007068237	0.002285717	0.002569049	0.00227882	0.002426367	0.004993694	0.001938578
± (95% CI = (Q97.5-Q2.5)/2 from MC var.)	2.43939E-06	5.28598E-07	5.83011E-07	4.3261E-07	4.2693E-07	1.24925E-06	3.09637E-07
233/235U	0.974668502	0.315138299	0.354190112	0.314176298	0.334586977	0.688608689	0.267412623
± (95% CI = (Q97.5-Q2.5)/2 from MC var.)	0.000386544	0.000148224	0.000109964	7.95298E-05	7.64237E-05	0.000226687	6.34984E-05
234/233U	0.007202772	0.025494601	0.024168844	0.025419479	0.023988259	0.010695476	0.026141629
± (95% CI = (Q97.5-Q2.5)/2 from MC var.)	8.14291E-06	6.64173E-05	1.66887E-05	1.85053E-05	1.55827E-05	7.36044E-06	1.76102E-05
[U] spike (ng/g)	0.642059087	0.442308789	0.442308789	0.442308789	0.442308789	0.442308789	0.442308789
± (2Stdev)	0.000280888	0.0004	0.0004	0.0004	0.0004	0.0004	0.0004
Spike Mass U(g)	0.5002	0.5002	0.5005	0.5005	0.5004	0.5007	0.501
± (2Stdev bal.)	0.00001	0.00001	0.00001	0.00001	0.00001	0.00001	0.00001
Sample Mass U(g)	0.1556	0.14868	0.13604	0.13079	0.13108	0.18069	0.15675
± (2Stdev bal.)	0.00001	0.00001	0.00001	0.00001	0.00001	0.00001	0.00001
Certification Date U Spike	{1, 7, 2007}	{1, 7, 2007}	{1, 7, 2007}	{1, 7, 2007}	{1, 7, 2007}	{1, 7, 2007}	{1, 7, 2007}
Measurement Date U	{1, 7, 2007}	{1, 7, 2007}	{1, 7, 2007}	{1, 7, 2007}	{1, 7, 2007}	{1, 7, 2007}	{1, 7, 2007}
230/229Th	6.62327E-05	0.001714271	0.000819815	0.000436649	0.00113881	0.000795074	0.003253215
± (95% CI = (Q97.5-Q2.5)/2 from MC var.)	8.76211E-07	4.55116E-06	2.22813E-06	1.86392E-06	3.6617E-06	2.29162E-06	6.76119E-06
232/229Th	0.37458133	64.52894781	1.092796029	7.623359108	42.58363685	1.156378127	0.952562163
± (95% CI = (Q97.5-Q2.5)/2 from MC var.)	0.021975359	0.021404244	0.003255277	0.003338733	0.017031671	0.002466614	0.003693128
230/232Th	0.00017801	2.65659E-05	0.000750213	5.72778E-05	2.67429E-05	0.000687568	0.003415333
± (95% CI = (Q97.5-Q2.5)/2 from MC var.)	1.01218E-05	6.9678E-08	2.7059E-06	2.47796E-07	8.49099E-08	2.91667E-06	1.40497E-05
[Th] spike (ng/g)	0.321385035	0.23360328	0.23360328	0.23360328	0.23360328	0.23360328	0.23360328
± (2Stdev)	0.000580697	0.0008	0.0008	0.0008	0.0008	0.0008	0.0008
Spike Mass Th(g)	0.5002	0.5002	0.5005	0.5005	0.5004	0.5007	0.501
± (2Stdev bal.)	0.00001	0.00001	0.00001	0.00001	0.00001	0.00001	0.00001
Sample Mass Th(g)	0.1556	0.14868	0.13604	0.13079	0.13108	0.18069	0.15675

241

Sample Name	EKC01	RC-01-3	RC-01-4	RC-01-1	RC-01-2	EKC01top	EKC01bot
± (2Stdev bal.)	0.00001	0.00001	0.00001	0.00001	0.00001	0.00001	0.00001
Certification Date Th Spike	{1, 7, 2007}	{1, 7, 2007}	{1, 7, 2007}	{1, 7, 2007}	{1, 7, 2007}	{1, 7, 2007}	{1, 7, 2007}
Measurement Date Th	{1, 7, 2007}	{1, 7, 2007}	{1, 7, 2007}	{1, 7, 2007}	{1, 7, 2007}	{1, 7, 2007}	{1, 7, 2007}
234/238U	5.09109E-05	5.82734E-05	6.20909E-05	5.79264E-05	5.82043E-05	5.34099E-05	5.06776E-05
± (95% CI = (Q97.5-Q2.5)/2 from MC var.)	5.48085E-08	1.51212E-07	4.04924E-08	4.07111E-08	3.63959E-08	3.42412E-08	3.31652E-08
235/238U	0.007251939	0.00725306	0.007253306	0.007253317	0.007251828	0.00725186	0.007249388
± (95% CI = (Q97.5-Q2.5)/2 from MC var.)	1.41693E-06	2.97059E-06	1.53675E-06	1.21457E-06	1.05618E-06	1.55175E-06	1.27377E-06
Molar Mass U Sample	238.0289333	238.0289009	238.028885	238.0289015	238.0289048	238.0289237	238.0289418
± (95% CI)	0.000328493	0.000689057	0.000356122	0.000281523	0.00024482	0.000359567	0.000295184
Abundance 234 Sample	5.05418E-05	5.78505E-05	6.164E-05	5.7506E-05	5.77819E-05	5.30226E-05	5.03103E-05
Abundance 235 Sample	0.007199363	0.007200416	0.00720063	0.007200671	0.007199202	0.007199267	0.00719685
Abundance 238 Sample	0.992750095	0.992741734	0.99273773	0.992741823	0.992743016	0.99274771	0.992752839
Atomic Weight 234 Sample	0.011828851	0.013539381	0.01442629	0.013458755	0.013523339	0.012409456	0.011774673
Atomic Weight 235 Sample	1.692166563	1.69241393	1.692464375	1.692473944	1.692128614	1.692143987	1.691575905
Atomic Weight 238 Sample	236.3249379	236.3229476	236.3219944	236.3229688	236.3232528	236.3243702	236.3255913
230/232Th	0.00017801	2.65659E-05	0.000750213	5.72778E-05	2.67429E-05	0.000687568	0.003415333
± (95% CI = (Q97.5-Q2.5)/2 from MC var.)	1.01218E-05	6.9678E-08	2.7059E-06	2.47796E-07	8.49099E-08	2.91667E-06	1.40497E-05
Molar Mass Th Sample	232.0376985	232.038002	232.0365523	232.0379405	232.0380017	232.0366777	232.0312311
± (95% CI)	0.002327515	1.60274E-05	0.000621513	5.69947E-05	1.9531E-05	0.000670008	0.00320993
Abundance 230 Sample	0.000177978	2.65652E-05	0.000749651	5.72745E-05	2.67422E-05	0.000687095	0.003403708
Abundance 232 Sample	0.999822022	0.999973435	0.999250349	0.999942725	0.999973258	0.999312905	0.996596292
Atomic Weight 230 Sample	0.040940799	0.006110883	0.172444455	0.013175034	0.006151591	0.15805469	0.782965583
Atomic Weight 232 Sample	231.9967577	232.0318912	231.8641079	232.0247654	232.0318501	231.878623	231.2482655
[234U] sample from MC	0.007112048	0.018832736	0.019508474	0.021357475	0.020089151	0.00637883	0.018352285
± (95% CI = (Q97.5-Q2.5)/2 from MC var.)	9.03112E-06	5.18739E-05	2.1701E-05	2.47017E-05	2.21285E-05	7.21111E-06	2.0348E-05
[235U] sample from MC	1.070776514	2.387657789	2.323185189	2.724211727	2.551862949	0.900014166	2.673216954
± (95% CI = (Q97.5-Q2.5)/2 from MC var.)	0.000620026	0.002369213	0.00216379	0.002523768	0.002303489	0.000853212	0.002440711
[238U] sample from MC	149.5490654	333.4087154	324.3947049	380.3920898	356.3994985	125.6994801	373.4719715
± (95% CI = (Q97.5-Q2.5)/2 from MC var.)	0.080761914	0.307579199	0.297129938	0.345394605	0.322279658	0.115078387	0.334501877
[U] sample from MC	150.6269539	335.815206	326.7373986	383.137659	358.9714506	126.6058731	376.1635407
± (95% CI = (Q97.5-Q2.5)/2 from MC var.)	0.081168538	0.3092171	0.299300247	0.347745779	0.32454583	0.115957573	0.3366472

Sample Name	EKC01	RC-01-3	RC-01-4	RC-01-1	RC-01-2	EKC01top	EKC01bot
[230Th] sample from MC	9.13263E-06	0.001307192	0.000657797	0.000340331	0.000968161	0.000479373	0.002395589
± (95% CI = (Q97.5-Q2.5)/2 from MC var.)	8.95979E-07	5.89676E-06	2.99945E-06	2.03151E-06	4.75806E-06	2.28839E-06	9.87069E-06
[232Th] sample from MC	0.391566591	51.35643987	0.950832913	6.901295342	38.45679083	0.757820291	0.720008281
± (95% CI = (Q97.5-Q2.5)/2 from MC var.)	0.022547078	0.184682878	0.004376543	0.024896461	0.138963401	0.003157236	0.003747891
[Th] sample from MC	0.391575724	51.35774706	0.95149071	6.901635673	38.45775899	0.758299663	0.72240387
± (95% CI = (Q97.5-Q2.5)/2 from MC var.)	0.022547337	0.184687966	0.004378233	0.024897181	0.138966018	0.003158418	0.003753366
Atom Nb 234U from MC	1.83001E+19	4.84588E+19	5.01975E+19	5.49552E+19	5.16917E+19	1.64135E+19	4.72225E+19
± (95% CI = (Q97.5-Q2.5)/2 from MC var.)	2.32381E+16	1.33477E+17	5.58392E+16	6.35603E+16	5.69391E+16	1.8555E+16	5.23578E+16
Atom Nb 235U from MC	2.74347E+21	6.1175E+21	5.95231E+21	6.9798E+21	6.53822E+21	2.30596E+21	6.84914E+21
± (95% CI = (Q97.5-Q2.5)/2 from MC var.)	1.58859E+18	6.07024E+18	5.54392E+18	6.46623E+18	5.90185E+18	2.18605E+18	6.25343E+18
Atom Nb 238U from MC	3.78325E+23	8.43448E+23	8.20645E+23	9.62305E+23	9.01609E+23	3.17991E+23	9.44799E+23
± (95% CI = (Q97.5-Q2.5)/2 from MC var.)	2.04309E+20	7.78105E+20	7.51671E+20	8.7377E+20	8.15294E+20	2.91122E+20	8.46213E+20
Atom Nb 230Th from MC	2.39087E+16	3.42216E+18	1.72208E+18	8.90968E+17	2.53459E+18	1.25497E+18	6.27152E+18
± (95% CI = (Q97.5-Q2.5)/2 from MC var.)	2.34562E+15	1.54374E+16	7.85241E+15	5.31839E+15	1.24564E+16	5.99088E+15	2.58409E+16
Atom Nb 232Th from MC	1.01624E+21	1.33287E+23	2.46772E+21	1.79111E+22	9.98079E+22	1.96679E+21	1.86866E+21
± (95% CI = (Q97.5-Q2.5)/2 from MC var.)	5.8517E+19	4.79312E+20	1.13586E+19	6.46144E+19	3.60655E+20	8.19406E+18	9.727E+18
Ratio U/Th from MC	385.0016799	6.538765538	343.3970963	55.51421253	9.334204859	166.96094	520.714411
± (95% CI = (Q97.5-Q2.5)/2 from MC var.)	22.21687832	0.02281205	1.572594044	0.193808744	0.03295139	0.678109472	2.665692948
Ratio 230/232Th from MC	2.33437E-05	2.54533E-05	0.000691812	4.93141E-05	2.51753E-05	0.000632568	0.003327181
± (95% CI = (Q97.5-Q2.5)/2 from MC var.)	2.62925E-06	6.90608E-08	2.8281E-06	2.4009E-07	8.42812E-08	2.37191E-06	1.45061E-05
Ratio 230Th/238U from MC	6.10678E-08	3.92069E-06	2.02777E-06	8.94684E-07	2.7165E-06	3.81364E-06	6.41437E-06
± (95% CI = (Q97.5-Q2.5)/2 from MC var.)	5.98041E-09	1.72918E-08	9.04011E-09	5.27414E-09	1.30424E-08	1.78062E-08	2.57224E-08
Ratio 232Th/238U from MC	0.002618315	0.154034488	0.002931099	0.018142584	0.107903607	0.006028826	0.001927878
± (95% CI = (Q97.5-Q2.5)/2 from MC var.)	0.000150697	0.00053768	1.34256E-05	6.33812E-05	0.000380832	2.44904E-05	9.8989E-06
Ratio 234/238U from MC	4.75566E-05	5.64854E-05	6.01381E-05	5.61459E-05	5.63669E-05	5.07467E-05	4.91397E-05
± (95% CI = (Q97.5-Q2.5)/2 from MC var.)	5.83673E-08	1.47583E-07	4.35605E-08	4.27234E-08	3.74257E-08	3.71351E-08	3.34444E-08
Ratio 235/238U from MC	0.007160035	0.007161354	0.0071616	0.007161589	0.007160119	0.007160047	0.007157745
± (95% CI = (Q97.5-Q2.5)/2 from MC var.)	3.6662E-06	3.69597E-06	2.69282E-06	2.23915E-06	2.0147E-06	2.8935E-06	2.04865E-06
Activity Ratio 230/232Th from MC	4.358414873	4.752383552	129.1691939	9.207247672	4.700462107	118.1023309	621.2272911
± (95% CI = (Q97.5-	0.492113772	0.023510695	0.735605168	0.05748106	0.024902227	0.659118017	3.759770829

Sample Name	EKC01	RC-01-3	RC-01-4	RC-01-1	RC-01-2	EKC01top	EKC01bot
Q2.5)/2 from MC var.)							
Activity Ratio 230Th/238U from MC	0.003730463	0.239511583	0.123871506	0.054654606	0.165946232	0.232957639	0.391839076
± (95% CI = (Q97.5-Q2.5)/2 from MC var.)	0.000365599	0.001303299	0.000678947	0.000364034	0.000963328	0.001296113	0.001998684
Activity Ratio 232Th/238U from MC	0.000856673	0.050398307	0.000958991	0.005936054	0.035304311	0.001972513	0.000630754
± (95% CI = (Q97.5-Q2.5)/2 from MC var.)	4.93639E-05	0.000229379	5.21299E-06	2.75072E-05	0.000162841	1.00942E-05	3.76707E-06
Activity Ratio 234/238U from MC	0.881600805	1.047142924	1.114837526	1.040817363	1.044925491	0.940713045	0.910941962
± (95% CI = (Q97.5-Q2.5)/2 from MC var.)	0.002220988	0.003577623	0.002600263	0.002429109	0.002429908	0.002165659	0.00210491
Activity Ratio 235/238U from MC	0.046035104	0.046045066	0.046045214	0.046045397	0.046036436	0.046035361	0.046020484
± (95% CI = (Q97.5-Q2.5)/2 from MC var.)	8.16E-05	8.0347E-05	7.95563E-05	7.98857E-05	7.92616E-05	8.10426E-05	7.79012E-05
Initial 230/232Th activity ratio	0.6	0.6	0.6	0.6	0.6	0.6	0.6
± (2Stdev)	0.2	0.2	0.2	0.2	0.2	0.2	0.2
Initial 230/232Th activity ratio from MC	0.60012722	0.59953478	0.599881564	0.600368185	0.59952368	0.600503035	0.600647887
± (95% CI = (Q97.5-Q2.5)/2 from MC var.)	0.19884778	0.193937089	0.197608243	0.197170776	0.196138212	0.196853553	0.194069048
Age UNCORRECTED from MC	463.0933748	28302.8966	12836.40996	5888.176711	18861.19459	31170.41468	62096.47508
± (2Stdev from MC var.)	45.84835496	181.2434471	68.47276624	38.50567365	109.7965883	190.5482689	404.8635334
Median	463.1705413	28303.11164	12836.06809	5888.330192	18861.21007	31171.24808	62094.97919
Quantile 97.5%	507.9271897	28482.51397	12902.86148	5926.002947	18970.60768	31355.07364	62490.86438
Quantile 2.5%	416.7885434	28123.53228	12769.48164	5850.493053	18751.90044	30982.24718	61700.21525
Quantile 97.5% - Median	44.7566484	179.4023341	66.79339224	37.67275426	109.3976158	183.8255659	395.8851871
Median - Quantile 2.5%	46.38199791	179.5793587	66.58644324	37.83713967	109.3096238	189.000893	394.7639407
(Quantile 97.5% - 2.5%)/2	45.56932315	179.4908464	66.68991774	37.75494696	109.3536198	186.4132294	395.3245639
Activity ratio 234U/238U initial	0.881445674	1.051070427	1.119082055	1.041502585	1.047386342	0.93525085	0.893848963
± (2Stdev from MC var.)	0.002280279	0.003949281	0.002737806	0.002526976	0.002610231	0.002431754	0.002587329
Median	0.881458014	1.051060479	1.119083819	1.041502039	1.047390037	0.935264604	0.893847251
Quantile 97.5%	0.883676988	1.055004806	1.121760837	1.044009308	1.049956018	0.937616167	0.896373379
Quantile 2.5%	0.879220909	1.047268084	1.116375024	1.039066733	1.044819713	0.932880632	0.891318682
Quantile 97.5% - Median	0.002218974	0.003944327	0.002677019	0.002507268	0.002565981	0.002351562	0.002526128
Median - Quantile 2.5%	0.002237105	0.003792395	0.002708795	0.002435306	0.002570324	0.002383973	0.002528569
(Quantile 97.5% - 2.5%)/2	0.002228039	0.003868361	0.002692907	0.002471287	0.002568152	0.002367767	0.002527348
Age CORRECTED from MC	399.3797277	25115.72295	12780.25991	5513.857531	16630.94415	31032.02177	62050.1814
± (2Stdev from MC var.)	50.52058694	1090.531401	70.95895902	131.0753734	753.0327538	195.6490403	405.2233011
Median	399.5883026	25119.22382	12780.13669	5513.38486	16631.729	31033.03016	62048.47444

Sample Name	EKC01	RC-01-3	RC-01-4	RC-01-1	RC-01-2	EKC01top	EKC01bot
Quantile 97.5%	448.2535606	26185.71853	12849.69329	5641.140247	17368.67458	31224.20139	62445.99406
Quantile 2.5%	348.9506151	24059.28469	12710.64419	5382.526299	15878.66404	30838.77067	61653.64817
Quantile 97.5% - Median	48.66525794	1066.494704	69.55660115	127.7553872	736.9455871	191.1712277	397.5196252
Median - Quantile 2.5%	50.63768753	1059.939132	69.4924986	130.8585611	753.0649546	194.2594935	394.8262666
(Quantile 97.5% - 2.5%)/2	49.65147273	1063.216918	69.52454987	129.3069741	745.0052709	192.7153606	396.1729459
Activity ratio 234U/238U initial	0.88146703	1.050612327	1.119063151	1.041458684	1.047088483	0.935276181	0.893862856
± (2Stdev from MC var.)	0.002279897	0.003917048	0.002737397	0.002524318	0.00259487	0.002430738	0.002587054
Median	0.881477665	1.050609564	1.119064092	1.041461994	1.047091217	0.935290738	0.893862153
Quantile 97.5%	0.88369737	1.054504339	1.121738251	1.043964329	1.049644165	0.93764354	0.896387901
Quantile 2.5%	0.879242474	1.046854381	1.116357338	1.039025199	1.044523699	0.932907824	0.891330617
Quantile 97.5% - Median	0.002219705	0.003894775	0.002674159	0.002502335	0.002552948	0.002352803	0.002525749
Median - Quantile 2.5%	0.002235191	0.003755183	0.002706754	0.002436795	0.002567518	0.002382913	0.002531535
(Quantile 97.5% - 2.5%)/2	0.002227448	0.003824979	0.002690456	0.002469565	0.002560233	0.002367858	0.002528642
Propagation of uncertainties from 230/232Th STD	1	1	1	1	1	1	1
Spike Type	1	1	1	1	1	1	1

8.16 Appendix 16: Results for U-Th geochronometry on the ECK-01 and RC-01 stalagmites, measured at NIL RSMAS laboratories by MC-ICP-MS.

Sample Name	Activity ratio 234U/238U initial	± (95% CI = (Q97.5-Q2.5)/2 from MC var.)	Ratio 230Th/238U from MC	± (95% CI = (Q97.5- Q2.5)/2 from MC var.)	230/232Th	± (95% CI = (Q97.5-Q2.5)/2 from MC var.)	Age UNCORRECTED	± (95% CI = (Q97.5-Q2.5)/2 from MC var.)	Age CORRECTED	± (95% CI = (Q97.5-Q2.5)/2 from MC var.)
RC-01-1	1.041458684	0.002469565	6.10678E-08	5.98041E-09	5.72778E-05	2.47796E-07	5888.176711	37.75494696	5513.857531	129.3069741
RC-01-2	1.047088483	0.002560233	3.92069E-06	1.72918E-08	2.67429E-05	8.49099E-08	18861.19459	109.3536198	16630.94415	745.0052709
RC-01-3	1.050612327	0.003824979	2.02777E-06	9.04011E-09	2.65659E-05	6.9678E-08	28302.8966	179.4908464	25115.72295	1063.216918
RC-01-4	1.119063151	0.002690456	8.94684E-07	5.27414E-09	0.000750213	2.7059E-06	12836.40996	66.68991774	12780.25991	69.52454987
EKC01top	0.935276181	0.002367858	2.7165E-06	1.30424E-08	0.000687568	2.91667E-06	31170.41468	186.4132294	31032.02177	192.7153606
EKC01bottom	0.893862856	0.002528642	3.81364E-06	1.78062E-08	0.003415333	1.40497E-05	62096.47508	395.3245639	62050.1814	396.1729459
EKC01	0.88146703	0.002227448	6.41437E-06	2.57224E-08	0.00017801	1.01218E-05	463.0933748	45.56932315	399.3797277	49.65147273

8.17 Appendix 17: Modern calcite sampling results and their locations

Sample	Number	Distance from center (cm)	std	std	Modern calcite $\delta^{13}C$	Modern calcite $\delta^{18}O$	Average calcite $\delta^{18}O$	Dripwater $\delta^{18}O$	Rainwater $\delta^{18}O$
EKC - Plate 1	Inside	0	0.02	0.02	-9.41	-5.33	-5.1	-5.805	-5.75
EKC - Plate 1	Middle	1	0.62	0.69	-13.06	-14.13			
EKC - Plate 1	Outside	2	0.02	0.03	-9.00	-4.87			
EKC - Plate 2	Center	0	0.02	0.04	-9.23	-5.36	-5.25	-5.805	-5.75
EKC - Plate 2	1cm	1	0.02	0.03	-9.14	-5.03			
EKC - Plate 2	2cm	2	0.02	0.04	-9.10	-5.32			
EKC - Plate 2	3cm	3	0.02	0.03	-8.63	-5.08			
EKC - Plate 2	4cm	4	0.01	0.04	-8.54	-5.46			
EKC Presidents Gallery	Scraped powder	-	0.02	0.02		-4.49	-4.49	-5.315	-5.75
EKC Forage Gallery	Scraped powder	-	0.15	0.31		-4.22	-4.22	-5.805	-5.75
Rahwe cave	Stalagmite tip	-	0.02	0.03		-5.14	-5.14	-8.52	-12.275

The yellow highlighted values have been removed from the assessment for these are probably contaminated from mud deposits or flooding events as values are way off the expected values.